Geochemical Characterization of Endmember Mantle Components

By

RHEA K. WORKMAN

B.S., UNIVERSITY OF MISSOURI – ROLLA, 1998

Submitted in partial fulfillment of the requirements for the degree of

Doctor of Philosophy

at the
MASSACHUSETTS INSTITUTE OF TECHNOLOGY
and the
WOODS HOLE OCEANOGRAPHIC INSTITUTION

June 2005

Author _____

Joint Program in Oceanography
Massachusetts Institute of Technology and
Woods Hole Oceanographic Institution
June 2005

Certified by _____

Dr. Stanley R. Hart
Thesis Supervisor, WHOI

Accepted by _____

Dr. Greg Hirth
Chair, Joint Committee for Marine Geology and Geophysics
Woods Hole Oceanographic Institution

Geochemical Characterization of Endmember Mantle Components

by

RHEA K. WORKMAN

Submitted in partial fulfillment for the requirements for the
degree of Doctor of Philosophy
at the Massachusetts Institute of Technology
and the Woods Hole oceanographic Institution
June 2005

Abstract

This thesis uses trace elements and radiogenic isotope tracers to define elemental abundances in reservoirs of the Earth's mantle, including EM2 (the Enriched Mantle 2), as seen in the Samoan hotspot track, and DMM (the depleted upper mantle), which is sampled at mid-ocean ridges. Together these components comprise up to ~50% of the total mantle mass. Much of the mantle's chemical heterogeneities are suspected to originate by either the removal of mass from the mantle (in the case of DMM) or the addition of mass to the mantle through subduction zones (in the case of EM2). We show that DMM represents mantle that 1) has been previously depleted by 2-3% melt removal, 2) mass-balances well with the continental crust, 3) has only 15% of the radiogenic heat production in primitive upper mantle and 4) can generate present-day ocean crust by 6% aggregated fractional melting. EM2 is classically interpreted as mantle material enriched in trace elements through the ancient, subduction-zone recycling of terrigenous sediments; here we show this model is unlikely and provide two other working hypotheses. The first is recycling of melt-impregnated oceanic lithosphere; the second is recycling of a mantle wedge impregnated with melt from a subducting oceanic plate.

Thesis Advisor: Dr. Stanley Hart, Woods Hole Oceanographic Institution

Thesis Chair: Dr. Nobu Shimizu, Woods Hole Oceanographic Institution

Committee:
Dr. Henry Dick, Woods Hole Oceanographic Institution
Prof. Fred Frey, Massachusetts Institute of Technology
Dr. Erik Hauri, Dept. of Terrestrial Magnetism, Carnegie Inst. of Washington
Dr. Jian Lin, Woods Hole Oceanographic Institution

Acknowledgments

Each of us have come to where we are today upon separate, unique and intricate pathways. Everyone we have encountered along the way has, in some form, shaped us into who we are and how we interact with our world. In this way, it is impossible to acknowledge them all, but there are a few who have done more shaping than the rest; and there are a few who believed in me before I did.

I met Stan during a summer student internship at WHOI and he quickly became the first reason I ever had for seeking a graduate degree. I'm nearly certain he has a sixth sense – knowing when to push, when to guide, when to teach and when to be a friend. Mantle geochemistry has been a medium for us to discuss the greater lessons of life, with "shop-talk" often ending in "life-talk". With thanks to Stan, I've learned much about science as well as much about myself.

Nobu has been a constant source of knowledge, support and great discussions. My experience here would not have been as vibrant or full without him. Fred taught me the first think I ever knew about trace element geochemistry and since then has been a reminder that 'the devil is in the details'. Erik has a wonderful and sincere way of seeing the world as a whole, but also the holes in our science – I hope it's rubbed off a little. Jian inspired me venture outside the realm of geochemistry; in doing so, I gained a great appreciation for geophysicists! Henry finally remembered my name after I finally saw the beauty of abyssal peridotites; we have since had great discussions about mantle rocks and life in general. Jurek taught me how to work in the clean lab, how to have patience, and how to perk up when things get a little dim. I have received nothing but unwaivering encouragement and support from Jurek, and I am forever grateful.

There is a very long list of very remarkable people from EAPS, Geology and Geophysics, and Marine Chemistry and Geochemistry who have contributed to my growth and overwhelmingly positive experience in the Joint Program: Peter K., Greg H., Glenn G., Mark K., Josh C., Wolfgang B., Bernhard P.-E., Wen-Lu Z., Rob R.-S., Peter C., Karen B., Jerry M., Bill C., Ken S., Susan H., Karen H., Jeff M., John H., Laurent M., Hans S., Dan F., Lary B., Graham L., Pete L., Dan M., Bob D., Jack W., Adam S., Andrew D., Grotz, Grove, and Bowring. I very much enjoyed our interactions and learned something important from each of them. Many of the same people regularly attended Geochemistry Seminar and prepared me for the piranhas.

I would like to thank those students who have gone before and who showed me the way of companionship, cooperation and comradery: Alberto, Ken K., Debbie H., Mark B., Amy D., Jen G., Robyn K., Mike B., and Astri. My fellow students are a wonderful and earthy group of people: Jeff, Margaret, Linda, Matt J., Cara, Jessica, Brian, Emily, Trish, Clare, Lynn, Sharon, Heidi, Mea, Fabian, Oscar, Chris, Janelle, Rose, Dave, Matt M., Steve DB and Kristy, my world-class officemate. May we meet many times and in many places! Special thanks go to the Ta'u Island Field Team – Jeff, Margaret and Matt – who put up with miles and miles of machete work, but got a great view! If it weren't for Kaeo, I likely never would have come to the east coast at all. The Geodynamics Seminar field trips were invaluable for solidifying an intuition for the world of geology.

Julia, Marsha, John and Judy from the Academic Programs Office care for us beyond their duty and always create an environment of true warmth and support. Pam, K., Maryanne, Elaine and Lynn from the G&G Administration are endlessly helpful, friendly and giving. To the Graphics Department - You guys are incredible!

I've had the fortune of living with people over the last two years who made our house feel like a home, filled with love and support, like a second family; thank you Margaret, Linda, and Cara! I also had the fortune of living with Emily, Charlie and Joe – they offered a very wide spectrum of personality, and were each great fun! Rose, you were always a shoulder, a kick or laugh right when I needed it – you will not be forgotten. Astri and Chanda made life exciting and always had something to talk about! Andy, thank you for the shelter and for showing me more patience than I thought was humanly possible.

I couldn't have been more fortunate with the wonderful family I have. If I had to live this life 100 times, I would pick each of them every time!

Very generous financial support for this thesis has been provided by WHOI's Academic Programs Office, NSF grants 81903800, 80489100 and 82591700 to Stan Hart and the Cole Ocean Ventures Fund.

To Boa, Patty, Marcie, Adam and Michael

Contents

Chapter 1:

Introduction

The field of mantle geochemistry is fundamentally concerned with the processes and history of Earth's differentiation. How has Earth developed its inner and outer cores, mantle, continental crust, oceanic crust, ocean and atmosphere? Can we track the growth and evolution of these reservoirs through the 4.56 billion years of Earth history – and can we project into the future? Though we are concerned with all these reservoirs, our field is self-named 'mantle' geochemistry since the Earth's mantle is the primary driver of differentiation. It mediates convective transfer of materials from deep to shallow Earth, resulting in the formation of crust, oceans and the atmosphere. It also returns bits of shallow, differentiated materials back to the deep Earth in places where the mantle is down-welling at subduction zones. The mantle essentially turns the Earth inside-out, trying to purge it of unwanted, incompatible elements (such as hydrogen, carbon, potassium and uranium) and retain in it the wanted, refractory elements (such as magnesium, iron and chromium). It is fascinating to think our human bodies are made of carbon once contained within the very deep, very hot inner Earth.

The Earth was born of materials condensed from our solar system about 4.56 billion years ago (Patterson, 1956; Birck and Allegre, 1978); it almost certainly had some small initial variations in chemical composition, but is thought to be, on average, similar in elemental and isotopic abundances to the class of meteorites called CI carbonaceous chondrites (Anders and Ebihara, 1982; Anders and Grevesse, 1989). From its mess of agglomerated materials, Earth formed (very early in its history) a dense, Fe-Ni metallic core, leaving the remaining lithophile materials to form the Bulk Silicate Earth (BSE); BSE is about 84% the volume of the Earth, but only 68% the mass of the Earth because its density is lower than that of the core. Knowing the approximate mass and composition of the core from seismic surveys through the Earth allows for a fairly good estimate of the chemical composition of the Bulk Silicate Earth (by subtracting the core from the CI composition; Hart and Zindler, 1986; McDonough and Sun, 1995); this simple estimate is inaccurate for

those elements, such as hydrogen, helium, sulfur and lead, that are strongly volatile and lost to space before the formation of Earth's atmosphere.

The BSE has further differentiated, or fractionated, into distinct chemical reservoirs – some of which are obvious at the surface of the Earth (like the oceans and continental crust) and some of which are held within the Earth's mantle. The focus of this thesis is on the compositional variations within the mantle, as determined from mantle melts erupted at both mid-ocean ridges and hotspots (i.e. mantle plumes). Zindler and Hart (1986) noted that there are 4 unique end-member mantle components based on $^{87}Sr/^{86}Sr$, $^{143}Nd/^{144}Nd$, $^{206}Pb/^{204}Pb$, $^{207}Pb/^{204}Pb$, and $^{208}Pb/^{204}Pb$ radiogenic isotope compositions of a global database of oceanic lavas. They described how most mid-ocean ridge basalts (MORBs) are isotopically similar and represent an upper mantle previously depleted of melt (i.e. oceanic and continental crust); this reservoir is termed the Depleted MORB Mantle (DMM). On the other hand, ocean island basalts (OIBs), erupted by hotspot volcanism, are isotopically heterogeneous in terms of most radiogenic isotope systems. Each hotspot chain is unique in radiogenic isotope space and represents a unique mixture of the Zindler and Hart mantle components. From parent isotope half-lives and parent-daughter ratios, it is inferred that end-member mantle sources for OIBs and MORBs must have been chemically isolated for billions of years in order to develop the observed differences in the abundance of daughter isotopes. Because isotopes of heavy elements are so little fractionated in the melting process, isotopic compositions of oceanic basalt are not only "clocks" for ancient reservoir development, but also "fingerprints" of a melt's solid source. The goal of mantle geochemistry in general and this thesis specifically is to determine the origins, ages and chemical compositions of these mantle components.

Although there have been many ideas regarding the origins of the classic mantle end-members seen in OIB chains, one model has been relied upon most commonly and received the most attention from a modeling point of view. We are in effect "outside looking in", so major differentiation processes occurring at the solid Earth's uppermost layers, namely the formation of continental and oceanic crust, are the most obvious explanations for the creation of volumetrically significant heterogeneities in composition. Return of these differentiated materials to the mantle through return flow at subduction zones creates *mantle* heterogeneity. Geochemical models attempting to accurately quantify the compositions of deeply-subducted materials need precise knowledge regarding: 1) hydrothermal alteration of the oceanic crust, 2) partition coefficients for both the dehydration and melting of crust and sediments, 3) the thermal structure of mantle wedges, 4) the compositions of subducting

sediments, and 5) the lifespan of a subducted slab in the deep mantle. Although much progress has been made in each of these topics, many parameters are not well defined through space and time, making it difficult to formulate a completely accurate model for any one of the OIB end-members.

In this thesis, I focus on describing the chemical character of 2 out of the 4 mantle reservoirs that were identified and 'fingerprinted' by Zindler and Hart (1986). The first is DMM; it is ubiquitously sampled along the global system of mid-ocean ridges and represents the largest accessible reservoir on Earth (at least 30% the BSE). It is called 'depleted' because we know from its isotopic fingerprint that melts were removed from this mantle a very long time ago (2 to 3 Ga), in a process we speculate to be much like the oceanic and continental crust formation that occurs today. We use the following constraints in deriving an average trace element composition of DMM: 1) trace element content of clinopyroxenes from abyssal peridotites, 2) isotopic evolution from primitive upper mantle (PUM) and 3) canonical trace element ratios in MORBs. The average trace element content of DMM, as deduced here, generally shows a very smooth pattern with increasing trace element compatibility, which to first order mass-balances with the continental crust. The degree of depletion indicated in DMM represents 2-3% melt removal from the primitive upper mantle; this means that DMM has only 15% the radiogenic heat production of PUM (from K, U and Th). Present-day ocean crust (i.e. average MORB) can be modeled with 6% aggregated fractional melting of the deduced DMM.

The second mantle reservoir studied in this thesis is nearly opposite in character from the depleted upper mantle – it is called the Enriched Mantle 2 (EM2) and is sampled from the inner Earth by the Samoan hotspot. EM2 has the highest $^{87}Sr/^{86}Sr$ of all oceanic lavas, whereas the depleted upper mantle has the lowest. Although EM2 may not be a volumetrically significant reservoir, its rare and unique composition is very significant because it allows us to eventually understand the details of BSE differentiation (for example, the growth rate of continental crust).

Chapters 2, 4 and 5 of this thesis address the geochemistry of the Samoan islands and seamounts in great detail. In Chapter 2, we use trace element abundances and radiogenic isotope tracers to establish the geochemical variability, character, and habits of the Samoan lavas, including the ones that are more extreme in their EM2 signature than any other lavas sampled on Earth. In Chapter 2, we establish that a model involving the recycling of only marine sediments will not successfully explain the origin of EM2. Instead, an alternative model is offered in which an oceanic lithosphere is impregnated with an upper mantle melt,

recycled through a subduction zone and stored for 2.5 Ga in the mantle – to be sampled today by the Samoan mantle plume.

In Chapter 4, we use volatile element abundances (water, carbon dioxide, fluorine, sulfur and chlorine) from Samoan glasses to comment on the general properties of these elements in igneous systems and the specific properties of water in the EM2 mantle reservoir. We find that absolute water contents are high for Samoan lavas (0.63 – 1.50 wt%), but relative enrichment of water compared to trace element enrichment is low. H_2O/Ce (58 – 157) and H_2O/La (120 – 350) correlate inversely with $^{87}Sr/^{86}Sr$ compositions (0.7045 – 0.7089). This leads us to believe that, because of very fast diffusion of hydrogen in olivine, recycled lithospheric material with high initial water content will lose water to the drier ambient mantle during storage within the inner Earth. This concept implies that water may be one of the few (if only) elements in the mantle that is close to chemical equilibrium over great distances.

Chapter 5 presents oxygen isotope data for Samoan olivine phenocrysts as a means to identify the presence of recycled material that was once at or near Earth's; oxygen isotope variations occur not because of production of a radiogenic oxygen isotope, but because oxygen's isotopes, ^{16}O and ^{18}O, have slightly different chemical behavior during low temperature reactions. Here we test two models for the generation of EM2. The first is (once-again) the standard sediment-recycling model. The second expands upon the metasomatic model of Chapter 2 by identifying a location for the metasomatism (the mantle wedge), and more accurately defining what the metasomatising agent is (an eclogite melt). Each model shows some major misfits to characteristics of end-member Samoan lavas, although the metasomatic model requires less 'special pleading'.

Chapter 6 investigates the correlation between geochemical and geophysical properties of Samoa. Excess crustal flux along the Samoan volcanic lineament decreases nearly monotonically approaching Vailulu'u Seamount, the easternmost and youngest volcano. This trend shows excellent correspondence to increasing $^{206}Pb/^{204}Pb$ compositions of the lavas with decreasing age along the hotspot track. We speculate this correlation could be due to either a lithosphere thickening toward the east or decreasing potential temperature of the mantle plume, and that the geochemical signatures observed in the lavas are partly a function of how mantle materials with differing solidus temperatures are sampled from the Earth.

References

Anders, E. and M. Ebihara, Solar-system abundances of the elements, *Geochim. Cosmochim. Acta*, 46, 2363-2380, 1982.

Anders, E. and N. Grevesse, Abundances of the elements: meteoritic and solar, *Geochim. Cosmochim. Acta*, 53, 197-214, 1989.

Birck, J.L. and C.J. Allegre, Chronology and chemical history of the parent body of basaltic achondrites studied by the ^{87}Rb-^{87}Sr method, *Earth Planet. Sci. Lett.*, 39, 37-51, 1978.

Patterson, C.C., Age of meteorites and the Earth, *Geochim. Cosmochim. Acta*, 10, 230-237, 1956.

Hart, S.R. and A. Zindler, In search of a bulk-Earth composition, *Chemical Geology*, 57, 247-267, 1986.

McDonough, W.F. and S.-s. Sun, The composition of the Earth, *Chemical Geology*, 120, 223-253, 1995.

Zindler, A., and Hart, S.R., Chemical Geodynamics, *Ann. Rev. Earth Planet. Sci.*, 14, 493-571, 1986.

Chapter 2:

Recycled metasomatized lithosphere as the origin of the Enriched Mantle II (EM2) Endmember: Evidence from the Samoan Volcanic Chain*

Abstract

An in-depth Sr-Nd-Pb-He-Os isotope and trace element study of the EMII-defining Samoan hotspot lavas leads to a new working hypothesis for the origin of this high $^{87}Sr/^{86}Sr$ mantle endmember. Systematics of the Samoan fingerprint include 1) increasing $^{206}Pb/^{204}Pb$ with time – from 18.6 at the older, western volcanoes to 19.4 at the present day hotspot center, Vailulu'u Seamount, 2) en-echelon arrays in $^{206}Pb/^{204}Pb$ – $^{208}Pb/^{204}Pb$ space which correspond to the two topographic lineaments of the 375 km long volcanic chain – this is much like the Kea and Loa Trends in Hawai'i, 3) the highest $^{87}Sr/^{86}Sr$ (0.7089) of all oceanic basalts, 4) an asymptotic decrease in $^{3}He/^{4}He$ from $24R_A$ (Farley et al., 1992) to the MORB value of $8R_A$ with increasing $^{87}Sr/^{86}Sr$, and 5) mixing among four components which are best described as the "enriched mantle", the depleted FOZO mantle, the (even more depleted) MORB Mantle, and a mild HIMU (high $^{238}U/^{204}Pb$) mantle component. A theoretical, "pure" EMII lava composition has been calculated and indicates an extremely smooth trace element pattern of this endmember mantle reservoir. The standard recycling model (of ocean crust/sediment) fails as an explanation for producing Samoan EM2, due to these smooth spidergrams for EM2 lavas, low $^{187}Os/^{188}Os$ ratios and high $^{3}He/^{4}He$ ($>8R_A$). Instead, the origin of EM2 has been modeled with the ancient formation of metasomatised oceanic lithosphere, followed by storage in the deep mantle and return to the surface in the Samoan plume.

* Published in G^3 Volume 5, No. 4, April 2004.

1. Introduction

Although intra-plate ocean island volcanism accounts for only a few percent of the total volcanism on Earth, these volcanic piles may be the surface manifestations of the deepest known samplings of the interior of the planet. The relative stationarity of mantle plumes with respect to upper mantle plate flow (Molnar and Stock, 1987; Steinberger and O'Connell, 1998; Wang and Wang, 2001; Koppers et al., 2001), and a growing catalogue of seismic evidence and tomographic images showing velocity anomalies beneath hot spots extending well into the mid-mantle and sometimes to the core-mantle boundary (Russell et al., 1998; Shen et al., 1998; Zhao, 2001; Montelli et al., 2003), all support the idea that mantle plumes sample the inner Earth at a much deeper level than do mid-ocean ridge spreading centers. Ocean island chains may thus provide some of the best clues to the chemical character of the lower mantle and the nature of convective interactions between the deep and shallow mantle.

Unlike mid-ocean ridge basalts (MORBs), which derive from a fairly uniform melt-depleted upper mantle, ocean island basalts (OIBs) are isotopically heterogeneous in terms of most radiogenic isotope systems (e.g. Zindler and Hart, 1986; Hart, 1988; Hofmann, 1997). Isotopic arrays from ocean island chains often extend from a "common" mantle, termed FOZO (i.e. Focus Zone; Hart et al., 1992), and tend toward one of three "endmember" mantle components: HIMU, the high time-integrated U/Pb mantle, EM1 or EM2, the Enriched Mantles 1 and 2 (Zindler and Hart, 1986). From parent isotope half-lives and parent-daughter ratios, it is inferred that mantle sources for OIBs and MORBs must have been chemically isolated for billions of years in order to develop the observed differences in the abundance of daughter isotopes. Because isotopes of heavy elements are so little fractionated in the melting process, isotopic compositions of oceanic basalt are not only "clocks" for ancient reservoir development, but also "fingerprints" of a melt's solid source. We are left, through geochemical interrogation and theoretical ingenuity, to reverse the processes by which mantle melts were generated and brought to Earth's surface. Ultimately, with some indication for source compositions, the origins and ages of chemically distinct, isolated mantle reservoirs can be deduced.

Although there have been many ideas regarding the origins of the classic mantle end members, one model has been relied upon most commonly and received the most attention from a modeling point of view. We are in effect "outside looking in", so major

differentiation processes occurring at the solid Earth's uppermost layers, namely the formation of continental and oceanic crust, are the most obvious explanations for the creation of volumetrically significant heterogeneities in composition. Many workers have applied this perspective and contributed to what is here referred to as the Standard Model for the origin of mantle components (Armstrong, 1968; Chase, 1981; Hofmann and White, 1982; Cohen and O'Nions, 1982; White, 1985; Zindler and Hart, 1986; Weaver, 1991; Hart et al., 1992). In summary, oceanic crust is subducted at convergent margins, dehydrated (increasing U/Pb, Th/Pb, and Sr/Rb ratios) and put into long term storage in the deep mantle to evolve to HIMU. EM1 and EM2 are generated when trace-element-enriched pelagic (i.e. deep-sea) and terrigenous (i.e. continental) sediment, respectively, accompany the subducted and stored oceanic crust (Fig. 1). Geochemical models attempting to accurately quantify the compositions of these deeply-subducted materials (Hart and Staudigel, 1989; Weaver, 1991; Stracke et al., 2003) are greatly hindered by a lack of knowledge regarding: 1) hydrothermal alteration of the oceanic crust, 2) partition coefficients for both the dehydration of crust and sediments and the melting of sediments, 3) the thermal structure of mantle wedges, 4) the variable compositions of sediments in space and time, and 5) the lifespan of a subducted slab in the deep mantle. Although much progress has been made in each of these topics, the constraints are not strong enough to provide the needed resolution in parent/daughter ratios. Ironically, it may be exactly the lack of constraints that ultimately makes the Standard Model nonviable. By all indications from today's geodynamical systems, sediments and the subduction zone processing of crust and sediments all display such variability that a specific composition (which evolves to HIMU, EM1 or EM2) almost certainly would not be produced twice, and there would be no discrete or recognizable "endmember" reservoirs. On the other hand, and often the strongest criticism of the Standard Model (e.g. Hawkesworth et al., 1984; Barling and Goldstein, 1990; Morgan, 2000), is that there may be no such things as mantle endmembers. Each ocean island array could consist of its own unique isotopic composition, which represents a unique subducted slab from a unique recycling time.

In the present study, we specifically deal with the origin of the Enriched Mantle II (EM2) endmember. Lavas from the Samoan Islands have long been recognized as holding the most extreme signal of EM2 (Zindler and Hart, 1986; Wright and White, 1986; Farley et al., 1992, Hauri and Hart, 1993). Here we use a new comprehensive geochemical study to assess possible origins of the EM2 reservoir. This paper outlines why the recycling of sediment/slab cannot be the origin of EM2, and offers an alternative model which will

generally result in consistent trace element compositions, and hence isotopic signatures, through time. We assume that mantle endmembers do, in fact, exist, and that one process, acting to varying degrees at a variety of times, will produce a fairly homogeneous endmember reservoir, which is available for mixing with other mantle components during upwelling of mantle plumes.

The working model introduced here for the origin of EM2 involves metasomatism (i.e. fluid/melt infiltration) of oceanic lithosphere, followed by subduction zone recycling and long-term storage of this lithosphere. As a process for creating trace-element-enriched mantle, metasomatism is not a new idea and has been invoked both for continental lithosphere (Frey and Green, 1974; Brooks et al., 1976; Menzies and Murthy, 1980; Menzies, 1983) and oceanic lithosphere (Zindler et al., 1979; Kay, 1979; Hawkesworth et al., 1979, 1984; Richardson et al., 1982; Roden et al., 1984; Hart et al., 1986; Halliday et al., 1992; Class and Goldstein, 1997; Niu et al., 1996; 1999; Niu and O'Hara, 2003). The process we envision is much like the SYS model of Zindler et al. (1979), and the auto-metasomatic model of Roden et al. (1984). We envision it operating on newly formed lithosphere close to spreading centers, as illustrated by Niu et al. (1999) and Niu and O'Hara (2003).

We show that a lithosphere impregnated 2.5 Ga with a small-degree upper mantle melt can evolve to the present day isotopic composition of EM2. This model provides an EM reservoir with much greater volume than that of oceanic crust and sediment. A more voluminous "package" will have greater resistance to mixing within the convecting mantle and therefore have greater possibility of staying an isolated body for the required 2.5 Ga evolution time. Another benefit of this model is that the lithosphere will be isolated and protected from subduction zone processing (such as elemental fractionations that occur within the subducted oceanic crust and sediments during metamorphism and devolatilization).

2. Geologic setting

The Samoan islands and seamounts are centered on 14°S latitude and stretch from 169-173°W longitude (Fig. 2). They sit ~100 km north of the northern termination of the Tonga Trench, on ~110 Ma oceanic crust of the Pacific Plate which is moving 25.8° WNW at 7 cm/yr (Sella et al., 2002). The Samoan volcanoes separate into two topographic ridges, both sub-parallel to the direction of plate motion: the Savai'i – Upolu – Tutuila – Malumalu

group define the southwestern (and generally older) lineament, and the Muli – Ofu/Olosega – Ta'u – Vailulu'u group define the northeastern (and younger) lineament. We will designate these the "Malu" and "Vai" Trends, respectively. The recently mapped leading-edge seamount, Vailulu'u, rises from 5000 meter seafloor to a summit depth of 590m (Hart et al., 2000). Recent volcanic activity at Vailulu'u has been documented with the following observations: elevated water temperatures and particulate contents within the summit crater, a halo of intense particulate matter surrounding the summit in the depth range of 600-800 meters, high Mn concentrations and $^{3}He/^{4}He$ ratios (up to 9 R_A) in the crater water, swarms of seismicity, and dredged rock samples with U-series ages of 5-50 years (Hart et al., 2000). The age-progression heading west from this present-day hot spot location approximately follows the plate velocity of 7 cm/yr and includes the seamounts Lalla Rookh, Combe, and Alexa, which is 1750 km west of Vailulu'u (Duncan, 1985; Natland and Turner, 1985; McDougall, 1985; Hart et al., 2000; Hart et al., unpubl. data). Malulu seamount and Rose Atoll to the east of Vailulu'u do not have Samoan isotopic signatures (Hart et al., unpubl. data), and are most likely associated with the Cook-Austral lineament.

As if burning the candle at both ends, post-erosional volcanism has been extensive on the westernmost island of Savai'i (with the most recent eruptive episode taking place from 1905-1911) as well as being documented on the islands of Upolu and Tutuila (but here, all pre-historic, and much less extensive) (Kear and Wood, 1959; Keating, 1992). Although the pervasive post-erosional veneer on Savaii has disrupted the age-progression model (Savai'i should be ~5Ma based on the plate velocity model) and has lead to debates about the origin of the Samoan volcanoes (e.g. Natland, 1980), we believe there is little doubt about the chain originating from hot spot volcanism. The atypical volume of post-erosional volcanism on Savai'i is possibly due to the complicated tectonic setting of the volcanic chain. Since Savai'i is closest to the Tonga Trench, it is reasonable that bending stresses are facilitating additional melt extraction from the upper mantle (e.g. Hawkins and Natland, 1975; Natland, submitted 2003).

Tectonic reconstruction of the region (Brocher, 1985; Pelletier et al., 1998; Zellmer and Taylor, 2001) show that the transform-fault bounding the northern Tonga Trench evolved ~6-8 million years ago from the fossil Vitiaz Trench in response to opening of the Lau back-arc basin. Studies of the chemical characteristics of the northern Lau back-arc basin seamounts and seismic profiling beneath the basin collectively suggest leakage of Samoan plume material into the northern Lau Basin through a tear, or window, in the paleo-slab of the Pacific Plate subducted at the Vitiaz Trench. Geochemical evidence includes high

$^{3}He/^{4}He$ lavas of some Lau Basin seamounts (Poreda and Craig, 1992; Turner and Hawksworth, 1998), with trace element and isotopic compositions which are more characteristic of OIBs than MORBs or IABs (Ewart et al, 1998; Danyushevsky et al, 1995; Wendt et al., 1997). Seismic studies by Millen and Hamburger (1998) and Chen and Brudzinski (2001) illustrate a remnant slab of the Vitiaz subduction that has detached from the warped Pacific Plate, thereby providing an unobstructed path for melt/mantle migration from the Samoan plume into the Lau Basin. By speculation, this suggests that the Samoan plume beneath the Pacific Plate is much more widespread than the discrete lineament of volcanoes would indicate. Also, the exact location of the Samoan volcanoes may not necessarily be where the plume upwelling is "strongest", but instead where the plume fortuitously intersects a structural weakness imparted to the lithosphere by tectonic stresses of the local area. The en-echelon nature of the volcanic edifices may provide witness to this structural control (see Natland, submitted 2003, for a full discussion of this idea).

3. Samples and Analytical Details

3.1. Sample locations and descriptions

Rock samples utilized in this study have been collected from both land and sea. The seamounts Vailulu'u, Muli, and Malumalu, along with submarine portions of Ta'u, were dredged during the 1999 AVON2/3 cruise of the R/V Melville. Land-based sampling of Savai'i and Upolu, conducted in 2001, was aimed at expanding the coverage of "old shield" (namely, the Fagaloa Volcanic Series; Kear and Wood, 1959), and thereby establishing a greater temporal coverage of the Samoan plume. On Upolu, we sampled the southwestern exposure of the Fagaloa Volcanics; this is a topographic massif with well-developed river valleys, referred to as A'ana by the local inhabitants. Our Upolu samples primarily come from along or near the Matafa'a coastline and Fagalei Bay. Samples from Savai'i were collected from the north-central shore, where exposures of Fagaloa Volcanics were mapped over a 20 km^2 relative topographic high (Kear and Wood, 1959). This area is bound to the east by the village of Vaipouli, contains the Muliolo and Eatelele Streams, and is bound to the west by an escarpment that leads down to the village Paia.

Subaerial sampling of Ta'u, the youngest island of the chain, was conducted in 1999 and was principally concentrated along the coastline. The sampling was temporally diverse, in that all five of the volcanic series mapped by Stice and McCoy (1968) are represented.

Unlike the older and larger islands of Savai'i and Upolu, Ta'u Island manifests from only one main shield volcano; this simplified structure is reflected in the isotopic homogeneity observed for Ta'u, as will be discussed in following sections.

Phenocryst abundances in Samoan lavas range from 0% to 50% and include the following minerals in decreasing modal abundance: olivine, clinopyroxene, plagioclase, orthopyroxene, and Ti-augite. Phenocrysts are most common in samples from Vailulu'u and least common in samples from Savai'i and Upolu. In thin section, some samples show two populations of olivine in which a coarse-grained population (2-10 mm) shows resorption boundaries and a smaller-grained population (1-2 mm) shows almost no embayed crystal boundaries. However, for most samples, olivine major element compositions (Jackson et al., unpubl.) show that phenocrystic olivines are in Mg-Fe equilibrium with the coexisting liquids. Some samples (especially T14) have glomerocrysts of olivine (±spinel). Plagioclase, clinopyroxene, and oxides are the most common matrix minerals. Hand-samples can generally be classified as aphanitic basalt, olivine basalt, picrite or (rarely) ankaramite. Alteration, in the form of iron-oxide, is most prevalent in the Savai'i and Upolu samples. Sample 63-11 from Vailulu'u crater shows hydrothermally-precipitated quartz rinds along some cracks and grain boundaries.

3.2. Analytical techniques

Techniques reported here are for samples described above. Additional subaerial samples from Savai'i, Upolu, Tutuila and Ta'u have been collected by K.A. Farley and J.H. Natland over the last two decades and analyzed by K.A. Farley for Sr-Nd-Pb-He isotopic compositions. Additional subaerial samples from Savai'i and Upolu have been collected and analysed for major and trace elements and Sr-Nd-Pb isotopes by M. Regelous. We include these data in the present manuscript, as they are previously unpublished; any differences in analytical techniques are reported in the corresponding data tables.

Sr, Nd, and Pb isotopic analyses were carried out with conventional ion exchange procedures (references in Taras and Hart, 1987), using whole rock powders, prepared in an agate shatterbox, and leached for 1 hour in warm 6.2 N HCl. The TIMS techniques are described by Hauri and Hart (1993). Sr and Nd isotope data carry 2σ precisions of ±35 ppm and ±40 ppm, and are reported relative to 0.71024 (NBS 987) and 0.511847 (La Jolla), respectively. Some samples run for Sr and Nd by NEPTUNE multi-collector ICP/MS at W.H.O.I. are of comparable precision to TIMS anaylses. The precision of TIMS Pb data is taken to be 0.05% per mass unit after fractionation-correcting to the NBS

981 values given by Todt et al. (1996). Pb isotopic compositions of some samples were also determined on the P54 multi-collector ICP/MS in Lyon, with 2σ precisions of all ratios of ~200 ppm. Additionally, the Upolu and Savai'i sample suite was analyzed on the NEPTUNE multi-collector ICP/MS at W.H.O.I.; using a Tl internal standard, the 2σ external reproducibility for these samples was ±100 ppm or better for all ratios (see Hart et al., 2002). Helium isotopic compositions ($^3He/^4He$ R_A, relative to atmospheric standard) of olivine and/or fresh glass separates (~1-3 mm) were determined at W.H.O.I. by *in vacuo* crushing, using methods described in Kurz et al. (1996). Analytical errors average ±0.2 Ra at 2σ, for helium concentrations ranging from $\sim10^{-8}$ to 10^{-6} cc/gram. Os isotopic compositions on a select group of olivine-rich samples were determined by sparging of OsO_4 into W.H.O.I.'s Finnigan Element Magnetic Sector ICP-MS, following a flux fusion sample preparation (see Hassler et al., 2000 for a detailed Os analytical technique). Fusion blank corrections resulted in 0.06-1.22% corrections to the $^{187}Os/^{188}Os$ ratios. Major elements and some trace elements (Ni, Cr, Sc, V, Ga, Cu, Zn) in unleached whole rock powders were measured by XRF, and all other trace elements by ICP/MS at Washington State University (Hooper et al, 1993). Submarine glasses have been analyzed for major elements by electron microprobe at Massachusetts Institute of Technology.

3.3. Sample preservation/quality

Despite sampling of lavas from older shield and submarine settings, the quality of preservation is generally very good. The Th/U ratios of the sample suite fall entirely within 4.5 ± 1.5 (with the exception of sample S15 at Th/U = 6.7) and show a slight (although rough) positive correlation with Th concentrations. The Ba/Rb ratios have an average of 9.3 ± 1.8 at 1σ (near the canonical value of ~12 for fresh ocean island basalts; Hofmann & White, 1983) and are inversely correlated with Rb concentrations; significant exceptions to this correlation are samples 79-4, S15, and S25, with Ba/Rb ratios of 17.2, 14.0, and 3.7, respectively. We take these two proxies of alteration as indications that elements as or less mobile than Rb and U are very nearly pristine for most samples. However, elevated Rb/Cs ratios (176 ± 70 at 1σ) in the subaerial Upolu and Ta'u samples are most likely explained by chemical weathering and contrast strongly with the roughly canonical values (85-95; Hofmann & White, 1983) represented by the remaining suite (97 ± 30 at 1σ).

4. Age Relationships and Age-Progression

Vailulu'u seamount, the most easterly volcano in the Samoan chain, is currently active and belived to be the present day hotspot center (Hart et al., 2000). U-series data constrain two samples from Vailulu'u's summit region to be less than 50 years old; 7 other samples from six dredge locations show excess $^{230}Th/^{238}U$, evidence of ages less than a few hundred thousand years (Sims and Hart, to be submitted). The oldest K-Ar age from Tau Island is 0.3 Ma (McDougall, 1985). The youngest volcanic series on Tau (Faleasao) is probably younger than 37,000 years, based on ^{14}C ages of coral inclusions in these volcanics (Hart, unpublished). Additionally, there was an underwater eruption just west of Tau in 1866 (see description in Keating, 1992), evidence that Tau is still in an active shield-building stage. As yet, we have no age constraints on Muli seamount, though the samples dredged from there appear "older" than those dredged from Vailulu'u or Tau. Samples from three dredges on Malumalu show $^{230}Th/^{238}U$ excesses similar to those on Vailulu'u (Sims and Hart, to be submitted), suggesting that Malumalu is not significantly older than Vailulu'u. K-Ar ages for the Pago and Masefau shields on Tutuila range from 1.0-1.9 Ma (McDougall, 1985; Natland and Turner, 1985), somewhat younger than the 2.3-2.7 Ma expected from plate motion considerations.

New high-quality $^{40}Ar/^{39}Ar$ step-release plateau ages are given in Table 1 for the northern shield on Savai'i and the SW shield on Upolu, along with an earlier 40/39 total fusion age for the Vanu River shield on Savai'i. Previous K-Ar ages on the eastern Upolu shield range from 1.54-2.74 Ma (Natland and Turner, 1985); our western shield ages are 0.93 and 2.65 Ma. The older age agrees with the older ages of the eastern shield, though both shields appear younger than the expected plate model age range of 3.9-4.5 Ma. The 0.93 Ma sample (U10) was collected from well within the interior of the eroded SW shield massif, and appears to be reliable evidence for an extended (~2 Ma) period of shield building on Upolu.

There are no published radiometric ages from Savai'i. Based on a plate velocity of 7 cm/year, the age expected for shield initiation on Savai'i is about 5.2 Ma; the two ages reported in Table 1 for the northern (Manase) shield, 0.24 and 0.39 Ma, are far younger than this expected plate age. Kear and Wood (1959) mapped this northern area as shield largely on the basis of abundant surface streamflow. However, we found no obvious evidence of unconformable erosional morphology in this area, and the geochemical evidence discussed below strongly suggests that this map unit is akin to the post-erosional basalts on

Savai'i and Upolu, and unlike the Upolu shield basalts. The young $^{40}Ar/^{39}Ar$ ages are consistent with a re-assignment of this unit to post-erosional status. In the southern interior of Savai'i, Kear and Wood (1959) mapped a small exposure of shield in a gorge on the upper Vanu River. This area is virtually inaccessible, but a trachyte cobble was collected from the lower Vanu River by one of us (KAF) in 1991, and the 40/39 total fusion age of this trachyte is 2.05 Ma (Table 1). While still significantly younger than a plate-model age, this trachyte age is nevertheless very important as it shows that not all of the volcanism on this island can be related to proximity to the Tonga trench, as suggested by Natland (1980); at 2 Ma, the corner of the Tonga trench was almost 400 km west of Savai'i (Bevis et al., 1995). On the other hand, there can be little doubt that Savai'i has been massively re-surfaced with post-erosional volcanism as proposed by Natland (1980). The early history of this island will probably only be accessed by dredging on the deeper flanks, where slope failure provides an exposed record.

All in all, the radiometric ages of shield lavas in Samoa are broadly consistent with a simple age-progressive hotspot track, in that ages generally increase from east to west. However, it is clear that shield ages are overall younger than those predicted by plate motion, most likely because the oldest incipient shield lavas are not sampled at the surface of present day volcanoes. While the earliest stages of shield building on Tutuila, Upolu and Savai'i are thus far missing from the sampled record, it would be premature to use this as evidence against a simple hotspot model for Samoa.

5. Magma Generation and Crystal Fractionation

In major element composition, the Samoan basalts and trachybasalts analyzed for this study are clustered just above the alkali-tholeiite line (MacDonald and Katsura, 1964) at 44-49 wt% SiO_2 (Fig. 3; Tables 2 and 5). Samples that fall into the tholeiitic field are, for the most part, from Vailulu'u Seamount, and three of these are highly picritic. Post-erosional lavas (on Savai'i, Upolu and Tutuila) overlap with the shield volcanics, but extend to much greater silica-undersaturation (basanites and nephelinites down to 36 wt% SiO_2; Hawkins and Natland, 1975; Johnson, 1983; Hauri and Hart, 1997). Mg#'s (molar percent $Mg/Mg+Fe^{2+}$) range from 40 in the differentiated Muli samples to 85 in the Vailulu'u picrites. The low MgO/high SiO_2 end of the suite is (vaguely) dominated by samples from Vailulu'u, Malumalu, and Upolu; on the other hand, high MgO/low SiO_2 samples are mainly from Savai'i, Tutuila, and Ta'u. Also plotted on some co-variation plots of Figure 3

are trajectories of near-solidus primary melt compositions at varying pressures of melting in the garnet stability field, using algorithms defined by Herzberg and Zhang (1996) through experiments on KLB-1 peridotite. Recent experiments on another fertile peridotite (KR4003 starting material; Walter, 1998) show primary melt compositions with a general shift to higher MgO at a given pressure (by ~5% in the 4-5 kbar pressure range). Most of the Samoan lavas have undergone some amount of crystal fractionation, as indicated by the fact that they have significantly lower Mg#'s than any estimated primary mantle melts.

The relationship between Mg#'s and CaO shown in Figure 4 provides information regarding both magma generation and crystal fractionation. Plotted along with lava compositions is the trajectory of primary mantle melt compositions (Herzberg and Zhang; 1996). To assess the extent of differentiation and the minerals involved, we have used the pMELTS program (Ghiorso et al., 2002) to model anhydrous fractional crystallization (at a best-fit pressure of 3-4 kbar) of some of the more primitive lavas (Ta'u samples T14 and T48, Vailulu'u sample 63-3, and Malumalu sample 78-1). PMELTS trajectories calculated with 1 wt% H_2O, at a given pressure, are nearly identical to anhydrous runs at 1kbar lower pressure (not shown). All starting compositions have olivine as the second liquidus phase (after spinel), leading to a negative slope for the liquid path on Mg# against CaO (Fig. 4). The kink to positive slopes on the liquid lines of descent marks the crystallization of cpx±olivine±plagioclase. As CaO content of the starting magma decreases, clinopyroxene (cpx) saturation occurs at lower Mg#'s. A suite of submarine Samoan glasses (Table 3) has also been plotted on Figure 4 and shows that true liquids follow the lines of crystal fractionation predicted by pMELTS.

Suites of lavas from each volcano cluster along fairly distinct Mg#-CaO fractionation trends. By projecting the olivine fractionation trends for the different volcanoes back to the primary mantle melt trajectory, we can interpret that the Samoan lavas were generated in the pressure range of 2.5-6 GPa; the order of increasing pressure of melting would be Vailulu'u < Ta'u/Malumalu < Tutuila/Upolu/Savai'i. The extrapolated primary magmas in this model have an extensive range in MgO, from 11 wt% at lowest pressure to 22 wt% at 6 GPa. To get integrated pressures of melting as high as 6 GPa, melting would have to initiate at depths exceeding 180 km and terminate at depths much deeper than the thickness of the lithosphere (~100 km). Given estimates for potential temperatures of plumes (~1550°C; Watson and McKenzie, 1991) and water-undersaturated solidi (Hirth and Kohlstedt, 1996), the depth of *initial* melting is close to 180 km and therefore cannot be the *integrated* depth of melting. The above approach is strictly valid only if the lavas from each

volcano are derived from a constant source composition. We conclude that this CaO index for pressure of melting is rather rickety, given the isotopic variations between volcanoes that will be discussed further into the paper, and that the order of "increasing pressure of melting" is clouded by the extent to which melts were generated from a depleted (low CaO) material.

The Vailulu'u samples are not only high in CaO (also Ca/(Ca+Na) and CaO/Al_2O_3) at a given MgO value, but they are also low in Na_2O, TiO_2, and FeO. This suggests they have the most promise in being interpreted as the shallowest, highest degree partial melts in the whole sample suite (Kinzler and Grove, 1992; Herzberg and Zhang, 1996; Walter, 1998). Melting beneath the other volcanoes may be initiated deeper in the mantle, possibly due to (1) differences in source composition (required by isotopic variations), (2) higher potential temperatures and mantle flow rates, or (3) mantle flow paths which affect melt-solid segregation. The Vailulu'u suite is fit fairly well by a crystal fractionation trend at a pressure of 3 kbar, and indicates cpx fractionation has likely occurred for most samples.

For Ta'u and Malumalu, olivine fractionation clearly dominates the spread in lava compositions. A few samples with Mg#'s greater than ~73 have obviously accumulated olivine (they are phenocryst-rich), but most samples lie along olivine fractionation lines or at the intersection of the olivine control line and cpx saturation (Fig. 4). Three Ta'u samples have compositions close to those of the Muli samples and have surely undergone cpx fractionation; these samples also have the lowest concentrations of the cpx-compatible elements vanadium and scandium in the whole suite (not shown). If parental magmas for all the Ta'u and Muli samples were of nearly the same composition, liquid lines of descent indicate that these low Mg# lavas have undergone about 15% more olivine fractionation than samples T14 and T48, along with 25% cpx fractionation.

6. Isotopes and Trace Elements

6.1 The Global Context

Plotted on the three-dimensional axes of Figure 5 is the mantle tetrahedron of Hart et al. (1992), with data from the ocean island chains which quintessentially define the coordinates for each of the mantle components, EM1, EM2, and HIMU. Data arrays for individual island chains, as well as groups of taxonomically similar island chains, quasi-linearly extend from one of the three OIB endmember components toward FOZO, the common mantle;

very notable is the serious lack of elongation of arrays along tie-lines between the three OIB components. It is clear that EM2 lavas in general, and Samoan lavas in particular, dominate the range in oceanic $^{87}Sr/^{86}Sr$ values, but are much less variable in $^{143}Nd/^{144}Nd$ than EM1. The variation in $^{206}Pb/^{204}Pb$ found in EM2 basalts is small relative to the composite oceanic suite.

Strontium, neodymium, lead, helium, and osmium isotope ratios for Samoan basalts are given in Tables 4 through 6. Isotope plots (Figs. 6-9) show this new data along with data reported in previous studies (Wright and White, 1986; Farley et al., 1992; Hauri and Hart, 1993). The wide range in $^{87}Sr/^{86}Sr$ values, 0.7044 – 0.7089, is correlated with the more narrow range of 0.51293 – 0.51251 for $^{143}Nd/^{144}Nd$ (Fig. 6). Each island or seamount tends to show a unique field of isotopic compositions that, as will be shown, evolve systematically through space and time. Malumalu Seamount contributes the furthest afield EM2 signature and now defines the most radiogenic $^{87}Sr/^{86}Sr$ value (0.7089) of all oceanic lavas. At lower $^{87}Sr/^{86}Sr$ (0.7044), near estimates for Bulk Silicate Earth (BSE), the Samoan array is split into two prongs – the "serpent's tongue". Both prongs, one comprised of lavas from Ta'u Island and the other, at higher $^{143}Nd/^{144}Nd$, comprised of lavas from Upolu and Tutuila, are significantly elevated (at ε_{Nd} of +3 and +5, respectively) over the BSE value of 0.512638 (Hamilton et al., 1983). The other notable EM2 hotspot, the Societies, overlaps the lower prong of the "serpents tongue", and is generally shifted to less-enriched Sr and Nd values. The classic EM1 array (Pitcairn) lies well below the Samoa array.

The sample group on the high $^{143}Nd/^{144}Nd$ prong is also the lowest in $^{206}Pb/^{204}Pb$ and $^{207}Pb/^{204}Pb$ of all the shield lavas (Fig. 7). All Samoan lavas lie to the right (high $^{206}Pb/^{204}Pb$ side) of the terrestrial Pb Geochron and are in the mid-range of the elongate, worldwide OIB cluster; they are situated entirely above the Northern Hemisphere Reference Line (NHRL; Hart, 1984) in both $^{207}Pb/^{204}Pb$ and $^{208}Pb/^{204}Pb$ (Figs. 7 and 8). The most radiogenic $^{206}Pb/^{204}Pb$ compositions (19.4) are found not in the highest $^{87}Sr/^{86}Sr$ samples, but in samples from Vailulu'u Seamount (of moderate $^{87}Sr/^{86}Sr \sim 0.7055$). On the other hand, the highest $^{207}Pb/^{204}Pb$ (15.65) and $^{208}Pb/^{204}Pb$ (39.8) correspond to the EM2-defining Malumalu lavas, implying that EM2 is an old reservoir of high time-integrated Th/U.

The Society array (not shown in Fig. 7) is much steeper, falling below the NHRL at low $^{206}Pb/^{204}Pb$ and crossing above it, to overlap the Malu trend data from Samoa. Interestingly, the highest $^{87}Sr/^{86}Sr$ sample from Tahaa (Societies) lies very close to our extreme $^{87}Sr/^{86}Sr$

sample in $^{207}Pb/^{204}Pb$ - $^{206}Pb/^{204}Pb$, but is far lower than it in $^{208}Pb/^{204}Pb$. Note in Figure 8 that the Society array lies close to the NHRL, and is totally distinct from the Samoa field.

The $^{3}He/^{4}He$ ratios of Samoan lavas range from 8 R_A at high $^{87}Sr/^{86}Sr$ to a maximum of 26 R_A at generally lower $^{87}Sr/^{86}Sr$ (Fig. 9). New data support the existence a primitive helium mantle (i.e. PHEM of Farley et al., 1992) but with depleted Sr and Nd isotopic compositions (i.e. FOZO of Hart et al., 1992). With increasing $^{87}Sr/^{86}Sr$, values of $^{3}He/^{4}He$ asymptotically approach ~8 R_A, showing that the helium isotopic composition of EM2 is approximately equivalent to that of MORB and much higher than the atmospheric values of recycled crustal materials (see discussion by Farley et al., 1992). This low $^{3}He/^{4}He$ value of EM2 is either inherent to the EM2 source, or is a product of diffusive equilibrium with the upper mantle over long timescales (see section 9).

The trace element character of the Samoan lavas display typical OIB features (Hofmann, 1988; Weaver, 1991), with trace element enrichments up to 100 times primitive upper mantle (PUM), the highest normalized concentrations at the highly incompatible elements, and negative anomalies at Cs, K and Pb (Fig. 10). The largest inter-volcano differences are at Pb, Rb, Ba, and Th. Weaver (1991) employed the trace element ratios Rb/Nb, Ba/Nb, Ba/Th, and Ba/La to distinguish between the EM1 and EM2 species. He used these trace elements to argue for a recycled sedimentary component as the cause for the EM signature, and ascribed the difference between EM1 and EM2 to a pelagic versus terrigenous sedimentary provenance. Therefore, a comparison between the Samoan lavas (extreme EM2) and those from Pitcairn (extreme EM1) should theoretically show the greatest differences in these ratios. However, recent studies on Pitcairn lavas (Dostal et al., 1998; Eisele et al., 2002) show nearly complete overlap with the Samoan lavas for Weaver's classification ratios, unlike the clear distinction between EM1 and EM2 previously reported for lavas with less extreme endmember signatures (Fig. 11). This result makes the trace element differences between EM1 and EM2 very difficult to resolve and discourages the description of EM1 and EM2 as having "pelagic" and "terrigenous" components, respectively. Furthermore, the Plank and Langmuir (1998) study of the compositions of sediment being subducted at today's convergent margins shows that pelagic and terrigenous sediments are: (1) not notably different in trace element ratios such as Ba/Th, and (2) not typically occurring alone in subducted sedimentary sections, but are instead components of the whole, mixed sedimentary package. Hence, generating mantle endmembers by recycling of only pelagic or only terrigenous sediment seems physically unlikely.

6.2 Shield vs. Post Erosional

As initially observed by Wright and White (1986), post-erosional (PE) lavas are isotopically distinct from all shield lavas. There is a commonality among the PE lavas from all along the chain (Savai'i, Upolu and Tutuila), in contrast to the observation that each island displays a unique isotopic birthmark in its shield lavas. The PE lavas show restricted $^{87}Sr/^{86}Sr$ values that plot mid-range in the Samoan field, have the lowest $^{206}Pb/^{204}Pb$ values and some of the lowest $^{208}Pb/^{204}Pb$ values of the whole sample suite (Figs. 6 and 8). The PE field on the $^{206}Pb/^{204}Pb$ versus $^{207}Pb/^{204}Pb$ plot (Fig. 7) is unusual, as it is elongate in an almost inverse direction to the shield trend (Wright and White, 1986).

Overall, the new Savaiian lavas are all of the same chemical nature as the post-erosionals, even though many are samples of the oldest-mapped flow series on the island (Fagaloa Series; Kear and Wood, 1959). These Savai'i lavas, as well as most other PE lavas, are clearly distinguishable from shield lavas by having the highest Nb/U and Ba/(La,Sm,Nb,Th) ratios of the whole sample suite (Fig. 12). Given the earlier discussion of the young radiometric ages for this "shield" series, we believe this sequence is in fact post-erosional, and not shield. The alternative explanation, that all of Savai'i is young and not part of an age-progressive Samoan hotspot track, is belied by the 2.05 my age for a trachyte cobble from the Vanu River valley (see above). Either way, we cannot rule out the possibility that PE lavas and shield lavas are geochemically the same on Savai'i, but nowhere else in Samoa.

What accounts for the distinct trace element and isotopic differences between shield and PE lavas? The commonality among Samoan PE lavas possibly derives from a similar history of being brewed and aged in the crust and lithosphere, unlike shield lavas that may have a shorter residence time in this shallow environment. Local Tongan sediments (from DSDP Site 595/596, about 1000 km southeast of Samoa) have Pb isotopic compositions (Plank and Langmuir, 1998) with the general characteristics of PE lavas (Figs. 7 and 8). Pb isotopic compositions of marine sediments are highly variable over short distances and other sediments could likely be found nearer to Samoa that provide closer fits to the Samoa post-erosional Pb field (which lies near the lower end of the general marine sediment array; Abouchami and Goldstein, 1995; O'Nions et al., 1998; Plank and Langmuir, 1998; Jones et al., 2000). In support of a sediment component in the PE lavas are values for $\delta^{18}O$ of olivine (5.5-5.7‰; Eiler et al., 1997) which are elevated over upper mantle values and can be interpreted to reflect the heavy values documented for marine sediments (also see discussion

below). In other words, we cannot rule out the late-stage incorporation of modern marine sediments in PE lavas based solely on isotopic compositions. Trace element ratios may provide a stronger constraint on the presence or absence of a modern sediment component; one would expect the PE lavas to inherit the high Pb/Ce, high REE/HFSE, low Sm/Yb, and Ba-enriched ratios characteristic of both local and globally averaged marine sediments (see Fig. 17; Plank and Langmuir, 1998). This is not the case for the PEs, which have, of all suspected traits, only notably high Ba (Figs. 11 and 12).

6.3 Mixing Arrays

The spread of isotopic compositions in the Samoan lavas can be attributed to either (1) processes that generate an infinite number of chemical (i.e. parent/daughter) heterogeneities within the mantle that, upon long-term storage, evolve into an infinite number of isotopic heterogeneities or (2) processes that produce a small number of unique chemical compositions that, upon long-term storage, result in a limited number of "end-member" isotopic compositions available for mixing. In order for the first option to produce sub-linear arrays in 2-D and 3-D isotope space, there must be a single process which acts systematically to varying degrees or at various times. Hence, talk of or modeling of the most extreme values (i.e. endmember mantle components) is the same in either case.

The lavas from Malumalu undeniably establish the existence of a reservoir with high $^{87}Sr/^{86}Sr$ (at least 0.7089), low $^{143}Nd/^{144}Nd$ (at most 0.5125), and $^{206}Pb/^{204}Pb$, $^{207}Pb/^{204}Pb$, and $^{208}Pb/^{204}Pb$ values near 19.3, 15.65 and 39.9, respectively. An unaltered sediment reservoir can be immediately ruled out as the cause of the EM2 component in Samoan shield lavas: although Global Subducting Sediment (GLOSS; Plank and Langmuir, 1998) and local Tongan sediment (Site 595/596; Plank and Langmuir, 1998) each have convincing $^{87}Sr/^{86}Sr$ and $^{207}Pb/^{204}Pb$ compositions (Figs. 6 and 7), they are severely inadequate (low) in $^{206}Pb/^{204}Pb$ and $^{208}Pb/^{204}Pb$ to generate the isotopic signatures displayed by the shield lavas (Fig. 8). Therefore, for recycled sediment to have evolved to the EM2 coordinate in Sr-Nd-Pb isotope space, subduction zone alteration of ancient sedimentary packages needed to be very specific: U/Pb and Th/Pb must increase, while Rb/Sr and Sm/Nd remain very much the same. In the dehydration of subducted oceanic crust, this is shown to be the case for all systems except Rb/Sr: Rb is about 5 times more mobile than Sr (Ayers, 1998), so the final dehydrated product has significantly lowered Rb/Sr ratios. Experiments on the dehydration and melting of sediments (Johnson and Plank, 1999) give rather inconclusive results for relative trace element partitioning of these parent/daughter ratios, and suggest that

partitioning can be extremely variable depending on the minerals present and the degree of dehydration.

Although the Samoan lavas are isotopically extreme, the "pure" EM2 signature may be even more extreme. For example, clinopyroxene and glass separates from peridotite xenoliths from Savai'i studied by Hauri et al. (1993) yield $^{87}Sr/^{86}Sr$ values up to 0.7128 and have been interpreted to represent metasomatism of oceanic lithosphere by a small degree carbonatitic melt (not diluted by mixing with depleted mantle) from the same source as that which provides melts for Samoan volcanism. However, the Pb isotopes in these rare xenoliths ($^{206}Pb/^{204}Pb$ ~18.86; $^{208}Pb/^{204}Pb$ ~39.76) lie well outside the isotopic array set by the Samoan lavas (Fig. 8); this suggests an origin for the enriched component in these xenoliths from a smaller, unique reservoir, unrelated to extant Samoan lavas.

Clearly, though, EM2-rich samples are more rare than samples of a less-enriched nature. On a plot of $^{206}Pb/^{204}Pb$ against $^{87}Sr/^{86}Sr$ (Fig. 13), the Samoan samples can be enclosed in a triangle where the high $^{87}Sr/^{86}Sr$ apex is defined by EM2. At lower $^{87}Sr/^{86}Sr$, there are two components, one with higher $^{206}Pb/^{204}Pb$ than EM2 and one with lower $^{206}Pb/^{204}Pb$, but both assuredly depleted according to their high $^{143}Nd/^{144}Nd$ values (Fig. 6). The low $^{206}Pb/^{204}Pb$, low $^{87}Sr/^{86}Sr$ apex (note the Upolu data cluster) has a signature tending toward DMM, but the strict use of the most depleted MORB/DMM isotopic values is not necessarily the only option for describing this component. The sub-Samoan upper mantle has been punctured by multiple mantle plumes in its 110 Myr lifespan, so may no longer be strictly, or homogeneously, pure DMM (see the South Pacific Isotopic and Thermal Anomaly; Staudigel et al., 1991). Also, we do not absolutely require the low $^{206}Pb/^{204}Pb$ depleted component to reside in the upper mantle (i.e. it could be part of the plume), although it's most easily visualized as being there given current notions of mantle dynamics. Regardless of these disclaimers, the use of anything but a generic DMM isotopic composition is arbitrary, and ultimately only compromises the generality of our observations and conclusions.

The high $^{206}Pb/^{204}Pb$, low $^{87}Sr/^{86}Sr$ component (obvious in the Ta'u and Vailulu'u lavas; Fig. 13) is suggestive of mixing with a HIMU mantle component. This component may also be present in the Samoan plume, but there is reason to believe HIMU material has under-plated the Samoan lithosphere in the past. Calculated hotspot tracks show that 20-25 million years ago, the Cook-Austral plume was located beneath the lithosphere on which the Samoan Islands presently sit (Norton, 2000). The Cook-Austral chain shows great variation in isotopic compositions (Fig. 14), not all of which would fit the Samoan data in multi-

isotope space. However, there is one volcano, Raivavae, which has the isotopic compositions appropriate to be a significant component in the Vai Trend lavas (Fig. 14; data from GEOROC database); we are not suggesting that Raivavae itself is contributing to the Samoan lavas, but that isotopically similar material may be underplating the Samoan island chain.

A fourth mixing component must be acknowledged when considering $^{3}He/^{4}He$ values. Figure 9 shows the inverse relationship between $^{87}Sr/^{86}Sr$ and $^{3}He/^{4}He$. The EM2 component can be classified as having a $^{3}He/^{4}He$ signal which asymptotically approaches the average DMM value of ~8 R_A (Kurz et al, 1982) at high $^{87}Sr/^{86}Sr$. HIMU has also been shown to have low $^{3}He/^{4}He$ values (Graham et al., 1993; Hanyu and Kaneoka, 1997; Hilton et al., 2000) and likely explains why Vailulu'u (with the largest HIMU component) is in parallel with Malumalu on Figure 9. Therefore, all three endmember components discussed above have low $^{3}He/^{4}He$, thus requiring an additional reservoir to account for high $^{3}He/^{4}He$. High $^{3}He/^{4}He$ values are found in the center of the Samoan Sr-Pb data array, at Ta'u and Tutuila, and generally decrease towards the outer fringes (Fig. 13). Farley et al. (1992) named this component the primitive helium mantle (PHEM) but new data suggest this reservoir has depleted $^{87}Sr/^{86}Sr$ and $^{143}Nd/^{144}Nd$ (like FOZO of Hart et al., 1992), and not bulk-earth-like values assigned to PHEM.

All four mantle components are in the Samoan plume from a magmatic standpoint. But what material is coming from the deep mantle is another story. We can make a good case for the depleted component coming from entrainment of the widely documented depleted upper mantle and the radiogenic Pb component (HIMU-ish) coming from entrainment of under-plated lithosphere from the HIMU Cook-Austral chain. This means the deep mantle material within the Samoan plume is dominantly EM2 and PHEM/FOZO. The sequence of mixing these components is difficult to ascertain, as the length scale of compositional heterogeneity and differences in solidus temperatures (i.e. solid vs. melt mixing) are unknown.

6.4 Spatial/Temporal Evolution

Samoan shield samples on the $^{206}Pb/^{204}Pb$ - $^{208}Pb/^{204}Pb$ plot form two *en echelon* trends of positive slope (Fig. 8) which are most distinctly separated at high $^{206}Pb/^{204}Pb$, and converge at lower $^{206}Pb/^{204}Pb$. The isotopic trends correspond to the two topographic ridges of the Samoan islands (Fig. 2); for a given $^{206}Pb/^{204}Pb$, the southern Malu Trend has higher $^{208}Pb/^{204}Pb$ than the northern Vai Trend. Within each of the two trends, isotopic enrichment

increases with decreasing age along the volcanic ridge. This relationship, shown clearly in a plot of distance versus $^{206}Pb/^{204}Pb$ (Fig. 15), has remarkable correlation and is striking in its implication of a systematic evolution of plume material or mantle processes. Figure 15 also shows how the Malu and Vai Trends form a continuum though time: even though each ridge independently displays isotopic enrichment with distance/time, the younger Vai Trend is generally higher in $^{206}Pb/^{204}Pb$ than the older Malu Trend (note that Malumalu may overlap in age with Ta'u and Vailulu'u). Of the four mixing components, low $^{206}Pb/^{204}Pb$ values are found only in the DMM reservoir (~18.0; Fig. 14). Therefore, the increase in $^{206}Pb/^{204}Pb$ with younging of volcanoes is interpreted to be a waning of the DMM component in the Samoan lavas, with a resulting increase in the abundance of EM2 and HIMU components. The separation of the Vai and Malu Trends in Pb-isotopic space indicates a higher HIMU/EM2 ratio in the Vai Trend.

Moving east along each of the two Trends, there are systematic increases in K/Na, Rb/Sr, La/Sm, La/Yb, Ba/Sm, Th/Nb, Th/Zr, Nb/Y, Nd/Sm, Nb/Zr, and U/Nb (Fig. 16); in other words, incompatible-element-enrichment increases with Pb isotopic enrichment, distance, and decreasing age. Due to correlations between isotopes and trace elements like those seen in Figure 16, variations in trace element ratios are easily attributed to differences in composition between the low $^{206}Pb/^{204}Pb$ source and the high $^{206}Pb/^{204}Pb$ sources. However, we are witness not to the source compositions, but to the products of "source processing". Because the process of melt generation has maintained (or not overly obscured) trace element correlations with isotopic compositions, we can infer some characteristics of the sub-Samoan mantle.

Possible explanations for the systematic chemical evolution of the Samoan plume include:

1. Horizontal zonation of plume material, implying a length-scale of heterogeneity on the order of volcano spacing, as has been suggested for the Hawaiian Islands (see below). In this case, trace element variations are truly source variations.

2. A lithologically-homogeneous mantle in which peridotite components of variable composition occur in the same proportions beneath all Samoa, but exist on a length-scale large enough to allow preservation of disequilibrium between the components. In this case, variable potential temperature of the plume would result in preferential sampling of components based on their respective solidus temperatures. Enriched materials would be sampled at small degrees of melting and trace element enrichment is partly a function of degree of melting.

3. A vertically-stratified plume, changing composition and/or physical properties as upwelling proceeds, and affecting the degree of entrainment of ambient upper mantle and lithospheric assimilation.

In the Hawaiian Islands (an EM1 plume), isotopically distinct, topographic *en echelons*, named the "Kea" and "Loa" Trends, have also been documented (Tatsumoto, 1978; Staudigel et al., 1984; Abouchami et al., 2000). The Society Islands (another EM2 archipelago) display similar sub-parallel trends in both geographic and Pb isotopic space (using data compiled in the GEOROC database). However, nothing so temporally systematic as that in Samoa has been previously reported. Chemical zonation of a mantle plume (e.g. Kurz et al., 1995; Hauri et al., 1996; Lassiter et al., 1996; DePaolo et al., 2001) may explain isotopic lineaments within island chains, but fails to address how this chemical heterogeneity may translate into topographic features. On the other hand, creation of topographic lineation as a consequence of either 1) the lithosphere's structural response to loading (e.g. Hieronymus and Bercovici, 1999; Hieronymus and Bercovici, 2000) or 2) magma rising in "plumlets" instead of a continuous stream (Ihinger, 1995) ignores the fact of correlative chemical variations. Even so, some common dynamic feature clearly exists, independent of mantle taxonomy, for the way in which plumes forge through the mantle/crust, melt, and arrive at Earth's surface.

7. Calculation of a "Pure" EM2 Lava

The following calculation is aimed at defogging the trace element pattern for lavas of the enriched endmember, through "un-mixing" (subtracting) Ta'u lavas (average $^{87}Sr/^{86}Sr$ = 0.7046) from the most EM2-rich Malumalu lavas, under the assumption that the highest $^{87}Sr/^{86}Sr$ lavas are, instead of pure EM2 melts, still somewhat contaminated by melts from a depleted/less enriched mantle. As a group, Ta'u lavas are closest to the PHEM mixing component (Figs. 13 and 14). By this calculation, trace element differences between un-enriched and enriched mantles are accentuated, and help to clarify the trace element characteristics of the EM2 source.

We extrapolate to the end-member trace element pattern of an EM2 melt in effect by subtracting the averaged trace element composition of Ta'u lavas from the Malumalu lavas until the $^{87}Sr/^{86}Sr$ composition equals 0.7128; this value derives from an analysis of cpx contained in a metasomatized peridotite xenolith from Savai'i (Hauri et al., 1993). Although

these xenoliths are not an extension of the Samoan Pb isotope array (Figs. 7 and 8), for lack of a better stopping point, they do place an upper limit on oceanic mantle Sr isotopic ratios.

Mixing between Ta'u and a "pure" EM2 component to make the most enriched Samoan samples (Malumalu samples 78-1 and 78-3) is calculated with the following two equations:

$$(^{87}Sr/^{86}Sr)_{78-1} = \frac{F[Sr]_{EM2}(^{87}Sr/^{86}Sr)_{EM2} + (1-F)[Sr]_{Tau}(^{87}Sr/^{86}Sr)_{Tau}}{F[Sr]_{EM2} + (1-F)[Sr]_{Tau}} \quad (1)$$

$$[Sr]_{78-1} = F[Sr]_{EM2} + (1-F)[Sr]_{Tau} \quad (2)$$

The concentration of Sr ([Sr]) in EM2 and the fraction of the EM2 melt, F, are solved simultaneously so that the right hand of equation (1) equals the $^{87}Sr/^{86}Sr$ composition of the two extreme Malumalu lavas (0.70889). With the value for F, concentrations of all trace elements can be calculated for the EM2 melt by using the structure of equation (2) and are reported in Table 7. Lava compositions used in this calculation have been corrected for crystal fractionation by incremental addition of olivine (or subtraction in the case of 78-1, 78-3 and 74-1) until the melt compositions reaches a Mg# of 73 (olivine addition ranges from 10-51%; olivine subtractions are 10%, 7% and 23%, respectively). Note from Figure 4 that Ta'u and Malumalu have very similar crystal fractionation trajectories with minimal cpx loss. All Ta'u samples have been utilized except for T21 which is plagioclase-rich and T44 which is an ankaramite.

The resulting fraction of EM2 "melt" in the Malumalu "mixture" is 51%, and the resulting $^{143}Nd/^{144}Nd$ ratio for the EM2 component equals 0.51235. Figure 17 shows the trace element pattern for the calculated "pure" EM2 melt component; note enrichments at Rb and Th that are almost 120 times PUM, negative anomalies at Cs and Ba, and an almost non-existent Pb anomaly. The REE slope of the calculated EM2 melt is steeper than both Malumalu and Vailulu'u, and the overall trace element pattern from U to the right is remarkably smoother than either the Malumalu or Vailulu'u pattern, save for dips at Sr and Ti. In general, the degree of enrichment in the EM2 melt is greatest for the highly incompatible elements.

The calculated trace element pattern of the "pure" EM2 melt is compared to: 1) an estimate of global subducting sediment (GLOSS; Plank and Langmuir, 1998) and 2) a local

sediment from DSDP Hole 595/596 analyzed for the GLOSS compilation (Fig. 17). Clearly, the sediment trace element patterns are very different from the calculated EM2 component. In particular, the sediment spidergrams are marked by large negative anomalies of the high-field-strength elements (HFSE; Nb, Ta, Zr, and Hf), and large positive Pb and Ba anomalies, whereas the calculated Samoan enriched component has no such features; in fact, the Ba anomaly becomes more *negative* in the EM2 melt. Also, the heavy rare-earth-element slope of the EM2 melt is significantly steeper than the sediment patterns: Sm/Yb for the sediments is 2.1 whereas for the EM2 melt is 7.2. The only argument in favor of sediment addition is the significantly decreased Pb anomaly in the EM2 melt. However, we (1) do not believe this alone lends credence to the sediment theory, and (2) show in our non-sediment model below how Pb in the EM2 source does not have a negative anomaly.

Ultimately, the calculated EM2 spidergram is inconsistent with standard models invoking ancient sediment recycling to explain the enrichment of the EM2 mantle source. As discussed below, it is unlikely that any chemical processing during subduction would so effectively "smooth out" the typically jagged spidergram of oceanic sediment. Alternatively, if the enriched plume material is argued to derive from addition of *present-day* sediments, the trace element patterns of local sediments should be directly reflected in the EM2 melt and they are not. Therefore, late-stage contamination of plume material with local sediment is also an unsatisfactory explanation for the observed chemical characteristics of the enriched Samoan basalts (and this point is strongly supported by the Pb isotope evidence shown in Figs. 7 & 8). Production of the EM component by deep mantle fractionations involving high-pressure phases such as Ca or Mg perovskite likewise will lead to jagged, not smooth, spidergrams (Hirose et al., 2004). Segregation of carbonatitic melts from mantle assemblages has been used to explain elevated trace element concentrations in oceanic lavas (see Zindler and Hart, 1986), but this process also causes irregular trace element patterns (e.g. Klemme et al., 1995; Sweeney et al., 1995; Hoernle et al., 2002). Instead, the remarkably smooth EM2 melt spidergram gives the uncanny impression of having originated from nothing but "unadulterated" melting processes within the upper mantle.

8. Sediment Recycling?

Osmium and oxygen isotopes are thought to be "smoking guns" for sediment/slab recycling (Eiler et al., 1997; Shirey and Walker, 1998; van Keken et al., 2002). Due to the

incompatibility of Re (Righter and Hauri, 1998) and compatibility of Os (Hart and Ravizza, 1996) in mantle melting, elevated Re/Os ratios in crustal materials should evolve to radiogenic osmium during long-term storage within the mantle. Altered upper MORB crust and marine sediments are enriched in heavy oxygen ($\delta^{18}O$ of ~15-25‰; Savin and Epstein, 1970; Lawrence et al., 1979; Staudigel et al., 1995; Alt, 2003) by low-temperature fractionation processes at the Earth's surface. This is high above the $\delta^{18}O$ value of 5.2‰ for upper mantle olivine (Ito et al, 1987; Mattey et al., 1994; Eiler et al., 1997). Therefore, the standard theory for the origin of EM2 involving recycling of mafic crust plus terrigenous sediment would suppose Samoan lavas to have both elevated $\delta^{18}O$ and $^{187}Os/^{188}Os$ compositions.

Eiler et al. (1997) demonstrated that EM2 basalts from Samoa (Savai'i post-erosional) and the Societies do have the highest $\delta^{18}O$ of all OIB's ($\delta^{18}O$ of olivine up to 6.1‰), explainable by the incorporation of ~5% terrigenous sediment addition to DMM. Using values chosen by Eiler et al. (1997) for the concentrations of Sr, Nd, and Pb in DMM and sediments, the sediment contribution to the trace element budget in the EM2 source will be 50%, 68% and 96%, respectively, for these elements. Clearly then, the trace element pattern of EM2 lavas should reflect the trace element patterns of sediment, but they do not (see Fig. 17). Eiler et al. (1997) also mention the possibility that metasomatism can elevate $\delta^{18}O$ values in magmas, and the present work recommends this idea be further explored.

Osmium isotopic compositions are likewise not so "smoking" of a sediment component. Combining data presented here (Table 4) with those from Hauri and Hart (1993), Samoan basalt samples with >80 ppt Os (ranging in $^{87}Sr/^{86}Sr$ from 0.7046 to 0.7089) reveal $^{187}Os/^{188}Os$ ratios of 0.124 - 0.130 which do not correlate with any other isotope system. Samples with <80 ppt Os (5 out of 21 in total) have elevated $^{187}Os/^{188}Os$ ratios and are interpreted to be contaminated with seawater (see Shirey and Walker, 1998). The small range in $^{187}Os/^{188}Os$ compositions of pristine samples spans values estimated for the primitive upper mantle (0.129; Meisel et al., 1996) and DMM (~0.125; Standish et al., 2002), and is much lower than the upper limit of 0.16 displayed in HIMU and EM1 lavas (Hauri and Hart, 1993; Reisberg et al., 1993; Eisele et al., 2002).

The unradiogenic $^{187}Os/^{188}Os$ values for these Samoan lavas represent either (1) a similarly unradiogenic mantle source, or (2) re-equilibration of more radiogenic Os components with unradiogenic upper/lower mantle through special processes that are not active beneath HIMU or EM1 hotspots. With regard to the former option, and to test the standard model, low Os concentrations in sediments may prevent a sediment component

from significantly elevating $^{187}Os/^{188}Os$ ratios in the EM2 source. In a simple case, if DMM with $^{187}Os/^{188}Os = 0.125$ and [Os] = 3000 ppt is mixed with sediment having $^{187}Os/^{188}Os$ = 1.0 and [Os] = 30 ppt (Peucker-Ehrenbrink and Jahn, 2001), then 35% of sediment is needed to change $^{187}Os/^{188}Os$ from 0.125 to 0.130. Here we are again left with an EM2 source whose trace element budget would be dominated by sediment, but do not observe such trace element patterns in the EM2 lavas nor see the implied correlations with other isotope systems. The second option, suggesting the Os budget derives from re-equilibration, can be ruled out since olivine phenocrysts are in approximate equilibrium with coexisting liquids (Jackson et al., unpubl.) and have high $^{3}He/^{4}He$ ratios (i.e. are not xenocrystic, but rather truly phenocrystic). We conclude that the mantle sources for Samoan lavas all have inherently unradiogenic $^{187}Os/^{188}Os$ values and are not influenced by a sediment/crustal component.

Although slab/sediment recycling has been a common theory for the origin of EM2 for over two decades (see Introduction), there are major flaws in this train of thought. The Standard Model for generating the EM2 reservoir involves the introduction into the deep mantle of 1) oceanic crust which has been depleted of fluid-mobile elements, such as the large-ion-lithophile elements (LILE; e.g. Cs, Rb, K and Pb), by dehydration and 2) a relatively pristine (i.e. elementally unfractionated) continental crust component (i.e. terrigenous sediments). Although not typically considered in the Standard Model, it seems logical that trace elements of subducted sediments (pelagic and/or terrigenous) must be fractionated by the same process by which the subducted ocean crust is fractionated (dehydration) – especially since sediments are closer to the mantle wedge and likely to have greater water contents than the altered ocean crust. Whereas there have been experimental studies showing high trace element mobility during dehydration of subducted ocean crust (especially for the isotopically important elements Rb and Pb; see Ayers [1998] and Stracke et al. [2003] for overviews), very little similar work has been done on dehydration of subducted sediments (i.e. Johnson and Plank, 1999). Actually, there is growing geochemical evidence that not only a fluid component, but also partial melts of subducted sediments contribute to arc magmas. The high recycling efficiencies (up to 40%) of elements which are not particularly fluid mobile, such as Be, Th and Nd (see discussion by Johnson and Plank, 1999), suggest sediment melting is a reality, even though many thermal models predict subsolidus temperatures within the subducted sediment column (e.g. Peacock, 1996). Regardless of the mechanism of trace element fractionations in subducted sediments, it is clear that fractionations will occur and will result in significant loss of incompatible

elements, and a decrease in the mass of a possible future EM2 reservoir. Ultimately, it is grossly inconsistent to use modern, surface sediment as an approximation of the trace element and isotopic composition of a "sediment" component in the mantle – once subducted, the sediment will never look the same, especially for parent/daughter ratios like Rb/Sr and Th/Pb.

Additionally, since today's surface, terrigeneous sediments represent what has been *extracted* by convergent margin volcanism and/or continental crust formation, it is the residue, or complement, to surface sediments which should be our concern for what material is actually recycled deep into the mantle. For example, depletion of the fluid immobile elements Na and Ta in arc volcanics (Pearce and Peate, 1995), and hence sediments (Plank and Langmuir, 1998), will be matched by Nb-Ta enrichments in the material that is ultimately introduced to the deep mantle. Experiments on partitioning between dehydration fluids and eclogite mineral assemblages (garnet, clinopyroxene and rutile) suggest that depletion of high field-strength elements (including Nb-Ta) in arc volcanics is due to their high compatibility in residual rutile (Stalder et al., 1998) and is therefore not a sediment signature. Enrichment of HFSE in the subducted slab will offset HFSE depletions in the subducted sediment. This is why *decreasing* Nb anomalies with increasing $^{87}Sr/^{86}Sr$ ratios, as documented for EM1 and EM2 lavas by Eisele et al. (2002), are not supporting evidence for sediment recycling.

We believe there is an alternative explanation for correlation between Nb anomalies and isotopic compositions. Figure 18 shows Nb/Nb* (calculated as $Nb_N/\sqrt{(Th_N \times La_N)}$,; Eisele et al., 2002) plotted with $^{208}Pb/^{204}Pb$ and La/Sm ratios of lavas from Samoa and Pitcairn. We have used $^{208}Pb/^{204}Pb$ as a measure of EM2 abundance instead of $^{87}Sr/^{86}Sr$ only because it provides better correlations. Samoan lavas show inverse relationships between Nb/Nb* and $^{208}Pb/^{204}Pb$ as well as La/Sm. Pitcairn lavas (from Eisele et al., 2003) show a negative correlation between Nb/Nb* and La/Sm, which overlaps with the Samoan lavas, and a more shallow slope than Samoa for Nb/Nb* against $^{208}Pb/^{204}Pb$ (the greatest isotopic variation in the Pitcairn lavas is in $^{143}Nd/^{144}Nd$). Pitcairn and Samoa samples have almost an identical range in both La/Sm and Nb/Nb*, even though the isotopic variability is greater in Samoa. Also plotted in Figure 18 is a trajectory for variable degree of melting of a depleted mantle, showing that small changes in F can produce large changes in both La/Sm and Nb/Nb*. Therefore, variable Nb/Nb* (previously interpreted as only a source effect) can be produced by recent variations in melt production, and is most likely what causes (1) scatter in the plots of Figure 18 and (2) the same Nb/Nb* variation in Pitcairn as Samoa given less isotopic

variation. The correlation of $^{208}Pb/^{204}Pb$ (and $^{87}Sr/^{86}Sr$) with Nb/Nb* can be interpreted as an ancient enrichment of mantle by a small degree (low Nb/Nb*) melt, as suggested by the calculated EM2 melt and modeled below.

9. Metasomatic Origin of EM2

Given the many failures of the "sediment recycling" model for EM2, as enumerated above, we propose here a new model that invokes metasomatic enrichment of ancient oceanic lithosphere, followed by long-term storage in the deep mantle and recent return to the surface as the Samoa plume. Conceptually, this model derives from the autometasomatic process proposed by Zindler et al. (1979) and Roden et al. (1984). Numerous authors have appealed to metasomatism of oceanic plates to generate chemical heterogeneities that can be tapped prior to plate subduction (Hawkesworth et al., 1979, 1984; Halliday et al., 1992; Class and Goldstein, 1997; Niu et al., 1996). Recycling of such metasomatized lithosphere, after long-term storage in the mantle, has been advocated by Richardson et al. (1982) and Niu and O'Hara (2003) as a source for enriched OIB.

If we start with the assumption that EM2 is a two-stage differentiate of bulk-earth, the slope on the $^{206}Pb/^{204}Pb$ - $^{207}Pb/^{204}Pb$ plot (Fig. 7) yields an age of 2.5 Ga. This is an age older than the commonly quoted average mantle differentiation age of 1.8 Byr (Hart, 1984). At that time, the composition of the mantle would have been more similar to primitive upper mantle than to the depleted mantle observed today (i.e. DMM). Assuming plate tectonics was operating 2.5 billion years ago in much the same way as it is today, this more primitive mantle material would have undergone depletion by melt extraction during upwelling under spreading ridges, then "turned the corner" and solidified to become depleted lithospheric mantle.

In the following calculations, we model the case in which small degree, deep melts not extracted at the ridge crest percolate up through the asthenosphere and impregnate the overlying lithosphere that had just undergone melt extraction on the ridge crest. This is essentially a metasomatic process. This metasomatized lithosphere then is recycled and stored in the mantle to become today's EM2 reservoir (Fig. 19). The melt fraction, amount of melt impregnation, and ratio of garnet to spinel peridotite melting are calculated so as to match parent/daughter ratios of EM2 for the Rb-Sr, Sm-Nd, U-Pb, Th-Pb and Lu-Hf systems, based on evolution from bulk earth 2.5 billion years ago. Bulk partition coefficients used for melting a primitive mantle source (McDonough and Sun, 1995) are

based on a compilation of D's from Kelemen et al. (2003) for melting of garnet and spinel peridotite, with the few exceptions listed in Figure 20. Bulk partition coefficients are weighted 72% garnet peridotite to 28% spinel peridotite. The best match to parent/daughter ratios is with a 1.1% impregnation of a depleted lithosphere by a 0.5% batch melt of a primitive mantle. The lithosphere represents a mantle depleted by 2% melt extraction, as calculated using the method of Workman and Hart (2003) and as reported in Table 8. Figure 20 shows the resulting trace element pattern of the EM2 source (also see Table 8). Rb/Sr has been fit to within <1%, Sm/Nd and Lu/Hf have been fit to within 3%, and Th/U has been fit to within 4%. The "unfortunate fits" are for U/Pb and Th/Pb, which are 53% and 58% too high respectively in the calculated EM2 source. This is clearly more a Pb problem than anything else. If the compatibility of Pb is lower by about a factor of two, as suggested by experimental partitioning data (Hauri et al., 1994; Salters et al., 2002), the U/Pb and Th/Pb ratios may be more precisely modeled. Because the mass fraction of melt added to the FOZO lithosphere (1.1%) is twice the degree of melting (0.5%) required to generate that impregnating melt, the mass of the mantle which melts must be twice as large as the mass of the metasomatized lithosphere.

Does this source lead to the observed $^{3}He/^{4}He$ values of 8 R_A for EM2? Given the general trace element enrichment in the impregnating melt, and making the standard assumption of extreme incompatibility of He, it is likely that the calculated EM2 source would have high He/U ratios and hence evolve to $^{3}He/^{4}He$ values higher than 8 R_A. There are two possible solutions. One concerns the relative compatibility of He and U; if at high pressure and low degree of melting He is more compatible than U (this has not been proven nor disproven), then the impregnating melt will have low He/U and potentially evolve to DMM-like $^{3}He/^{4}He$ values (by coincidence). The second option is that the EM2 "package" has had a residence time in the upper mantle long enough (~1-2 Ga) to result in diffusive equilibrium of He (see model by Moreira and Kurz, 2001, for example); this option has obvious implications for the primary home of recycled lithosphere.

Although the above model leaves several questions unanswered, such as the scale-length of the heterogeneities created by the metasomatism, and the resulting lithologies (mafic veins or enriched peridotite), it is successful in producing the observed isotopic and trace element characteristics of the Samoan mantle source. It does not require *ad hoc* chemical manipulations in the subduction zone, as does the standard crust/sediment-recycling model. In fact, as the enrichment zone is limited to the lower parts of the lithosphere, it will be nearly invulnerable to subduction zone processing. It calls on a process for which there is

abundant evidence, particularly in the sub-continental lithosphere (Frey and Green, 1974; Menzies and Murthy, 1980; Menzies, 1983; Menzies and Hawkesworth, 1987). And insofar as small-degree melts are ubiquitous in the upper oceanic asthenosphere, the process is virtually guaranteed. We note also that the small-scale convection usually invoked for this part of the mantle (i.e. Richter rolls) provides an efficient means of upward advection of standing melt fractions, as well as the consequent decompression that will augment the melt fractions and facilitate melt/solid segregation.

10. Conclusions

A large suite of recently collected basalts from the Samoa hotspot chain have been analyzed for Sr, Nd, Pb, Os and He isotopes, and major and trace elements. Localities include the sub-aerial islands of Savai'i, Upolu and Ta'u, and the submarine seamounts Muli, Malumalu and Vailulu'u.

1. Samoan basalts are isotopically (Sr-Nd-Pb) the most extreme EM2 lavas in the oceanic database ($^{87}Sr/^{86}Sr$ up to 0.7089). The Samoan isotopic arrays can be explained by mixing among four mantle components: DMM, EM2, HIMU and PHEM/FOZO. The deep plume material is most likely composed of EM2 and PHEM/FOZO, whereas the HIMU and DMM components are entrained into the plume in the upper mantle.

2. Systematic temporal and spatial variations in lava chemistry occur while going from west (older) to east (younger) along the chain: e.g., $^{206}Pb/^{204}Pb$, La/Sm, Rb/Sr, Th/Zr. This indicates a waning of the DMM component and waxing of the EM2 and HIMU components in Samoan volcanoes over the last few million years.

3. The standard recycling model (ocean crust plus terrigenous sediment) fails as an explanation for producing Samoan EM2, as witnessed by the smooth spidergrams for EM2 lavas with negative Ba anomalies, low $^{187}Os/^{188}Os$ ratios, high $^{3}He/^{4}He$ (>8Ra) and mismatched Pb isotopic compositions.

4. The EM2 mantle source can be successfully modeled with the ancient (2.5 Ga) formation of metasomatised oceanic lithosphere, followed by storage in the deep mantle and return to the surface in the Samoan plume.

Appendix 2-1

Samples analyzed by M. Regelous were crushed in a steel jaw crusher to 3-5 mm sized chips, washed in deionised water, dried and handpicked in order to avoid chips which were visibly altered, or which contained vesicles. A portion of these chips was set aside for isotope analysis, the rest was powdered in an agate swing mill. Major element analyses were carried out by X-ray fluoresence at the Universität Mainz, Germany, using a Phillips PW 1404 instrument. Trace element concentrations were determined by ICPMS using a Fisons Plasmaquad II instrument at the University of Queensland, Australia. Full details of the procedure are given in Niu and Batiza (1997). The external precision on the concentrations of most of the trace elements measured is < 3%. The long-term average values for the BHVO-1 rock standard are reported in Table 5. Pb isotope measurements were carried out at the Max Planck Institut für Chemie, Mainz, following the procedure outlined by Abouchami et al. (2000). Between 50 and 100 mg of rock chips were washed in deionised water in an ultrasonic bath, then ultrasonicated in 6M HCl for 15 minutes, before being leached in hot 6M HCl for 1 hour. The HCl leachate was pipetted off, and the residue was rinsed, soaked in deionised water for 15 minutes, rinsed again and dried. This leaching procedure appears to remove much of the non-magmatic Pb that is contained in less-resistant components (surface contamination or alteration products), as discussed by Abouchami et al. (2000) and Eisele et al. (2003). The leached residues were dissolved in HF-HNO3, treated repeatedly with HNO_3 and HCl until completely in solution, and Pb separated on anion exchange resin using HBr-HNO_3 mixtures (Abouchami et al., 2000). All reagents used were double-distilled, and total precedural blanks for the Pb chemistry were below 50pg. The eluent from the Pb columns was twice evaporated to dryness with 15M HNO_3, and redissolved in 3M HNO_3. Sr and Nd were separated from this fraction at the University of Bristol, U.K., using methods adapted from Pin et al. (1994). The sample in 3M HNO_3 was loaded onto columns containing 0.15ml of TRU spec resin, positioned so as to drip directly into a second column containing 0.1ml of Sr spec resin. After rinsing with 3M HNO_3, the columns were separated, and Sr was eluted from the Sr spec column in H_2O. The light- and middle-rare earth elements were recovered from the TRU spec resin by rinsing with 2.5M HCl. Nd was separated from this fraction using conventional HDEHP columns and 0.3M HCl. Pb isotope analyses were carried out using a triple spike technique to correct for instrumental mass fractionation. About 5% of the purified Pb fraction was transferred to a second beaker and spiked with a ^{204}Pb-^{206}Pb-^{207}Pb triple spike. The spiked and unspiked fractions were loaded onto separate Re filaments with silica gel-H_3PO_4. Isotope compositions were measured using a Finnigan MAT-261 multicollector mass spectrometer (M.P.I. Mainz) in static mode, and the data for spiked and unspiked fractions were combined off-line to obtain the fractionation-corrected Pb isotope composition of the sample (Galer, 1999). During this study, the NBS981 Pb standard gave $^{206}Pb/^{204}Pb$, $^{207}Pb/^{204}Pb$ and $^{208}Pb/^{204}Pb$ ratios of 16.9403±0.0022, 15.4974±0.0020 and 36.7246±0.0058 respectively (2s, n=19). Sr and Nd isotope measurements were carried out on a Finnigan Triton multicollector mass spectrometer (University of Bristol) in static

mode, and within-run exponential fractionation corrections applied using $^{86}Sr/^{88}Sr=0.1194$ and $^{146}Nd/^{144}Nd=0.7219$. The NBS987 Sr and J&M Nd standards gave $^{87}Sr/^{86}Sr$ and $^{143}Nd/^{144}Nd$ ratios of 0.710247 ± 0.000008 (2 sigma, n=15) and 0.511113 ± 0.000004 (n=12) respectively, during the period of the sample measurements.

References

Abouchami, W. and S. L. Goldstein, A lead isotopic study of Circum-Antarctic manganese nodules, *Geochim. Cosmochim. Acta,* 59. 1809-1820, 1995.

Abouchami, W., Galer, S.J.G., and Hofmann, A.W., High precision lead isotope systematics of lavas from the Hawaiian Scientific Drilling Project, *Chemical Geology, 169*, 187-209, 2000.

Alt, J. C., Stable isotopic composition of the upper oceanic crust formed at a fast spreading ridge, ODP Site 801, *Geochemistry, Geophysics, Geosystems, 4(5)*, 10.1029/2002GC000400, 2003.

Armstrong, R. L., A model for the evolution of strontium and lead isotopes in a dynamic Earth, *Reviews of Geophysics 6,* 175-199, 1968.

Ayers, J., Trace element modeling of aqueous fluid - peridotite interaction in the mantle wedge of subduction zones, *Contributions to Mineralogy and Petrology 132*, 390-404, 1998.

Barling, J., and Goldstein, S.L., Extreme isotopic variations in Heard Island lavas and the nature of mantle reservoirs, *Nature, 348*(6296), 59-62, 1990.

Bevis, F. W. Taylor, B. E. Schutz, J. Recy, B. L. Isacks, S. Helu, R. Singh, E. Kendrick, J. Stowell, B. Taylor and S. Calmant, Geodetic observations of very rapid convergence and back-arc extension at the Tonga arc, *Nature, 374,* 249-251, 1995.

Brocher, T. M. and R. Holmes, Tectonic and Geochemical Framework of the Northern Melanesian Borderland: An Overview of the KK820316 Leg 2 Objectives and Results. In *Investigations of the Northern Melanesian Borderland, Circum-Pacific Council for Energy and Mineral Resources Earth Science Series 3*, edited by T. M. Brocher, Vol. 3, pp. 1-12, 1985.

Brooks, C., James, D.E., and Hart, S.R., Ancient lithosphere: its role in young continental volcanism, *Science, 193*, 1086-1094, 1976.

Chase, C. G., Ocean island Pb: two-stage histories and mantle evolution, *Earth Planet. Sci. Lett., 52*, 277-284, 1981.

Chen, W., and Brudzinski, M. R., Evidence for a Large-Scale Remnant of Subducted Lithosphere Beneath Fiji, *Science, 292*, 2475-2479, 2001.

Class, C., and S.L. Goldstein, Plume-lithosphere interactions in the ocean basins: constraints from the source mineralogy, *Earth Planet. Sci. Lett., 150*, 245-260, 1997.

Cohen, R. S., and O'Nions, R.K., Identification of recycled continental material in the mantle from Sr, Nd and Pb isotope investigations, *Earth Planet. Sci. Lett., 61*, 73-84, 1982.

Danyushevsky, L. V., Sobolev, A.V., and Falloon, T.J., Northern Tongan high-Ca boninite petrogenesis: the role of Samoan plume and subduction zone-transform fault transition, *Journal of Geodynamics, 20*(3), 219-241, 1995.

DePaolo, D. J., and Manga, M., Deep Origins of Hotspots - the Mantle Plume Model, *Science, 300*, 920-921, 2003.

Dostal, J., B. L. Cousins and C. Dupuy, The incompatible element characteristics of an ancient subducted sedimentary component in ocean island basalts from French Polynesia, *J. Petrol. 39*, 937-952, 1998.

Duncan, R. A., Radiometric ages from volcanic rocks along the New Hebrides-Samoa lineament, in *Geological investigations of the Northern Melanesian Borderland, Circum-Pacific Council for Energy and Mineral Resources Earth Science Series 3*, edited by T.M. Brocher, pp. 67-76, 1985.

Eiler, J. M., Farley, K.A., Valley, J.W., Hauri, E.H., Craig, H., Hart, S.R., and Stolper, E.M., Oxygen isotope variations in ocean island basalt phenocrysts, *Geochim. Cosmochim. Acta, 61*(11), 2281-2293, 1997.

Eisele, J., W. Abouchami, S. J. G. Galer, and A. W. Hofmann, The 320kyr Pb isotope evolution of Mauna Kea lavas recorded in the HSDP-2 drill core, *Geochemistry, Geophysics, Geosystems,* 4(5), doi:10.1029/2002GC000339, 2003.

Eisele, J., Sharma, M., Galer, S.J.G., Blichert-Toft, J., Devey, C.W., and Hofmann, A.W., The role of sediment recycling in EM-1 inferred from Os, Pb, Hf, Nd, Sr isotope and trace element systematics of the Pitcairn hotspot, *Earth Planet. Sci. Lett., 196*, 197-212, 2002.

Ewart, A., Collerson, K.D., Regelous, M., Wendt, J.I., and Niu, Y., Geochemical Evolution within the Tonga-Kermedec-Lau Arc-Back-arc Systems: the Role of Varying Mantle Wedge Composition in Space and Time, *J. Petrol., 39*(3), 331-368, 1998.

Farley, K. A., Natland, J.H., and Craig, H., Binary mixing of enriched and undegassed (primitive?) mantle components (He, Sr, Nd, Pb) in Samoan lavas, *Earth Planet. Sci. Lett., 111*, 183-199, 1992.

Frey, F. A., and Green, D.H, The mineralogy, geochemistry, and origin of lherzolite inclusions in Victorian basanites, *Geochim. Cosmochim. Acta, 38*, 1023-1059, 1974.

Galer, S. J. G., Optimal double and triple spiking for high precision lead isotopic

measurement, *Chem. Geol., 157*, 255-274, 1999.

Ghiorso, M. S., Hirschmann, M.M., Reiners, P.W., and Kress, V.C. III, The pMELTS: A revision of MELTS for improved calculation of phase relations and major element partitioning related to partial melting of the mantle to 3 GPa, *Geochemistry, Geophysics, Geosystems, 3*(5), 10.1029/2001GC000217, 2002.

Graham, D. W., S. E. Humphris, W. J. Jenkins, M. D. Kurz, Helium isotope geochemistry of some volcanic rocks from Saint Helena, *Earth Planet. Sci. Lett., 110*, 121-131, 1993.

Halliday, A. N., G. R. Davies, D-C. Lee, S. Tommasini, C. R. Paslick, J. G. Fitton, D. E. James, Lead Isotope Evidence for Young Trace Element Enrichment in the Oceanic Upper Mantle, *Nature 359*, 623-627, 1992.

Hamilton, P.J., R.K. O'Nions, D. Bridgewater, and A. Nutman, Sm-Nd studies of Archean metasediments and metavolcanics from West Greenland and their implications for the Earth's early history, *Earth Planet. Sci. Lett., 38*, 26-43, 1983.

Hanyu, T. and Kanoeka, I, The uniform and low $^{3}He/^{4}He$ ratios of HIMU basalts as evidence for their origin as recycled materials, *Nature, 390*, 2730376, 1997.

Hart, S. R., A large-scale isotope anomaly in the Southern Hemisphere mantle, *Nature, 309*(5971), 753-757, 1984.

Hart, S. R., Heterogeneous mantle domains: signatures, genesis and mixing chronologies, *Earth Planet. Sci. Lett., 90*, 273-296, 1988.

Hart, S. R., and H. Staudigel, Isotopic characterization and identification of recycled components, 15-28. In *Crust/Mantle Recycling at Convergence Zones*, edited by S. R. Hart and L. Gulen, NATO ASI Series, Vol. 258, Series C, Kluwer Academic Publishers, Dordrecht, The Netherlands, 1989.

Hart, S. R., and Ravizza, G.E., Os Partitioning Between Phases in Lherzolite and Basalt, in *Earth Processes: Reading the Isotopic Code*, edited by R. Basu and S.R. Hart, Geophysical Monograph Series 95, AGU, Washington, D.C., 1996.

Hart, S. R., Gerlach, D.C., and White, W.M., A possible new Sr-Nd-Pb mantle array and consequences for mantle mixing, *Geochim. Cosmochim. Acta, 50*, 1551-1557, 1986.

Hart, S. R., Hauri, E.H., Oschmann, L.A., and Whitehead, J.A., Mantle Plumes and Entrainment: Isotopic Evidence, *Science, 256*, 517-520, 1992.

Hart, S. R., Staudigel, H., Koppers, A.A.P., Blusztajn, J., Baker, E.T., Workman, R., Jackson, M., Hauri, E., Kurz, M., Sims, K., Fornari, D., Saal, A., and Lyons, S., Vailulu'u undersea volcano: The New Samoa, *Geochemistry, Geophysics, Geosystems, 1*, 2000GC000108, 2000.

Hart, S.R., R. K. Workman, M. Coetzee, J. Blusztajn, L. Ball and K. T. M. Johnson, The Pb Isotope Pedigree of Western Samoan Volcanics: New Insights From High-Precision Analysis by NEPTUNE ICP/MS, *EOS, 83*, F20, 2002.

Hassler, D. R., B. Peucker-Ehrenbrink and G. E. Ravizza, Rapid determination of Os isotopic composition by sparging OsO_4 into a magnetic-sector ICP-MS, *Chem. Geol., 166,* 1-14, 2000.

Hauri, E. H., and Hart, S.R., Re-Os isotope systematics of HIMU and EMII oceanic island basalts from the south Pacific Ocean, *Earth Planet. Sci. Lett., 114*, 353-371, 1993.

Hauri, E. H., and Hart, S.R., Rhenium abundances and systematics in oceanic basalts, *Chemical Geology, 139*, 185-205, 1997.

Hauri, E. H., Shimizu, N., Dieu, J.J., and Hart, S.R, Evidence for hotspot-related carbonatite metasomatism in the oceanic upper mantle, *Nature, 365*, 221-227, 1993.

Hauri, E. H., Wagner, T.P., and Grove, T.L., Experimental and natural partitioning of Th, U, Pb and other trace element between garnet, clinopyroxene and basaltic melts, *Chemical Geology, 117*, 149-166, 1994.

Hauri, E. H., Lassiter, J.C., and DePaolo, D.J., Osmium isotope systematics of drilled lavas from Mauna Loa, Hawaii, *J. Geophys. Res., 101*, 11793-11806, 1996.

Hawkesworth, C. J., Norry, M.J., Roddick, J.C., and Vollmer, R., $^{143}Nd/^{144}Nd$ and $^{87}Sr/^{86}Sr$ ratios from the Azores and their significance in LIL-element enriched mantle, *Nature, 280*, 28, 1979.

Hawkesworth, C. J., Rogers, N.W., van Calsteren, P.C.W., Menzies, M.A., Mantle enrichment processes, *Nature, 311*, 331-335, 1984.

Hawkins, J. W., and Natland, J.H., Nephelinites and Basanites of the Samoan linear volcanic chain: their possible tectonic significance, *Earth Planet. Sci. Lett., 24*, 427-439, 1975.

Herzberg, C., and Zhang, J., Melting experiments on anhydrous peridotite KLB-1: Compositions of magmas in the upper mantle and transition zone, *J. Geophys. Res., 101*, 8271-8295, 1996.

Hieronymus, C. F., and Bercovici, D., Discrete alternating hotspot islands formed by interaction of magma transport and lithospheric flexure, *Nature, 397*, 604-607, 1999.

Hieronymus, C. F., and Bercovici, D., Non-hotspot formation of volcanic chains: control of tectonic and flexural stresses on magma transport, *Earth Planet. Sci. Lett., 181*, 539-554, 2000.

Hilton, D.R., C.G. Macpherson, and T.R. Elliott, Helium isotope ratios in mafic phenocrysts

and geothermal fluids from La Palma, the Canary Islands (Spain): Implications for HIMU mantle sources, *Geochim. Cosmochim. Acta, 64*, 2119-2132, 2000.

Hirose, K., Shimizu, N., van Westrenen, W., and Fei, Y., Trace element partitioning in Earth's lower mantle, *Physics of the Earth and Planetary Interiors*, in press, 2004.

Hirth, G., and Kohlstedt, D.L., Water in the oceanic upper mantle: implications for rheology, melt extraction and the evolution of the lithosphere, *Earth Planet. Sci. Lett., 144*, 93-108, 1996.

Hoernle, Kaj, G. Tilton, M. J. LeBas, S. Duggen and D. Garbe-Schönberg, Geochemistry of oceanic carbonatites compared with continental carbonatites: mantle recycling of oceanic crustal carbonate, Contrib. Mineral Petrol., 142, 520-542, 2002.

Hofmann, A. W., Chemical differentiation of the Earth: the relationship between mantle, continental crust and oceanic crust, *Earth Planet. Sci. Lett., 90*, 297-314, 1988.

Hofmann, A. W., Mantle geochemistry: the message from oceanic volcanism, Nature 385, 219-229, 1997.

Hofmann, A. E., and White, W.M., Mantle plumes from ancient oceanic crust, *Earth Planet. Sci. Lett., 57*, 421-436, 1982.

Hofmann, A. W., and White, W.M., Ba, Rb and Cs in the Earth's Mantle, Z. *Naturforsch, 38*(a), 256-266, 1983.

Hooper, P. R., Johnson, D.M., and Conrey, R.M., *Major and trace element analyses of rocks and minerals by automated x-ray spectrometry*, Washington State University, Geology Dept., 1993.

Ihinger, P.D., Mantle flow beneath the Pacific Plate: evidence from seamount segments in the Hawaiian-Emperor Chain, *Amer. J. Science, 295*, 1035-1057, 1995.

Ito, E., White, W.M., and Gopel, C., The O, Sr, Nd, and Pb isotope geochemistry of MORB, *Chemical Geology, 62*, 157-176, 1987.

Johnson, K. T. M., *The petrology and tectonic evolution of seamounts and banks of the Northern Melanesian Borderland*, southwest Pacific. Thesis, University of Hawaii, 1983.

Johnson, M. C., and Plank, T., Dehydration and Melting Experiments Constrain the Fate of Subducted Sediments, *Geochemistry, Geophysics, Geosystems,* 1, 1999GC000014, 1999.

Jones, C. E., A. N. Halliday, D. K. Rea, R. M. Owen, Eolian inputs of lead in the North Pacific, *Geochim. Cosmochim. Acta, 64,* 1405-1416, 2000.

Kay, R.W., Zone refining at the base of lithospheric plates: A model for a steady-state

asthenosphere, In *Processes at Mid-Ocean Ridges*, ed. J. Francheteau, Tectonophysics, 55, 1-6, 1979.

Kear, D. and B. L. Wood, The geology and hydrology of Western Samoa: *New Zealand Geological Survey Bulletin, 63*, 1-90, 1959.

Keating, B. H., The geology of the Samoan Islands. In *Geology and offshore mineral resources of the Central Pacific basin*, edited by B. H. Keating and B. R. Bolton, Circum-pacific Council for Energy and Mineral Resources Earth Science Series, 14, 127-178, 1992.

Kelemen, P.B., G.M. Yogodzinski and D.W. Scholl, Along-strike variation in the Aleutian island arc: Genesis of high Mg# andesite and implications for continental crust, in *Inside the Subduction Factory, Geophysical Monograph 139*, John Eiler, editor, American Geophysical Union, Washington DC, 223-276, 2003.

Kinzler, R. J., and Grove, T.L., Primary Magmas of Mid-Ocean Ridge Basalts 1. Experiments and Methods, *J. Geophys. Res., 97*, 6885-6906, 1992.

Klemme, S., S. R. van der Laan, S. F. Foley and D. Günther, Experimentally determined trace and minor element partitioning between clinopyroxene and carbonatite melt under upper mantle conditions, *Earth, Planet. Sci. Letts.*, 133, 439-448, 1995.

Koppers, A. A. P., Morgan, J.P., Morgan, J.W., and Staudigel, H., Testing the fixed hotspot hypothesis using $^{40}Ar/^{39}Ar$ age progressions along seamount trails, *Earth Planet. Sci. Lett., 185*, 237-252, 2001.

Kurz, M. D., T.C. Kenna, J.C. Lassiter, D.J. Depaolo, Helium isotopic evolution of Mauna Kea: First results from the 1-km drill core, *J. Geophys. Res.,* 101 (B5), 11,781-11-791, 1996.

Kurz, M. D., Jenkins, W.J., Shilling, J.G., and Hart, S.R., Helium isotopic variations in the mantle beneath the central North Atlantic Ocean, *Earth Planet. Sci. Lett., 58*, 1-14, 1982.

Kurz, M. D., Kenna, T.C., Kammer, D.P., Rhodes, J.M., and Garcia, M.O., Isotopic evolution of Mauna Loa volcano: A view from the submarine southwest rift, in *Mauna Loa Revealed: Structure, Composition, History and Hazards*, edited by J.M. Rhodes, and Lockwood, J.P., Geophysical Monograph Series 92, pp. 289-306, AGU, Washington, 1995.

Lassiter, J. C., DePaolo, D.J., and Tatsumoto, M., Isotopic evidence of Mauna Kea volcano: Results from the initial phase of the Hawaiian Scientific Drilling Project, *J. Geophys. Res., 101*, 11769-11780, 1996.

Lawrence, J. R., Drever, J., Anderson, T.F., and Brueckner, H.K., Importance of alteration of

volcanic material in the sediments of Deep Sea Drilling Site 323, $^{18}O/^{16}O$ and $^{87}Sr/^{86}Sr$, *Geochim. Cosmochim. Acta, 43*, 537-588, 1979.

MacDonald, G. A. and T. Katsura, Chemical composition of the Hawaiian lavas, *J. Petrol., 5*, 83-133, 1964.

Moreira, M., and M.D. Kurz, Subducted oceanic lithosphere and the origin of the 'high μ' basalt helium isotopic signature, *Earth Planet. Sci. Lett., 189,* 49-57, 2001.

Mattey, D., Lowry, D., and Macpherson, C., Oxygen isotope composition of mantle peridotite, *Earth Planet. Sci. Lett., 128*, 231-241, 1994.

McDonough, W. F. and S.-s. Sun, The composition of the Earth, *Chemical Geology, 120*, 223-253, 1995.

McDougall, I., Age and Evolution of the Volcanoes of Tutuila, American Samoa, *Pacific Science, 39*, 311-320, 1985.

Meisel, T., R. J. Walker and J. W. Morgan, The osmium isotopic composition of the Earth's primitive upper mantle, *Nature, 383*, 517-520, 1996.

Menzies, M., Mantle ultramafic xenoliths in alkaline magmas: evidence for mantle heterogeneity modified by magmatic activity, in *Continental Basalts and Mantle Xenoliths*, edited by C.J. Hawkesworth, and Norry, M.J., pp. 92-110, Shiva, Cheshire, 1983.

Menzies, M., and Murthy, V.R., Nd and Sr isotope geochemistry of hydrous mantle nodules and their host alkali basalts: implications for local heterogeneities in metasomatically veined mantle, *Earth Planet. Sci. Lett., 46*, 323-334, 1980.

Menzies, M. A. and C. J. Hawkesworth, Editors, *Mantle Metasomatism,* Academic Press, London, 1987.

Millen, D. W., and Hamburger, M.W, Seismological evidence for tearing of the Pacific plate at the northern termination of the Tonga subduction zone, *Geology, 26*(7), 659-662, 1998.

Molnar, P., and Stock, J., Relative motions of hotspots in the Pacific, Atlantic and Indian Oceans since late Cretaceous time, *Nature, 327*(6123), 587-591, 1987.

Montelli, R., G. Nolet, F.A. Dahlen, G. Masters, E.R. Engdahl, S-H. Hung, Finite-Frequency Tomography Reveals a Variety of Plumes in the Mantle, *Science*, 10.1126/science.1092485, 2003.

Morgan, J. P., Isotope Topology of Individual Hoptspot Basalt Arrays: Mixing curves or Melt Extraction Trajectories, *Geochemistry, Geophysics, Geosystems, 1*, 1999GC000004, 2000.

Natland, J., H. The progression of volcanism in the Samoan linear volcanic chain, *American Journal of Science, 280-A*, 709-735, 1980.

Natland, J. H., *The Samoan Chain: A shallow lithospheric fracture system*, 2003, in prep.

Natland, J. H. and D. L. Turner, Age Progression and Petrological Development of Samoan Shield Volcanoes: Evidence from K-Ar Ages, Lava compositions, and mineral studies, *Investigations of the Northern Melanesian Borderland Circum-Pacific Council for Energy and Mineral Resources Earth Science Series 3*, edited by T. M. Brocher, Vol. 3, pp. 139-171, 1985.

Niu, Y., and R. Batiza, Trace element evidence from seamounts for recycled oceanic crust in the Eastern Pacific mantle, *Earth Planet. Sci. Lett., 148*, 471-483, 1997.

Niu, Y. K., D. Collerson, R. Batiza, J. I. Wendt and M. Regelous, The origin of E-type MORB at ridges far from mantle plumes: The East Pacific Rise at 11°20', *J. Geophys. Res., 104*, 7067-7087, 1999.

Niu, Y. and M. J. O'Hara, Origin of ocean island basalts: A new perspective from petrology, geochemistry, and mineral physics considerations, *J. of Geophys. Res., 108*, 2209, doi:10.1029/2002JB002048, 2003.

Niu, Y., G. Waggoner, J.M. Sinton, J.J. Mahoney, Mantle source heterogeneity and melting processes beneath seafloor spreading centers: The East Pacific Rise 18°-19°S, *J. Geophys. Res., 101*, 27,711-27,733, 1996.

Norton, I. O., Global Hotspot Reference Frames and Plate Motion, pp. 339-357, in *The History and Dynamics of Global Plate Motions*, eds. M. A. Richards, R. G. Gordon and R. D. van de Hilst, Geophysical Monograph 121, American Geophysical Union, 2000.

Peacock, S. M, Thermal and petrologic structure of subduction zones, in *Subduction Top to Bottom, Geophys. Monogr. Ser., 96,* edited by G. E. Bebout et al., 119-133, AGU Washington, D.C., 1996.

Pearce, J.A. and D.W. Peate, Tectonic implications of the composition of volcanic arc magmas, *Ann. Rev. Earth Planet. Sci., 23*, 251-285, 1995.

Pelletier, B., Calmant, S., and Pillet, R., Current tectonics of the Tonga-Hebrides region, *Earth Planet. Sci. Lett., 164*, 263-276, 1998.

Peucker-Ehrenbrink, B., and B.-m. Jahn, Rhenium-osmium isotope systematics and platinum group element concentrations: Loess and the upper continental crust, *Geochem. Geophys. Geosyst.,* 2, 2001GC000172, 2001.

Pin, C., D. Briot, C. Bassin, and F. Poitrasson, Concomitant separation of strontium and

samarium-neodymium for isotopic analysis in silicate samples, based on specific extraction chromatography, *Anal. Chim. Acta, 298*, 209-217, 1994.

Plank, T. and C. H. Langmuir, The chemical compositions of subducting sediments and its consequences for the crust and mantle, *Chem. Geol., 145*, 325-394, 1998.

Poreda, R. J., and Craig, H., He and Sr isotopes in the Lau Basin mantle: Depleted and primitive mantle components, *Earth Planet. Sci. Lett., 113*, 487-493, 1992.

Reisberg, L., Zindler, A., Marcantonio, F., White, W., Wyman, D., and Weaver, B., Os isotope systematics in ocean island basalts, *Earth Planet. Sci. Lett., 120*, 149-167, 1993.

Richardson, S. H., Erlank, A.J., Duncan A.R., and Reid, D.L., Correlated Nd, Sr and Pb isotope variation in Walvis Ridge basalts and implications for their mantle source, *Earth Planet. Sci. Lett., 59*, 327-342, 1982.

Righter, K., and Hauri, E.H., Compatibility of Rhenium in Garnet During Mantle Melting and Magma Genesis, *Science, 280*, 1737-1741, 1998.

Roden, M. F., Hart, S.R., Frey, F.A., and Melson, W.G., Sr, Nd and Pb isotopic and REE geochemistry of St. Paul's Rocks: the metamorphic and metasomatic development of an alkali basalt mantle source, *Contributions to Mineralogy and Petrology, 85*, 376-390, 1984.

Russell, S. A., Lay, T., and Garnero, E.J., Seismic evidence for small-scale dynamics in the lowermost mantle at the root of the Hawaiian hotspot, *Nature, 396*, 255-258, 1998.

Salters, V. J. M., Longhi, J.E., and Bizimis, M., Near mantle solidus trace element partitioning at pressures up to 3.4 GPa, *Geochemistry, Geophysics, Geosystems, 3*(7), 10.1029/2001GC000148, 2002.

Savin, S. M., and Epstein, S., The oxygen and hydrogen isotope geochemistry of ocean sediments and shales, *Geochim. Cosmochim. Acta, 34*, 43-63, 1970.

Sella, G. F., Dixon, T.H., and Mao, A., REVEL: A model for recent plate velocities from space geodesy, *J. Geophys. Res., 107*, EGT 11-1 to 11-32, 2002.

Shen, Y., Solomon, S.C., Bjarnason, I.T., and Wolfe, C.J., Seismic evidence for a lower-mantle origin of the Iceland plume, *Nature, 395*(6697), 62-65, 1998.

Shirey, S. B., and Walker, R.J., The Re-Os isotope system in cosmochemistry and high-temperature geochemistry, *Annual Reviews in Earth and Planetary Science, 26*, 423-500, 1998.

Smith, W. H. F. and D. T. Sandwell, *Sea floor topography predicted from satellite altimetry and ship depth measurements*, Rep. MGG-09. World Data Cent. A for Mar. Geol. and Geophys., Natl. Geophys. Data Cent., U. S. Dep. Comer., Boulder, Colo.,

1994.

Standish, J. J., Hart, S.R., Blusztajn, J., Dick, H.J.B., and Lee, K.L., Abyssal peridotite osmium isotopic compositions from Cr-spinel, *Geochemistry, Geophysics, Geosystems, 3*(1), 10.1029/2001GC000161, 2002.

Staudigel, H., Zindler, A., Hart, S.R., Leslie, T., Chen, C.-Y., and Clague, D., The isotope systematics of a juvenile intraplate volcano: Pb, Nd, and Sr isotope ratios from Loihi Seamount, Hawaii, *Earth Planet. Sci. Lett., 69*, 13-29, 1984.

Staudigel, H. K.-H. Park, M. Pringle, J. L. Rubenstone, W.H.F. Smith and A. Zindler, The longevity of the south Pacific isotopic and thermal anomaly, *Earth Planet. Sci. Lett., 102*, 24-44, 1991.

Staudigel, H., Davies, G.R., Hart, S.R., Marchant, K.M., and Smith, B.M., Large scale isotopic Sr, Nd, and O isotopic anatomy of altered oceanic crust: DSDP/ODP sites 417/418, *Earth Planet. Sci. Lett., 130*, 169-185, 1995.

Steinberger, B., and O'Connell, R.J., Advection of plumes in the mantle flow: implications for hotspot motion, mantle viscosity and plume distribution, *Geophys. J. Int., 132*(412-434), 1998.

Stice, G. C. and F. W. McCoy, Jr., The Geology of the Manu'a Islands, Samoa, *Pacific Science, 22*, 427-457, 1968.

Stracke, A., Bizimis, M., and Salters, V.J.M., Recycling oceanic crust: Quantitative constraints, *Geochemistry, Geophysics, Geosystems, 4*(3), 10.1029/2001GC000223, 2003.

Sweeney, R. J., V. Prozesky and W. Przybylowicz, Selected trace and minor element partitioning between peridotite minerals and carbonatite melts at 18-46 kb pressure, *Geochim. Cosmochim. Acta, 59*, 3671-3683, 1995.

Taras, B.D., and S.R. Hart, Geochemical evolution of the New England seamount chain: isotopic and trace-element constraints, *Chemical Geology, 64*, 35-54, 1987.

Tatsumoto, M., Isotopic composition of lead in oceanic basalts and its implication to mantle evolution, *Earth Planet. Sci. Lett., 38*, 63-87, 1978.

Todt, W., R.A. Cliff, A. Hanser, A.W. Hofmann, $^{202}Pb + {}^{205}Pb$ double spike for lead isotopic analyses, *Terra Cognita, 4*, 209, 1984.

Turner, S., and Hawkesworth, C., Using geochemistry to map flow beneath the Lau Basin, *Geology, 26*(11), 1019-1022, 1998.

van Keken, P. E., E. H. Hauri, and C. J. Ballentine, Mantle Mixing: The Generation, Preservation, and Destruction of Chemical Heterogeneity, *Annu. Rev. Earth Plant. Sci.,*

30, 493-525, 2002.

Walter, M. J., Melting of Garnet Peridotite and the Origin of Komatiite and Depleted Lithosphere, *J. Petrol., 39*, 29-60, 1998.

Wang, S., and Wang, R., Current plate velocities relative to hotspots: implications for hotspot motion, mantle viscosity and the global reference frame, *Earth Planet. Sci. Lett., 189*, 133-140, 2001.

Watson, S. and D. McKenzie, Melt Generation by Plumes: A Study of Hawaiian Volcanism, *J. Petrology, 32*, 501-537, 1991.

Weaver, B. L., The origin of ocean island basalt end-member compositions: trace element and isotopic constraints, *Earth Planet. Sci. Lett., 104*, 381-397, 1991.

Wendt, J. I., Regelous, M., Collerson, K.D., and Ewart, A., Evidence for a contribution from two mantle plumes to island-arc lavas from northern Tonga, *Geology, 25*(7), 611-614, 1997.

White, W. M., Source of oceanic basalts: Radiogenic isotopic evidence, *Geology, 13*, 115-118, 1985.

Workman, R.K., and S.R Hart, Trace element composition of the depleted upper mantle, *Eos Trans. AGU, 84(46)*, Fall Meet. Suppl., Abstract V52D-02, 2003.

Wright, E., and White, W.M., The origin of Samoa: new evidence from Sr, Nd, and Pb isotopes, *Earth Planet. Sci. Lett., 81*, 151-162, 1986/87.

Zellmer, K. E., and Taylor, B., A three-plate kinematic model for Lau Basin opening, *Geochemistry, Geophysics, Geosystems, 2*, 2000GC000106, 2001.

Zhao, D., Seismic structure and origin of hotspots and mantle plumes, *Earth Planet. Sci. Lett., 192*, 251-265, 2001.

Zindler, A., and Hart, S.R., Chemical Geodynamics, *Annual Reviews Earth and Planetary Sciences, 14*, 493-571, 1986.

Zindler, A, S. R. Hart, F. A. Frey and S. Jakobsson, Nd and Sr isotope ratios and REE abundances in Reykjanes peninsula basalts: Evidence for mantle heterogeneity beneath Iceland, *Earth Planet. Sci. Lett., 45*, 249-262, 1979.

Figures

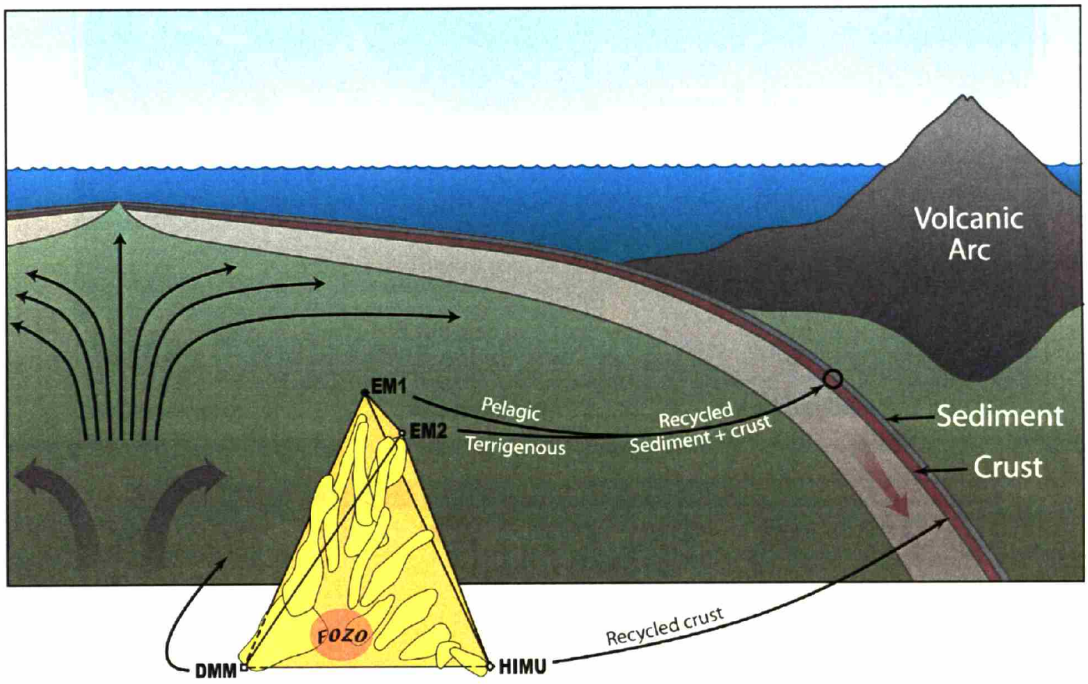

Figure 2-1. Schematic diagram of the Standard Model for the origin of isotopically defined mantle components. DMM (the Depleted MORB Mantle) is the melt-depleted upper mantle that supplies melts to mid-ocean ridges; HIMU (high U/Pb mantle) is a reservoir derived from recycling and long-term storage (billions of years) of oceanic crust; EM1 and EM2 are derived from recycling and long-term storage of oceanic crust along with pelagic or terrigenous sediment, respectively. Major contributions to the model have been from Armstrong (1968), Chase (1981), Hofmann and White (1982), Cohen and O'Nions (1982), White (1985), Zindler and Hart (1986), Weaver (1991), and Hart et al. (1992).

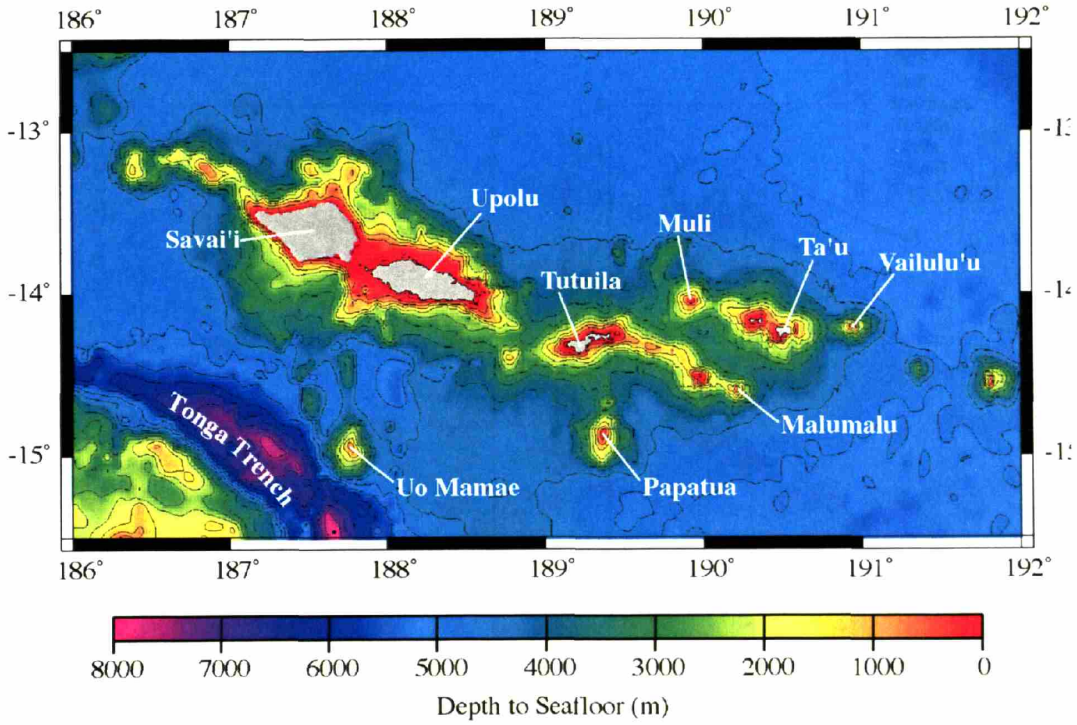

Figure 2-2. Bathymetric map of the Samoan volcanic chain made from merging inferred bathymetry from Smith and Sandwell (1994) with ship-track data from both the AVON 2/3 cruise (see Hart et al., 2000) and the GEODAS track-line database. Western Samoa is comprised of the two western islands, Savai'i and Upolu; American Samoa is comprised on Tutuila, Ofu, Olosega, and Ta'u. In the southwest corner of the map, where depths are down to 8000 m, is the northern termination of the Tonga Trench. Just off to the west at about 14.5°S is a transform fault bounding the Lau Backarc Basin to the south.

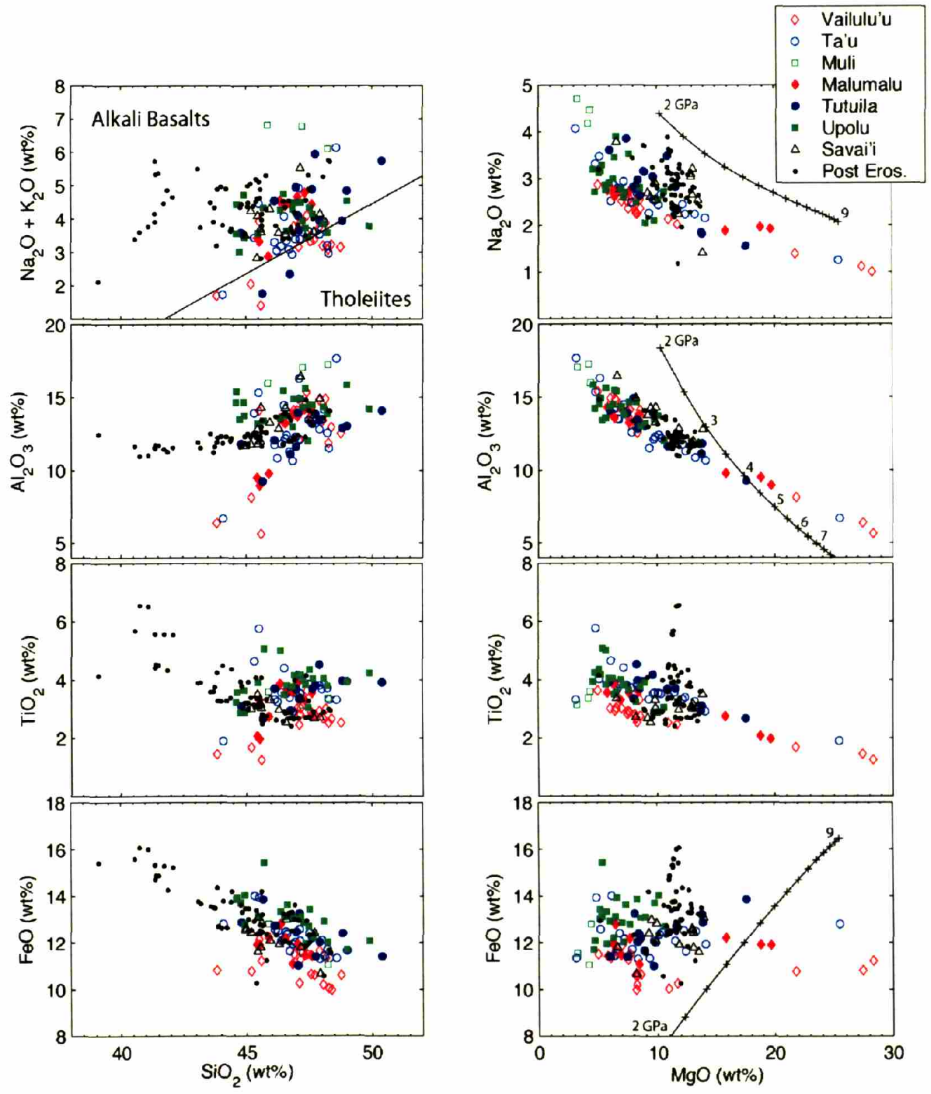

Figure 2-3. Major element compositions of Samoan basalts. Plots include data from Hauri and Hart (1997) for Savai'i lavas. Alkali-tholeiite line is from MacDonald and Katsura (1964). Trajectories of compositions for primary melts from fertile peridotites are plotted on some of the MgO diagrams, using the algorithms of Herzberg and Zhang (1996) in the pressure range of 2-8 GPa (tick marks every 0.5 GPa).

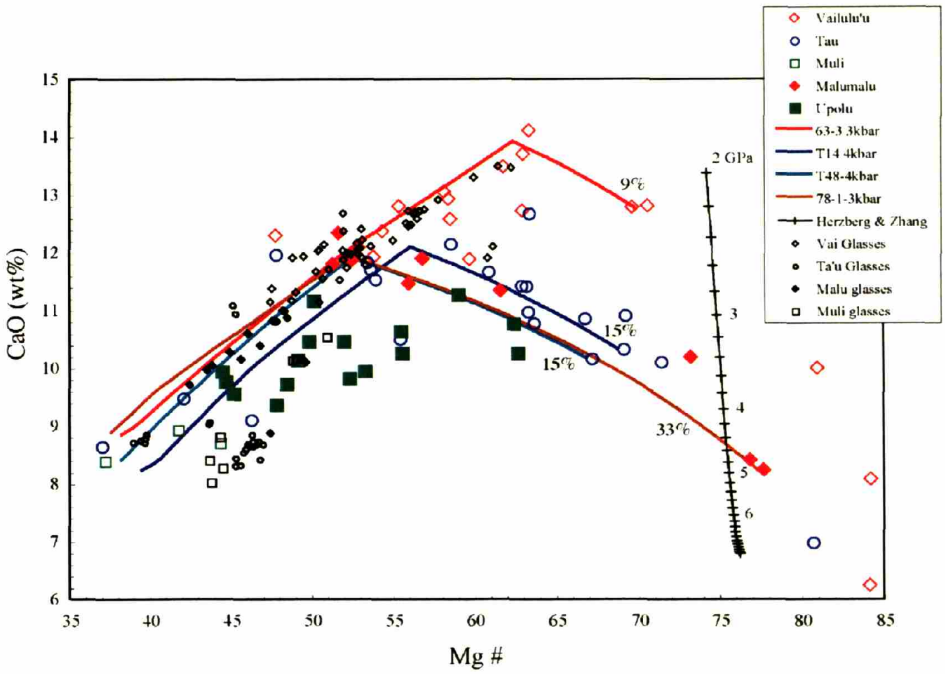

Figure 2-4. CaO plotted with Mg#'s for Samoan lavas. Mg# is calculated as molar percentage of $Mg/(Mg+Fe^{2+})$ where Fe^{2+} is taken to be 85% of reported FeO. Compositions of primary melts from fertile peridotite are plotted using algorithms from Herzberg and Zhang (1996) in the pressure range of 2-8 GPa; tic marks are every 0.2 GPa. Crystal fractionation trends have been calculated using pMELTS at pressures of 3 and 4 kbar for best fits to compositional trends starting with some of the most MgO-rich lavas. Mass of olivine crystallized (expressed as a percent of the total initial mass) before clinopyroxene saturation is noted at the high Mg# end of the liquid lines of descent. Primary melts can be interpreted to have integrated depths of melting from 2.5-6 GPa, but CaO variations in the lavas more likely represent CaO contents of a heterogeneous mantle source. Plot includes data from Hauri and Hart (1997) for Savai'i lavas.

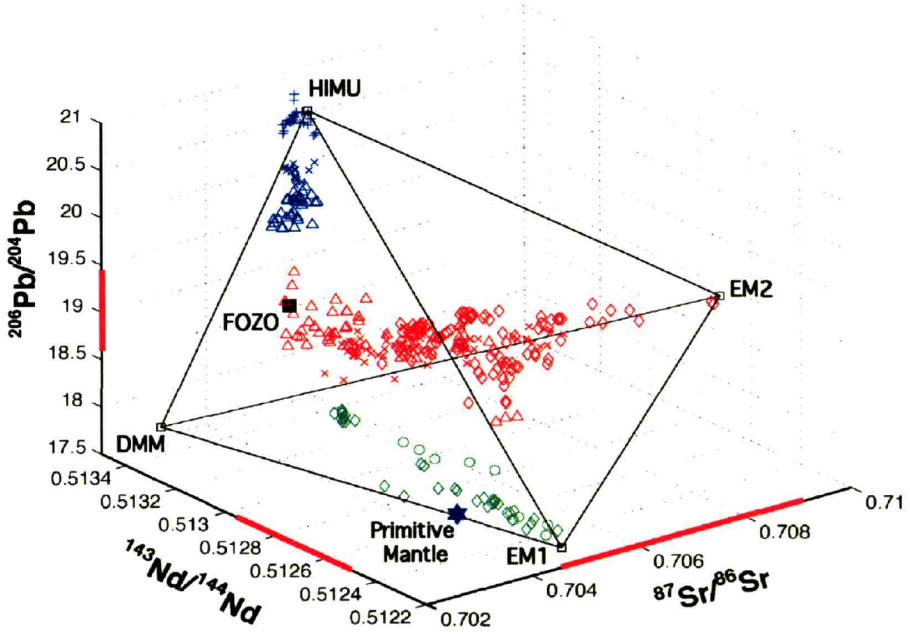

Figure 2-5. Mantle tetrahedron of Hart et al. (1992). Arrays from endmember defining island chains have been plotted using the GEOROC database and data presented in this manuscript. Island chains plotted for HIMU are in blue and include Tubuaii (×), Mangaia (+) and St. Helena (△). EM1 islands are in green and include Pitcairn (◊) and Walvis Ridge (○). EM2 islands are in red and include Samoa (◊), Societies (×), and the Marquesas (△). Red bars along the axes mark the range of values for the Samoan Islands. EM2 has been extended from its previous coordinate (Zindler and Hart, 1986) to values for $^{87}Sr/^{86}Sr$, $^{143}Nd/^{144}Nd$, and $^{206}Pb/^{204}Pb$ at 0.7090, 0.5125, and 19.3, respectively.

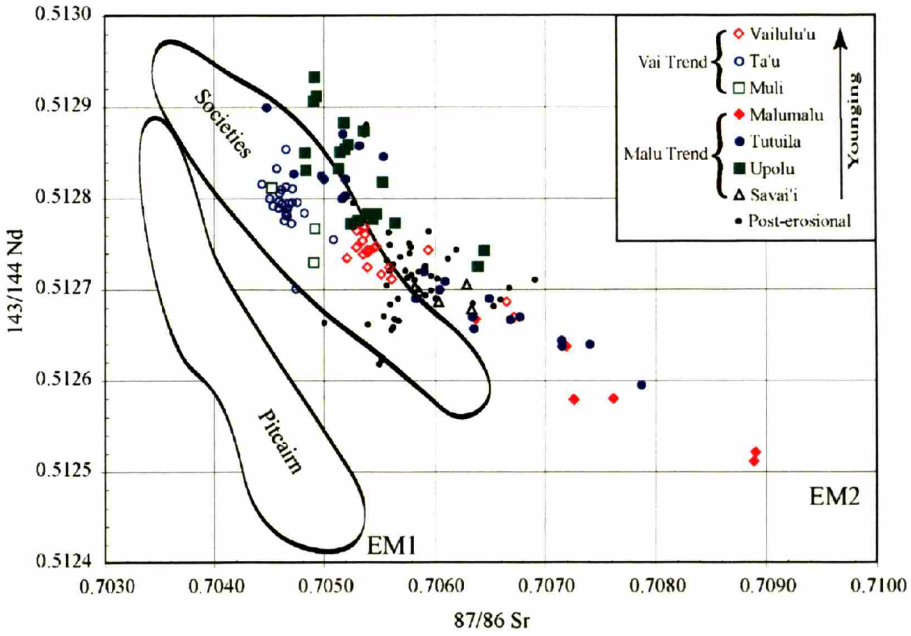

Figure 2-6. Sr and Nd isotopes for Samoan lavas. This as well as other isotope plots includes data from Wright and White (1987), Farley et al. (1992), and Hauri and Hart (1993). The legend here applies to all other isotope plots. The Vai Trend and Malu Trend correspond to topographic ridges of the volcanic chain (see Fig. 2). Savai'i samples marked with triangles are all from the Fagaloa Volcanic series. Post-erosional lavas include samples from Upolu and Savai'i. Fields for the Societies and Pitcairn were obtained from the GEOROC database. Coordinates for Globally Subducting Sediment (GLOSS) and local Tongan sediment are from Plank and Langmuir (1998).

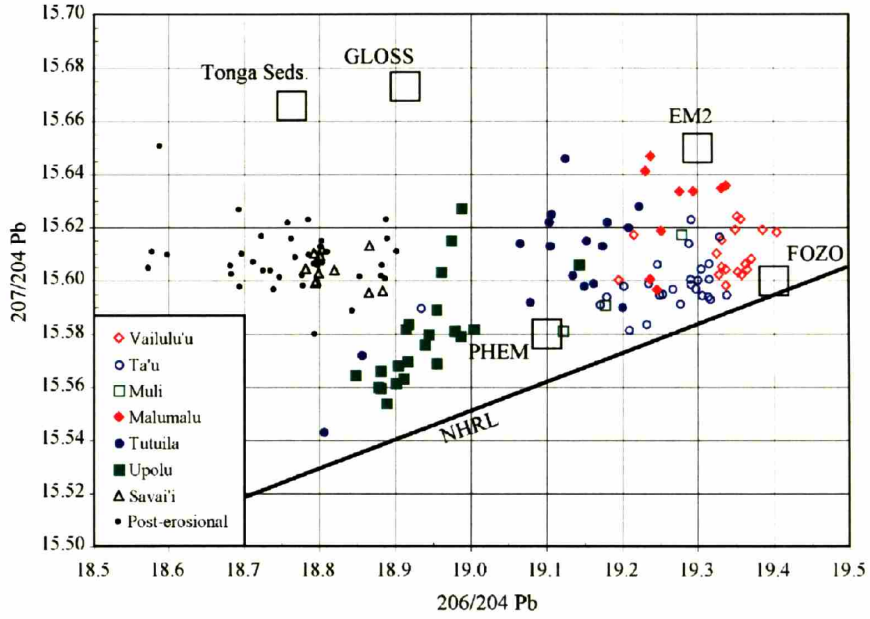

Figure 2-7. Plot of $^{206}Pb/^{204}Pb$ with $^{207}Pb/^{204}Pb$ of Samoan lavas. The Northern Hemisphere Reference Line (NHRL) lies significantly below the EM2 coordinate. Here, the Vai and Malu topographic lineaments can be distinguished as separate isotopic trends. Note how the post-erosional lavas are askew to the overall array of shield lavas. GLOSS = Globally Subducting Sediment (Plank and Langmuir, 1998); PHEM = Primtive Helium Mantle (Farley et al., 1992). Hauri et al. (1993) xenolith data derives from cpx and glass separates from Savaiian xenoliths. See Figure 6 for other references.

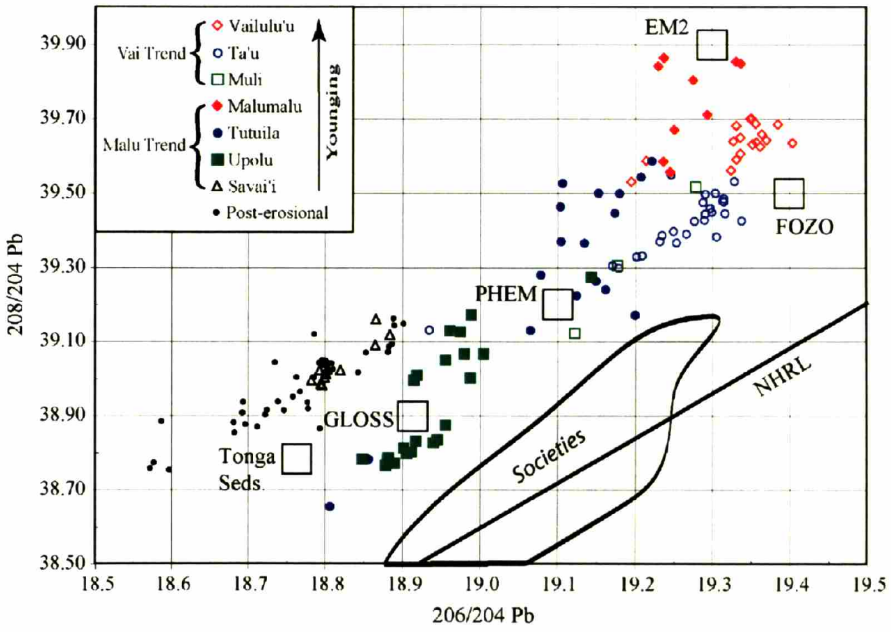

Figure 2-8. Plot of $^{206}Pb/^{204}Pb$ and $^{208}Pb/^{204}Pb$ of Samoan lavas. Again, the Vai and Malu Trends are separated into two isotopic arrays. Along each trend, the age of volcanoes increases in the direction of lower $^{206}Pb/^{204}Pb$ and $^{208}Pb/^{204}Pb$. See Figure 6 for references.

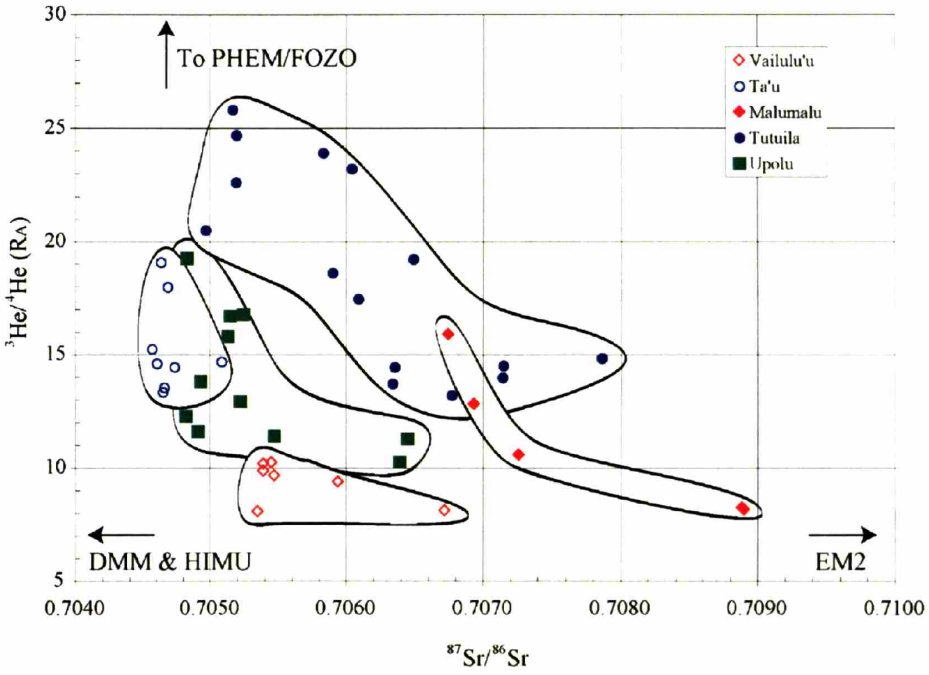

Figure 2-9. Plot of $^{87}Sr/^{86}Sr$ compositions of Samoan basalts with $^3He/^4He$ (R_A) of olivine phenocrysts and submarine glasses obtained from the same basalts. Some Tutuila samples are from Farley et al. (1992). EM2 is shown here to approach the DMM $^3He/^4He$ value of ~8 R_A at high $^{87}Sr/^{86}Sr$.

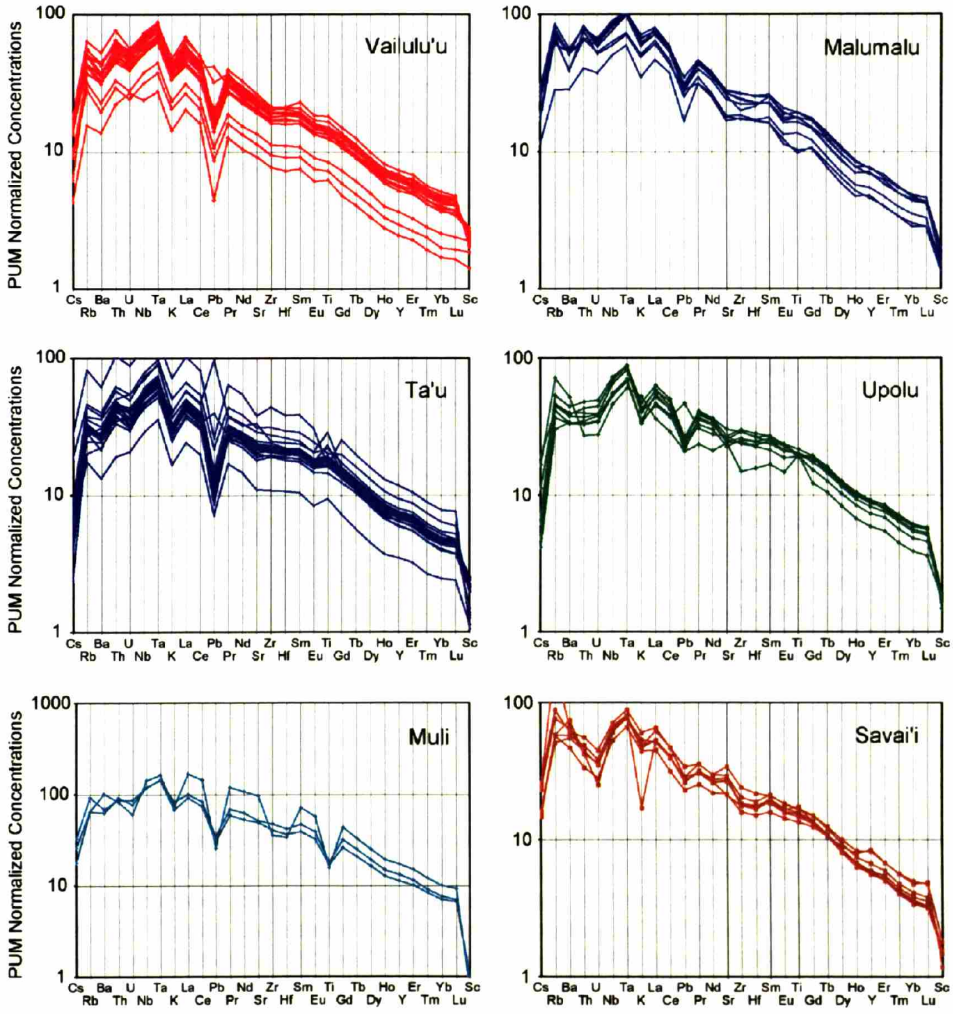

Figure 2-10. Trace element concentrations of Samoan lavas normalized to primitive upper mantle (PUM) of McDonough and Sun (1995). Note the difference in scale for the Muli lavas. Low concentration patterns are typically picrites (for example, the lowest three samples from Vailulu'u and lowest one from Ta'u). The highest concentration sample from Ta'u is T21, with 50% plagioclase phenocrysts.

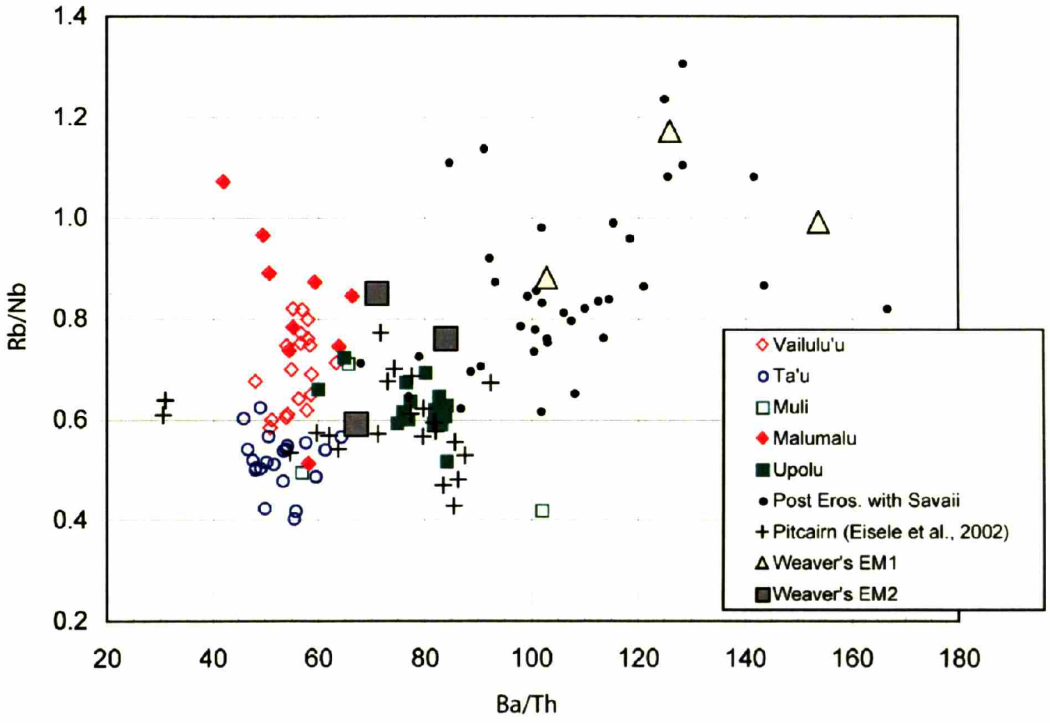

Figure 2-11. Ba/Th vs. Rb/Nb for lavas from Samoa (this study; Regelous et al., unpubl.; Hauri and Hart, 1997) and Pitcairn (Eisele et al., 2003) showing that Weaver's (1991) distinction between EM1 and EM2 trace element characteristics do not hold up to comparisons of lavas from endmember defining island chains (see Fig. 5). Pitcairn and Samoa show complete overlap in Ba/Th and Rb/Nb, whereas Weaver (1991) showed separate fields for EM1 and EM2 lavas. Plank and Langmuir (1998) report that terrigenous and pelagic sediments have indistinguishable Ba/Th ratios, each with a range of 10-220, with exceptions being rare hydrothermal clays and hemipelagic clays that are heavily-enriched in Ba. Therefore, the reason for initially identifying EM1 and EM2 as having recycled "pelagic" and "terrigenous" sediment, respectively, proves unfounded with further data collection.

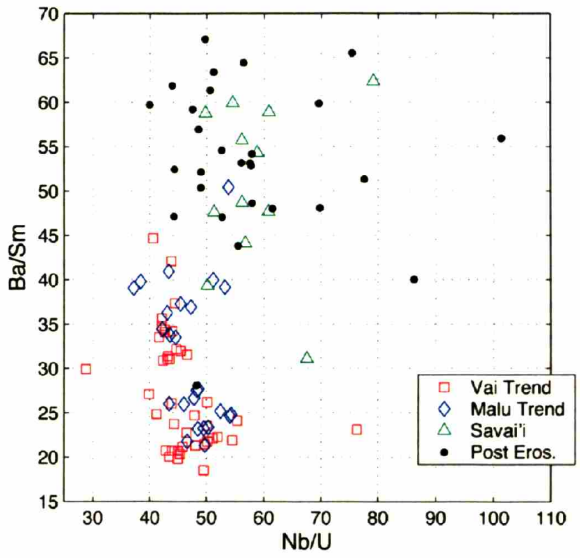

Figure 2-12. Plot of Nb/U vs. Ba/Sm used to highlight the trace element differences between shield and post-erosional lavas in Samoa. The new Savai'i lavas, sampled from the oldest mapped volcanic series on the island (Fagaloa Series; Kear and Wood, 1959), plot in the same field as post erosional lavas from all along the Samoan chain. This leads to the conclusion that either post-erosional lavas and shield lavas are the same on Savai'i, or post-erosional volcanism has been unusually extensive.

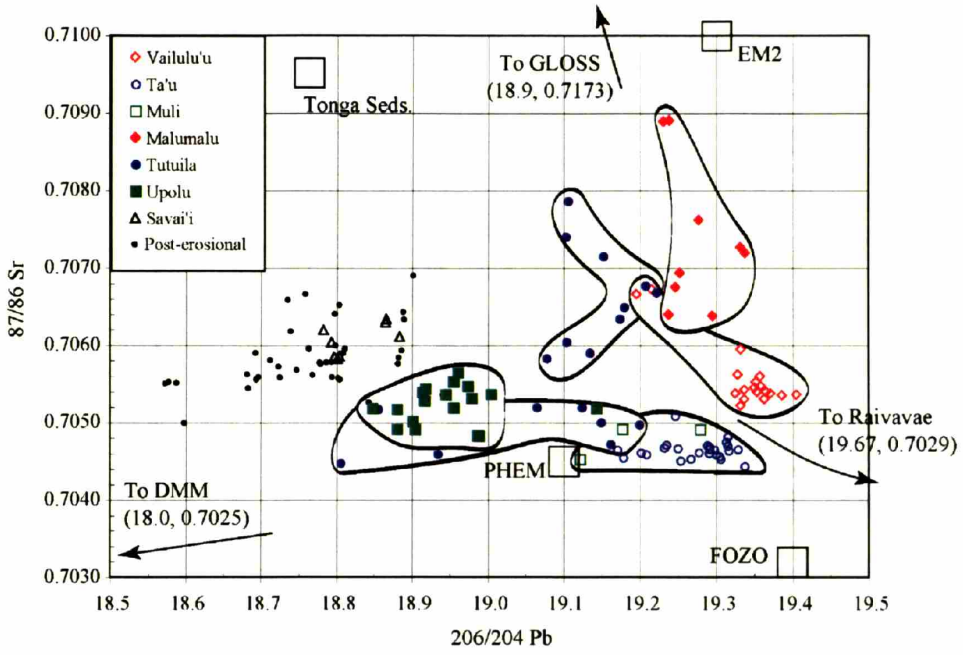

Figure 2-13. Sr and Pb isotope plot showing two classes of volcanoes – those which are elongate on the $^{206}Pb/^{204}Pb$ axis (Upolu, Tutuila Pago shield, Muli, and Ta'u) and those elongate on the $^{87}Sr/^{86}Sr$ axis. Mixing components are identified as DMM, HIMU, EM2 and the high $^{3}He/^{4}He$ reservoir, PHEM/FOZO. See Figure 6 for references.

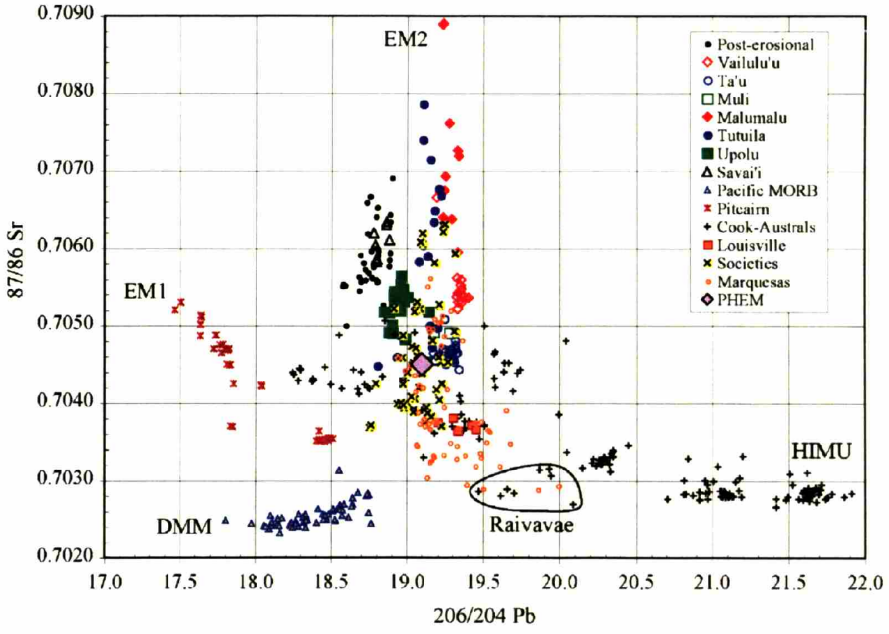

Figure 2-14. Plot showing Sr and Pb isotopic compositions for ocean islands of the Pacific Ocean. Data has been compiled from this study and the GEOROC database. EM2 dominates the spread in composition for the volcanoes Malumalu and Tutuila. Upolu volcano has a significant DMM component and Vailulu'u and Ta'u have been contaminated by HIMU from the Cook-Austral under-plated Pacific lithosphere.

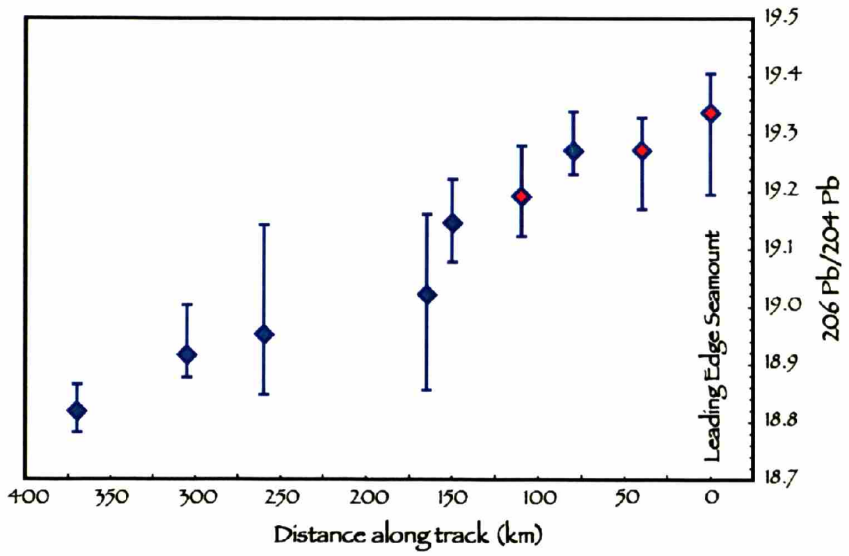

Figure 2-15. Plot showing a systematic increase in $^{206}Pb/^{204}Pb$ with eastward younging of volcanoes. Distance is measured from the zero-aged leading edge seamount, Vailulu'u. The "oldest" volcano (at a distance of 370 km from Vailulu'u) is Savai'i, though no lavas have been shown to be as old as the theoretical 5 Myr age of the island as suggested from age progression models. High $^{206}Pb/^{204}Pb$ values are found in EM2 and HIMU; low $^{206}Pb/^{204}Pb$ values are found in DMM. The increase in $^{206}Pb/^{204}Pb$ with time is therefore a waning of the DMM component in Samoan lavas.

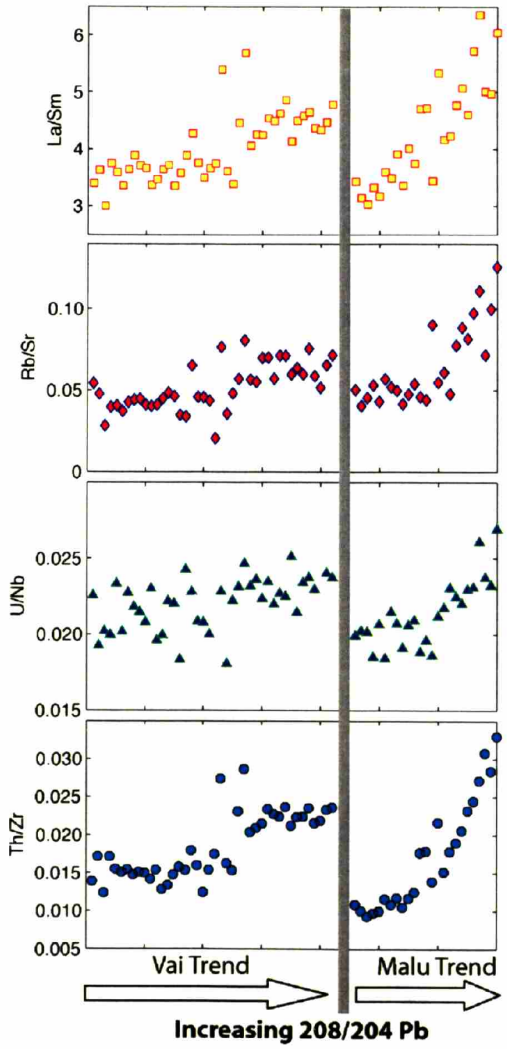

Figure 2-16. Trace element ratios of Samoan lavas, with the more incompatible element in the numerator, showing correlation with $^{208}Pb/^{204}Pb$ isotopic compositions. The Vai and Malu Trends have been separated into two groups, each sorted by increasing $^{208}Pb/^{204}Pb$, and plotted with trace element ratios.

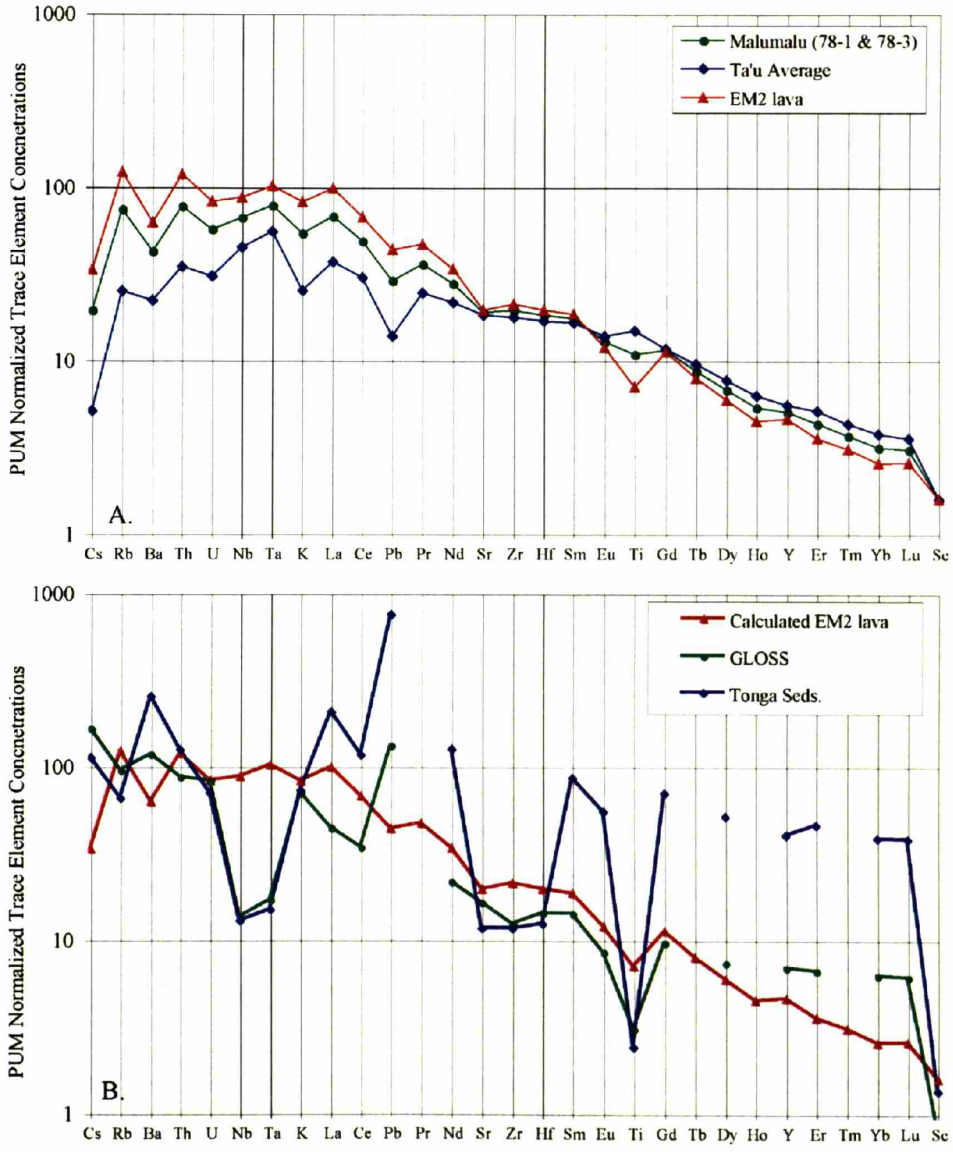

Figure 2-17. Spidergrams in a) show the average of Ta'u lavas, the average of the two most enriched Malumalu lavas, and a calculated EM2 lavas based on extrapolation between Ta'u and Malumalu trace element patterns shown here. All lavas have been corrected for olivine fractionation. In b), the calculated EM2 lava is compared to trace element patterns for globally subducting sediment (GLOSS) and a local Tongan sediment (both from Plank and Langmiur, 1998). Clearly, the trace element patterns between the EM2 lava and sediment are a near-zero match.

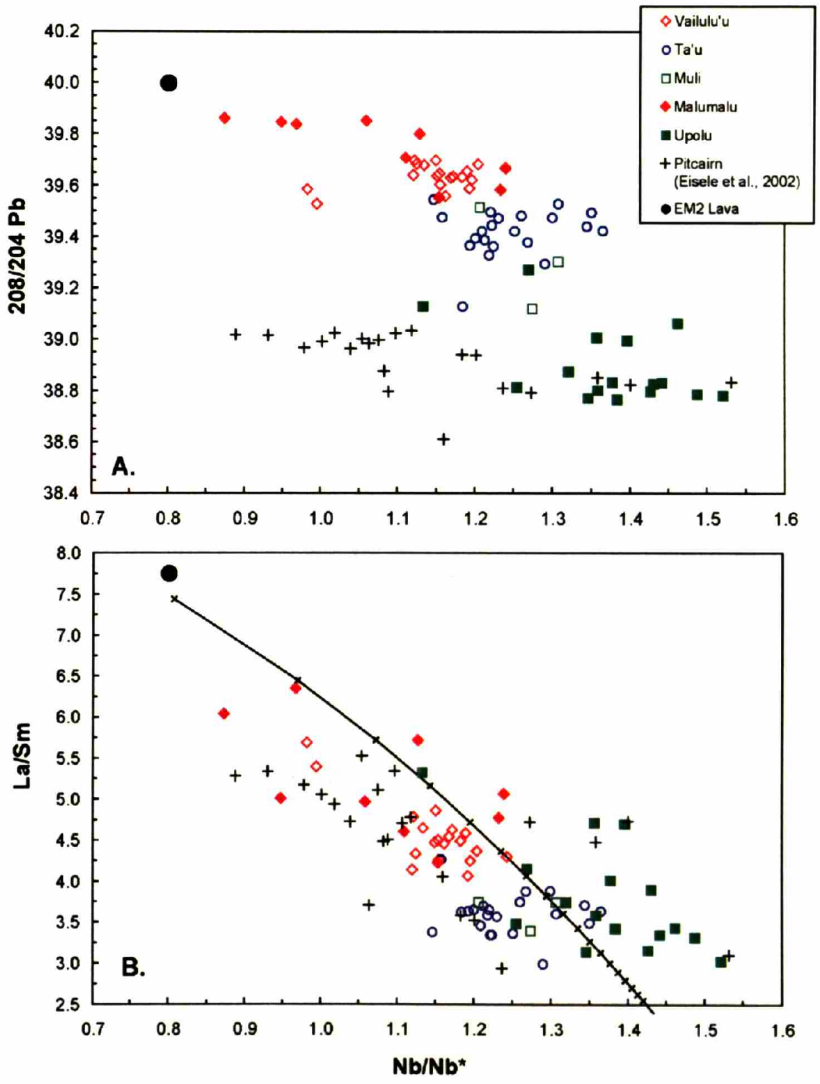

Figure 2-18. Nb/Nb* (calculated as $Nb_N/\sqrt{(Th_N \times La_N)}$, as in Eisele et al. [2002]) plotted with a) $^{208}Pb/^{204}Pb$ and b) La/Sm, of Samoan lavas and Pitcairn lavas (from Eisele et al., 2002). Pitcairn lavas have little source variation, as seen by a narrow range in $^{208}Pb/^{204}Pb$, but they have a range in Nb/Nb* and La/Sm that is nearly identical to Samoa. This indicates that varying degrees of melting of the same source can provide a wide range of trace element ratios otherwise interpreted to be source variations. The negative correlation in Samoa shows that at small degrees of melting (i.e. high La/Sm and low Nb/Nb*), the enriched component may be preferentially sampled from the mantle. The melting curve is for bacth melting of a mantle with the following concentrations in ppm: Th = 0.032, Nb = 0.457, La = 0.32, Sm = 0.326. D values for these elements are respectively 0.00038, 0.0043, 0.0045, 0.04. Tick marks are every 0.1% melting, increasing toward low La/Sm.

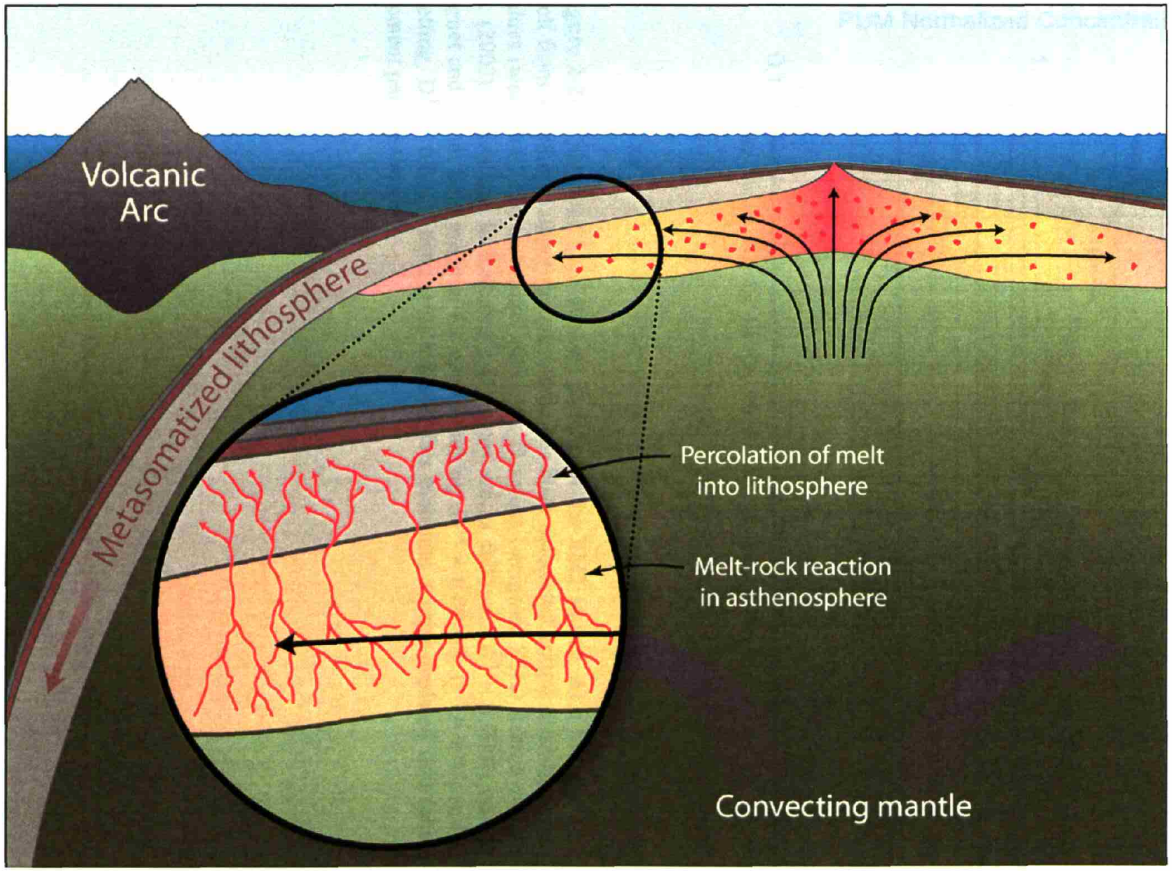

Figure 2-19. Schematic diagram illustrating a working hypothesis for the origin of the EM2 mantle reservoir. Starting 2.5 Ga, small degree (0.5%) batch melts of the primitive upper mantle migrate through the asthenosphere an impregnate the lithosphere. A mixture of depleted lithosphere with 1.1% of the 0.5% batch melts has the trace element pattern required to evolve to the present day Sr, Nd, and Hf isotopic compositions of EM2.

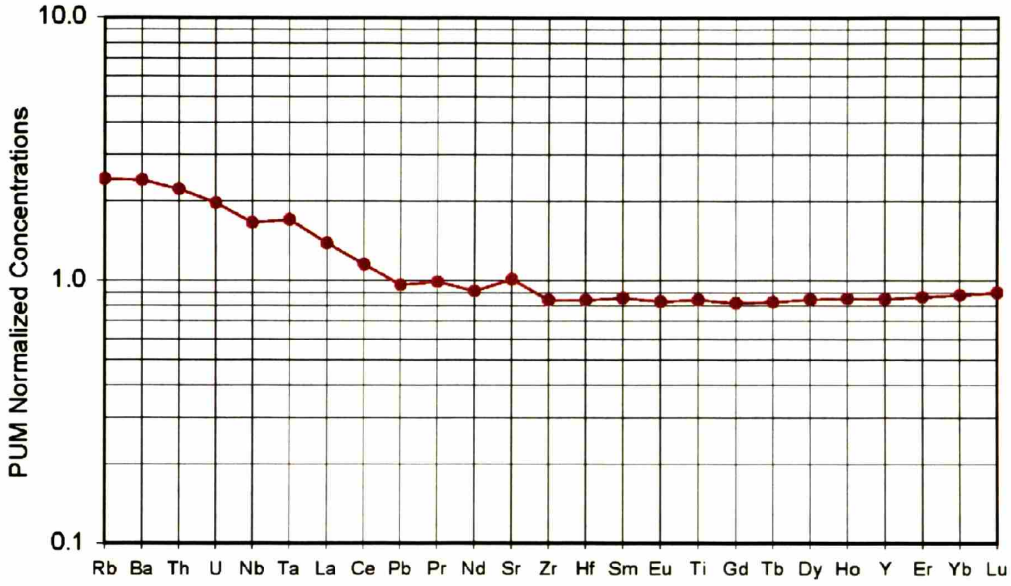

Figure 2-20. Calculated trace element pattern for the EM2 source. At a theoretical 2.5 Ga, a 0.5% batch melt from a primitive upper mantle source has been calculated with a combination of garnet peridotite D values (weighted 72%) and spinel peridotite D values (weighted 28%) from a compilation by Kelemen et al. (2003). Exceptions to Kelemen's D values are as follows: $D^{Rb} = 0.0001$, and $D^{U} = 0.0016$ for both garnet and spinel field melting; for garnet melting, $D^{Th} = 0.00038$, $D^{Zr} = 0.05$, and $D^{Hf} = 0.08$; for spinel melting, $D^{Th} = 0.0011$. Mixing of 1.1% of this melt into a semi-depleted lithosphere results in the trace element pattern shown.

Tables

Table 2-1. 40/39 Argon Ages from Upolu and Savai'i, Western Samoa

Sample Number	Location	Steps Used/ Total Steps	^{39}Ar Fraction Used	40/39 Total Fusion (my)	Weighted Plateau (my)
U10	Upolu, A'ana Shield	5/7	3.1-98.8%	0.972±0.020	**0.933±0.011**
U12	Upolu, A'ana Shield	5/6	0-92.8%	2.68±0.03	**2.65±0.02**
S11	Savai'i, Manase Shield	3/6	4.4-64.7%	0.900±0.122	**0.236±0.052**
S23	Savai'i, Manase Shield	5/6	0-91.3%	0.590±0.024	**0.386±0.014**
91SVK-7	Savai'i, Vanu River Shield	-	-	2.05±0.?	-

- Step-release heating from 600°-1400°C
- 2-sigma errors include measurement uncertainties, and uncertainty in J-value (flux gradient from FCT-3 biotite monitor), but not uncertainty in monitor age.
- 91SVK-7 is a trachyte cobble from the lower Vanu River, analyzed by K. A. Farley

Table 2-2. Sample information and chemical data for Samoan basalts

Volcano	Vailulu'u	Vailulu'u	Vailulu'u	Vailulu'u	Vailulu'u	Vailulu'u	Vailulu'u
Sample	**63-3**	**63-5**	**63-13**	**64-1**	**68-3**	**68-10**	**68-11**
Latitude (°S)	14.218	14.218	14.218	14.260	14.217	14.217	14.217
Longitude (°W)	169.059	169.059	169.059	169.056	169.064	169.064	169.064
Water Depth (m)	920	920	920	2630	780	780	780
Phenocrysts	10% Ol	5% Ol Tr Cpx	Aphyric	3% Ol 2% Cpx	10% Ol	Aphyric	60% Ol
Major elements	*(wt%)*						
SiO_2	48.29	48.07	47.16	47.71	47.84	48.18	45.61
Al_2O_3	11.88	13.42	14.76	13.38	11.86	14.90	5.64
TiO_2	2.52	2.67	3.01	2.80	2.55	3.00	1.24
FeO*	10.03	10.19	11.59	10.60	10.51	11.34	11.21
MnO	0.17	0.17	0.18	0.17	0.17	0.19	0.17
CaO	12.78	13.70	12.37	13.48	12.75	12.09	6.23
MgO	10.94	8.26	6.57	8.15	10.68	6.06	28.34
K_2O	0.96	0.96	1.28	1.07	0.99	1.13	0.41
Na_2O	2.13	2.24	2.72	2.31	2.36	2.76	1.00
P_2O_5	0.29	0.32	0.37	0.33	0.29	0.36	0.14
Mg#	69.58	62.96	54.31	61.72	68.07	52.85	84.13
Trace Elements	*(ppm)*						
Ni	285	110	59	104	285	47	1067
Cr	879	498	110	455	822	66	2771
V	299	335	339	329	300	351	154
Ga	16	20	20	19	20	18	6
Cu	86	59	58	85	82	68	103
Zn	84	85	95	82	89	94	86
Cs	0.29	0.13	0.28	0.33	0.30	0.38	0.09
Rb	24.7	22.2	33.6	29.6	26.6	24.7	9.3
Ba	216	210	279	236	218	239	90
Th	3.92	3.72	5.15	4.06	4.04	4.67	1.75
U	0.85	0.82	1.07	0.87	0.87	0.98	0.54
Nb	35.41	34.74	45.14	38.97	36.44	42.41	15.57
Ta	2.41	2.32	3.08	2.59	2.50	2.90	1.01
La	28.82	28.95	37.44	31.12	29.29	33.97	13.04
Ce	58.36	58.29	74.35	63.12	58.67	67.35	26.90
Pb	2.41	2.08	2.76	3.04	2.50	2.96	0.66
Pr	6.84	7.00	8.74	7.58	6.86	8.07	3.19
Nd	27.84	29.05	35.38	31.29	29	32.91	12.96
Sr	378	404	470	424	387	434	181
Zr	168	178	218	189	168	202	80
Hf	4.46	4.69	5.76	5.13	4.43	5.45	2.03
Sm	6.45	6.80	7.83	7.33	6.46	7.62	3.01
Eu	2.03	2.13	2.45	2.26	1.99	2.39	0.93
Gd	5.75	6.16	7.09	6.72	5.81	6.83	2.58
Tb	0.88	0.92	1.08	1.02	0.86	1.06	0.40
Dy	4.90	5.17	5.88	5.68	4.83	5.95	2.24
Ho	0.87	0.94	1.10	1.01	0.88	1.11	0.41
Y	22.08	24.09	27.50	26.43	22.46	27.93	10.47
Er	2.14	2.32	2.70	2.53	2.13	2.77	0.99
Tm	0.28	0.30	0.35	0.33	0.28	0.36	0.13
Yb	1.60	1.75	2.02	1.91	1.63	2.12	0.74
Lu	0.24	0.25	0.30	0.27	0.24	0.31	0.11
Sc	40.4	42.6	33.4	42.2	40.9	34.0	22.8

** Mg# = molar ratio of MgO/(MgO + 0.85*FeO)

Table 2-2, page 2.

Volcano	Vailulu'u	Vailulu'u	Vailulu'u	Vailulu'u	Vailulu'u	Vailulu'u	Vailulu'u
Sample	**68-28**	**68-30**	**70-1**	**70-2**	**70-9**	**71-2**	**71-11**
Latitude (°S)	14.217	14.217	14.208	14.208	14.208	14.337	14.337
Longitude (°W)	169.064	169.064	169.032	169.032	169.032	169.980	169.980
Water Depth (m)	780	780	1130	1130	1130	4170	4170
Phenocrysts	Tr Ol	Aphyric	Aphyric	Tr Cpx	Tr Ol Tr cpx	40% Ol Tr Cpx	2% Ol 1% Cpx
Major elements	*(wt%)*						
SiO_2	47.42	48.41	47.57	47.02	47.92	43.85	47.57
Al_2O_3	15.37	12.96	13.63	14.12	14.84	6.37	13.71
TiO_2	3.62	2.66	2.91	3.01	2.92	1.44	2.75
FeO*	11.49	9.97	11.44	11.88	11.65	10.80	10.64
MnO	0.18	0.17	0.18	0.18	0.18	0.17	0.18
CaO	12.30	14.11	13.05	12.80	11.93	8.07	12.72
MgO	5.01	8.21	7.56	7.02	6.47	27.44	8.60
K_2O	1.25	0.96	0.98	1.11	1.05	0.59	1.15
Na_2O	2.86	2.27	2.35	2.51	2.70	1.11	2.35
P_2O_5	0.50	0.30	0.34	0.35	0.35	0.17	0.33
Mg#	47.77	63.33	58.09	55.34	53.80	84.20	62.90
Trace Elements	*(ppm)*						
Ni	21	124	57	44	49	1080	135
Cr	50	542	98	72	60	2141	316
V	394	314	338	357	345	177	324
Ga	24	21	21	20	21	9	19
Cu	26	79	82	58	62	138	91
Zn	99	82	92	92	94	77	92
Cs	0.38	0.19	0.31	0.32	0.31	0.19	0.34
Rb	33.1	22.1	25.0	25.8	25.2	16.9	30.4
Ba	292	209	203	245	233	128	247
Th	4.96	3.56	4.20	4.53	4.29	2.31	4.35
U	1.03	0.79	0.93	0.94	0.95	0.49	0.95
Nb	48.08	34.11	37.07	42.81	41.41	20.66	40.53
Ta	3.25	2.31	2.50	2.90	2.76	1.38	2.75
La	41.67	27.34	31.03	34.38	32.79	17.10	32.93
Ce	84.11	55.47	64.97	67.72	66.48	34.37	65.58
Pb	2.65	2.36	2.23	2.72	2.64	1.28	2.31
Pr	10.01	6.83	7.57	8.06	7.97	4.04	7.85
Nd	40.82	28.27	31.51	32.96	32.41	16.52	31.64
Sr	521	392	420	453	430	224	434
Zr	222	175	198	199	199	98	186
Hf	5.92	4.72	5.36	5.42	5.24	2.55	5.17
Sm	9.26	6.73	7.50	7.66	7.51	3.68	7.25
Eu	2.81	2.13	2.30	2.38	2.37	1.14	2.25
Gd	8.06	6.06	6.78	6.76	6.77	3.17	6.36
Tb	1.23	0.93	1.02	1.05	1.04	0.48	0.99
Dy	6.64	5.27	5.67	5.79	5.78	2.72	5.44
Ho	1.20	0.94	1.01	1.06	1.07	0.49	0.98
Y	31.28	24.21	26.38	27.34	27.97	12.57	25.93
Er	2.96	2.28	2.48	2.56	2.71	1.15	2.39
Tm	0.38	0.30	0.33	0.34	0.36	0.16	0.32
Yb	2.24	1.68	1.87	1.95	2.07	0.87	1.83
Lu	0.32	0.25	0.27	0.29	0.31	0.13	0.27
Sc	32.8	45.1	41.9	38.6	35.1	29.8	39.2

Table 2-2, page 3.

Volcano	Vailulu'u	Vailulu'u	Vailulu'u	Vailulu'u	Vailulu'u	Vailulu'u	Ta'u
Sample	**71-22**	**72-2**	**73-1**	**73-2**	**73-3**	**73-12**	**T10**
Latitude (°S)	14.337	14.184	14.214	14.214	14.214	14.214	14.218
Longitude (°W)	169.980	169.894	169.059	169.059	169.059	169.059	169.509
Water Depth(m)	4170	3835	960	960	960	960	-
Phenocrysts	40% Ol	Aphyric	Tr Cpx	15% Ol	1% Ol Tr Cpx	15% Ol	Tr Ol
Major elements	*(wt%)*						
SiO_2	45.21	45.53	47.14	47.42	46.90	47.10	46.60
Al_2O_3	8.13	14.10	13.97	11.29	14.12	12.07	12.41
TiO_2	1.68	3.31	2.80	2.34	2.87	2.46	3.54
FeO*	10.77	12.13	11.26	10.66	11.49	10.25	12.35
MnO	0.17	0.19	0.18	0.17	0.18	0.18	0.19
CaO	9.99	11.88	12.93	13.18	12.58	12.80	10.98
MgO	21.79	8.56	7.52	11.43	7.71	11.70	10.13
K_2O	0.67	1.40	1.37	0.95	1.23	1.15	0.92
Na_2O	1.39	2.54	2.50	2.30	2.56	2.02	2.43
P_2O_5	0.20	0.37	0.34	0.26	0.35	0.28	0.45
Mg#	80.93	59.68	58.34	69.23	58.46	70.53	63.24
Trace Elements	*(ppm)*						
Ni	778	110	79	303	101	220	214
Cr	1687	227	202	840	241	768	579
V	212	367	325	292	328	295	336
Ga	14	23	14	17	22	17	19
Cu	156	79	70	109	66	59	72
Zn	78	102	86	84	89	77	111
Cs	0.21	0.39	0.38	0.11	0.32	0.31	0.12
Rb	19.0	29.3	38.1	24.5	33.2	30.4	19.9
Ba	149	287	347	203	283	282	178
Th	2.62	4.95	6.08	3.90	4.83	4.85	2.77
U	0.56	1.11	1.15	0.83	1.00	0.87	0.73
Nb	24.69	47.47	46.68	34.41	44.50	38.17	35.18
Ta	1.64	3.18	3.09	2.31	2.93	2.53	2.52
La	20.16	38.26	44.17	27.56	36.83	36.11	29.20
Ce	40.44	76.30	83.63	54.86	72.25	68.75	62.19
Pb	1.59	2.53	4.79	1.78	2.62	6.23	2.02
Pr	4.73	9.08	9.36	6.38	8.48	7.78	8.14
Nd	19.03	37.20	35.97	26.50	33.93	30.18	34.70
Sr	267	492	473	360	467	398	437
Zr	117	221	212	159	204	177	223
Hf	3.11	5.89	5.77	4.21	5.33	4.89	5.97
Sm	4.36	8.35	7.77	6.15	7.58	6.70	8.35
Eu	1.38	2.60	2.36	1.92	2.36	2.07	2.55
Gd	3.92	7.32	6.77	5.51	6.67	5.95	7.92
Tb	0.60	1.11	1.05	0.84	1.03	0.90	1.14
Dy	3.34	6.03	5.64	4.59	5.57	4.96	6.14
Ho	0.59	1.10	1.04	0.86	1.02	0.90	1.11
Y	15.55	29.25	27.27	21.99	27.61	23.49	29.41
Er	1.42	2.66	2.50	2.02	2.50	2.19	2.78
Tm	0.19	0.35	0.33	0.28	0.33	0.28	0.37
Yb	1.11	2.02	1.90	1.54	1.88	1.64	2.14
Lu	0.16	0.29	0.28	0.23	0.28	0.23	0.32
Sc	36.0	38.0	39.1	43.1	37.3	42.7	21.5

Table 2-2, page 4.

Volcano	Ta'u	Ta'u	Ta'u	Ta'u	Ta'u	Ta'u	Ta'u
Sample	**T14**	**T16**	**T19**	**T21**	**T22**	**T23**	**T25**
Latitude (°S)	14.2163	14.2164	14.2192	14.2160	14.2160	14.2174	14.2163
Longitude (°W)	169.5079	169.5094	169.5037	169.4762	169.4726	169.4648	169.4652
Water Depth (m)	-	-	-	-	-	-	-
Phenocrysts	2% Ol Tr Cpx	8% Ol	2% Ol	50% Plag Tr Ol, Cpx	Aphyric	Aphyric	25% Ol
Major elements	*(wt%)*						
SiO_2	46.25	46.71	47.14	48.61	46.51	47.49	45.23
Al_2O_3	10.84	11.27	12.12	17.66	14.47	13.44	8.37
TiO_2	3.24	3.38	3.52	3.31	4.40	3.85	2.42
FeO*	12.48	11.63	12.07	11.34	12.15	12.39	12.80
MnO	0.19	0.18	0.18	0.19	0.18	0.18	0.19
CaO	10.33	10.91	11.43	8.65	10.51	11.84	8.41
MgO	13.26	12.42	9.73	3.18	7.20	6.77	19.87
K_2O	0.82	0.86	0.86	2.07	1.15	0.92	0.66
Na_2O	2.23	2.23	2.55	4.07	2.93	2.71	1.78
P_2O_5	0.37	0.39	0.39	0.93	0.52	0.42	0.28
Mg#	69.02	69.13	62.83	37.03	55.41	53.40	76.50
Trace Elements	*(ppm)*						
Ni	396	360	194	9	83	79	723
Cr	943	729	542	5	185	112	1406
V	333	340	345	182	369	373	254
Ga	20	20	20	27	22	22	13
Cu	116	32	110	101	70	105	69
Zn	126	102	127	150	124	123	111
Cs	0.12	0.09	0.09	0.58	0.19	0.05	0.16
Rb	18.0	19.8	18.8	49.1	26.3	16.4	15.9
Ba	164	177	164	406	248	190	126
Th	3.51	2.89	3.24	8.26	4.58	3.80	2.59
U	0.64	0.73	0.73	1.79	1.00	0.71	0.57
Nb	33.26	36.62	33.16	78.63	47.97	38.73	24.03
Ta	2.27	2.60	2.30	5.09	3.29	2.64	1.66
La	26.79	29.68	27.08	66.60	37.70	31.06	19.90
Ce	55.65	63.08	56.61	136.19	79.07	65.26	41.81
Pb	5.95	1.82	1.47	3.89	2.25	1.46	1.40
Pr	6.80	8.24	7.06	16.23	9.62	7.98	5.20
Nd	29.62	35.06	31.01	67.87	41.52	35.00	22.45
Sr	377	442	407	754	575	472	294
Zr	205	225	220	460	287	241	154
Hf	5.34	5.83	5.52	10.79	7.40	6.14	3.92
Sm	7.37	8.15	8.07	15.59	10.04	8.68	5.61
Eu	2.41	2.47	2.53	4.69	3.13	2.75	1.78
Gd	7.20	7.64	7.70	13.74	9.38	8.25	5.22
Tb	1.08	1.08	1.15	1.96	1.37	1.21	0.79
Dy	5.61	5.77	6.41	10.77	7.46	6.82	4.27
Ho	1.00	1.03	1.17	1.94	1.34	1.21	0.79
Y	25.74	27.91	28.94	50.43	34.20	30.48	20.21
Er	2.39	2.55	2.72	4.58	3.27	2.94	1.85
Tm	0.31	0.33	0.36	0.60	0.42	0.38	0.24
Yb	1.78	1.97	2.04	3.43	2.38	2.10	1.37
Lu	0.25	0.29	0.30	0.51	0.35	0.30	0.19
Sc	32.4	24.2	35.7	17.0	32.7	34.9	26.8

Table 2-2, page 5.

Volcano	Ta'u	Ta'u	Ta'u	Ta'u	Ta'u	Ta'u	Ta'u
Sample	**T27**	**T30**	**T32**	**T33**	**T38**	**T44**	**T45**
Latitude (°S)	14.2161	14.2161	14.2163	14.2163	14.2161	14.2564	14.2556
Longitude (°W)	169.4774	169.4774	169.4390	169.4421	169.4774	169.4312	169.4319
Water Depth (m)	-	-	-	-	-	-	-
Phenocrysts	3% Ol Tr cpx	3% Ol 1% Cpx	Aphyric	10% Ol 2% Cpx	Aphyric	15% Ol 10% Cpx	3% Ol
Major elements	*(wt%)*						
SiO_2	48.12	46.41	48.02	47.32	45.34	46.84	47.93
Al_2O_3	14.17	11.80	13.50	10.61	13.93	10.63	12.81
TiO_2	3.86	3.57	3.68	3.09	4.64	2.90	3.80
FeO*	11.42	12.07	12.10	11.61	14.00	11.92	11.30
MnO	0.17	0.18	0.18	0.17	0.20	0.18	0.17
CaO	11.54	10.86	11.71	11.54	11.97	10.11	11.67
MgO	6.36	11.52	6.67	12.40	6.11	14.15	8.36
K_2O	1.06	0.83	0.93	0.75	0.93	0.79	0.87
Na_2O	2.85	2.36	2.78	2.19	2.51	2.15	2.67
P_2O_5	0.46	0.41	0.42	0.33	0.39	0.33	0.43
Mg#	53.87	66.68	53.62	69.15	47.79	71.34	60.81
Trace Elements	*(ppm)*						
Ni	95	298	86	288	63	439	162
Cr	290	682	100	988	59	764	549
V	334	313	356	308	489	283	353
Ga	25	19	22	18	24	17	25
Cu	131	102	133	61	120	92	99
Zn	122	121	121	103	121	115	113
Cs	0.09	0.17	0.10	0.11	0.08	0.09	0.14
Rb	21.4	19.0	19.0	15.7	16.7	17.1	18.4
Ba	208	166	180	140	203	140	170
Th	3.86	3.44	3.66	2.83	3.64	3.05	3.38
U	0.79	0.82	0.88	0.58	0.72	0.63	0.82
Nb	39.56	37.63	37.74	28.68	39.88	28.37	35.66
Ta	2.68	2.55	2.56	1.98	2.76	1.91	2.43
La	32.43	30.50	31.24	23.65	30.45	23.94	28.63
Ce	67.26	62.61	64.88	50.60	63.59	50.56	60.31
Pb	1.86	1.43	2.32	1.94	1.45	1.90	1.36
Pr	8.24	7.45	7.94	6.38	7.78	6.32	7.44
Nd	35.65	32.06	34.68	27.80	33.84	27.82	32.80
Sr	492	431	469	366	471	356	458
Zr	251	233	236	190	224	199	239
Hf	6.22	5.66	6.11	4.96	5.98	5.08	6.07
Sm	8.85	7.85	8.69	7.09	8.43	7.07	8.49
Eu	2.82	2.50	2.77	2.25	2.69	2.24	2.74
Gd	8.54	7.39	8.30	6.69	8.06	6.70	8.21
Tb	1.29	1.11	1.24	1.02	1.19	1.03	1.23
Dy	7.01	6.03	6.78	5.62	6.48	5.66	6.87
Ho	1.28	1.07	1.21	1.01	1.18	1.01	1.24
Y	32.55	27.50	31.25	26.16	29.69	25.28	31.49
Er	3.10	2.62	2.93	2.39	2.78	2.40	2.88
Tm	0.40	0.33	0.38	0.31	0.36	0.31	0.38
Yb	2.28	1.91	2.13	1.74	2.05	1.72	2.16
Lu	0.32	0.28	0.31	0.25	0.29	0.25	0.31
Sc	31.5	32.5	34.6	36.9	40.0	32.4	36.5

Table 2-2, page 6.

Volcano	Ta'u	Ta'u	Ta'u	Ta'u	Ta'u	Ta'u	Ta'u
Sample	**T46**	**T47**	**T48**	**T51**	**T55**	**74-1**	**74-4**
Latitude (°S)	14.2312	14.2131	14.2176	14.2179	14.2650	14.363	14.363
Longitude (°W)	169.4200	169.4361	169.4202	169.4846	169.4968	169.386	169.386
Water Depth (m)	-	-	-	-	-	2544	2544
Phenocrysts	3% Ol 2% Cpx	2% Ol 1% Cpx	1% Ol	2% Ol	3% Ol 2% Cpx	25% Ol	Aphyric
Major elements	*(wt%)*						
SiO_2	46.56	48.31	46.13	46.95	48.25	44.09	45.52
Al_2O_3	12.19	11.51	11.75	12.26	12.56	6.67	15.33
TiO_2	3.51	3.33	3.33	3.55	3.71	1.89	5.76
FeO*	12.46	11.34	12.52	12.02	11.70	12.79	13.92
MnO	0.19	0.17	0.18	0.18	0.18	0.19	0.19
CaO	10.78	12.68	10.17	11.42	12.15	6.98	9.48
MgO	10.38	9.33	12.19	9.82	7.85	25.45	4.83
K_2O	0.85	0.71	0.87	0.87	0.73	0.48	1.17
Na_2O	2.66	2.26	2.44	2.53	2.48	1.25	3.31
P_2O_5	0.43	0.36	0.41	0.40	0.38	0.22	0.51
Mg#	63.60	63.31	67.13	63.14	58.46	80.67	42.12
Trace Elements	*(ppm)*						
Ni	230	171	351	194	112	1019	36
Cr	515	654	687	540	331	1655	32
V	323	346	308	341	355	187	472
Ga	20	21	22	22	22	13	24
Cu	115	106	85	110	104	69	145
Zn	130	112	120	126	124	103	142
Cs	0.20	0.16	0.05	0.10	0.10	0.13	0.15
Rb	19.2	14.7	17.8	17.5	12.0	10.5	22.3
Ba	176	160	171	177	147	87	237
Th	3.69	3.00	3.55	3.43	2.65	1.51	3.98
U	0.84	0.62	0.74	0.67	0.60	0.42	1.11
Nb	36.94	30.76	35.58	34.21	29.72	18.94	45.78
Ta	2.54	2.14	2.43	2.34	2.04	1.32	3.38
La	30.96	25.08	29.49	27.81	23.86	15.66	37.13
Ce	63.70	53.29	60.93	58.49	51.28	33.14	77.39
Pb	1.66	1.28	1.58	2.05	1.95	1.06	14.60
Pr	7.76	6.62	7.39	7.28	6.52	4.30	9.44
Nd	33.77	29.37	32.39	31.76	29.68	18.16	40.30
Sr	451	396	434	427	427	217	660
Zr	239	199	237	223	214	113	259
Hf	6.18	5.28	5.94	5.72	5.60	3.01	6.79
Sm	8.50	7.47	8.05	8.02	7.95	4.21	9.55
Eu	2.72	2.40	2.57	2.56	2.64	1.28	3.20
Gd	8.17	7.29	7.53	7.72	7.89	3.92	8.68
Tb	1.24	1.09	1.14	1.16	1.20	0.56	1.29
Dy	6.76	6.09	6.28	6.36	6.64	3.04	7.11
Ho	1.21	1.09	1.14	1.17	1.21	0.55	1.27
Y	31.09	27.53	28.85	28.91	30.30	14.91	32.34
Er	2.90	2.61	2.74	2.74	2.88	1.40	3.00
Tm	0.37	0.34	0.35	0.36	0.38	0.18	0.40
Yb	2.13	1.91	2.00	1.97	2.10	1.08	2.27
Lu	0.30	0.28	0.29	0.29	0.30	0.16	0.32
Sc	34.0	41.1	31.5	35.8	38.5	18.3	22.5

Table 2-2, page 7.

Volcano	Ta'u	Muli	Muli	Muli	Malumalu	Malumalu	Malumalu
Sample	**75-10**	**79-4**	**79-7**	**80-23**	**76-1**	**76-8**	**76-9**
Latitude (°S)	14.181	13.916	13.916	14.129	14.569	14.569	14.569
Longitude (°W)	169.304	169.993	169.993	170.062	169.718	169.718	169.718
Water Depth (m)	2675	3484	3484	2368	2785	2785	2785
Phenocrysts	Aphyric	1% Plag Tr Ol, Cpx	Tr Cpx	Aphyric	Aphyric	2% Ol	10% Ol 3% Cpx
Major elements	*(wt%)*						
SiO_2	47.10	47.23	45.88	48.27	47.62	47.04	45.91
Al_2O_3	16.29	17.06	15.99	17.23	14.30	13.69	9.77
TiO_2	4.02	3.13	3.58	3.36	3.54	3.88	2.74
FeO*	12.56	11.55	12.78	11.05	11.41	11.93	12.20
MnO	0.20	0.22	0.22	0.20	0.16	0.18	0.17
CaO	9.11	8.39	8.93	8.70	12.34	11.86	10.19
MgO	5.16	3.27	4.38	4.21	5.81	6.27	15.84
K_2O	1.46	2.09	2.37	1.94	1.69	1.92	1.00
Na_2O	3.47	4.70	4.46	4.17	2.75	2.75	1.88
P_2O_5	0.63	2.37	1.40	0.87	0.38	0.49	0.32
Mg#	46.28	37.25	41.82	44.41	51.64	52.43	73.14
Trace Elements	*(ppm)*						
Ni	5	4	0	0	46	65	458
Cr	15	1	6	7	94	137	889
V	282	144	168	205	370	356	276
Ga	26	23	27	28	23	22	19
Cu	21	10	6	13	138	72	56
Zn	140	188	191	163	109	121	107
Cs	0.39	0.54	0.68	0.37	0.64	0.51	0.24
Rb	27.6	38.6	54.8	38.4	36.6	44.3	16.9
Ba	264	662	447	409	351	355	187
Th	4.94	6.48	6.82	7.18	6.43	6.41	3.21
U	1.10	1.21	1.74	1.55	1.18	1.30	0.76
Nb	51.26	92.26	77.19	77.72	49.78	56.67	33.01
Ta	3.59	5.95	5.28	5.24	3.64	3.93	2.20
La	43.08	107.50	64.09	58.62	51.07	48.43	30.37
Ce	90.50	238.81	137.70	122.09	97.08	95.90	62.55
Pb	3.26	3.80	5.06	4.52	4.32	4.24	2.50
Pr	11.08	29.95	17.21	14.81	11.13	11.17	7.94
Nd	47.98	132.41	77.37	65.12	45.11	46.27	32.42
Sr	617	1901	1010	967	512	544	356
Zr	327	371	492	419	209	276	180
Hf	8.31	9.45	11.73	10.18	6.01	7.23	4.79
Sm	11.62	28.68	18.84	15.63	10.20	10.52	7.19
Eu	3.75	8.77	5.94	4.94	2.98	3.19	2.05
Gd	10.74	23.57	17.17	14.04	9.17	9.49	6.56
Tb	1.60	3.22	2.46	2.04	1.33	1.38	0.91
Dy	8.83	16.70	12.86	10.92	7.08	7.42	4.81
Ho	1.59	2.85	2.19	1.88	1.25	1.28	0.85
Y	40.24	73.39	56.38	48.07	32.32	32.16	23.37
Er	3.81	6.52	4.97	4.39	2.97	2.97	2.06
Tm	0.50	0.81	0.61	0.56	0.38	0.38	0.27
Yb	2.80	4.39	3.34	3.07	2.09	2.05	1.54
Lu	0.40	0.62	0.47	0.45	0.31	0.29	0.22
Sc	20.5	10.4	14.1	15.7	32.8	31.0	24.0

Table 2-2, page 8.

Volcano	Malumalu	Malumalu	Malumalu	Malumalu	Malumalu	Malumalu	Upolu
Sample	**76-13**	**77-1**	**77-9**	**78-1**	**78-3**	**78-8**	**U10**
Latitude (°S)	14.569	14.701	14.701	14.623	14.623	14.623	13.9283
Longitude (°W)	169.718	169.767	169.767	169.726	169.726	169.726	171.9813
Water Depth (m)	2785	3605	3605	2264	2264	2264	-
Phenocrysts	Aphyric	3% Ol 2% Cpx	3% Ol	25% Ol 5% Cpx	30% Ol 5% Cpx	2% Ol Tr Cpx	Aphyric
Major elements	*(wt%)*						
SiO_2	46.35	46.55	46.83	45.54	45.44	47.33	45.46
Al_2O_3	13.55	13.22	13.80	8.94	9.49	14.19	13.21
TiO_2	3.86	3.55	3.58	1.96	2.06	3.29	3.91
FeO*	12.78	12.17	11.08	11.89	11.91	11.45	13.09
MnO	0.20	0.17	0.17	0.17	0.17	0.17	0.19
CaO	11.80	11.90	11.34	8.23	8.41	11.47	11.27
MgO	6.42	7.62	8.45	19.68	18.81	6.93	8.97
K_2O	1.94	1.70	1.81	1.41	1.47	2.05	1.52
Na_2O	2.61	2.70	2.59	1.92	1.96	2.74	2.05
P_2O_5	0.49	0.42	0.36	0.27	0.28	0.40	0.34
Mg#	51.30	56.77	61.53	77.63	76.81	55.93	58.97
Trace Elements	*(ppm)*						
Ni	71	116	154	616	578	97	142
Cr	130	252	391	1289	1175	106	433
V	384	356	370	194	213	342	346
Ga	26	24	21	14	16	21	21
Cu	95	97	62	49	53	79	51
Zn	125	109	108	102	101	104	106
Cs	0.50	0.51	0.55	0.39	0.36	0.60	0.35
Rb	42.8	46.8	47.5	41.8	40.0	51.4	42.8
Ba	341	341	336	255	261	372	341
Th	5.33	5.14	6.59	6.03	5.24	6.26	2.16
U	1.29	1.22	1.24	1.05	1.08	1.36	0.56
Nb	57.53	55.47	53.44	39.02	41.45	58.97	30.02
Ta	3.84	3.70	3.64	2.63	2.71	3.84	2.22
La	48.57	46.34	46.05	39.44	41.66	51.99	23.29
Ce	96.33	90.88	89.34	73.02	77.38	98.76	48.32
Pb	5.18	4.14	4.18	4.19	3.77	4.58	3.11
Pr	11.80	11.05	10.13	7.93	8.85	11.52	5.93
Nd	47.24	43.33	41.30	31.00	32.86	44.15	26.24
Sr	554	530	477	333	361	529	475
Zr	281	250	232	183	193	256	155
Hf	7.11	6.38	6.23	4.71	4.80	6.42	4.41
Sm	10.18	9.15	9.27	6.53	6.56	9.09	6.77
Eu	2.87	2.59	2.72	1.89	1.75	2.51	2.25
Gd	9.10	8.09	8.16	5.81	5.67	7.96	6.60
Tb	1.26	1.12	1.22	0.82	0.77	1.11	1.03
Dy	6.57	5.96	6.52	4.40	4.00	5.84	5.59
Ho	1.15	1.04	1.15	0.77	0.70	1.04	1.00
Y	33.12	29.97	29.31	19.57	20.49	30.47	25.19
Er	2.82	2.55	2.72	1.76	1.73	2.53	2.38
Tm	0.37	0.34	0.34	0.23	0.23	0.34	0.30
Yb	2.13	1.92	1.92	1.24	1.32	1.97	1.70
Lu	0.31	0.29	0.28	0.19	0.19	0.29	0.24
Sc	25.0	27.4	31.2	25.2	21.9	28.5	28.0

Table 2-2, page 9.

Volcano	Upolu	Upolu	Upolu	Upolu	Upolu	Upolu	Upolu
Sample	**U12**	**U14**	**U16**	**U19**	**U21**	**U22**	**U24**
Latitude (°S)	13.9456	13.9383	13.9355	13.9392	13.8926	13.8922	13.9314
Longitude (°W)	171.9766	171.9805	171.9991	171.9938	171.9640	171.9630	171.9661
Water Depth (m)	-	-	-	-	-	-	-
Phenocrysts	Tr Ol,Plag Tr Cpx	2% Plag	3% Plag, Ol Tr Cpx	8% Plag 2% Cpx	2% Cpx Tr Ol, Plag	4% Cpx 2% Ol	5% Plag Tr Ol, Cpx
Major elements	*(wt%)*						
SiO_2	48.08	47.51	47.65	47.36	48.24	47.24	49.01
Al_2O_3	14.32	14.53	14.49	15.63	13.88	14.32	15.85
TiO_2	4.04	4.34	4.03	3.83	3.79	4.00	3.92
FeO*	12.91	13.41	12.20	11.94	12.04	12.84	11.71
MnO	0.19	0.20	0.18	0.17	0.17	0.18	0.18
CaO	10.14	9.94	10.47	11.17	10.64	9.95	9.56
MgO	5.95	5.13	6.30	5.72	7.15	6.98	4.61
K_2O	0.96	1.22	1.16	0.99	1.00	1.19	1.35
Na_2O	2.90	3.12	2.99	2.74	2.59	2.77	3.19
P_2O_5	0.51	0.60	0.54	0.46	0.49	0.54	0.63
Mg#	49.15	44.51	51.99	50.12	55.46	53.27	45.22
Trace Elements	*(ppm)*						
Ni	72	43	95	73	122	131	43
Cr	137	59	191	162	246	211	64
V	360	361	353	338	354	368	341
Ga	24	24	24	22	23	22	22
Cu	31	38	75	61	48	92	35
Zn	122	130	112	105	116	125	117
Cs	0.09	0.13	0.15	0.10	0.40	0.23	0.15
Rb	18.0	26.8	26.7	21.9	24.8	27.7	32.1
Ba	223	255	247	218	220	260	290
Th	2.64	3.40	2.93	2.59	2.74	3.14	3.79
U	0.70	0.90	0.79	0.69	0.77	0.79	0.99
Nb	34.81	45.28	42.59	36.23	35.77	42.88	47.60
Ta	2.47	3.21	3.02	2.59	2.54	3.02	3.26
La	30.14	37.48	33.30	29.03	35.27	37.73	40.81
Ce	63.91	80.50	71.31	61.80	70.00	73.99	83.91
Pb	3.32	3.70	3.54	6.98	3.14	3.79	3.93
Pr	8.24	10.11	8.98	7.73	9.26	9.78	10.37
Nd	37.45	44.40	40.23	34.51	41.25	43.19	45.31
Sr	447	535	505	530	479	488	597
Zr	263	313	302	247	253	271	303
Hf	6.85	7.91	7.42	6.35	6.49	6.92	7.51
Sm	9.59	10.93	10.03	8.65	10.12	10.50	10.90
Eu	3.21	3.60	3.28	2.86	3.50	3.55	3.60
Gd	9.35	10.47	9.45	8.27	9.96	10.12	10.35
Tb	1.46	1.59	1.42	1.25	1.48	1.51	1.56
Dy	8.06	8.51	7.76	6.87	7.99	8.34	8.44
Ho	1.47	1.56	1.38	1.25	1.45	1.50	1.53
Y	37.16	39.30	35.14	31.35	37.88	38.35	39.08
Er	3.53	3.68	3.29	2.99	3.43	3.54	3.70
Tm	0.46	0.49	0.43	0.38	0.44	0.47	0.47
Yb	2.62	2.68	2.36	2.12	2.46	2.59	2.65
Lu	0.37	0.39	0.34	0.31	0.35	0.38	0.38
Sc	31.1	26.8	29.4	29.4	30.1	28.5	23.9

Table 2-2, page 10.

Volcano	Savai'i	Savai'i	Savai'i	Savai'i	Savai'i	Savai'i	Savai'i
Sample	**S11**	**S12**	**S15**	**S16**	**S18**	**S23**	**S25**
Latitude (°S)	13.4840	13.4614	13.4561	13.4767	13.4751	13.4469	13.4469
Longitude (°W)	172.3787	172.3654	172.3939	172.3950	172.3929	172.3900	172.3864
Water Depth (m)	-	-	-	-	-	-	-
Phenocrysts	3% Ol 2% Cpx	2% Ol	2% Ol Tr Cpx	Aphyric	Aphyric	2% Ol	1% Ol
Major elements	*(wt%)*						
SiO_2	45.95	46.30	45.45	47.16	47.95	45.46	45.57
Al_2O_3	13.27	12.84	12.80	16.43	14.92	11.80	12.00
TiO_2	3.31	2.96	3.49	3.35	2.70	3.09	3.16
FeO*	12.08	11.91	13.06	11.78	10.66	11.60	11.79
MnO	0.17	0.17	0.18	0.17	0.17	0.17	0.17
CaO	10.54	9.91	7.81	8.45	10.87	9.81	10.07
MgO	9.86	11.86	13.94	6.62	8.23	13.54	13.09
K_2O	1.39	1.35	1.42	1.75	1.28	1.55	0.49
Na_2O	2.91	2.24	1.41	3.78	2.87	2.54	3.21
P_2O_5	0.53	0.46	0.44	0.52	0.36	0.44	0.46
Mg#	63.12	67.62	69.12	54.10	61.82	71.00	69.96
Trace Elements	*(ppm)*						
Ni	193	286	451	86	137	406	383
Cr	415	502	612	77	298	555	568
V	294	271	243	258	271	250	258
Ga	20	18	23	25	22	19	17
Cu	39	44	55	22	57	51	50
Zn	109	106	112	111	85	99	101
Cs	0.31	0.34	0.33	0.54	0.31	0.49	0.52
Rb	34.7	30.4	34.8	53.1	34.4	45.8	116.3
Ba	379	363	489	404	308	430	435
Th	3.87	3.53	3.41	4.43	2.67	3.35	3.46
U	0.78	0.71	0.51	0.91	0.57	0.74	0.72
Nb	44.21	40.01	40.20	46.64	34.71	41.43	42.42
Ta	2.99	2.87	2.89	3.28	2.46	2.85	2.97
La	40.18	34.41	33.75	42.60	29.28	33.20	34.48
Ce	78.56	67.10	66.36	78.71	52.74	66.01	68.38
Pb	4.30	4.06	4.05	5.11	3.44	4.29	3.92
Pr	9.02	7.76	7.76	9.03	6.43	7.75	8.08
Nd	37.22	32.31	33.13	37.01	27.41	32.74	34.15
Sr	581	532	420	680	429	544	564
Zr	213	194	185	251	167	186	189
Hf	5.34	4.97	4.90	6.14	4.27	4.70	4.91
Sm	8.58	7.46	7.84	8.49	6.46	7.72	8.02
Eu	2.81	2.43	2.54	2.84	2.21	2.47	2.60
Gd	8.14	7.09	7.32	8.22	6.74	7.14	7.42
Tb	1.19	1.05	1.06	1.23	1.04	1.05	1.08
Dy	6.37	5.74	5.56	6.76	6.03	5.45	5.73
Ho	1.11	1.01	0.96	1.24	1.17	0.94	0.98
Y	28.79	25.35	24.13	35.14	36.39	24.49	24.90
Er	2.59	2.39	2.22	2.96	2.97	2.20	2.26
Tm	0.33	0.30	0.28	0.39	0.38	0.27	0.29
Yb	1.82	1.68	1.54	2.19	2.09	1.50	1.60
Lu	0.26	0.24	0.22	0.32	0.33	0.21	0.22
Sc	24.9	23.8	25.2	19.0	29.1	24.4	24.7

Table 2-3. Major element electron probe data on submarine glasses from Samoa. Normalized to 100%

Sample #	Volcano	SiO_2	TiO_2	Al_2O_3	FeO*	MnO	MgO	CaO	Na_2O	K_2O	P_2O_5	n
63-13	Vailulu'u	47.223	3.428	14.612	12.744	0.187	5.486	11.147	3.045	1.639	0.489	2
68-03	Vailulu'u	47.454	3.079	14.899	11.726	0.152	6.037	12.039	2.820	1.359	0.436	2
68-34	Vailulu'u	46.896	3.167	14.484	12.175	0.171	6.283	12.376	2.697	1.304	0.447	2
68-35	Vailulu'u	47.208	3.230	14.546	12.739	0.177	5.797	11.912	2.683	1.251	0.456	2
68-36	Vailulu'u	46.954	3.237	14.642	12.239	0.144	6.016	12.136	2.873	1.326	0.433	2
68-37	Vailulu'u	47.071	3.285	14.595	12.647	0.177	5.914	11.937	2.662	1.279	0.432	2
68-38	Vailulu'u	48.142	3.128	14.846	11.631	0.162	5.948	11.528	2.924	1.256	0.435	2
68-43	Vailulu'u	47.054	3.297	14.792	12.297	0.173	5.966	12.045	2.572	1.349	0.456	2
68-44	Vailulu'u	47.011	3.217	14.534	12.444	0.171	6.026	12.028	2.776	1.336	0.456	3
70-01	Vailulu'u	48.043	3.001	14.474	11.821	0.194	6.316	11.996	2.674	1.104	0.378	4
70-02	Vailulu'u	47.548	3.229	14.855	12.204	0.170	5.880	11.668	2.705	1.305	0.437	2
70-09	Vailulu'u	48.094	3.206	14.672	12.364	0.191	5.669	11.317	2.827	1.229	0.433	2
71-03	Vailulu'u	46.986	3.187	14.150	10.839	0.129	7.055	12.911	2.834	1.473	0.437	2
71-04	Vailulu'u	47.034	3.137	13.900	11.492	0.148	6.950	12.722	2.731	1.458	0.429	2
71-05	Vailulu'u	47.735	2.955	14.670	11.278	0.176	6.568	12.212	2.609	1.379	0.419	2
71-06	Vailulu'u	47.631	3.161	14.503	11.581	0.176	5.968	12.676	2.392	1.498	0.414	4
71-09	Vailulu'u	46.874	3.119	14.172	11.304	0.166	7.022	12.716	2.721	1.452	0.453	2
71-10	Vailulu'u	47.149	3.119	14.375	11.286	0.156	6.823	12.458	2.737	1.489	0.409	4
71-11	Vailulu'u	47.492	2.984	15.202	11.487	0.151	6.208	11.908	2.785	1.346	0.438	2
71-13	Vailulu'u	47.680	2.956	15.156	11.521	0.159	6.214	11.923	2.646	1.340	0.406	2
71-13D	Vailulu'u	47.799	2.994	15.288	11.351	0.180	6.188	11.792	2.723	1.300	0.385	4
71-14	Vailulu'u	46.956	3.133	14.127	11.395	0.148	6.994	12.668	2.676	1.460	0.444	2
71-16	Vailulu'u	47.679	3.013	15.199	11.551	0.168	6.013	11.736	2.837	1.351	0.451	3
71-22	Vailulu'u	48.190	2.961	15.655	11.406	0.176	5.540	11.138	3.042	1.490	0.403	4
71-23	Vailulu'u	46.975	3.129	14.136	11.314	0.155	6.959	12.697	2.689	1.483	0.462	2
71-24	Vailulu'u	46.963	3.077	14.133	11.199	0.164	6.979	12.717	2.860	1.457	0.451	2
71-25	Vailulu'u	47.021	3.163	14.108	11.105	0.162	6.987	12.746	2.804	1.480	0.425	2
71-26	Vailulu'u	47.099	3.099	14.144	11.369	0.191	6.841	12.510	2.822	1.486	0.441	2
71-27	Vailulu'u	47.094	3.100	14.074	11.273	0.168	6.973	12.581	2.807	1.473	0.457	2
71-28	Vailulu'u	46.886	3.090	14.304	11.446	0.215	6.969	12.483	2.773	1.452	0.382	3
72-02	Vailulu'u	45.953	3.662	15.543	12.494	0.179	5.401	11.380	3.268	1.613	0.508	2
72-04	Vailulu'u	46.292	3.432	14.939	11.785	0.172	6.365	12.222	2.915	1.415	0.463	2

n = number of analyses
*=All Fe reported as FeO

Table 2-3, Page 2

Sample #	Volcano	SiO_2	TiO_2	Al_2O_3	FeO*	MnO	MgO	CaO	Na_2O	K_2O	P_2O_5	n
72-07	Vailulu'u	46.014	3.488	15.055	11.808	0.173	6.359	12.410	2.794	1.449	0.449	2
72-10	Vailulu'u	46.842	2.944	13.296	11.599	0.157	8.682	12.103	2.641	1.268	0.468	2
72-12	Vailulu'u	46.324	3.465	15.072	11.824	0.180	6.298	12.159	2.850	1.417	0.412	4
72-13	Vailulu'u	46.549	3.000	13.300	11.869	0.183	8.775	11.905	2.664	1.307	0.448	2
73-01	Vailulu'u	47.342	2.933	15.048	11.551	0.160	6.028	11.977	2.881	1.639	0.442	3
73-03	Vailulu'u	47.213	3.140	15.089	11.877	0.165	5.905	11.709	2.922	1.510	0.470	2
73-04	Vailulu'u	47.495	2.942	15.108	11.582	0.194	5.972	11.872	2.766	1.636	0.431	2
73-07	Vailulu'u	47.364	2.985	15.016	11.470	0.140	6.162	12.073	2.975	1.402	0.412	2
73-12	Vailulu'u	47.585	2.955	15.137	11.211	0.176	5.996	11.976	2.860	1.655	0.449	2
73-13	Vailulu'u	47.603	3.020	15.122	11.447	0.160	6.111	12.052	2.695	1.374	0.417	2
73-15	Vailulu'u	47.268	2.991	15.260	11.335	0.199	5.963	11.967	2.995	1.614	0.409	2
WC1	Vailulu'u	48.855	2.527	12.550	10.614	0.178	8.339	13.467	2.242	0.919	0.309	3
WC2	Vailulu'u	48.765	2.588	12.860	10.628	0.113	8.062	13.491	2.270	0.913	0.310	3
WC3	Vailulu'u	47.956	3.268	14.805	11.958	0.138	5.427	11.164	3.220	1.602	0.463	3
WC4	Vailulu'u	47.921	3.377	14.836	11.645	0.159	5.708	11.546	2.941	1.450	0.416	3
WC6	Vailulu'u	47.966	3.035	14.887	11.251	0.168	6.199	12.108	2.706	1.291	0.388	3
WC7	Vailulu'u	48.467	2.689	13.209	10.765	0.197	7.676	13.297	2.388	0.982	0.329	3
74-2	Ta'u	48.214	3.654	14.988	13.116	0.236	3.984	8.720	4.147	1.953	0.988	2
74-3	Ta'u	45.513	5.399	14.097	14.034	0.216	5.537	10.951	2.784	1.007	0.462	2
74-5	Ta'u	48.400	3.728	15.000	12.699	0.220	3.999	8.854	4.157	1.942	1.002	2
74-10	Ta'u	48.508	3.688	14.903	12.865	0.231	3.987	8.752	4.124	1.946	0.995	2
74-11	Ta'u	48.409	3.715	14.991	12.852	0.235	4.030	8.715	4.151	1.924	0.977	2
74-12	Ta'u	45.473	5.356	14.017	14.165	0.220	5.556	11.096	2.668	0.991	0.459	2
74-13	Ta'u	48.502	3.708	14.870	12.819	0.217	4.024	8.786	4.197	1.916	0.960	2
74-14	Ta'u	48.315	3.737	15.028	12.813	0.210	4.032	8.858	4.123	1.914	0.971	2
75-1	Ta'u	47.977	3.847	16.455	12.320	0.185	4.920	8.330	3.775	1.479	0.713	2
75-2	Ta'u	47.857	3.762	16.359	12.515	0.223	4.941	8.315	3.843	1.480	0.706	2
75-3	Ta'u	46.874	4.073	16.119	12.920	0.209	5.320	8.657	3.813	1.376	0.639	2
75-4	Ta'u	48.175	3.842	16.475	11.959	0.211	5.011	8.420	3.703	1.467	0.736	2
75-5	Ta'u	46.782	4.210	16.203	12.953	0.223	5.287	8.663	3.666	1.375	0.640	2
75-7	Ta'u	46.724	4.096	16.323	12.928	0.196	5.324	8.734	3.663	1.378	0.635	2
75-8	Ta'u	47.096	4.030	16.311	12.661	0.222	5.258	8.687	3.748	1.361	0.627	2

Table 2-3, Page 3

Sample #	Volcano	SiO_2	TiO_2	Al_2O_3	FeO*	MnO	MgO	CaO	Na_2O	K_2O	P_2O_5	n
75-12	Ta'u	47.820	3.838	16.317	12.280	0.220	4.850	8.447	3.956	1.562	0.710	2
75-13	Ta'u	46.771	4.691	14.903	13.400	0.235	4.961	9.076	3.794	1.474	0.695	2
75-15	Ta'u	47.671	3.924	16.476	12.460	0.215	5.017	8.547	3.582	1.460	0.648	2
75-16	Ta'u	47.054	4.064	16.334	12.966	0.222	5.248	8.605	3.541	1.381	0.583	2
75-17	Ta'u	46.752	4.726	15.082	13.335	0.247	4.925	9.039	3.689	1.489	0.716	2
75-18	Ta'u	46.895	4.097	16.234	12.755	0.198	5.329	8.741	3.811	1.352	0.588	2
76-1	Malumalu	46.986	3.831	14.854	12.706	0.179	5.169	10.602	3.262	1.945	0.467	2
76-2	Malumalu	47.471	3.689	15.298	12.818	0.187	4.710	9.971	3.444	2.012	0.400	2
76-3	Malumalu	46.960	3.952	14.469	12.521	0.199	5.455	10.813	3.303	1.830	0.498	2
76-4	Malumalu	46.786	3.963	14.467	12.713	0.179	5.502	10.826	3.222	1.865	0.477	2
76-5	Malumalu	48.855	3.407	15.699	12.653	0.210	5.447	8.873	3.092	1.346	0.418	3
76-6	Malumalu	47.388	3.576	15.274	12.282	0.166	5.151	10.393	3.160	2.195	0.416	2
76-7	Malumalu	47.544	3.718	15.316	12.705	0.220	4.736	10.050	3.362	1.963	0.386	2
76-8	Malumalu	46.737	3.892	14.358	12.583	0.187	5.585	11.002	3.346	1.824	0.485	2
76-10	Malumalu	47.377	3.982	15.507	12.673	0.191	4.458	9.716	3.464	2.098	0.534	2
76-11	Malumalu	47.393	3.608	15.316	12.639	0.199	4.920	10.278	3.389	1.893	0.364	2
76-12	Malumalu	46.948	3.957	14.504	12.546	0.197	5.486	10.818	3.180	1.869	0.495	2
76-13	Malumalu	46.869	3.958	14.567	12.434	0.188	5.579	10.875	3.240	1.839	0.451	2
76-14	Malumalu	47.499	3.611	15.355	12.479	0.189	4.997	10.163	3.203	2.100	0.404	2
77-6	Malumalu	47.023	3.764	14.467	12.561	0.209	5.598	10.995	3.009	1.957	0.417	2
78-2	Malumalu	48.530	3.255	16.109	10.645	0.196	4.957	10.164	3.214	2.450	0.481	2
78-10	Malumalu	48.627	3.252	15.758	10.580	0.163	4.965	10.107	3.491	2.612	0.444	2
79-2	Muli	44.232	5.043	15.262	11.764	0.229	5.401	10.162	4.357	2.520	1.030	2
79-3	Muli	44.495	5.024	15.139	11.580	0.209	5.271	10.135	4.587	2.550	1.009	2
79-5	Muli	48.855	3.153	16.510	10.307	0.243	3.822	8.401	5.013	2.580	1.117	2
79-8	Muli	48.850	3.143	16.528	10.319	0.228	3.955	8.269	4.962	2.555	1.190	2
79-18	Muli	48.876	3.046	16.681	10.241	0.255	3.813	8.022	5.319	2.661	1.086	2
80-1	Muli	46.873	4.430	15.752	12.337	0.250	4.696	8.808	4.215	1.821	0.820	2
80-28	Muli	48.194	4.849	14.002	11.626	0.169	5.757	10.540	3.146	1.223	0.493	2

Table 2-4. Isotopic compositions of Samoan lavas.

Volcano	Sample	$^{86}Sr/^{87}Sr$	$^{143}Nd/^{144}Nd$	$^{206}Pb/^{204}Pb$	$^{207}Pb/^{204}Pb$	$^{208}Pb/^{204}Pb$	$^{3}He/^{4}He$	[He] in cc/gm		$^{187}Os/^{188}Os$	Os (ppb)
Vailulu'u	**63-3**	0.705453	0.512745	19.350	15.619	39.698	-	-		0.1275	0.261
Vailulu'u	**63-5**	0.705299	0.512746	19.337	15.604	39.604	-	-		-	-
Vailulu'u	**63-13**	0.705520	0.512716	19.352	15.624	39.699	-	-		-	-
Vailulu'u	**64-1**	0.705303	0.512764	19.363	15.606	39.623	-	-		-	-
Vailulu'u	**68-3**	0.705396	-	19.337	15.621	39.651	10.04 (2)	1.16E-07	ol, gl	-	-
Vailulu'u	**68-10**	0.705373	0.512760	19.325	15.610	39.560	-	-		-	-
Vailulu'u	**68-11**	0.705594	0.512724	19.357	15.623	39.685	-	-		0.1280	2.039
Vailulu'u	**68-28**	0.705419	0.512743	19.337	15.598	39.648	-	-		-	-
Vailulu'u	**68-30**	0.705215	0.512734	19.332	15.615	39.589	-	-		-	-
Vailulu'u	**70-1**	0.705371	0.512768	19.371	15.608	39.641	-	-		-	-
Vailulu'u	**70-2**	0.705359	0.512738	19.405	15.618	39.633	-	-		-	-
Vailulu'u	**70-9**	0.705352	0.512753	19.386	15.619	39.683	8.05	5.78E-08	gl	-	-
Vailulu'u	**71-2**	0.705943	0.512743	19.332	15.605	39.680	9.48 (2)	1.76E-07	ol, gl	0.1300	1.357
Vailulu'u	**71-11**	0.705394	0.512743	19.353	15.603	39.630	9.85	5.48E-07	ol	-	-
Vailulu'u	**71-22**	0.705473	0.512747	19.358	15.602	39.635	9.64	2.99E-08	ol	-	-
Vailulu'u	**72-2**	0.705395	0.512740	19.365	15.604	39.657	-	-		-	-
Vailulu'u	**73-1**	0.706720	0.512669	19.215	15.617	39.585	8.1 (3)	2.09E-08	gl	-	-
Vailulu'u	**73-2**	0.705424	0.512742	19.329	15.621	39.616	9.28	1.07E-08	ol	-	-
Vailulu'u	**73-3**	0.705616	0.512711	19.328	15.602	39.638	-	-		-	-
Vailulu'u	**73-12**	0.706653	0.512686	19.195	15.600	39.529	-	-		0.1288	0.105
Ta'u	**T10**	0.704657	0.512789	19.291	15.623	39.497	-	-		-	-
Ta'u	**T14**	0.704591	0.512806	*18.934*	*15.590*	*39.131*	-	-		-	-
Ta'u	**T16**	0.704605	0.512818	19.290	15.601	39.426	15.13	5.73E-09	ol	0.1294	0.279
Ta'u	**T19**	0.704582	0.512790	*19.299*	*15.600*	*39.448*	-	-		-	-
Ta'u	**T21**	0.704751	0.512796	19.313	15.594	39.479	-	-		-	-
Ta'u	**T22**	0.704701	0.512773	*19.314*	*15.606*	*39.485*	-	-		-	-
Ta'u	**T23**	0.704706	0.512796	*19.288*	*15.614*	*39.476*	-	-		-	-
Ta'u	**T25**	0.704708	0.512790	-	-	-	13.26	1.05E-07	ol	0.1290	0.206
Ta'u	**T27**	0.704561	0.512806	*19.304*	*15.604*	*39.500*	-	-		-	-
Ta'u	**T30**	0.704528	0.512822	*19.305*	*15.594*	*39.382*	-	-		0.1364	0.080
Ta'u	**T32**	0.704588	0.512797	*19.208*	*15.581*	*39.332*	-	-		-	-
Ta'u	**T33**	0.704736	0.512780	19.284	15.596	39.445	16.62	4.35E-09	ol	-	-
Ta'u	**T38**	0.704651	0.512785	*19.328*	*15.617*	*39.532*	-	-		-	-
Ta'u	**T44**	0.705086	0.512755	*19.246*	*15.606*	*39.549*	14.86	9.61E-09	ol	-	-
Ta'u	**T45**	0.704434	0.512816	*19.337*	*15.595*	*39.425*	-	-		-	-
Ta'u	**T46**	0.704676	0.512795	*19.231*	*15.584*	*39.369*	-	-		-	-
Ta'u	**T47**	0.704504	0.512800	*19.253*	*15.595*	*39.366*	-	-		-	-

** Analyses in plain text are from TIMS, in italics are from MC-ICP-MS in Lyon, and underlined are from MC-ICP-MS at WHOI.

Table 2-4. Page 2

Volcano	Sample	$^{86}Sr/^{87}Sr$	$^{143}Nd/^{144}Nd$	$^{206}Pb/^{204}Pb$	$^{207}Pb/^{204}Pb$	$^{208}Pb/^{204}Pb$	$^{3}He/^{4}He$	[He] in cc/gm		$^{187}Os/^{188}Os$	Os (ppb)
Ta'u	**T48**	0.704664	0.512789	*19.249*	*15.595*	*39.397*	-	-		0.1351	0.062
Ta'u	**T51**	0.704614	0.512794	*19.276*	*15.591*	*39.425*	-	-		-	-
Ta'u	**T55**	0.704545	0.512815	19.178	15.594	39.298	-	-		-	-
Ta'u	**74-1**	0.704686	0.512786	19.29	15.599	39.443	17.97	4.97E-08	ol	0.1291	1.397
Ta'u	**74-4**	0.704815	0.512784	*19.314*	*15.601*	*39.477*	-	-		-	-
Ta'u	**75-10**	0.704533	0.512792	*19.266*	*15.597*	*39.39*	-	-		-	-
Muli	**79-4**	0.704904	0.512730	*19.279*	*15.617*	*39.517*	-	-		-	-
Muli	**79-7**	0.704524	0.512812	*19.122*	*15.581*	*39.122*	-	-		-	-
Muli	**80-23**	0.704914	0.512767	*19.177*	*15.591*	*39.305*	-	-		-	-
Malumalu	**76-1**	0.707192	0.512637	*19.338*	*15.636*	*39.847*	-	-		-	-
Malumalu	**76-8**	0.706374	0.512667	*19.294*	*15.633*	*39.710*	-	-		-	-
Malumalu	**76-9**	0.706745	0.512669	19.245	15.596	39.555	15.89	2.12E-08	ol	-	-
Malumalu	**76-13**	0.706395	0.512680	19.237	15.600	39.584	-	-		-	-
Malumalu	**77-1**	0.706930	0.512663	19.251	15.619	39.669	13.45	3.30E-08	ol	-	-
Malumalu	**77-9**	0.707260	0.512579	*19.331*	*15.635*	*39.853*	10.56	1.92E-08	ol	-	-
Malumalu	**78-1**	0.708901	0.512521	*19.237*	*15.647*	*39.862*	8.09	9.61E-08	ol	0.1293	0.130
Malumalu	**78-3**	0.708886	0.512511	19.230	15.641	39.840	8.22	9.15E-08	ol	0.1288	0.427
Malumalu	**78-8**	0.707614	0.512580	19.276	15.633	39.803	-	-		-	-
Upolu	**U10**	0.705365	0.512774	19.044	15.582	39.067	-	-		0.1407	0.013
Upolu	**U12**	-	-	18.889	15.554	38.772	-	-		-	-
Upolu	**U14**	-	-	18.878	15.560	38.767	-	-		-	-
Upolu	**U16**	0.705171	0.512883	18.881	15.559	38.787	-	-		-	-
Upolu	**U19**	0.705278	0.512870	18.917	15.569	38.832	-	-		-	-
Upolu	**U21**	0.705011	-	18.901	15.561	38.814	-	-		-	-
Upolu	**U22**	-	-	18.912	15.563	38.802	-	-		0.1509	0.022
Upolu	**U24**	0.705191	0.512854	18.955	15.569	38.875	-	-		-	-
Savai'i	**S11**	0.706195	0.512693	18.782	15.604	38.995	-	-		0.1299	0.107
Savai'i	**S12**	-	-	18.799	15.603	39.002	-	-		-	-
Savai'i	**S15**	0.706039	0.512686	18.793	15.610	39.022	-	-		-	-
Savai'i	**S16**	0.706296	0.512705	18.865	15.595	39.089	-	-		-	-
Savai'i	**S18**	0.706110	0.512730	18.884	15.596	39.118	-	-		-	-
Savai'i	**S23**	-	-	18.795	15.599	38.985	-	-		0.1270	0.491
Savai'i	**S25**	0.705848	0.512706	18.797	15.600	38.982	-	-		0.1353	0.034

** Analyses in plain text are from TIMS, in italics are from MC-ICP-MS in Lyon, and underlined are from MC-ICP-MS at WHOI.

Table 2-5. ***Sample information and chemical data for Samoan basalts collected by M. Regelous****

Volcano	Upolu	Upolu	Upolu	Upolu	Upolu	Upolu	Upolu
Sample	**U 11 F**	**U 13 F**	**U 14 F**	**U 38 F**	**U 39 F**	**U 40 F**	**U 41 F**
Volcanic Series	Fagaloa	Fagaloa	Fagaloa	Fagaloa	Fagaloa	Fagaloa	Fagaloa
Lat. (°S)	13.8537	13.8533	13.9422	13.8453	13.8512	13.8597	13.8648
Long. (°W)	171.6886	171.6582	171.5848	171.7093	171.7033	171.6523	171.6436
Major elements (wt%)							
SiO_2	48.06	45.65	45.78	48.28	47.33	47.53	46.01
Al_2O_3	15.20	13.98	15.79	15.32	13.86	14.00	13.87
TiO_2	4.24	2.92	3.65	4.28	5.09	3.88	2.96
FeO*	12.01	12.82	12.84	12.05	12.25	12.50	12.67
MnO	0.16	0.18	0.19	0.17	0.16	0.17	0.18
CaO	9.73	10.27	9.82	9.37	10.47	10.26	10.77
MgO	5.38	10.24	6.72	5.27	5.80	7.45	10.00
K_2O	1.37	0.91	0.56	1.41	1.44	0.97	0.94
Na_2O	3.22	2.59	4.00	3.22	2.92	2.75	2.16
P_2O_5	0.63	0.44	0.65	0.63	0.68	0.48	0.45
Mg#	48.44	62.63	52.31	47.85	49.82	55.54	62.35
Trace Elements (ppm)							
Ni	72	249	72	73	79	140	248
Cr	105	389	75	98	73	220	411
V	312	272	293	311	341	316	280
Ga	25	20	23	25	25	22	21
Cu	71	92	38	69	120	101	98
Zn	144	123	134	150	154	130	124
Cs	0.20	0.40	0.54	0.32	0.47	0.14	0.23
Rb	32.3	23.8	38.2	33.0	38.2	21.2	23.8
Ba	311	259	341	292	305	203	272
Th	3.79	3.17	5.27	3.77	5.08	2.64	3.27
U	1.07	0.76	1.12	1.07	1.26	0.73	0.79
Nb	52.18	40.16	52.88	51.82	58.00	35.35	40.33
Ta	3.26	2.48	3.07	3.19	3.60	2.23	2.50
La	45.10	31.13	49.32	41.43	48.93	27.74	32.16
Ce	96.38	66.54	102.63	93.74	105.67	65.00	67.97
Pb	2.82	2.40	3.72	2.98	3.48	1.70	2.27
Pr	13.21	8.21	12.34	12.49	13.99	9.03	8.43
Nd	53.08	31.72	46.48	50.08	55.92	38.14	32.80
Sr	683	521	699	664	631	494	543
Zr	324	179	243	322	335	264	183
Hf	7.79	4.35	5.71	7.71	8.13	6.46	4.51
Sm	11.24	6.62	9.25	10.61	11.76	8.76	6.82
Eu	3.60	2.11	2.89	3.36	3.66	2.79	2.18
Gd	10.52	6.11	8.19	9.57	10.63	8.18	6.33
Tb	1.46	0.87	1.14	1.34	1.46	1.17	0.89
Dy	8.11	4.82	6.25	7.37	7.97	6.56	4.95
Ho	1.49	0.88	1.13	1.33	1.42	1.21	0.90
Y	39.25	21.40	27.44	31.82	34.83	28.89	21.98
Er	3.69	2.17	2.75	3.21	3.44	2.94	2.23
Tm	0.47	0.29	0.36	0.42	0.44	0.39	0.29
Yb	2.69	1.69	2.10	2.42	2.53	2.25	1.71
Lu	0.38	0.24	0.30	0.34	0.35	0.32	0.24
Sc	22.2	22.7	19.0	21.9	25.3	25.9	24.0
$^{86}Sr/^{87}Sr$	0.705361	0.705391	0.705644		0.705180	0.704904	0.705439
$^{143}Nd/^{144}Nd$	0.512874	0.512783	0.512773			0.512907	0.512777
$^{206}Pb/^{204}Pb$	18.944	18.914	18.961	18.940	19.143	18.905	18.918
$^{207}Pb/^{204}Pb$	15.580	15.582	15.603	15.576	15.606	15.568	15.584
$^{208}Pb/^{204}Pb$	38.835	38.996	39.130	38.827	39.273	38.798	39.009

*See Appendix 1 for analytical techniques.

** Mg# = molar ratio of MgO/(MgO + 0.85*FeO)

Table 2-5, Page 2

Volcano	Upolu	Savai'i	Savai'i	Savai'i	Savai'i	Savai'i	Savai'i PE
Sample	**U 43 F**	**S 36 F**	**S 44 F**	**S 45 F**	**S 46 F**	**S 47 F**	**S 10 M**
Volcanic Series	Fagaloa	Fagaloa	Fagaloa	Fagaloa	Fagaloa	Fagaloa	Mulifanua
Lat. (°S)	13.8895	13.2642	13.2662	13.2662	13.2642	13.2637	13.3058
Long. (°W)	171.5614	172.3815	172.3677	172.3674	172.3813	172.3841	172.6411
Major elements (wt%)							
SiO_2	46.66	45.93	47.24	11.94	13.93	14.70	12.70
Al_2O_3	13.69	11.92	14.48	3.04	2.72	3.11	3.37
TiO_2	5.16	3.12	2.57	11.34	11.29	11.86	11.25
FeO*	14.15	11.59	11.86	0.16	0.16	0.16	0.15
MnO	0.18	0.16	0.16	9.70	10.35	9.18	9.26
CaO	9.76	10.05	10.19	13.24	9.34	10.16	11.01
MgO	5.46	13.21	9.62	1.61	0.94	1.08	2.10
K_2O	1.07	0.48	0.96	2.69	2.73	2.62	3.28
Na_2O	3.35	3.10	2.64	0.44	0.29	0.31	0.56
P_2O_5	0.50	0.44	0.27	71.01	63.44	64.24	67.25
Mg#	44.72	70.51	62.98	11.94	13.93	14.70	12.70
Trace Elements (ppm)							
Ni	35	386	214	385	174	202	281
Cr	4	603	339	600	423	526	440
V	389	238	252	233	251	265	224
Ga	25	19	21	19	20	22	21
Cu	84	76	73	77	81	54	63
Zn	160	120	121	115	110	122	132
Cs	0.28	0.40	0.14	0.43	0.14	0.13	0.62
Rb	25.0	55.9	23.2	48.0	25.1	16.8	55.2
Ba	213	431	235	437	224	323	543
Th	2.80	3.36	2.18	3.48	2.41	2.23	4.93
U	0.82	0.70	0.43	0.81	0.57	0.73	1.19
Nb	40.56	42.85	29.16	44.36	28.81	36.51	67.26
Ta	2.59	2.65	1.80	2.70	1.76	2.58	4.15
La	30.24	31.95	41.87	31.95	22.82	20.37	41.90
Ce	72.09	69.29	47.58	69.49	49.31	44.97	87.77
Pb	3.15	2.79	2.01	2.87	2.07	2.06	4.22
Pr	9.91	8.76	8.94	8.80	6.36	5.94	10.91
Nd	42.30	34.84	36.05	34.74	25.53	24.21	41.94
Sr	552	585	436	821	419	394	679
Zr	301	188	161	191	156	189	267
Hf	7.55	4.71	4.00	4.69	3.90	4.74	6.35
Sm	9.98	7.32	7.55	7.29	5.70	5.50	8.42
Eu	3.23	2.35	2.67	2.33	1.92	1.83	2.62
Gd	9.57	6.67	9.17	6.60	5.62	5.38	7.48
Tb	1.37	0.92	1.32	0.92	0.83	0.81	1.03
Dy	7.65	4.99	7.93	4.93	4.74	4.64	5.47
Ho	1.38	0.87	1.59	0.86	0.87	0.86	0.95
Y	33.23	20.89	46.87	20.84	21.40	21.05	23.34
Er	3.36	2.06	4.10	2.07	2.20	2.19	2.24
Tm	0.44	0.27	0.54	0.26	0.29	0.30	0.28
Yb	2.50	1.49	3.09	1.49	1.71	1.72	1.59
Lu	0.35	0.21	0.49	0.21	0.25	0.25	0.22
Sc	26.0	22.2	24.4	21.4	25.2	21.5	18.7
$^{86}Sr/^{87}Sr$	0.705179	0.705823	0.706670	0.705856	0.706338		0.706528
$^{143}Nd/^{144}Nd$	0.512883	0.512702		0.512698	0.512678	0.512725	0.512682
$^{206}Pb/^{204}Pb$	18.848	18.801		18.804	18.866	18.821	18.803
$^{207}Pb/^{204}Pb$	15.564	15.609		15.612	15.613	15.604	15.615
$^{208}Pb/^{204}Pb$	38.783	39.012		39.024	39.159	39.022	39.019

Table 2-5, Page 3

Volcano	Savai'i PE	Savai'i PE	Savai'i PE	Savai'i PE	Savai'i PE	Savai'i PE	Savai'i PE
Sample	**S 15 Ma**	**S 26 S**	**S 28 Pb**	**S 31 P**	**S 32 M**	**S 33 P**	**S 34 A**
Volcanic Series	Mulifanua	Salani	Puapua	Puapua	Mulifanua	Puapua	Aopo
Lat. (°S)	13.3094	13.4327	13.4611	13.4753	13.3799	13.3099	13.318
Long (°W)	172.7021	172.314	172.3728	172.513	172.6655	172.7404	172.5523
Major elements (wt%)							
SiO_2	44.62	45.51	48.64	48.76	45.39	48.05	45.89
Al_2O_3	12.40	12.64	14.20	14.18	11.84	14.25	12.38
TiO_2	3.30	3.24	3.01	2.96	3.83	2.73	3.13
FeO*	11.46	11.80	10.58	10.48	12.11	10.91	11.23
MnO	0.16	0.15	0.14	0.14	0.15	0.15	0.16
CaO	10.48	9.07	8.07	8.05	9.07	8.57	9.51
MgO	11.92	12.04	8.98	9.08	12.75	9.76	12.31
K_2O	1.91	1.80	2.09	2.06	1.88	1.68	1.78
Na_2O	3.04	3.25	3.73	3.72	2.62	3.28	3.15
P_2O_5	0.71	0.52	0.56	0.56	0.36	0.61	0.47
Mg#	68.57	68.14	64.03	64.50	68.82	65.24	69.68
Trace Elements (ppm)							
Ni	275	329		233	361	236	340
Cr	500	405		315	520	350	535
V	244	238		196	268	201	240
Ga	21	22		23	22	22	20
Cu	69	59		55	75	50	60
Zn	128	139		133	134	129	118
Cs	0.58	0.52		0.75	0.65	0.48	0.50
Rb	51.0	46.1		61.4	55.2	44.9	49.3
Ba	500	388		451	399	503	401
Th	6.34	3.39		5.33	2.82	4.75	3.94
U	1.43	0.89		1.39	0.73	1.11	0.87
Nb	70.27	54.93		55.33	50.96	55.28	50.26
Ta	4.27	3.42		3.55	3.63	3.43	3.28
La	54.90	32.20		36.37	24.26	39.62	36.60
Ce	112.66	71.92		75.05	54.51	81.56	77.21
Pb	5.24	3.06		4.21	2.32	3.94	3.08
Pr	13.50	9.34		9.26	7.17	9.82	9.48
Nd	50.24	37.53		35.63	29.73	37.02	36.57
Sr	748	670		610	491	606	556
Zr	272	251		284	250	253	225
Hf	6.39	6.00		6.64	6.40	5.93	5.57
Sm	9.59	8.09		7.55	6.66	7.50	7.58
Eu	2.92	2.57		2.43	2.15	2.37	2.30
Gd	8.11	7.31		7.00	6.18	6.83	6.88
Tb	1.11	1.02		0.99	0.86	0.98	0.95
Dy	5.78	5.35		5.31	4.60	5.46	5.15
Ho	0.99	0.91		0.91	0.79	0.98	0.90
Y	24.41	21.99		22.24	19.21	24.02	21.52
Er	2.39	2.10		2.14	1.87	2.39	2.11
Tm	0.30	0.26		0.28	0.24	0.31	0.27
Yb	1.67	1.43		1.54	1.31	1.84	1.53
Lu	0.24	0.20		0.22	0.18	0.26	0.22
Sc	21.3	18.4		15.8	20.4	17.2	20.3
$^{86}Sr/^{87}Sr$	0.706435	0.705597	0.705784	0.705765	0.705267	0.705451	0.706409
$^{143}Nd/^{144}Nd$			0.512747	0.512751	0.512795	0.512776	
$^{206}Pb/^{204}Pb$	18.888	18.793	18.776	18.777	18.842	18.682	18.796
$^{207}Pb/^{204}Pb$	15.623	15.580	15.602	15.598	15.589	15.603	15.607
$^{208}Pb/^{204}Pb$	39.163	38.866	38.938	38.921	39.017	38.856	39.051

Table 2-5, Page 4

Volcano	Savai'i PE	Savai'i PE	Savai'i PE	Savai'i PE	Savai'i PE	Savai'i PE	Upolu PE
Sample	**S 35 P**	**S 39 A**	**S 42 A**	**S 43 P**	**S 50 S**	**S 52 M**	**U 10 S**
Volcanic Series	Puapua	Aopo	Aopo	Puapua	Salani	Mulifanua	Salani
Lat. (°S)	13.2957	13.2703	13.2673	13.32	13.3596	13.42	13.8368
Long.(°W)	172.4654	172.3123	172.3106	172.2362	172.2673	172.2024	171.7362
Major elements (wt%)							
SiO_2	48.30	47.33	46.05	44.72	45.94	45.83	48.41
Al_2O_3	13.32	12.47	11.76	11.45	12.59	11.98	15.15
TiO_2	2.94	2.70	2.83	3.67	3.27	3.04	4.23
FeO*	11.29	11.71	11.98	12.42	12.37	11.45	11.88
MnO	0.15	0.16	0.16	0.16	0.17	0.15	0.16
CaO	9.44	9.45	9.28	9.13	9.79	9.24	9.64
MgO	10.16	12.04	13.75	14.06	11.95	13.33	5.21
K_2O	1.23	0.96	1.19	1.56	1.32	1.59	1.40
Na_2O	2.84	2.88	2.66	2.45	2.32	2.86	3.26
P_2O_5	0.33	0.31	0.35	0.39	0.27	0.52	0.65
Mg#	65.38	68.32	70.64	70.37	66.94	70.93	47.92
Trace Elements (ppm)							
Ni	255	340	412		302	402	62
Cr	456	570	594		552	491	86
V	236	231	231		266	223	309
Ga	21	20	19		21	20	25
Cu	55	72	66		83	65	78
Zn	114	121	124		123	126	146
Cs	0.15	0.30	0.36		0.51	0.66	0.31
Rb	29.5	24.8	31.0		38.6	44.0	33.7
Ba	277	245	288		314	438	298
Th	2.44	2.44	2.91		1.88	4.35	3.87
U	0.55	0.57	0.70		0.46	1.06	1.08
Nb	38.69	31.82	36.65		47.12	51.33	52.29
Ta	2.73	2.12	2.40		3.45	3.13	3.27
La	21.29	22.02	26.43		19.08	37.49	42.54
Ce	47.10	47.50	56.59		44.93	78.41	97.06
Pb	3.18	1.98	2.38		1.72	3.78	3.03
Pr	6.10	6.08	7.15		6.04	9.67	12.72
Nd	25.00	24.42	28.34		25.09	37.30	51.10
Sr	402	398	437		409	794	676
Zr	187	159	175		211	225	326
Hf	4.95	4.16	4.47		5.53	5.39	7.96
Sm	5.76	5.60	6.13		5.62	7.70	10.63
Eu	1.90	1.81	1.92		1.85	2.44	3.33
Gd	5.70	5.57	5.84		5.38	6.94	9.68
Tb	0.84	0.83	0.85		0.77	0.97	1.37
Dy	4.75	4.74	4.73		4.29	5.20	7.50
Ho	0.86	0.87	0.85		0.77	0.90	1.35
Y	20.55	20.92	20.49		18.63	21.87	32.62
Er	2.12	2.16	2.09		1.90	2.15	3.32
Tm	0.28	0.28	0.27		0.25	0.27	0.44
Yb	1.60	1.61	1.54		1.43	1.53	2.50
Lu	0.23	0.23	0.22		0.20	0.21	0.35
Sc	21.5	22.1	20.8		22.5	19.0	21.6
$^{86}Sr/^{87}Sr$		0.705564	0.705793	0.706018	0.706907	0.705686	0.705363
$^{143}Nd/^{144}Nd$		0.512705		0.512712	0.512711	0.512736	0.512870
$^{206}Pb/^{204}Pb$	18.853	18.803	18.792		18.901	18.746	18.940
$^{207}Pb/^{204}Pb$	15.602	15.607	15.607		15.611	15.602	15.577
$^{208}Pb/^{204}Pb$	39.071	39.039	39.044		39.150	38.916	38.826

Table 2-5, Page 5

Volcano	Upolu PE	Upolu PE	Upolu PE	Upolu PE	Upolu PE	Upolu PE	Upolu PE
Sample	**U 15 S**	**U 16 S**	**U 17 S (1)**	**U 17 S (2)**	**U 21 S**	**U 23 P**	**U 24 L**
Volcanic Series	Salani	Salani	Salani	Salani	Salani	Puapua	Lefaga
Lat. (°S)	13.9983	14.0306	14.0357	Same Flow	13.9541	14.0221	13.9668
Long. (°W)	171.4222	171.4325	171.4619	Few meters	171.7674	171.731	171.9434
Major elements (wt%)							
SiO_2	44.68	47.20	45.13		45.29	41.85	44.11
Al_2O_3	12.02	12.21	11.67		12.26	11.79	12.63
TiO_2	4.53	3.99	3.96		3.45	4.52	3.62
FeO*	12.55	12.32	12.33		12.61	13.48	12.32
MnO	0.16	0.15	0.16		0.17	0.17	0.17
CaO	9.96	8.99	9.87		10.45	10.91	10.83
MgO	11.63	10.57	11.94		11.51	11.14	11.04
K_2O	1.66	1.54	1.51		1.19	1.85	1.40
Na_2O	2.21	2.67	2.88		2.52	3.56	3.15
P_2O_5	0.59	0.36	0.56		0.55	0.72	0.72
Mg#	66.02	64.28	67.00		65.68	63.42	65.27
Trace Elements (ppm)							
Ni	315		327		284	248	240
Cr	427		430		441	325	419
V	275		257		245	288	270
Ga	22		20		21	21	21
Cu	21		81		67	66	69
Zn	151		134		131	145	128
Cs	0.19		0.47		0.43	0.63	0.19
Rb	43.7		56.8		31.9	53.3	38.4
Ba	533		466		403	677	486
Th	4.41		3.73		4.54	6.73	7.17
U	1.06		0.87		1.03	1.43	0.93
Nb	50.54		45.98		45.85	72.56	54.02
Ta	3.09		2.85		2.80	4.09	3.03
La	41.63		36.96		42.94	63.55	65.36
Ce	88.37		79.28		89.24	129.64	130.00
Pb	2.26		2.99		3.68	4.95	4.48
Pr	11.01		9.96		11.00	15.49	14.99
Nd	43.34		39.79		42.36	57.75	53.99
Sr	643		613		623	892	823
Zr	219		203		225	264	231
Hf	5.49		5.24		5.70	6.36	5.40
Sm	9.01		8.54		8.54	11.03	10.00
Eu	2.76		2.61		2.60	3.37	3.00
Gd	8.27		7.84		7.52	9.40	8.39
Tb	1.13		1.09		1.04	1.28	1.16
Dy	6.06		5.89		5.69	6.70	6.23
Ho	1.04		1.02		0.99	1.15	1.09
Y	24.89		24.32		23.80	27.84	27.05
Er	2.41		2.38		2.35	2.64	2.63
Tm	0.30		0.30		0.30	0.32	0.33
Yb	1.67		1.66		1.67	1.78	1.94
Lu	0.23		0.23		0.23	0.24	0.27
Sc	21.3		21.2		21.4	21.5	22.3
$^{86}Sr/^{87}Sr$		0.706088	0.705813	0.705750	0.705393	0.705536	0.705670
$^{143}Nd/^{144}Nd$			0.512711	0.512713	0.512662	0.512671	0.512666
$^{206}Pb/^{204}Pb$	18.785		18.711			18.577	
$^{207}Pb/^{204}Pb$	15.623		15.607			15.611	
$^{208}Pb/^{204}Pb$	39.004		38.871			38.775	

Table 2-5, Page 6

Volcano	Upolu PE	Upolu PE	Upolu PE	Upolu PE	Upolu PE	Upolu PE	Upolu PE
Sample	**U 26 L**	**U 28 L**	**U 30 L**	**U 32 M**	**U 33 M**	**U 35 M (1)**	**U 35 M (2)**
Volcanic Series	Lefaga	Lefaga	Lefaga	Mulifanua	Mulifanua	Mulifanua	Mulifanua
Lat. (°S)	13.9728	13.9677	13.9804	13.7917	13.8265	13.8359	Same Flow
Long.(°W)	171.9399	171.9416	171.9329	171.9007	171.9974	171.9469	Few meters
Major elements (wt%)							
SiO_2	41.64	42.25	42.10	44.65	48.37	41.58	
Al_2O_3	11.95	11.58	11.74	12.14	13.63	11.14	
TiO_2	5.82	5.63	5.67	4.31	3.34	6.58	
FeO*	14.39	13.92	14.02	13.14	11.30	14.55	
MnO	0.18	0.16	0.17	0.16	0.14	0.17	
CaO	10.26	9.90	10.03	9.67	9.01	9.97	
MgO	11.67	11.44	11.45	12.35	8.12	11.77	
K_2O	1.20	1.65	1.54	1.27	1.92	1.39	
Na_2O	2.29	2.87	2.69	1.99	3.50	2.42	
P_2O_5	0.61	0.59	0.58	0.34	0.68	0.42	
Mg#	62.99	63.29	63.14	66.35	60.11	62.92	
Trace Elements (ppm)							
Ni	299	301		357	171	328	
Cr	376	375		489	204	460	
V	322	320		292	189	379	
Ga	22	22		20	23	20	
Cu	67	69		68	29	87	
Zn	145	145		129	142	140	
Cs	0.54	0.54		0.29	0.51	0.41	
Rb	37.8	50.2		32.3	47.9	40.4	
Ba	509	499		425	576	429	
Th	5.00	4.90		2.26	4.86	3.81	
U	1.07	1.08		0.47	1.14	0.84	
Nb	61.34	60.31		35.56	49.91	48.46	
Ta	3.73	3.66		2.40	2.84	3.08	
La	47.75	47.09		24.93	44.65	36.18	
Ce	100.15	98.79		52.55	91.89	77.47	
Pb	3.51	3.37		1.94	4.03	2.74	
Pr	12.26	12.15		7.00	11.32	9.72	
Nd	46.86	46.38		28.67	44.05	37.78	
Sr	704	689		641	766	524	
Zr	260	256		186	235	226	
Hf	6.51	6.33		4.99	5.72	6.02	
Sm	9.58	9.39		6.48	9.30	7.92	
Eu	2.95	2.88		2.08	2.98	2.46	
Gd	8.50	8.32		6.25	8.54	7.21	
Tb	1.18	1.15		0.89	1.19	1.01	
Dy	6.19	6.08		4.83	6.27	5.56	
Ho	1.08	1.06		0.87	1.07	0.99	
Y	25.96	25.48		21.69	26.33	23.61	
Er	2.49	2.44		2.09	2.46	2.35	
Tm	0.31	0.30		0.27	0.30	0.30	
Yb	1.73	1.68		1.53	1.64	1.74	
Lu	0.24	0.23		0.21	0.22	0.23	
Sc	22.8	22.6		23.8	16.1	27.4	
$^{86}Sr/^{87}Sr$	0.705620	0.705594	0.705379	0.706113	0.705664	0.705631	0.705607
$^{143}Nd/^{144}Nd$	0.512728	0.512684	0.512881	0.512734	0.512690	0.512668	0.512656
$^{206}Pb/^{204}Pb$		18.696				18.681	
$^{207}Pb/^{204}Pb$		15.610				15.606	
$^{208}Pb/^{204}Pb$		38.878				38.883	

Table 2-5, Page 7

Volcano	Upolu PE	BHVO-1 Standard		
Sample	**U 37 P**			
Volcanic Series	Puapua			
Lat. (°S)	14.0068			
Long. (°W)	171.7292	Long-term average, U. Queensland		
Major elements (wt%)				
SiO_2	41.75			
Al_2O_3	11.84			
TiO_2	4.45	Ti 49	16376	1.02
FeO*	13.34			
MnO	0.18			
CaO	10.92			
MgO	11.06			
K_2O	1.86			
Na_2O	3.92			
P_2O_5	0.69			
Mg#	63.49			
Trace Elements (ppm)				
Ni	241	Ni 60	116	2.57
Cr	312	Cr 52	295	2.37
V	290	V 51	286	1.39
Ga	21	Ga 71	21.2	1.18
Cu	67	Cu 65	137	0.94
Zn	142	Zn 66	106	1.81
Cs	0.63	Cs 133	0.0967	1.21
Rb	53.6	Rb 85	9.27	0.83
Ba	678	Ba 137	132	0.75
Th	6.58	Th 232	1.19	1.09
U	1.39	U 238	0.433	1.09
Nb	71.19	Nb 93	18.4	0.86
Ta	4.04	Ta 181	1.15	1.31
La	61.31	La 139	15.1	0.74
Ce	125.23	Ce 140	37.7	0.65
Pb	95.09	Pb 208	1.97	3.87
Pr	15.00	Pr 141	5.45	0.55
Nd	55.86	Nd 146	24.1	0.52
Sr	861	Sr 86	394	0.52
Zr	256	Zr 90	165	0.94
Hf	6.20	Hf 178	4.37	1.28
Sm	10.69	Sm 149	5.95	0.79
Eu	3.27	Eu 151	2.04	0.98
Gd	9.10	Gd 160	5.97	0.68
Tb	1.25	Tb 159	0.886	0.97
Dy	6.59	Dy 161	5.11	0.85
Ho	1.13	Ho 165	0.953	0.84
Y	27.60	Y 89	22.9	0.76
Er	2.63	Er 167	2.42	1.32
Tm	0.32	Tm 169	0.324	1.28
Yb	1.79	Yb 172	1.90	1.05
Lu	0.24	Lu 175	0.268	1.36
Sc	22.2	Sc 45	29.9	1.68
$^{86}Sr/^{87}Sr$	0.705492			
$^{143}Nd/^{144}Nd$	0.512618			
$^{206}Pb/^{204}Pb$				
$^{207}Pb/^{204}Pb$				
$^{208}Pb/^{204}Pb$				

*Table 2-6. Isotopic compositions of samples previously collected by KAF**.*

Volcano	Sample	Type	$^{86}Sr/^{87}Sr$	$^{143}Nd/^{144}Nd$	$^{3}He/^{4}He$	$^{206}Pb/^{204}Pb$	$^{207}Pb/^{204}Pb$	$^{208}Pb/^{204}Pb$
Tutuila	91TP-128	upper shield	0.705535	0.512846	-	-	-	-
Tutuila	91TP-134	dike	0.705195	0.512821	24.67	19.065	15.614	39.13
Tutuila	91TP-165	dike	0.705166	0.5128	25.79	-	-	-
Tutuila	91TP-201	dike	0.704971	0.512825	20.49	19.199	15.59	39.171
Tutuila	91TP-133	lower shield	0.70609	0.512709	17.44	-	-	-
Tutuila	91TP-203	lower shield	0.707863	0.512595	14.83	19.106	15.625	39.526
Tutuila	91TP-207	lower shield	0.707143	0.512644	13.97	-	-	-
Tutuila	91TP-144	upper shield	0.705317	0.512858	-	-	-	-
Tutuila	91TP-196	upper shield	0.704476	0.5129	-	18.806	15.543	38.656
Tutuila	91TP-228	upper shield	0.705225	0.512453	-	-	-	-
Tutuila	91TP-252	upper shield	0.706354	0.512657	14.44	-	-	-
Tutuila	91TPK-5	upper shield	0.705192	0.512803	22.59	19.124	15.646	39.224
Upolu	91UF-65B	shield	0.70547	0.512783	11.4	18.974	15.615	39.126
Upolu	91UF-86	shield	0.706389	0.512725	10.25	-	-	-
Upolu	91UF-89B	shield	0.705245	0.512772	16.78	-	-	-
Upolu	91UFK-4	shield	0.705147	0.512851	16.7	-	-	-
Upolu	91UFK-6A	shield	0.704821	0.51285	12.28	18.988	15.627	39.171
Upolu	UPO-10C	shield	0.706447	0.512743	11.27	-	-	-
Upolu	UPO-F-19	shield	0.705133	0.512833	15.8	-	-	-
Upolu	UPO-F-20	shield	0.70522	0.512859	12.92	-	-	-
Upolu	UPO-F9-7	shield	0.70493	0.512912	13.8	-	-	-
Manua	82MT11	shield	0.704569	0.512833	15.23	-	-	-
Manua	82MT17	shield	0.704649	0.512783	13.34	-	-	-
Manua	82MT18	shield	0.704661	0.512781	13.54	-	-	-
Manua	82MT8B	shield	0.704637	0.512776	19.06	19.316	15.593	39.445
Savaii	91SVK-1	PE	0.705589	0.512721	13.7	-	-	-
Savaii	91SVK7	COBBLE	0.7072	0.51277	-	18.872	15.587	39.021

** Analytical techniques as described in Farley et al. (1992).

Table 2-7. Calculated trace element composition of a "pure" EM2 melt.

	Average Ta'u	Average Malumalu	EM2 Melt
$^{87}Sr/^{86}Sr$	0.7046	0.70889	0.7128
Cs	0.11	0.41	0.70
Rb	15.17	44.73	73.47
Ba	146.96	281.99	413.29
Th	2.78	6.17	9.46
U	0.62	1.16	1.69
Nb	29.71	43.96	57.83
Ta	2.06	2.92	3.76
K	0.73	1.57	2.39
La	24.16	44.31	63.90
Ce	50.61	82.17	112.85
Pb	2.09	4.35	6.56
Pr	6.27	9.16	11.98
Nd	27.24	34.89	42.33
Sr	367.00	379.09	390.83
Zr	187.15	205.43	223.20
Hf	4.82	5.20	5.57
Sm	6.74	7.15	7.56
Eu	2.15	1.99	1.84
Ti	2.99	2.20	1.42
Gd	6.41	6.28	6.15
Tb	0.95	0.87	0.79
Dy	5.21	4.59	4.00
Ho	0.94	0.80	0.67
Y	24.00	21.89	19.84
Er	2.26	1.91	1.57
Tm	0.29	0.25	0.21
Yb	1.67	1.40	1.13
Lu	0.24	0.21	0.17
Sc	25.76	25.77	25.79

**All reported as ppm except K and Ti in wt%.

**All samples in averages are olivine corrected to Mg# 73.

Table 2-8. Source composition of EM2

	Primitive Mantle* (ppm)	Depleted mantle (2% melt depleted) (ppm)	Bulk D values	EM2 Source (ppm)	PUM Normalized
Rb	0.6	0.140	0.00001	1.456	2.427
Ba	6.6	1.587	0.00008	15.857	2.403
Th	0.0795	0.020	0.00058	0.177	2.224
U	0.0203	0.006	0.0016	0.040	1.968
Nb	0.658	0.289	0.0040	1.087	1.653
Ta	0.037	0.019	0.0042	0.063	1.698
La	0.648	0.287	0.0067	0.895	1.381
Ce	1.675	0.823	0.0117	1.923	1.148
Pb	0.15	0.027	0.0092	0.144	0.959
Pr	0.254	0.146	0.0214	0.251	0.987
Nd	1.25	0.772	0.0317	1.140	0.912
Sr	19.9	10.803	0.0185	20.044	1.007
Zr	10.5	6.686	0.0472	8.835	0.841
Hf	0.283	0.195	0.0644	0.238	0.841
Sm	0.406	0.290	0.0692	0.347	0.855
Eu	0.154	0.114	0.1088	0.128	0.829
Ti	1072.1	829.471	0.1428	900.5	0.840
Gd	0.544	0.417	0.1800	0.445	0.818
Tb	0.099	0.079	0.2730	0.082	0.826
Dy	0.674	0.554	0.3504	0.569	0.845
Ho	0.149	0.125	0.4649	0.127	0.853
Y	4.3	3.651	1.0829	3.655	0.850
Er	0.438	0.374	0.5708	0.378	0.864
Yb	0.441	0.387	1.0784	0.387	0.878

* Primtive Upper Mantle (PUM) from McDonough and Sun (1995).

Chapter 3:

Major and Trace Element Composition of the Depleted MORB Mantle (DMM)*

Abstract

We derive an estimate for the chemical composition of the depleted MORB mantle (DMM), the source reservoir to mid-ocean ridge basalts (MORBs), which represents at least 30% the mass of the whole silicate Earth. A database for the chemical and physical properties of abyssal peridotites has become robust and complete enough to truly access a reference DMM. Using trace element depletion trends from the abyssal peridotites, it is possible to construct a large part of DMM's trace element pattern. Splicing this information with isotopic constraints (Sr-Nd-Pb-Hf) and canonical ratios (Ce/Pb, Nb/Ta, Nb/U, Ba/Rb, H_2O/Ce, CO_2/Nb and Cl/K), we can extend abundance estimates to all the incompatible elements including volatile content. The resulting trace element pattern for average DMM constrains parental MORB to be generated by 6% aggregated fractional melting – consistent with recent models for hydrous melting of the mantle (Asimow et al., 2004). We show that DMM is roughly balanced by the continental crust and better balanced upon inclusion of ocean island basalt source and oceanic crust components. Compared to the primitive mantle, DMM has been depleted by 2-3% melt extraction and has only 15% the radiogenic heat production.

* Published in EPSL Volume 231, Feb. 2005

1. Introduction

The trace element composition of the depleted upper mantle (DMM) is a fundamental parameter in modeling the generation of mid-ocean ridge basalts (MORBs), calculating the crust-mantle mass balance, and establishing the chemical and thermal evolution of the Earth. To date, all attempts to establish an average composition for the upper mantle, whether by parent/daughter derivations from isotopic systems (Allègre et al., 1983; Galer and O'Nions; 1985; Albarede and Brouxel, 1987; Shimizu, 1998; Elliot et al., 1999; Salters and Stracke, 2004) or by MORB trace element inversions (Salters and Stracke, 2004; McKenzie and O'Nions, 1991, Hofmann, 1988, Sun and McDonough, 1989), have centered on MORB liquids and include major assumptions about melt generation, melt transport and differentiation processes that have affected these upper mantle melts. Unfortunately, it is just these processes that we are trying to understand, rather than assume *a priori*.

The most compelling evidence for upper mantle depletion comes from the heavy-element isotopic composition of MORBs. Although MORBs and their residues, abyssal peridotites, have some degree of heterogeneity in radiogenic isotope ratios (Sr-Nd-Pb-Hf), they are focused within a small range of values relative to ocean island basalts and are, with very few exceptions, depleted from bulk earth values in $^{87}Sr/^{86}Sr$, $^{143}Nd/^{144}Nd$ and $^{176}Hf/^{177}Hf$, thus requiring a long-term history of low Rb/Sr, Hf/Lu and Nd/Sm (i.e. incompatible element depletion). Direct evidence for upper mantle depletion came with the classic trace element studies of Johnson et al. (1990) and Johnson and Dick (1992) on abyssal peridotites, but most of the observed depletion in these peridotites is due to melt extraction during the latest spreading events, so that the composition of the general ambient upper mantle has been severely overprinted by this latest melting episode.

Ultimately, we know that this mantle, which has been estimated to comprise 30-70% by mass of the bulk silicate earth, has been depleted over time in the highly incompatible (lithophile) elements (Allègre et al., 1983; Hofmann, 1988, refs. therein). Most models ascribe the depletion of the upper mantle to the extraction of the enriched continental crust, a process that has removed up to 90% of the most incompatible elements, and 80-85% of the heat-producing elements (e.g. Hofmann, 1988). Some part of the depletion may also be created by the preservation of recycled oceanic crust that is currently sequestered in unknown regions of the mantle. It is possible the lower mantle (below 670 km) has also been depleted by such processes, but this question is highly controversial at present.

In place of assuming a set of bulk partition coefficients or a degree of melt extraction, we use in this paper the following constraints in deriving an average trace element composition of DMM: 1) trace element content of clinopyroxenes from abyssal peridotites, 2) isotopic evolution from primitive upper mantle (PUM) and 3) canonical trace element ratios in MORBs. Abyssal peridotite data from the literature, the backbone of this study, are treated in a way reminiscent of studies such as Loubet et al. (1975), Hart and Zindler (1986) and McDonough and Sun (1995). Abyssal peridotites, unlike basalts, are not modified by secondary processes such as fractional crystallization, magma mixing and crustal assimilation (Dick et al., 1984), but may be subject to melt impregnation (Dick, 1989) and melt/rock reaction (Kelemen et al., 1992). We show that melt impregnation can be recognized and therefore filtered from the abyssal peridotite dataset and suggest that melt/rock reaction in the dataset we have used has had more effect on major element chemistry than trace element chemistry. Overall, it seems that, for the moderately incompatible elements, abyssal peridotites more accurately record the trend of upper mantle depletion than do MORBs.

The average trace element content of DMM, as deduced here, generally shows a very smooth pattern with increasing trace element compatibility, which to first order mass-balances with the continental crust. The degree of depletion indicated in DMM represents 2-3% melt removal from the primitive upper mantle (PUM) of McDonough and Sun (1995); this means that DMM has only 15% the radiogenic heat production of PUM (from K, U and Th). Present-day ocean crust (i.e. MORBs) can be modeled with 6% aggregated fractional melting of the deduced DMM.

2. Trace Element Composition of DMM

2.1 Abyssal Peridotites

Abyssal peridotites have been shown to be residues of fractional or near-fractional melting that produces MORB (e.g. Johnson et al., 1990). Although bulk trace element compositions of these peridotites are heavily modified by alteration on the seafloor, many workers have analyzed the trace element compositions (Sr, Zr, Ti, Ce, Nd, Sm, Eu, Gd, Dy, Er, Yb, and Y) of relict, unaltered clinopyroxene grains as a means of chemical characterization (Johnson et al., 1990; Johnson and Dick, 1992; Dick and Natland, 1996; Hellebrand et al., 2002; Salters and Dick, 2002; Tartarotti et al., 2002). Using such

clinopyroxene compositions, bulk compositions ($C_{WholeRock}$) of the peridotites can be calculated for each trace element with the following equation:

$$C_{WholeRock} = C_{cpx}\left(\frac{D_{bulk}}{D_{cpx}}\right) \quad (1)$$

where the bulk partition coefficient (D_{bulk}) is determined from modal abundances ($x_{mineral}$) of olivine (ol), orthopyroxene (opx), clinopyroxene (cpx) and spinel (sp), and mineral/melt partition coefficients ($D_{mineral}$) as follows:

$$D_{bulk} = x_{ol}D_{ol} + x_{opx}D_{opx} + x_{cpx}D_{cpx} + x_{sp}D_{sp} \quad (2)$$

This method of calculating bulk peridotite compositions is a substitute for a more accurate method, which would be to sum the concentrations of trace elements in minerals according to their modal proportions. Converting to whole rock compositions from clinopyroxene alone is done simply due to the fact that almost no trace element data exists for other minerals in the peridotite samples.

We have compiled a data set from the literature that includes abyssal peridotites having both cpx trace element analyses and modal abundances (data sources are Johnson et al., 1990; Johnson and Dick, 1992; Dick et al., 1984; Dick and Natland, 1996; Hellebrand et al., 2002; Salters and Dick, 2002; Tartarotti et al., 2002). All samples containing more than 1% modal plagioclase are excluded on the basis that most plagioclase in abyssal peridotites has been interpreted as a secondary phase representative of melt impregnation (Dick, 1989; Tartarotti et al., 2002); as a result, only 5 out of almost 90 samples included have any reported modal plagioclase at all. Anomalously high Ce and Sr values have also been excluded for some samples. For Sr, some anomalous values are suspected seawater alteration; such Sr anomalies are not accompanied by Eu anomalies and therefore are not suspected to be plagioclase reaction products. For both Sr and Ce, the most incompatible elements of the sample suite and therefore the most depleted in abyssal peridotites, elevated concentrations are probably due to small amounts of melt impregnation (see discussion below).

The final trace element data set for the abyssal peridotites, corrected to whole rock compositions using mineral/melt partition coefficients from Kelemen et al. (2003),

published modal abundances and the above equations, is shown in Figure 1 and the Supp. Data Table 1. It is important to note that the geographical distribution of the sample suite is highly focused on the Southern Ocean; 90% of the samples originate from the American-Antarctic, Southwest Indian and Central Indian Mid-Ocean Ridges, with the remaining 10% obtained from the Mid-Atlantic Ridge and East Pacific Rise. The question of whether or not this geographical bias manifests as a chemical bias will not be answered until larger datasets from other localities are established.

The purpose of compiling bulk rock information is to derive the inter-relationships between different trace elements (i.e. to what degree the various incompatible trace elements are depleted relative to each other over the entire history of mantle depletion). A formulation of the trace element "system" begins by interpreting the trace element compositions of peridotites using the equation for a residue of fractional melting (see Zou, 1998, for review of melting models). Calculations show that modal fractional melting used to interpret residues of melting is a fine approximation for any number of more complicated melting models (see Appendix 1). The ratio of the concentration of a given element in a solid, C_s, to its original concentration, C_o, after some fraction of melting, F, is as follows:

$$\frac{C_s}{C_o} = (1-F)^{(\frac{1}{D}-1)} \tag{3}$$

where D is the bulk solid/melt partition coefficient for modal melting.

The relationship between the concentrations of two elements in the residue, [A] and [B], can be linearized upon equating two equations solved for F:

$$\ln(C_s^A) = R\ln(C_s^B) + \ln\left(\frac{C_o^A}{\left(C_o^B\right)^R}\right) \tag{4}$$

where the slope, R, on the linear ln([A]) versus ln([B]) array is a function of the bulk partition coefficients for elements A and B:

$$R = \frac{D_B(1-D_A)}{D_A(1-D_B)} \tag{5}$$

Given that we have information for 12 different elements (see fig. 1), there are 132 of the ln([A]) vs. ln([B]) relationships to consider in the overall reduction of this dataset;

Figure 2 shows a sampling of these linear arrays, with the more incompatible of a given element pair plotted on the x-axis. The peridotites show an extremely wide range in degree of depletion and form well-correlated depletion trends for upper mantle melting. Correlations are best for those element pairs having similar bulk D values (see the Sm-Nd, Sm-Eu and Dy-Er panels in fig. 2), and fall off slightly for elements with increasingly dissimilar bulk D's (see Zr-Ti and Sm-Yb). Some of the scatter in correlations may have been produced by melt impregnation. For instance, impregnation of low degree melts into highly depleted residues would cause points to fall off the depletion trends toward the more incompatible element, as shown in Figure 2. Melt impregnation trajectories for relationships among the HREE (e.g. Dy-Er) very closely overlap their well-correlated arrays (not shown for clarity), thereby indicating that melt impregnation has none to very little effect on the slopes or positions of these depletion trends.

The ln([A]) vs. ln([B]) depletion trends have been fit by a York (1996) two-error regression (fig. 2), assuming a blanket error of 10% for all points. The regressions have also been forced through the primitive upper mantle (PUM) coordinate of McDonough and Sun (1995); most regressions intersect the PUM coordinate without forcing, but this treatment becomes appropriate for some regressions with poor correlations (for example, see the Ce-Nd panel in fig. 2) and we find it necessary for obtaining robust output from the regression scheme.

The upper mantle is certainly not a unique composition (isotopic or otherwise), but rather a range of compositions reflecting variable amounts of depletion and/or re-enrichment. A given peridotite's bulk trace element composition represents the culmination of melt depletion and enrichment over the entire history of that peridotite. Also, integrated within the trace element trends (fig. 2) is the net transfer of material out of the mantle by oceanic and continental crust generation as well as crustal recycling, in so far as the recycled material is well-mixed within the upper mantle. In this sense, some of the more complicated processes affecting upper mantle composition are incorporated into the abyssal peridotite trends, but are not required to explain the trace element data.

Knowing that much of the depletion observed in abyssal peridotites is caused by the most recent melting event, we need to define where today's *average*, *unmelted* upper mantle lies on the depletion trends. For this we need another constraint, the most obvious being the isotopic evolution of DMM: calculating the present-day Sm/Nd ratio from $^{143}Nd/^{144}Nd$ signatures in MORBs defines a unique position on the abyssal peridotite depletion trends.

2.2 Isotope Constraints

Although there has been much written on the homogeneity of MORBs relative to OIBs (Zindler and Hart,1986; Hart, 1988; Hofmann, 1997), it is clear from the global database (fig. 3) that the MORB mantle is not one sole isotopic composition and by inference not one sole trace element composition. The variation in MORB $^{87}Sr/^{86}Sr$, $^{143}Nd/^{144}Nd$, and $^{206}Pb/^{204}Pb$ compared to all oceanic basalts is 18%, 35% and 47%, respectively. To address this issue of compositional heterogeneity in the upper mantle we derive three different trace element compositions for the MORB source by calculating present-day parent/daughter ratios from isotopic signatures and relating those ratios to the abyssal peridotite depletion trends. A study by Su and Langmuir (2003), who have filtered global MORB data for proximity to subduction zones and known plumes/hot spots (fig. 3; Table 1), provides an average MORB isotopic composition (Sr-Nd-Pb) as well as a standard deviation of the isotope data. We use the Su and Langmuir (2003) data analysis to define the following: 1) the average DMM composition, 2) an E-DMM based on isotopes that are 2σ enriched over the average, and 3) a D-DMM based on isotopes that are 2σ depleted from the average. The $^{176}Hf/^{177}Hf$ value of DMM is selected by averaging MORB values from Nowell et al. (1998), Chauvel and Blichert-Toft (2001) and Andres et al. (2002); $^{176}Hf/^{177}Hf$ values for E-DMM and D-DMM are based on correlations with $^{143}Nd/^{144}Nd$ (e.g. Chauvel and Blichert-Toft, 2001).

To derive present-day parent/daughter ratios, a depletion model must be assumed. It is common to use a two-stage evolution model with a single, instantaneous depletion event at a time (t) equal to the average age of the continental crust. An example from the Rb-Sr system, where T is the age of the Earth and parent/daughter ratios are for present-day is the following:

$$\left(\frac{^{87}Sr}{^{86}Sr}\right)_{DMM} = \left(\frac{^{87}Sr}{^{86}Sr}\right)_{o} + \left(\frac{^{87}Rb}{^{86}Sr}\right)_{BSE}\left(e^{\lambda T} - e^{\lambda u}\right) + \left(\frac{^{87}Rb}{^{86}Sr}\right)_{DMM}\left(e^{\lambda u} - 1\right) \qquad (6)$$

However, because mantle depletion is largely the result of continental crust extraction, it is important to consider continental growth through time and the fact that it is not a single depletion event as modeled in the above equation. Although there is debate about continuous growth (Hurley and Rand, 1969) or constant volume with crustal recycling (Armstrong, 1968; Armstrong, 1981; Fyfe, 1978), somewhere in between (such as episodic growth) is probably the reality (McColloch and Bennett, 1994; Taylor and McLennan, 1995; Condie,

2000). Models suggesting continuous growth generally agree that the real increase in continental mass was at about 3 Ga (Taylor and McLennan, 1995). Models in favor of constant crustal volume suggest rapid (or at least effective) recycling of crust greater than 3 billion years old (e.g. Armstrong, 1981; Bowring and Housh, 1995). For our purpose, it is really preservation that is of issue; even though there are isotopic arguments for a 4.0 Ga depleted mantle of similar size and degree of depletion as the modern depleted mantle (e.g. Bowring and Housh, 1995; Vervoort et al., 1996), it is more important here that the abundance of that old crust is low compared to crust younger than 3.0 Ga. Isotopically, the recycling of old crust would make depletion appear to be younger on average and smear out (or even negate) the signal of ancient depletion.

Here we have improved on the classical methods by using a continuous transport, melt depletion model starting at 3 Ga. The equation for the Sr isotopic composition of DMM at time, t, as derived by Allègre (1969) and Hart and Brooks (1970) is:

$$\left(\frac{^{87}Sr}{^{86}Sr}\right)_t = \left(\frac{^{87}Sr}{^{86}Sr}\right)_o + \frac{\lambda\left(^{87}Rb/^{86}Sr\right)_o [1 - e^{-(\lambda+k)t}]}{\lambda + k} \quad (7)$$

where λ is the decay constant for ^{87}Rb and k is the difference in transport coefficients between Rb and Sr and essentially relates to the difference between bulk partitioning of the two elements. The initial conditions are values for bulk silicate Earth at the time when depletion begins (3.0 Ga). The parameter, k, is solved for by knowing the isotopic composition of bulk Earth at 3 Ga and DMM at time zero (i.e. present-day), as shown in Table 1. The parent/daughter variation through time is then:

$$\left(^{87}Rb/^{86}Sr\right)_t = \left(^{87}Rb/^{86}Sr\right)_o e^{-(\lambda+k)t} \quad (8)$$

Figure 4 shows how this model, as used for the Rb/Sr system, gives a factor of ~2 lower estimate for the present-day Rb/Sr ratio of DMM, compared to the usual two-stage model. Decreasing the age of depletion requires lower Rb/Sr ratios for the same present-day ^{87}Sr/^{86}Sr ratio. In the same way that the Sr isotopes are used to constrain the Rb/Sr ratio of DMM, similar constraints result in determinations for Sm/Nd, Lu/Hf, and U/Pb (Table 1). The choice of depletion model does not greatly affect the Sm-Nd system, but is important for the whole suite of parent/daughter ratios.

Most important to the abyssal peridotite inversion is the present-day Sm/Nd ratio for DMM, since this identifies the present-day position of DMM on the mantle depletion arrays. Figure 5 shows how the Sm/Nd ratio of 0.411 in average DMM has a unique intersection with the Sm-Nd abyssal peridotite regression line, defining unique Sm and Nd concentrations of 0.239 ppm and 0.581 ppm, respectively. Given the absolute concentrations of Sm and Nd, we can derive the absolute concentrations of all the other trace elements that have been analyzed in abyssal peridotites (REE, Sr, Zr, Ti, Y; Table 2). Ultimately, estimates for every element concentration are obtained based on relationships with every other element. Standard deviations of various estimates for a given element are on the order of 1-2% for REE's and Ti and 5-6% for Sr, Zr and Ce, indicating that the depletion trends are internally very consistent; note that these standard deviations do not testify to the *accuracy* of the model. With other parent/daughter ratios, other pieces of the trace element pattern for DMM are estimated: Rb derives directly from the Sr; Hf derives from extrapolation to Lu from the REE's; Pb derives from the Ce/Pb canonical ratio (see below) and U follows (Table 2). The same procedure is applied with the E-DMM and D-DMM isotopic compositions.

It is possible to derive Th concentrations from Th/U ratios inferred from $^{208}Pb/^{204}Pb$ and $^{206}Pb/^{204}Pb$ isotopic evolution. However, it has been widely recognized that inferred Th/U ratios are generally much higher than observed Th/U ratios in MORBs; this has been termed the 'kappa conundrum' (Galer and O'Nions, 1985; Elliot et al., 1999; Tatsumoto, 1996). Since Th and U are both highly incompatible during mantle melting, with Th being slightly more incompatible, the Th/U ratios of MORBs should provide an upper limit to the source Th/U. Due to the extremely long half-life of ^{232}Th (14 Byr), we interpret the kappa conundrum to be a problem where the Th-Pb system has not "caught-up" with the U-Pb system. For a more accurate representation of present-day upper mantle, we use Th/U ratios measured by careful U-Series studies on MORBs (Lundstrom et al., 1999; Sims et al., 2002; Sims et al., 2003) over the range in isotopic composition used to define our D-DMM through to E-DMM (Table 1).

2.3 Canonical Ratios and Volatile Contents

There are a few trace element ratios in MORBs (as well as many OIBs) that remain constant over variable degree of melting and variable isotopic composition. These ratios (Ce/Pb, Nb/Ta, Nb/U, and Ba/Rb) are termed "canonical" and their constancy is interpreted to be due to bulk partition coefficients being very nearly the same for the element pairs

during upper mantle melting, preventing significant fractionation (Hofmann and White, 1983; Hofmann et al., 1986; Jochum et al., 1997; Sims and DePaolo, 1997; Pfänder et al., 2002; Weyer et al., 2002). Hence, ratios in the melts are presumed to be identical to ratios of these elements in the source.

We employ these canonical ratios in order to complete the trace element pattern of DMM. It is clear though, from Figure 6, that some canonical ratios are better behaved than others; Nb/Ta, Nb/U and Ba/Rb all hover about their published values of 15.5, 47 and 11.3 respectively (Hofmann and White, 1983; Hofmann et al., 1986; Jochum et al., 1997; Pfänder et al., 2002; Weyer et al., 2002), whereas Ce/Pb ratios display much more scatter with a significant distribution of data higher than either published canonical values of 25 and 20 (Hofmann et al., 1986; Sims and DePaolo, 1997). As a mid-value of the MORB data, we use a Ce/Pb ratio of 30; if, in studies to come, it is determined that Ce/Pb should be lower, we recommend changing only the Pb concentration in DMM, as the U-Nb-Ta-La-Ce segment of the trace element patterns derived is consistent with MORB trace element characteristics (see section 3.2). This would imply that the derived U/Pb ratios from Pb isotopic inversions are not accurate – i.e. that U and Pb cycling in the upper mantle is more complicated than is assumed to be here. All other canonical ratios used are as previously published.

There is also a suite of canonical ratios involving the volatile elements H, C and Cl that are useful for estimating the budget of these elements in the upper mantle. Volatile elements play an important role in melt generation and transport, so the following estimates are crucial input parameters for modeling such processes. The compatibility of water has been shown to be similar to that of Ce, and MORBs have on average an H_2O/Ce ratio of ~200 (Michael, 1995). Using Ce = 0.550 ppm (Table 2), H_2O is calculated to be 110 ppm in DMM. Using a lower limit of 150 and upper limit of 250 for H_2O/Ce (Michael, 1995) along with our lower and upper estimates for Ce (Table 2), respectively, the range of water content in DMM is 70-160 ppm.

In a recent study on volatile undersaturated basaltic melt inclusions from the Siqueiros transform fault, Saal et al. (2002) have established two new working canonical ratios: CO_2/Nb at 239 ± 46 and Cl/K at 0.0075 ± 0.0025. Using our Nb min/max estimates from Table 2 and our K estimate from Table 3 (see section 3.1 below), average DMM has a CO_2 content of 36 ± 12 ppm and a Cl content of 0.38 ± 0.25 ppm. These estimates are about 2 times lower than those reported by Saal et al. (2002) due to their use of different trace

element abundances in DMM, but within error of recent estimates by Salters and Stracke (2004).

2.4 Final product

Combining the mantle depletion trends from the abyssal peridotites, parent/daughter ratios from the isotopic evolution of DMM, and a handful of canonical ratios, trace element patterns ("spidergrams") of average DMM, E-DMM (enriched from the average) and D-DMM (depleted from the average) have been derived (fig. 7a; Table 1 for isotope values; Table 2 for trace element compositions). Overall, the spidergrams are very smooth except for a dip in Sr along with an expected Pb anomaly (see Hofmann, 1988). The greatest difference between the three compositions is in the highly incompatible elements; for example, Rb and Ba vary by a factor of ~5, but Sm varies by only 30%.

Because it is difficult to assign errors to the estimated compositions, we have provided minimum and maximum estimates for trace element concentrations in the average DMM by using starting ages for the continuous depletion model at 2.5 and 3.5 Ga, respectively (see the grey lines on Figure 7b; Table 2). By changing the initial assumption of depletion age, we are effectively saying DMM is more or less depleted and all elements together move up or down the depletion arrays in proportion to their compatibilities during melting. Each of these patterns is internally consistent, and therefore not a true range for each element but rather a coherent solution for the assumptions made. It is not advisable to "mix and match" values from different patterns, since the elements behave as a system, not independently, and should be regarded as such. However, the Ba/Th ratios for the 2.5 and 3.5 Ga patterns are, respectively, too high and too low to generate realistic MORB compositions (see section 3.2) and support the idea that 3.0 Ga is an appropriate assumption for initiation of mantle depletion. As an aside, using a classical 1.8 Ga instantaneous depletion model results in a spidergram (not shown) very similar to that of the 3.5 Ga pattern but with Rb and Ba close to values for the 3.0 Ga (preferred) pattern.

The Salters and Stracke (2004) spidergram (fig. 7b) for average DMM, based on depleted MORB elemental ratios and isotopic evolution, is generally less depleted than the average DMM of this study. In particular, they show significantly higher estimates for the whole left side of the spidergram (Rb to Ce), as well as higher Zr, Hf and Y, than predicted even for our maximum estimate; this is most likely due to their use of an instantaneous (two-stage) depletion model for isotopic evolution instead of the gradual depletion model described in this paper.

Please note that in the following sections, only average DMM is discussed.

3. Physical and Chemical Properties of DMM

3.1 Modal abundances & major elements

Abyssal peridotites from all over the world show depletion trends not only in trace element content, but also in major element content in the form of modal abundances and mineral compositions (Dick et al., 1984; Dick and Natland, 1996; Hellebrand et al., 2002; Michael and Bonatti, 1985; Niu et al., 1997; Baker and Beckett, 1999). In general, these observations are supported by experimental and theoretical studies of peridotite melting (Kinzler and Grove, 1992a; Walter et al., 1995; Gaetani and Grove, 1998; Hirschmann et al., 1998). With increasing degree of melt depletion, olivine increases in modal proportion while orthopyroxene, clinopyroxene and spinel decrease. Al, Ca, Na, K and Ti are more incompatible during melting than Mg, Cr and Ni, so have the highest mineral and whole rock concentrations in the least depleted peridotites (e.g. Baker and Beckett, 1999).

Since we have established the systematics of incompatible trace elements in abyssal peridotites (see above), we use their relationship to modes to estimate the proportion of minerals in today's average DMM, then challenge the results with considerations of melt extraction and a comparison to the primitive mantle. Using the same data set as employed earlier (Suppl. Data Table 1), we have plotted bulk trace element concentrations against modal abundances in individual abyssal peridotites (see examples in fig. 8); note that these are not completely independent parameters since modes in part determine bulk trace element contents. By extrapolating the trends like those in Figure 8 to the DMM trace element concentrations (Table 2), we find DMM to be composed of 57% ol, 28% opx, 13% cpx and 2% sp (Table 3); orthopyroxene does not correlate with any trace elements and has been solved for by summation to 100%. These modes are very close to those found by extrapolating the modal abundance correlations for the South-West Indian Ridge abyssal peridotites (Dick, 1989) for which, without spinel, yields 60% ol, 30% opx and 10% cpx.

Constructing the bulk depleted mantle composition from mineral modes requires fairly precise knowledge of oxide abundances in the mantle minerals. Baker and Beckett (1999) have reduced mineral data for abyssal peridotites and provided algorithms for estimating major element compositions of minerals according to the modal abundance of olivine. Using the Baker and Beckett (1999) mineral compositions at 57% olivine and combining

the minerals in the given proportions, results in a bulk DMM having an Al_2O_3 content nearly that of the primitive upper mantle (PUM; McDonough and Sun, 1995), along with a very low Ca/Al ratio compared to PUM. Since Al is depleted during melt extraction and Al is more enriched than Ca in mantle melts (see Table 3), it is reasonable to expect the depleted mantle to have lower Ca and Al concentrations and a equal or higher Ca/Al ratio than that of PUM. This seems to be a problem only with Al abundance and is interpreted to be due to extrapolating mineral compositions beyond the limit of data used by Baker and Beckett (1999). For this reason, we find it more appropriate to use mineral compositions at 60% olivine, the lowermost (i.e. fertile) limit of their regressed data. In doing so, we calculate the major element composition of DMM as reported in Table 3.

Compared to PUM, estimated DMM has, as expected, lower SiO_2, TiO_2, Al_2O_3, CaO, Na_2O, and K_2O with higher MgO and Cr_2O_3 (Table 3). The TiO_2 content of 0.13 wt% is very close to the 0.12 wt% calculated from the trace element derivation (Table 2). The CaO/Al_2O_3 ratio is equal to that of PUM (0.80), and would increase to 0.86 by lowering the spinel abundance by only 0.5%. As previously mentioned, much of the trace element depletion in the upper mantle can be attributed to the continental crust. The question now is: can the newly estimated *major element* depletion also be attributed to the continental crust? The continental crust budget (see mass-balance section below and bulk continental crust of Rudnick and Fountain, 1997) does largely account for the low TiO_2 and K_2O, the most incompatible of the major elements, and partially accounts for the Na_2O. However, owing to the small mass of continental crust, major elements with less contrast between the crust and mantle cannot be balanced solely by the continents. As a possible solution, Table 3 shows a rudimentary mass balance of the DMM major elements in which 3% of primary MORB is subtracted from PUM (note that this is not a melting model). The major elements calculated in this way show striking similarity to the estimated DMM composition, implying that there is a isolated reservoir of oceanic crust somewhere within in the silicate Earth, as also suggested by Hauri and Hart (1997). A second estimate for Na_2O based on mass balance with both the continental crust and a MORB reservoir is also provided in Table 3 and is most likely more accurate than the original sum of mineral compositions.

To convert mineral modes into practical information for those who study abyssal peridotites, we have calculated the trace element composition of the constituent minerals in unmelted, average DMM by using Eqns. (1) and (2) with mineral/melt partition coefficients compiled by Kelemen et al. (2003). This effectively distributes the DMM trace element

budget among the minerals according to their relative affinity for incompatible elements. The resulting mineral compositions are reported as Suppl. Data Table 2

As a cautionary note, the reported modes and mineral compositions will only apply to the very shallow mantle, owing to variable mineral compositions and phases with pressure and temperature, but the average bulk composition of unmelted, upper mantle should be similar at any depth in this reservoir.

3.2 MORB generation

Here we present the average DMM trace element composition, so should be able to produce an average parental N-MORB. To model MORB generation, we first calculate bulk partition coefficients (D) from Eqn. (5) applied to the abyssal peridotite depletion trends. Because the slopes of the depletion trends (fig. 2) only supply information about *ratios* of D values, we initially have to assume a D for one element and then calculate the remainder in relation to that one. We have chosen a bulk D_{Nd} of 0.031, according to a compilation from Kelemen et al. (2003) for upper mantle melting, since the bulk compatibility of Nd is almost identical in both the spinel and garnet facies.

The set of partition coefficients resulting from the inversion of all abyssal peridotite depletion trends is reported in Table 2. Figure 9 shows the calculated D values compared to both garnet and spinel facies bulk D's from Kelemen et al. (2003); clearly the slope of the calculated D values very closely matches that of spinel facies melting and is far off the slope of garnet facies melting. Note that choosing a different D_{Nd} will change the absolute position but not the slope of the D values shown in Figure 9 (meaning the ratios of D's will not change). The above observation does not exclude a contribution of trace elements from small degree melts in the garnet facies, especially for elements with low D values; this may be why Sr and Ce are a little lower than the spinel facies prediction. For elements with higher bulk D's in the garnet facies, the majority of depletion will happen in the spinel facies, thus is reflected in the depletion arrays. If depletion for the middle to heavy REE's was significant in garnet melting, the trace element pattern across the REE would be steeper, even if the last D values to act on the peridotites were those of spinel melting. This is a straightforward effect of fractional melting on residues.

As an average MORB trace element pattern to be fit by our modeling, we use the parental (fractionation-corrected) N-MORB reported by Su and Langmuir (2003). A point generally agreed upon, and hence applied here, is that MORBs are aggregated fractional or near-fractional melts over a range of pressures, as initially confirmed by Sobolev and

Shimizu (1993). The highly incompatible elements are enriched ~16-fold over DMM, thus requiring 6% aggregated fractional melting of DMM. Figure 10 shows the excellent fit to N-MORB using the D values derived here and reported in Table 2.

The 6% degree of melting to generate MORB is on the low side of previous estimates ranging from 6-20% (Langmuir et al., 1992; Kinzler and Grove, 1992b). A higher F could be obtained if a greater fractionation correction is applied to the already-corrected parental N-MORB of Su and Langmuir (2003) since F is mainly limited by the concentration of highly incompatible elements (i.e. Rb, Ba, U, Th, Nb, Ta) in the modeled MORB; however, this requires generally higher D's to maintain the proper slope for M- to HREE. To get to F = 10%, at least another 30% fractionation is necessary and this seems unlikely. This low value for F, as compared to previous models, may be due to the fact that older estimates are based on anhydrous melting. Water content in the upper mantle is increasingly recognized as a very important aspect of mantle viscosity and convection (Hirth and Kohlstedt, 1996) as well and mantle melting (Hirth and Kohlstedt, 1996; Asimow and Langmuir, 2003; Asimow et al., 2004; Parman and Grove, 2004). To test the validity of 6% mean F, we apply our estimated concentration of H_2O to the recent model by Asimow et al. (2004) for hydrous mantle melting (the pHMELTS model).

A pHMELTS model run, using 110 ppm water, the major element compositions in Table 3, a potential temperature of 1360°C, a 2-D passive triangle melting regime and near-fractional melting, results in 7.0% mean melting to produce MORB and a crustal thickness of 6.3 km (P. Asimow, pers. comm., 2004). This confirms that the mean degree of melting (as defined by Plank et al., 1995) for hydrous models is generally on the low side of previous estimates from anhydrous models.

For average DMM, the derived D values (Table 2) translate into 2-3% melt depletion from primitive mantle using either non-modal or modal fractional melting models. Because average DMM is only 2-3% melt depleted, but average MORB is generated by 6% melting, one or all of the following is implied: 1) the degree of melting was lower in the past, 2) the mantle is a cannibal, recycling some crust and lithosphere back into itself, 3) depleted mantle has exchanged with the less depleted mantle, or 4) MORB generation is not the process that depletes the mantle.

4. Crust-Mantle Mass Balance

Classic works based on continental crust and the depleted mantle being sole complementaries calculate that from 30% to 70% of the mantle is depleted according to isotope and parent/daughter constraints [Allègre et al., 1983, refs. therein]. In the following paragraphs, we provide three different scenarios for the balance of chemical reservoirs in the silicate earth, with each scenario progressively involving additional reservoirs. We believe that using the entire trace element suite to assess the extent to which the silicate earth does or does not mass-balance is a robust way to calculate relative proportions of reservoirs. The mass of the continental crust is fixed to be 0.6% the mass of the silicate Earth. For each scenario, the best estimates of reservoir masses along with uncertainty in the estimates are derived from a Monte Carlo simulation with 10^5 trials in which element concentrations for each reservoir are considered as normal random variables with means given as PUM normalized concentrations and 1σ equal to 10%; in each trial, the relative reservoir masses are determined by a linear least-squares fit to the input parameters. Uncertainties are quoted as 2σ.

Scenario 1 is our own mass-balance involving only DMM and the continental crust, meaning in what proportion do DMM and the continental crust have to be added in order to sum back to primitive mantle? Our calculations indicate that 33±3% the mass of the silicate Earth has to be DMM, with the remainder being primitive mantle, to best balance the bulk continental crust composition as estimated by Rudnick and Fountain (1997). For this particular 'reconstituted' mantle, all elements sum to within 15% of the primitive mantle except Rb and Pb which are in excess by 28% and 21%, respectively. This scenario is no doubt overly simplistic. For one, there is no real evidence for the existence of a primitive mantle reservoir (see review by van Keken et al., 2002). However, there is evidence for a lower mantle that is less depleted than DMM, but depleted nonetheless; this reservoir is implied from many OIB isotopic arrays and termed FOZO by Hart et al. (1992). If a depleted lower mantle were accounted for here, the DMM reservoir would be significantly smaller than 33% in order to allow for the moderate depletion of the lower mantle.

Scenario 2 is the mass-balance of DMM, continental crust, and recycled oceanic crust. The idea of a recycled MORB component in the mantle is corroborated by the observation that the major element composition of DMM cannot be balanced by continental crust alone (see Table 3). At 43±6% DMM and 2.0±0.6% parental N-MORB of Su and Langmuir (2003), this scenario provides a better fit for most elements than does the first scenario; all

elements here are fit to within 8% except Rb and Pb with 20% and 15% excesses and Nb with a 17% deficit. The abundance of MORB cannot be increased greatly without having elevated M- to HREE that cannot be compensated by adding more DMM. However, we have not considered subduction zone alteration of oceanic crust, which almost certainly affects this mass balance.

Scenario 3 is the mass-balance of DMM, continental crust, recycled oceanic crust and an OIB source component (from Workman et al., 2004). To show upper limits on the sizes of enriched mantle components, the mass balance calculation has been made assuming 0% primitive mantle. The resulting balance is 74±5% DMM, 4.7±1.0% MORB and 21±5% OIB source; all elements are fit to within 15% except Rb and Nb with 23% excess and 21% deficit, respectively.

In each scenario 2 and 3, the fraction of MORB in the mass-balance is less than the mass of oceanic crust generated throughout Earth history (6-7% of the mantle mass, assuming constant rates for 4.55 Ga). As such, it is suggestive of the mantle being partially cannibalistic with respect to subducted oceanic crust. However, these mass balances do not include a depleted lithosphere, and could therefore be misrepresentative if oceanic crust and lithosphere are shown to be absolutely mechanically and thermally coupled.

5. Conclusions

Through abyssal peridotite trends, the isotopic composition of N-MORB and a few canonical ratios, we have constructed a major and trace element reference model for average, unmelted, depleted MORB mantle (DMM). From this DMM, parental MORB is generated by about 6% aggregated fractional melting as constrained primarily from the enrichment factor for the highly incompatible elements in parental MORB. Melting occurs mainly in the spinel facies mantle, but is most likely initiated within the uppermost garnet facies, as suggested by pHMELTS model runs. The water content inferred by the derived trace element composition is between 70 and 160 ppm, and is an integral ingredient in modeling mantle melting (Asimow et al., 2004) and mantle viscosity (Hirth and Kohlstedt, 1996; 2004). We have provided trace element compositions for minerals in the uppermost mantle which can be better estimated in the future with increasingly accurate information on mineral/mineral partitioning of trace elements and compositional variations of minerals with temperature and pressure.

The radiogenic heat production of DMM (from U, Th, and K) is only 15% that of the bulk silicate Earth at 2.43 x 10^{-9} Watts/m^3, using a density of 3.20 g/cm^3 and radiogenic heat production values from Durrance (1986). It takes ~33% of the mantle mass to be composed of DMM, the remaining being primitive mantle, to balance the continental crust alone, and ~43% if including an oceanic crust component. If there is no primitive mantle, the maximum masses of the oceanic crust and OIB reservoirs are 5% and 21%, respectively, if these enriched reservoirs are balanced purely by DMM.

Overall, the composition constructed here is a robust estimate for average upper mantle and can be used as an input parameter for a variety of models concerning mantle processes.

Acknowledgements

We are endlessly grateful to Henry Dick, whose decades of toils over mid-ocean ridges and abyssal peridotites have made possible the work presented here; in jest we question his sanity for counting over half a million points on abyssal peridotite modal abundances. Many stimulating conversations have been had with Nobu Shimizu, Jessica Warren, Glenn Gaetani, Peter Kelemen and Greg Hirth on the nature of the depleted mantle. We especially thank Paul Asimow for a sneak-preview application of his new pHMELTS model, as well as E. Hauri and W. McDonough for their helpful reviews.

Appendix 3-1.

Calculations for other melting models show that the fractional melting model used here to interpret residues of melting is a fine approximation for any number of more complicated (and maybe more realistic) melting models. Figure A1 plots melt depletion trends for Sm and Nd in residues of melting, starting with PUM of McDonough and Sun [14], and using equations for modal fractional, non-modal fractional, dynamic and non-modal dynamic melting as derived or summarized in Zou [23]. Residual porosity is chosen to be 0.5% for dynamic melting. Mineral/melt partition coefficients have been borrowed from Kelemen et al. [22] and the empirical coefficients of melting are from Niu [79] as follows: olivine = -0.17, orthopyroxene = 0.65, clinopyroxene = 0.47, spinel = 0.05. Bulk D values for Sm and Nd are taken from Table 2 in main text.

By definition, the two modal melting models are linear in Figure A1, with dynamic melting resulting in slightly less depletion for a given degree of melting (both curves end at 25% melting). Non-modal melting results in much greater depletion for a given degree of melting than modal melting and in slightly curved trajectories of melt depletion, but not severely enough to make a linear approximation (i.e. modal melting) invalid. For the upper few decades of melt depletion, the melting models are all nearly identical (fig. A1). Even at the point where they are clearly distinguishable from each other, the models all are contained within the scatter of the abyssal peridotite data (not shown on fig. A1 for clarity, but see figs. 2 and 5 above). Using modal fractional melting as an approximation for any of the other melting models will primarily lead to different D values than may be truly "Bulk D's", but will not change the ultimate estimate of DMM. For example, if the real melting style beneath ridges is non-modal dynamic melting, a linear fit by modal fractional melting will lead to estimates of 'effective' partition coefficients, meaning the 'non-modal' part of melting will be incorporated into the D outputs. Because we solve for relative partition coefficients (and do not assume them *a priori*), it is almost inconsequential which model is used given the resolution of the peridotite dataset. However, the estimate for the degree of melt depletion in DMM could be over-estimated if assuming an initial absolute D that is too high.

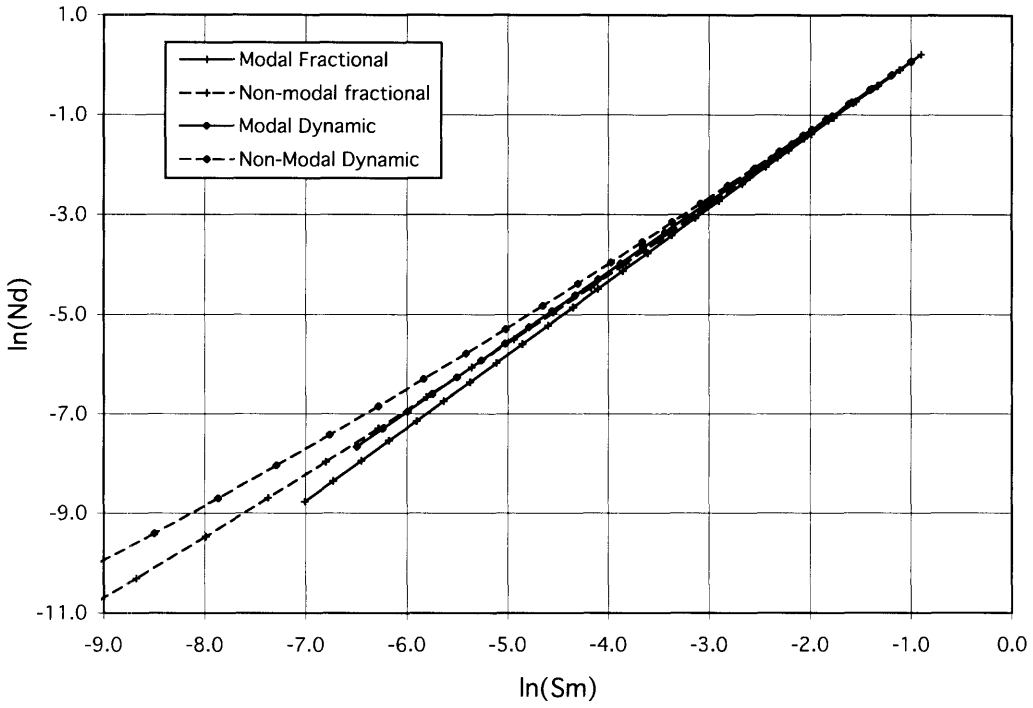

Figure A1.

Melting models showing depletion trends for Sm and Nd in residues of melt extraction. See text for details. Curves for modal melting models (fractional and dynamic) both end at 25% melt extraction. Non-modal fractional and dynamic curves are fall off the plot at 21% and 22% melting, respectively. Although not shown, the scatter in the abyssal peridotite data brackets all the melting model curves.

References

Albarede, F. and M. Brouxel, The Sm/Nd secular evolution of the continental crust and depleted mantle, Earth and Planet. Sci. Letters 82 (1987) 25-35.

Allègre, C. J., Comportement des systemes U-Th-Pb dans le manteau superieur et modele d'evolution de ce dernier au cours des temps geologiques, Earth and Planet. Sci. Letters 5 (1969) 261-269.

Allègre, C. J., S. R. Hart, and J. F. Minster, Chemical structure and evolution of the mantle and the continents determined by inversion of Nd and Sr isotopic data, II. Numerical experiments and discussion, Earth Planet. Sci. Lett. 66 (1983) 191-213.

Andres, M., J. Blichert-Toft, J. Schilling, Hafnium isotopes in basalts from the southern Mid-Atlantic Ridge from 40°S to 55°S: Discovery and Shona plume-ridge interactions and the role of recycled sediments, Geochem., Geophys., Geosyst. 3 (2002) doi:10.1029/2002GC000324.

Armstrong, R. L., A Model for the Evolution of Strontium and Lead Isotopes in a Dynamic Earth, Rev. of Geophysics 6 (1968) 175-199.

Armstrong, R. L., Radiogenic isotopes: the case for crustal recycling on a near-steady-state no-continental-growth Earth, Phil. Trans. R. Soc. London 301 (1981) 443-472.

Asimow, P. D. and C. H. Langmuir, The importance of water to oceanic mantle melting regimes, Nature 421 (2003) 815-820.

Asimow, P. D., J. E. Dixon and C. H. Langmuir, A hydrous melting and fractionation model for mid-ocean ridge basalts: Application to the Mid-Atlantic Ridge near the Azores, Geochem., Geophys., Geosyst. 5 (2004) doi:10.1029/2003GC000568.

Baker, M.B. and J.R. Beckett, The origin of abyssal peridotites: a reinterpretation of constraints based on primary bulk compositions, Earth and Planet. Sci. Lett. 171 (1999) 49-61.

Bowring, S. A. and T. Housh, The Earth's Early Evolution, Science 269 (1995) 1535-1540.

Chauvel, C. and J. Blichert-Toft, A hafnium isotope and trace element perspective on melting of the depleted mantle, Earth and Planet. Sci. Letters 190 (2001) 137-151.

Condie, K. C., Episodic continental growth models: afterthoughts and extensions, Tectonophysics 322 (2000) 153-162.

Dick, H. J. B., Abyssal-peridotites, very slow spreading ridges and oceanic ridge magmatism, in: A.D. Saunders, M.J. Norry (Eds.), Magmatism in the Ocean Basins,

Geological Society, London, 1989, pp. 71-105.

Dick, H. J. B. and J. H. Natland, Late-stage melt evolution and transport in the shallow mantle beneath the East Pacific Rise, in: C. Mevel, K. M. Gillis, J. F. Allan, P. S. Meyer (Eds.), Proceedings of the Ocean Drilling Program, Scientific Results 147, 1996, pp.103-134.

Dick, H. J. B., R. L. Fisher, and W. B. Bryan, Mineralogical variability of the uppermost mantle along mid-ocean ridges, Earth and Planet. Sci. Letters 69 (1984) 88-106.

Dickin, A.P., Radiogenic Isotope Geology, Cambridge University Press, Cambridge, UK, 1995, 490 pp.

Durrance, E. M., Radioactivity on Geology: Principles and Applications, Ellis Horwood Limited, Chichester, 1986.

Elliott, T., A. Zindler, and B. Bourdon, Exploring the kappa conundrum: the role of recycling in the lead isotope evolution of the mantle, Earth and Planet. Sci. Letters 169 (1999) 129-145.

Fyfe, W. S., The evolution of the Earth's crust; modern plate tectonics to ancient hot spot tectonics, Chemical Geology 23 (1978) 89-114.

Gaetani, G. A. and T. L. Grove, The influence of water on melting of mantle peridotite, Contrib. Mineral. Petrol. 131 (1998) 323-346.

Galer, J.J.G. and R.K. O'Nions, Residence time of thorium, uranium and lead in the mantle and implications for mantle convection, Nature 316 (1985) 778-782.

Hart, S. R., Heterogeneous mantle domains: signatures, genesis and mixing chronologies, Earth Planet. Sci. Lett. 90 (1988) 273-296.

Hart, S. R. and C. Brooks, Rb-Sr Mantle Evolution Models, Carnegie Institution Yearbook 68 (1970) 426-429.

Hart, S. R., and A. Zindler, In search of a bulk-earth composition, Chem. Geol. 57 (1986) 247-267.

Hart, S. R., Hauri, E.H., Oschmann, L.A., and Whitehead, J.A., Mantle Plumes and Entrainment: Isotopic Evidence, Science 256 (1992) 517-520.

Hauri, E. and S. R. Hart, Rhenium abundances and systematics in oceanic basalts, Chem. Geology 139 (1997) 185-205.

Hellebrand, E., J. E. Snow, P. Hoppe and A. W. Hofmann, Garnet-field Melting and Late-stage Refertilization in 'Residual' Abyssal Peridotites from the Central Indian Ridge, J. of Petrology 43 (2002) 2305-2338.

Hirschmann, M. M., M. S. Ghiorso, L. E. Wasylenki, P. D. Asimow and E. M. Stolper

Calculation of peridotite partial melting from thermodynamic models of minerals and melts. I. Review of methods and comparison with experiments, J. Petrol. 39 (1998) 1091-1115.

Hirth, G. and D. L. Kohlstedt, Water in the oceanic upper mantle: implications for rheology, melt extraction, and the evolution of the lithosphere, Earth and Planet. Sci. 144 (1996) 93-108.

Hirth, G. and D. L. Kohlstedt, Rheology of the Upper Mantle and the Mantle Wedge: A View from the Experimentalists, in: J. Eiler (Ed.), Inside the Subduction Factory, AGU Monograph 138, AGU, Washington D.C., 2004, pp. 83-105.

Hofmann, A.W., K. P. Jochum, H. M. Seufert, and W. M. White, Nb and Pb in oceanic basalts: new constraints on mantle evolution, Earth Planet. Sci. Lett. 79 (1986) 33-45.

Hofmann, A. W., Chemical differentiation of the Earth: the relationship between mantle, continental crust, and oceanic crust, Earth and Planet. Sci. Letters 90 (1988) 297-314.

Hofmann, A. W., Mantle geochemistry: the message from oceanic volcanism, Nature 385 (1997) 219-229.

Hofmann, A. W., and W. M. White, Ba, Rb and Cs in the Earth's Mantle, Z. Naturforsch 38 (1983) 256-266.

Hurley, P. M. and J. R. Rand, Pre-drift continental nuclei, Science 164 (1969) 1229-1242.

Jochum, K. P., J. A. Pfänder, J. E. Snow and A. W. Hofmann, Nb/Ta in Mantle and Crust, EOS 78 (1997) F805.

Johnson, K. T. M. and H. J. B. Dick, Open system melting and temporal and spatial variation of peridotite and basalt at the Atlantis II fracture zone, J. Geophys. Res. 97 (1992) 9219-9241.

Johnson, K. T. M., H. J. B. Dick, and N. Shimizu, Melting in the oceanic upper mantle; an ion microprobe study of diopsides in abyssal peridotites, J. of Geophys. Res. 95 (1990) 2661-2678.

Kelemen, P. B., H. J.B. Dick and J. E. Quick, Formation of harzburgite by pervasive melt/rock reaction in the upper mantle, Nature 358 (1992) 635-641.

Kelemen, P.B., G.M. Yogodzinski and D.W. Scholl, Along-strike variation in lavas of the Aleutian island arc: Implications for the genesis of high Mg# andesite and the continental crust, in: J. Eiler (Ed.), Inside the Subduction Factory, AGU Monograph 138, AGU, Washington D.C., 2003, pp. 223-276.

Kinzler, R. J. and T. L. Grove, Primary magmas of Mid-Ocean Ridge Basalts 1. Experiments and Methods, J. Geophys. Res. 97 (1992a) 6885-6906.

Kinzler, R. J. and T. L. Grove, Primary magmas of Mid-Ocean Ridge Basalts 2. Applications, J. Geophys. Res. 97 (1992b) 6907-6926.

Langmuir, C.H., E.M. Klein and T. Plank, Petrological systematics of mid-ocean ridge basalts: Constraints on melt generation beneath ocean ridges, in: J.P Morgan, D.K. Blackman, J.M. Sinton, (Eds.), Mantle Flow and Melt Generation at Mid-Ocean Ridges, Geophys. Monogr. Ser. 71, AGU, Washington, D.C., 1992, pp. 183-180.

Loubet, M., N. Shimizu and C. J. Allegre, Rare Earth Elements in Alpine Peridotites, Contrib. Mineral. Petrol. 53 (1975) 1-12.

Lundstrom, C.C., D.E. Sampson, M.R. Perfit, J. Gill, Q. Williams, Insights into mid-ocean ridge basalt petrogenesis: U-series disequilibria from the Siqueiros Transform, Lamont Seamounts, and the Pacific Rise, J. Geophys. Res. 104 (1999) 13,035-13,048.

McCulloch, M.T., V.C. Bennett, Progressive growth of the Earth's continental crust and depleted mantle; geochemical constraints, Geochimica et Cosmochimica Acta 58 (1994) 4717-4738.

McDonough, W.F., and S.-s. Sun, The composition of the Earth, Chem. Geol. 120 (1995) 223-253.

McKenzie, D. and R.K. O'Nions, Partial Melt Distributions from Inversion of Rare Earth Element Concentrations, J. Pet. 32 (1991) 1021-1091.

Michael, P., Regionally distinctive sources of depleted MORB: Evidence from trace elements and H_2O, Earth and Planet. Sci. Letters, 131 (1995) 301-320.

Michael, P. J., and E. Bonatti, Peridotite compositions from the North Atlantic: regional and tectonic variations and implications for partial melting, Earth and Planet. Sci. Letters 73 (1985) 91-104.

Niu, Y., Mantle Melting and Melt Extraction Processes beneath Ocean Ridges: Evidence from Abyssal Peridotites, J. Pet. 38 (1997) 1047-1074.

Niu, Y., C. H. Langmuir and R. J. Kinzler, The origin of abyssal peridotites: a new perspective, Earth and Planet. Sci. Letters, 152, 251-265, 1997.

Nowell, G.M., P.D. Kempton, S.R. Noble, J.G. Fitton, A.D. Saunders, J.J. Mahoney and R.N. Taylor, High precision Hf isotope measurements of MORB and OIB by thermal ionization mass spectrometry: insights into the depleted mantle, Chemical Geology 149 (1998) 211-233.

Parman, S.W., T.L. Grove, Harzburgite melting with and without H_2O: Experimental data and predictive modeling, J. Geophys. Res. 109 (2004) doi:10.1029/2003JB002566.

Pfänder, J. A., C. Münker, K. Mezger and A. W. Hofmann, In search of a superchondritic

Nb/Ta reservoir: High-precision Nb/Ta and Zr/Hf ratios in ocean island and interplate basalts, Goldschmidt Conference Abstracts 66 (2002) A597.

Plank, T., M. Spiegelman, C.H. Langmuir, D.W. Forsyth, The meaning of "mean F": Clarifying the mean extent of melting at ocean ridges, J. Geophys. Res. 100 (1995) 15,045-15,052.

Presnall, D.C, and J.D. Hoover, High pressure phase equlibrium constraints on the origin of mid-ocean ridge basalts, in: B.O. Mysen (Ed.), Magmatic Processes: Physicochemical Principles, The Geochemical Society Special Publication No. 1, 1987, 75-89.

Rudnick, R. L. and D. M. Fountain, Nature and composition of the continental crust: a lower crustal perspective. Rev. Geophysics 33, (1995) 267-309.

Saal., A., E. H. Hauri, C. H. Langmuir and M. R. Perfit, Vapor undersaturation in primitive mid-ocean-ridge basalt and the volatile content of Earth's upper mantle, Nature, 419 (2002) 451-455.

Salters, V. J. M., and H. J. B. Dick, Mineralogy of the mid-ocean ridge basalt source from neodymium isotopic composition in abyssal peridotites, Nature 418 (2002) 68-72.

Salters, V. J. M, and A. Stracke, The composition of the depleted mantle, Geochem., Geophys., Geosyst. 5 (5) (2004).doi: 10.1029/2003GC00097.

Shimizu, N., The geochemistry of olivine-hosted melt inclusions in a FAMOUS basalt ALV519-4-1, Phys. of the Earth and Planet. Int. 107 (1998) 183-201.

Sims, K. W. W. and D. J. DePaolo, Inferences about mantle magma sources from incompatible trace element concentration ratios in oceanic basalts, Geochimica et Cosmochimica Acta 61 (1997) 765-784.

Sims, K.W.W., S.J. Goldstein, J. Blichert-Toft, M.R. Perfit, P. Kelemen, D.J. Fornari, P. Michael, M.T. Murrell, S.R. Hart, D.J. DePaolo, G.D. Layne, L.A. Ball, M. Jull, J. Bender, Chemical and isotopic constraints on the generation and transport of magma beneath the East Pacific Rise, Geochimica et Cosmochimica Acta 66 (2002) 3481-3504.

Sims, K.W.W., J. Blichert-Toft, D.J. Fornari, M.R. Perfit, S.J. Goldstein, P. Johnson, D.J. DePaolo, S.R. Hart, M.T. Murrell, P.J. Michael, G.D. Layne, L.A. Ball, Aberrant Youth: Chemical and isotopic constraints on the origin of off-axis lavas from the East Pacific Rise, 9°-10°N, Cheochem. Geophys., Geosyst. 4 (2003) doi:10.1029/2002GC000443.

Sobolev, A. V. and Shimizu, N., Ultra-depleted primary melt included in an olivine from the Mid-Atlantic Ridge, Nature 363 (1993) 151-154.

Su, Y. and C.H. Langmuir, Global MORB chemistry compilation at the segment scale, Ph.D. Thesis, Department of Earth and Environmental Sciences, Columbia University

(2003) Available at: http://petdb.ldeo.columbia.edu/documentation/morbcompilation/.

Sun, S.-s., and W.F. McDonough, Chemical and isotopic systematics of oceanic basalts: implications for mantle composition and processes, in: A.D. Saunders, M.J. Norry (Eds.), Magmatism in the Ocean Basins, Geological Society, London, 1989, pp. 313-345.

Tartarotti, P., S. Susini, P. Nimis and L. Ottolini, Melt migration in the upper mantle along the Romanche Fracture Zone (Equatorial Atlantic), Lithos 63 (2002) 125-149.

Tatsumoto, M., Genetic relations of oceanic basalts as indicated by lead isotopes, Science 153 (1996) 1094-1101.

Taylor, S. R. and S. M. McLennan, The geochemical evolution of the continental crust, Rev. of Geophysics 33 (1995) 241-265.

Van Keken, P. E., E. H. Hauri, C. J. Ballentine, Mantle Mixing: The Generation, Preservation, and Destruction of Chemical Heterogeneity, Ann. Rev. Earth and Planet. Sci 30 (2002) 493-525.

Vervoort, J. D., P. J. Patchett, G. E. Gehrels, A. P. Nutman, Constraints on early Earth differentiation from hafnium and neodymium isotopes, Nature 379 (1996) 624-627.

Walter, M. J., T. W. Sisson and D. C. Presnall, A mass proportion method for calculating melting reactions and application to melting of model upper mantle lherzolite, Earth and Planet. Sci. Letters 135 (1995) 77-90.

Weyer, S., C. Munker, M. Rehkamper, and K. Mezger, Determination of ultra-low Nb, Ta, Zr and Hf concentrations and the chondritic Zr/Hf and Nb/Ta ratios by isotope dilution analyses with multiple collector ICP-MS, Chemical Geology 187 (2002) 295-313.

Workman, R.K., S. R. Hart, M. Jackson, M. Regelous, K. A. Farley, J. Blusztajn, M. Kurz and H. Staudigel, Recycled metasomatized lithosphere as the origin of the Enriched Mantle II (EM2) Endmember: Evidence from the Samoan Volcanic Chain, Geochem., Geophys., Geosyst. 5 (2004) doi:10.1029/2003GC000623.

York, D., Least-squares fitting of a straight line, Can. J. Phys. 44 (1966) 1079-1086.

Zindler, A., S.R. Hart, Chemical Geodynamics, Ann. Rev. Earth Planet. Sci. 14 (1986) 493-571.

Zou, H., Trace element fractionation during modal and nonmodal dynamic melting and open-system melting: A mathematical treatment, Geochimica et Cosmochimica Acta 62 (1998) 1937-1945.

Figures

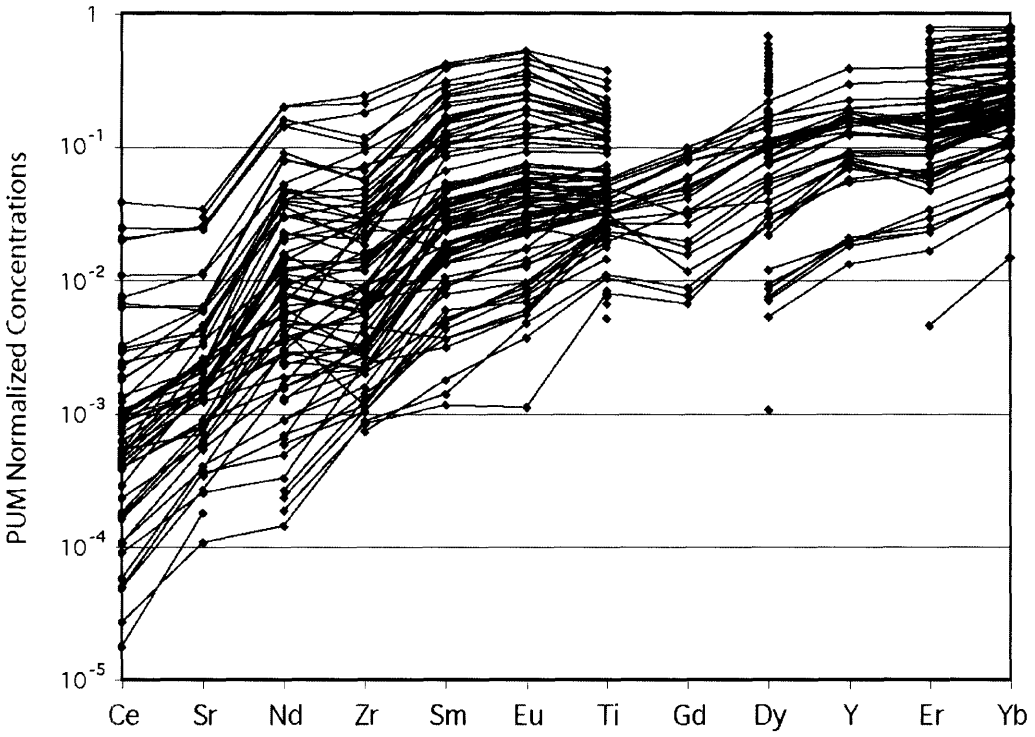

Figure 3-1. Calculated whole rock trace element compositions of abyssal peridotites. Data can be found in Suppl. Data Table 1; data sources as quoted in the text.

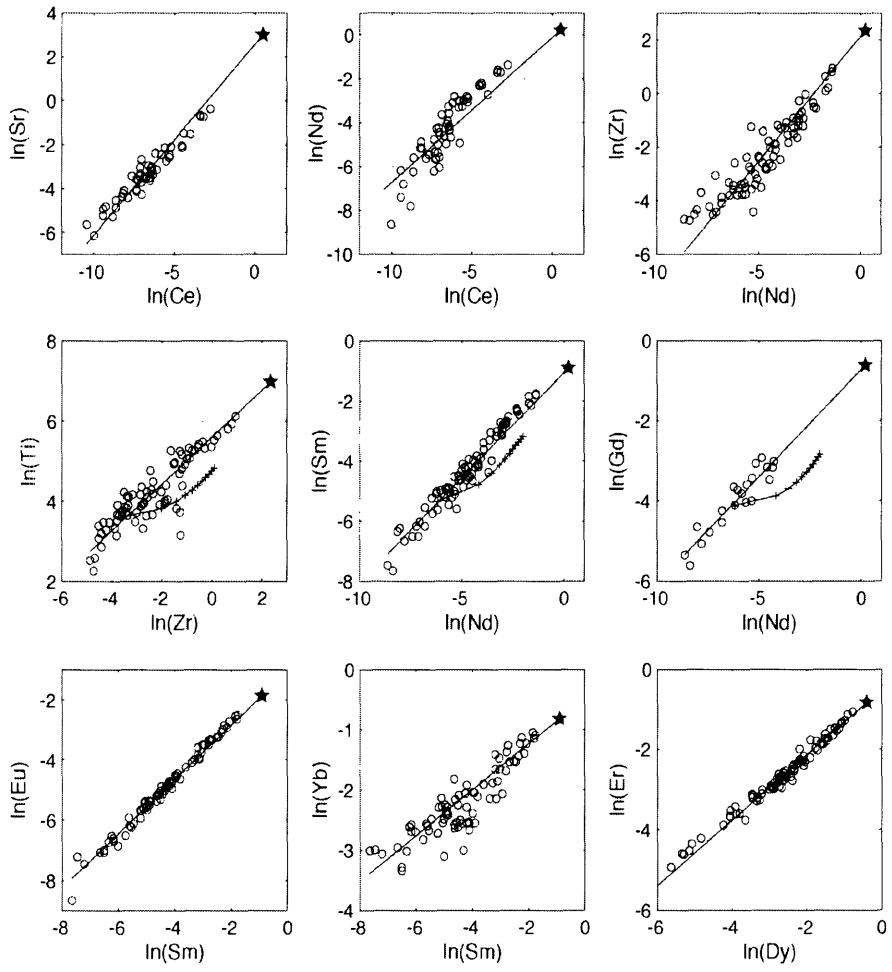

Figure 3-2. Co-variation diagrams for trace elements in abyssal peridotites, plotted as ln([A]) against ln([B]) in accordance with Eq. 4; the more incompatible element is on the x-axis for each plot. Star symbol is Primitive Upper Mantle (PUM; also Bulk Silicate Earth, BSE) of McDonough and Sun (1995). Solid line is the best-fit regression, forced through the PUM coordinate and with assigned errors of 10% for each point. The curved lines with crosses (in the middle three panels) are trajectories for impregnation of a 1% melt of DMM (see Fig. 7; D values from Kelemen et al., 2004) into a depleted mantle of composition indicated by the points of origin on the regression lines; ticks are in increments of 0.1% up to a total of 1% melt impregnation.

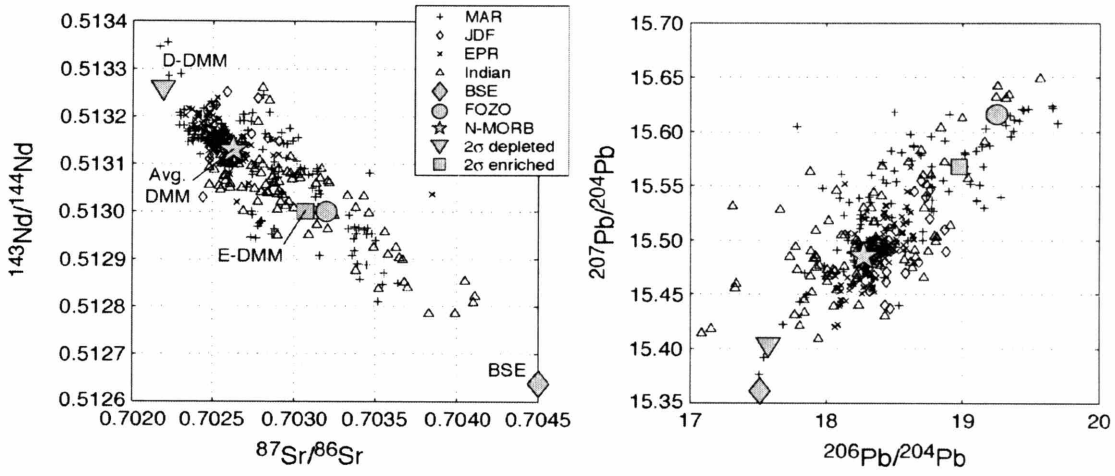

Figure 3-3. Two panels showing the Sr-Nd-Pb isotopic compositions of global MORB data obtained from the PETDB database (http://petdb.ldeo.columbia.edu/petdb/) MAR = Mid-Atlantic Ridge; JDF = Juan de Fuca Ridge; EPR = East Pacific Rise; Indian = Indian Ocean ridge systems; BSE = Bulk Silicate Earth; FOZO = Focus Zone (Hart et al., 1992); N-MORB and All-MORB are, respectively, the average composition for normal MORBs and unfiltered (all) MORBs according to Su and Langmuir (2003). The variation in N-MORB $^{87}Sr/^{86}Sr$, $^{143}Nd/^{144}Nd$, and $^{206}Pb/^{204}Pb$ compared to all of oceanic basalts is 18%, 35% and 47%, respectively.

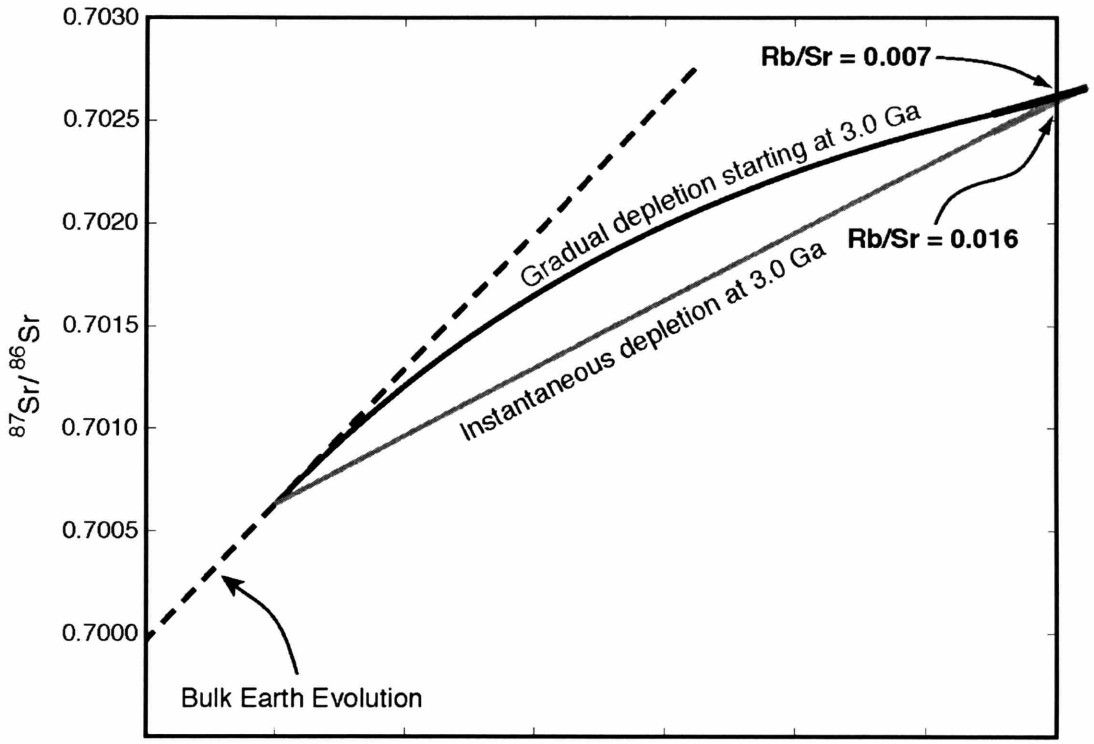

Figure 3-4. Plot showing examples of instantaneous depletion and continuous depletion models for the isotopic evolution of Sr in DMM. Note that the derived Rb/Sr ratio of today's upper mantle varies by a factor of about two between the models - the Rb/Sr ratio is defined by the slope of the evolution curves. Nd isotopic evolution by continuous depletion is not shown since it is essentially linear through time. See Table 1 for isotope evolution parameters and Eqs. 7 and 8 for continuous depletion model.

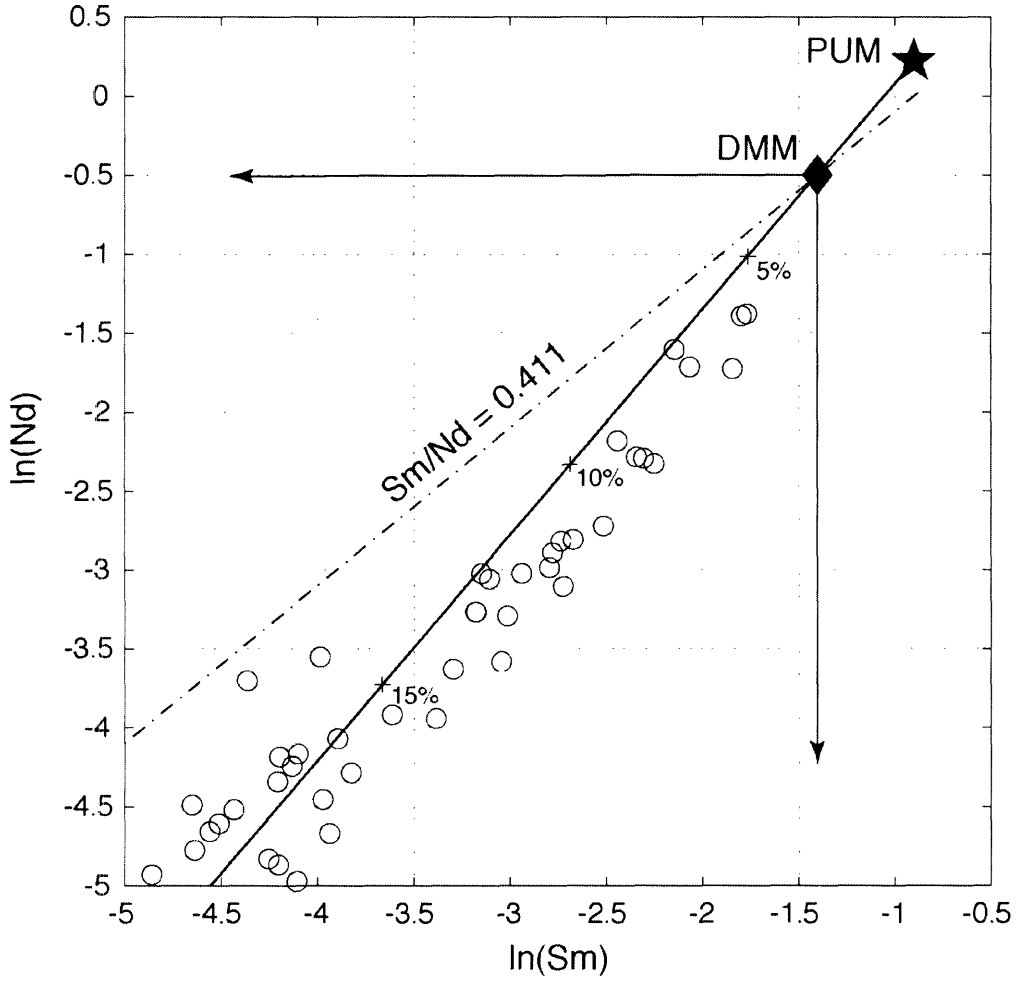

Figure 3-5. Plot of ln([Sm]) versus ln([Nd]) of abyssal peridotites showing the upper half of the mantle depletion array (see fig. 2 for full scale). Star symbol marks the PUM coordinate (i.e. BSE) of McDonough and Sun (1995). Crosses on the mantle depletion line mark percent melt extraction for fractional melting using bulk D values as reported in Table 2. Line of constant Sm/Nd of 0.411 is derived from the Nd isotopic evolution of DMM; the intersection of this line with the mantle depletion line marks today's average composition of DMM. From Sm and Nd concentrations, concentrations of all other elements reported for abyssal peridotites (see fig. 1) can be derived from the system of mantle depletion arrays like those shown in fig. 2.

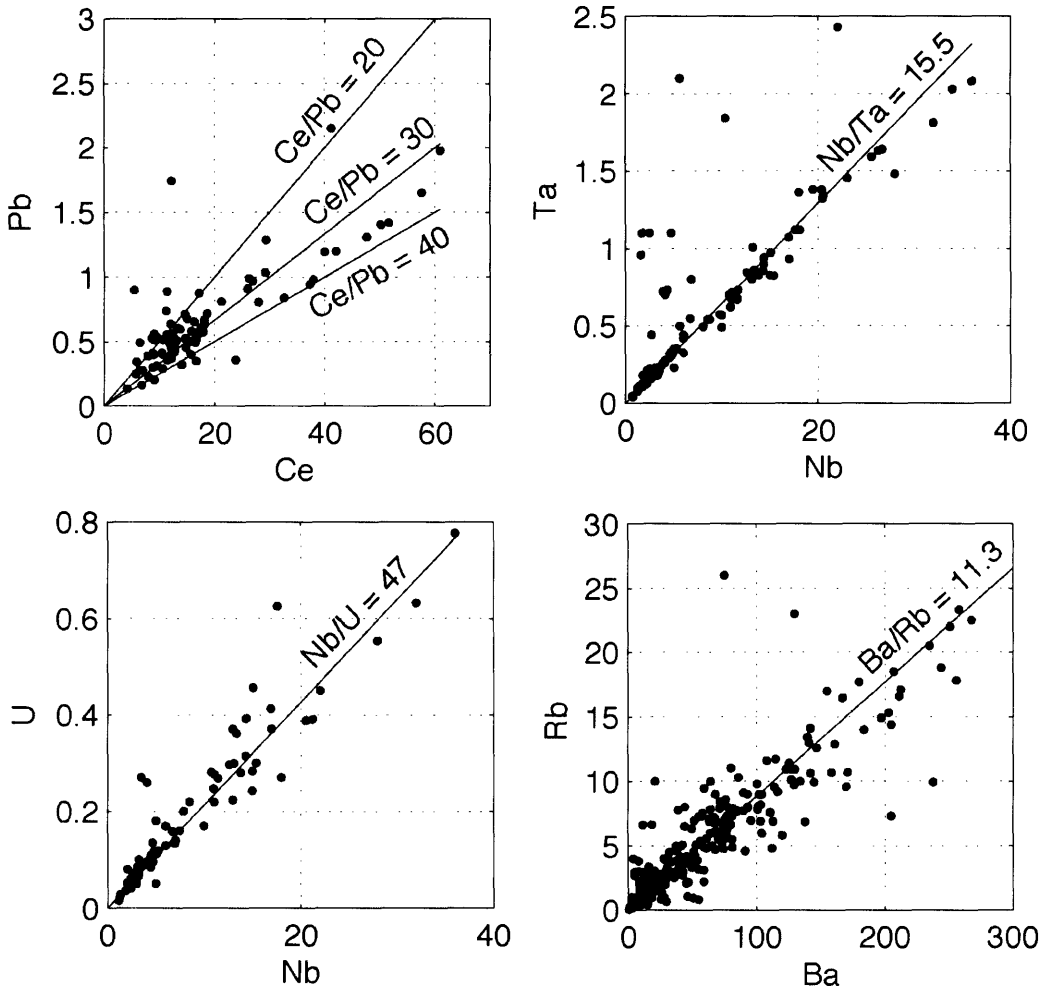

Figure 3-6. Four panels showing co-variation plots for elements in MORBs having canonical ratios. Data acquired from the PETDB database (http://petdb.ldeo.columbia.edu/petdb/) and reported as ppm. Literature values for canonical ratios (see text for references) are plotted for all panels except Ce-Pb, for which bounding and median values are shown.

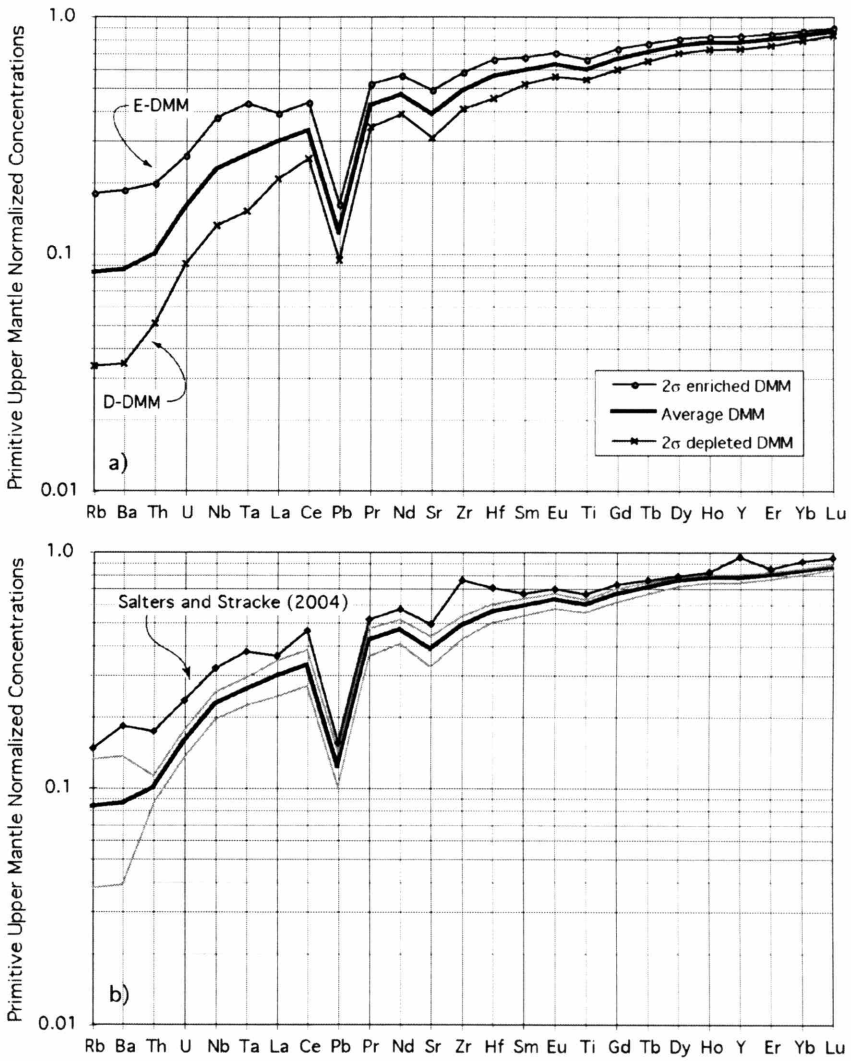

Figure 3-7. Panel a) shows trace element patterns for average Depleted MORB Mantle (DMM), E-DMM and D-DMM (E- and D- are, respectively, enriched and depleted over the average DMM, as based on a isotopic compositions reported in Table 1). Trace element compositions have been derived from abyssal peridotite depletion trends (see fig. 2), isotopic evolution based on the average N-MORB Sr-Nd-Pb-Hf isotopic compositions with a gradual depletion model starting at 3Ga (Table 1; Fig. 3), and canonical ratios (fig. 6). In panel b) the upper and lower grey lines result from using gradual depletion models starting at 3.5 Ga and 2.5 Ga, respectively, for the average DMM isotopic composition. The Salters and Stracke (2004) trace element pattern for average DMM is shown for comparison.

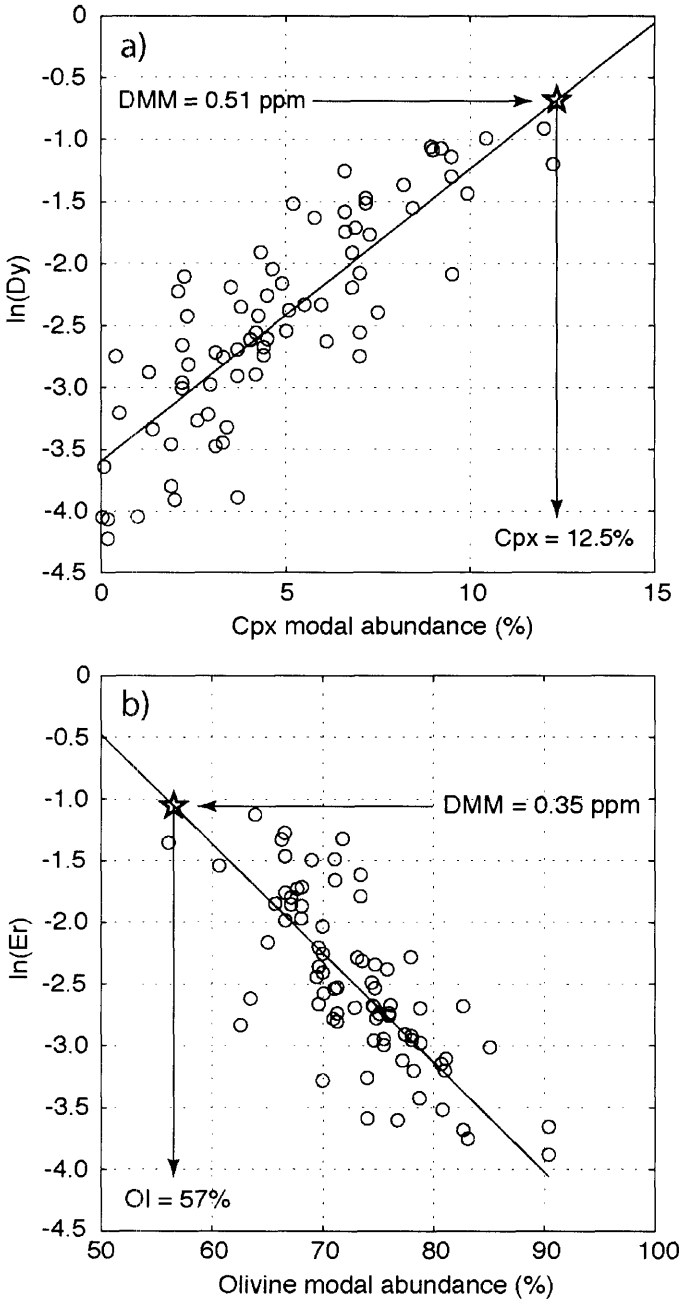

Figure 3-8. Modal abundances of a) clinopyroxene and b) olivine plotted with calculated (in the same way as for Figures 1 and 2) bulk trace element compositions of individual peridotites. Determination of the modal composition of DMM results from extrapolating the two-error regressions here to our best estimate for DMM's trace element concentrations (from Table 2).

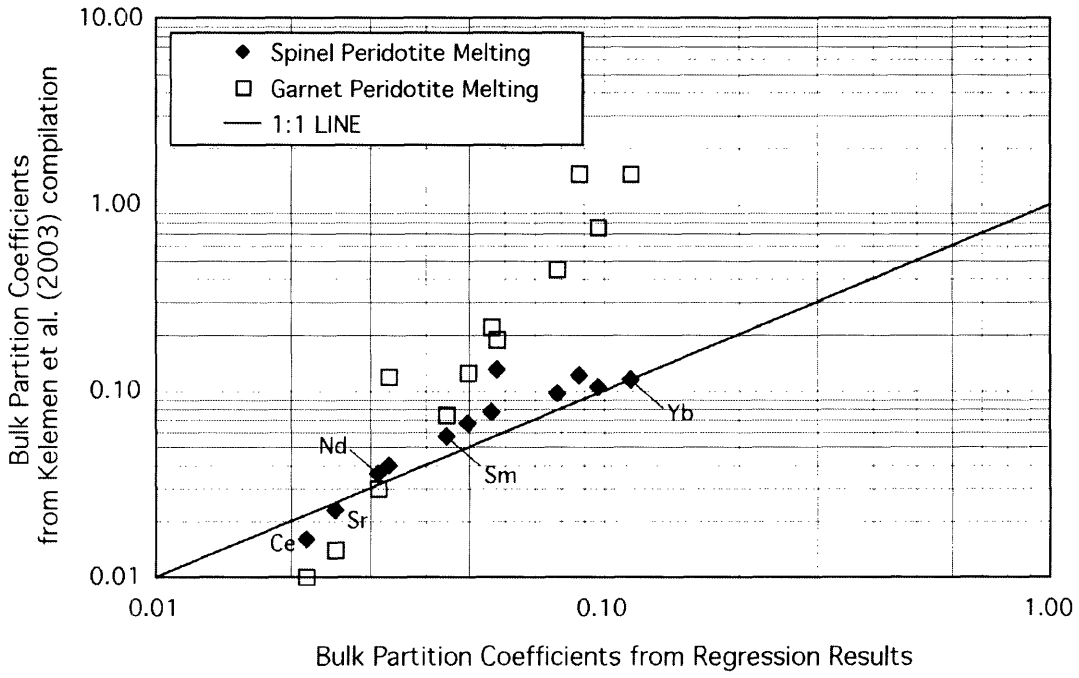

Figure 3-9. Bulk partition coefficients (D's) as obtained from abyssal peridotite trends (fig. 2, Table 2) plotted against both spinel and garnet facies bulk D values from Kelemen et al. (2003). Regression-based D values are calculated with Eqn. 5 and assuming $D_{Nd} = 0.031$. It is clear that the slope of the D values obtained reflect melting more in the spinel facies than the garnet facies, as the garnet facies is much steeper. Another choice for D_{Nd} will change the absolute concentrations, but not the slope, of the points plotted here.

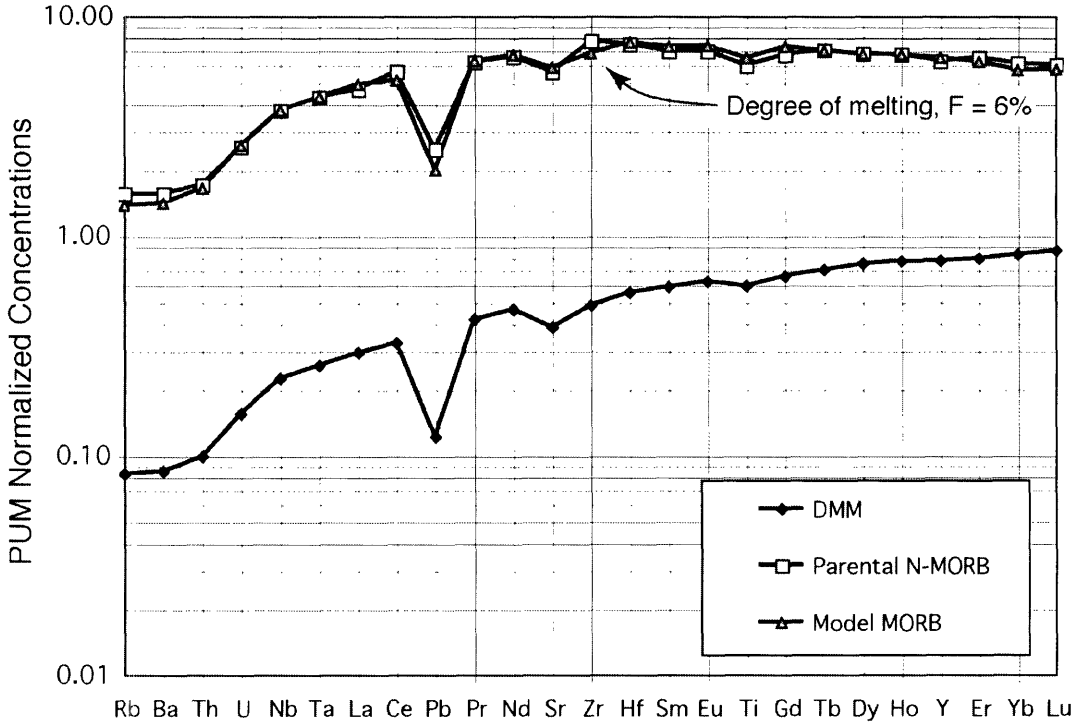

Figure 3-10. Plot showing the spectacular fit of parental N-MORB (from Su and Langmuir (2003) by 6% aggregated fractional melting of DMM (from this study) using Bulk D values in Table 2. The Rb, Ba, Th, U, and Pb for the parental MORB are taken from the N-MORB average of Hofmann (1988) and adjusted according to fractionation corrections provided by Su and Langmuir (2003).

Tables

Table 3-1. Isotopic constraints on the depleted MORB mantle (DMM).

	BSE [a]	DMM [b]	D-DMM	E-DMM	λ
$^{87}Sr/^{86}Sr$	0.7045	0.70263	0.70219	0.70307	1.42×10^{-11}
$^{143}Nd/^{144}Nd$	0.512638	0.51313	0.51326	0.51300	6.54×10^{-12}
$^{176}Hf/^{177}Hf$	0.28276	0.28326	0.28350	0.28310	1.876×10^{-11}
$^{206}Pb/^{204}Pb$	17.511	18.275	17.573	18.977	1.55125×10^{-10}
$^{207}Pb/^{204}Pb$	15.361	15.486	15.404	15.568	9.8485×10^{-10}
Rb/Sr [c]	0.0307	0.0065	0.0033	0.0111	
Sm/Nd	0.325	0.411	0.435	0.388	
Lu/Hf	0.239	0.369	0.439	0.325	
U/Pb	0.130	0.172	0.131	0.217	
Th/U [d]	3.9	2.5	2.2	3.0	

[a] Age of Earth = 4.55 Ga.

[b] Sr-Nd-Pb isotopic compositions taken from Su &Langmuir [28]; DMM is their average for MORBs far from plumes, D-DMM is 2σ depleted and E-DMM is 2σ enriched over the average. See text for Hf isotope references.

[c] Present-day parent/daughter ratios, calculated with a continuous depletion model starting 3 Ga. Decay constants (λ's) are summarized in Dickin [77].

[d] Th/U ratios taken from U-Series disequilibrium studies on MORBs, as quoted in text.

Table 3-2. Trace element composition of DMM.

	Average DMM (ppm)	Normalized [a]	Range [b] Min	Range [b] Max	Enriched DMM (ppm)	Depleted DMM (ppm)	Constraint	Calculated Bulk D [c]	1σ (%)
Rb	**0.050**	0.083	0.023	0.079	0.108	0.020	Isotopes	*0.00001*	
Ba	**0.563**	0.085	0.256	0.896	1.219	0.227	Canonical Ratio	*0.00012*	
Th	**0.0079**	0.099	0.0068	0.0089	0.0157	0.0040	U-Series	*0.001*	
U	**0.0032**	0.156	0.0027	0.0036	0.0052	0.0018	Isotopes	*0.0011*	
Nb	**0.1485**	0.226	0.1277	0.1671	0.2462	0.0864	Canonical Ratio	*0.0034*	
Ta	**0.0096**	0.259	0.0082	0.0108	0.0159	0.0056	Canonical Ratio	*0.0034*	
La	**0.192**	0.296	0.157	0.222	0.253	0.134	Extrapolated	*0.01*	
Ce	**0.550**	0.329	0.451	0.639	0.726	0.421	Regression	0.022	3.9
Pb	**0.018**	0.122	0.015	0.021	0.024	0.014	Canonical Ratio	*0.014*	
Pr	**0.107**	0.420	0.091	0.120	0.132	0.087	Interpolated	0.027	
Nd	**0.581**	0.465	0.507	0.644	0.703	0.483	Regression	0.031	3.6
Sr	**7.664**	0.385	6.462	8.709	9.718	6.092	Regression	0.025	4.7
Zr	**5.082**	0.484	4.465	5.601	6.087	4.269	Regression	0.033	7.2
Hf	**0.157**	0.555	0.142	0.170	0.186	0.127	Isotopes	0.035	
Sm	**0.239**	0.588	0.217	0.256	0.273	0.210	Regression	0.045	2.2
Eu	**0.096**	0.624	0.088	0.102	0.108	0.086	Regression	0.050	2.5
Ti	**716.3**	0.594	666.5	756.1	792.0	650.0	Regression	0.058	2.9
Gd	**0.358**	0.658	0.332	0.379	0.397	0.324	Regression	0.056	4.5
Tb	**0.070**	0.704	0.065	0.073	0.076	0.064	Interpolated	0.068	
Dy	**0.505**	0.749	0.480	0.525	0.543	0.471	Regression	0.079	7.3
Ho	**0.115**	0.772	0.110	0.119	0.123	0.108	Interpolated	0.084	
Y	**3.328**	0.774	3.179	3.445	3.548	3.129	Regression	0.088	5.0
Er	**0.348**	0.795	0.334	0.359	0.369	0.329	Regression	0.097	8.7
Yb	**0.365**	0.827	0.353	0.374	0.382	0.348	Regression	0.115	8.1
Lu	**0.058**	0.859	0.056	0.059	0.060	0.056	Extrapolated	0.120	

[a] Normalized to primitive upper mantle (PUM) with values from McDonough and Sun (1995).

[b] Minimum and maximum estimates for average DMM concentrations, based on assuming initiation of continuous depletion at 2.5 Ga and 3.5 Ga, respectively.

[c] Bulk partition coefficients calculated from Eqn. 5, assuming $D_{Nd} = 0.031$ and solving for all other D's; 1σ errors (%) are based on the variation of D estimates obtained from various regressions involving a given element. Values in italics are from Kelemen et al. (2003), except Rb, which is assumed, and U and Th, which are based on our own literature compilation. Underlined values are interpolated between regression outputs.

Table 3-3. Modal abundances and major element composition of DMM.

	Modal Abundances in DMM (%):							
	Olivine	Opx	Cpx	Spinel				
	57	28	13	2				
	Mineral compositions:							
	Olivine	Opx	Cpx	Spinel	Bulk DMM	PUM [a]	Primary N-MORB[b]	PUM minus 3% N-MORB
SiO_2	40.70	53.36	50.61		44.71	44.90	49.51	44.87
Al_2O_3		6.46	7.87	57.54	3.98	4.44	16.75	4.07
FeO*	10.16	6.27	2.94	12.56	8.18	8.03	8.05	8.05
MnO	0.14	0.12	0.09	0.16	0.13	0.13	0.14	0.13
MgO	48.59	30.55	16.19	19.27	38.73	37.71	9.74	38.68
CaO	0.05	2.18	19.52		3.17	3.54	12.50	3.27
Na_2O					0.13			
		0.05	0.89		(0.28)[c]	0.36	2.18	0.30
Cr_2O_3		0.76	1.20	10.23	0.57	0.38	0.07	0.39
TiO_2		0.16	0.63		0.13	0.20	0.90	0.18
NiO	0.36	0.09	0.06	0.24	0.24	0.25	-	-
K_2O					0.006 [d]	0.029	0.065	0.028
P_2O_5					0.019 [e]	0.021	0.095	0.019
Total	100.00	100.00	100.00	100.00	100.00	100.00	100.00	100.00
Mg # [f]	89.5	89.7	90.8	73.2	89.4	89.3	70.6	89.5
Cr # [g]				10.7				
CaO/Al_2O_3		0.34	2.48		0.80	0.80	0.75	0.80

* Total Fe as FeO.

[a] Primitive Upper Mantle (PUM) from McDonough and Sun (1995).

[b] Primary N-MORB from averaged glass compositions in Presnall and Hoover (1987).

[c] Value in parentheses is Na_2O estimated from the mass balance with continental crust (see text).

[d] Calculated by inverting parental N-MORB at 0.1 wt% K_2O for 6% melting and assuming $D_K = 0.0013$.

[e] Calculated by extracting 3% primary N-MORB (shown here) from PUM.

[f] Mg # = molar ratio of $Mg/(Mg+Fe^{2+})$; Mg # of N-MORB uses 90% total FeO as Fe^{2+}.

[g] Cr # = molar ratio of Cr/(Cr+Al).

Supplementary Data Table 3-1. Abyssal peridotite modes and compositions

Sample Number	Location	Ridge Segment	Source Ref. (modes)	Modal Data						Source Ref. (Cpx TE)
				OL	OPX	CPX	SP	Plag	Sum	
Vulc5:41-13(5)	Vulcan FZ	American-Antarctic	Dick (1989) G.S. Sp. Pub.	71.80	18.10	8.94	1.21	0.00	100.05	Johnson et al. (1990)
Vulc5:41-15(8)	Vulcan FZ	American-Antarctic	Dick (1989) G.S. Sp. Pub.	63.90	22.70	12.00	1.44	0.00	100.04	Johnson et al. (1990)
Vulc5:41-30(3)	Vulcan FZ	American-Antarctic	Dick (1989) G.S. Sp. Pub.	65.70	27.20	5.79	1.33	0.00	100.02	Johnson et al. (1990)
Vulc5:41-33(6)	Vulcan FZ	American-Antarctic	Dick (1989) G.S. Sp. Pub.	68.10	21.00	9.93	0.96	0.04	100.03	Johnson et al. (1990)
Vulc5:41-45(7)	Vulcan FZ	American-Antarctic	Dick (1989) G.S. Sp. Pub.	68.10	22.30	8.45	1.14	0.04	100.03	Johnson et al. (1990)
Vulc5:34-56(3)	Bullard FZ	American-Antarctic	Dick (1989) G.S. Sp. Pub.	74.80	17.10	7.50	0.60	0.00	100.00	Johnson et al. (1990)
Vulc5:35-1(4)	Bullard FZ	American-Antarctic	Dick (1989) G.S. Sp. Pub.	74.40	19.20	5.97	0.44	0.00	100.01	Johnson et al. (1990)
Vulc5:35-19(2)	Bullard FZ	American-Antarctic	Dick (1989) G.S. Sp. Pub.	70.00	22.10	6.89	1.09	0.00	100.08	Johnson et al. (1990)
Vulc5:35-22(4)	Bullard FZ	American-Antarctic	Dick (1989) G.S. Sp. Pub.	77.40	18.90	2.96	0.73	0.04	100.03	Johnson et al. (1990)
Vulc5:35-30(8)	Bullard FZ	American-Antarctic	Dick (1989) G.S. Sp. Pub.	74.70	20.10	4.27	1.00	0.00	100.07	Johnson et al. (1990)
Vulc5:37-3(2)	Bullard FZ	American-Antarctic	Dick (1989) G.S. Sp. Pub.	82.70	13.90	2.35	0.05	1.05	100.05	Johnson et al. (1990)
AII107:40-6(5)	Bouvet FZ	SW Indian	Dick (1989) G.S. Sp. Pub.	78.20	18.10	3.40	0.30	0.00	100.00	Johnson et al. (1990)
AII107:40-8(6)	Bouvet FZ	SW Indian	Dick (1989) G.S. Sp. Pub.	77.20	19.60	3.10	0.10	0.00	100.00	Johnson et al. (1990)
AII107:40-11(9)	Bouvet FZ	SW Indian	Dick (1989) G.S. Sp. Pub.	81.10	15.50	2.90	0.40	0.00	99.90	Johnson et al. (1990)
AII107:40-13(5)	Bouvet FZ	SW Indian	Dick (1989) G.S. Sp. Pub.	78.70	18.80	2.00	0.50	0.00	100.00	Johnson et al. (1990)
AII107:40-27(5)	Bouvet FZ	SW Indian	Dick (1989) G.S. Sp. Pub.	80.70	15.50	3.30	0.40	0.00	99.90	Johnson et al. (1990)
IO11/76:56-57(4)	Islas Orcadas FZ	SW Indian	Dick (1989) G.S. Sp. Pub.	69.60	24.50	4.32	1.66	0.00	100.08	Johnson et al. (1990)
IO11/76:56-10(10)	Islas Orcadas FZ	SW Indian	Dick (1989) G.S. Sp. Pub.	73.40	18.70	7.18	0.67	0.00	99.95	Johnson et al. (1990)
IO11/76:56-54(4)	Islas Orcadas FZ	SW Indian	Dick (1989) G.S. Sp. Pub.	69.00	21.70	8.20	1.14	0.00	100.04	Johnson et al. (1990)
IO11/76:58-34(4)	Islas Orcadas FZ	SW Indian	Dick (1989) G.S. Sp. Pub.	70.00	25.90	3.51	0.62	0.00	100.03	Johnson et al. (1990)
PS86:6-37(3)	E. of Shaka FZ	SW Indian	Johnson et al. (1990)	66.56	21.85	10.43	1.13	0.00	99.97	Johnson et al. (1990)
Prot5:15-90(8)	Andrew Bain FZ	SW Indian	Johnson et al. (1990)	70.00	22.00	7.00	1.00	0.00	100.00	Johnson et al. (1990)
Prot5:19-2(8)	Pnc. Edward FZ	SW Indian	Johnson et al. (1990)	72.90	23.40	3.10	0.60	0.00	100.00	Johnson et al. (1990)
Prot5:29-26(6)	Discovery II FZ	SW Indian	Johnson et al. (1990)	63.50	28.60	7.00	0.90	0.00	100.00	Johnson et al. (1990)
Prot5:38-1(3)	Indomed FZ	SW Indian	Johnson et al. (1990)	69.40	24.80	5.10	0.70	0.00	100.00	Johnson et al. (1990)
RC27-9:6-3(7)	Atlantis II FZ	SW Indian	Johnson et al. (1990)	67.10	25.60	6.60	0.60	0.00	99.90	Johnson et al. (1990)
RC27-9:6-8(8)	Atlantis II FZ	SW Indian	Johnson et al. (1990)	66.60	25.80	6.60	0.80	0.00	99.80	Johnson et al. (1990)
RC27-9:25-142(6)	Atlantis II FZ	SW Indian	Johnson et al. (1990)	56.10	33.50	9.00	1.50	0.00	100.10	Johnson et al. (1990)
RC27-9:18-23	Atlantis II FZ	SW Indian	Johnson & Dick (1992)	73.38	18.59	7.18	0.86	0.00	100.01	Johnson & Dick (1992)
RC27-9:18-45	Atlantis II FZ	SW Indian	Johnson & Dick (1992)	77.92	19.39	2.25	0.43	0.00	99.99	Johnson & Dick (1992)
RC27-9:25-138	Atlantis II FZ	SW Indian	Johnson & Dick (1992)	71.08	18.26	9.50	1.13	0.04	100.01	Johnson & Dick (1992)
RC27-9:30-32	Atlantis II FZ	SW Indian	Johnson & Dick (1992)	42.50	42.10	15.09	0.46	0.00	100.15	Johnson & Dick (1992)
RC27-9:30-40	Atlantis II FZ	SW Indian	Johnson & Dick (1992)	66.29	23.74	9.22	0.75	0.00	100.00	Johnson & Dick (1992)
RC27-9:34-58	Atlantis II FZ	SW Indian	Johnson & Dick (1992)	70.94	25.37	3.31	0.37	0.00	99.99	Johnson & Dick (1992)
RC27-9:34-63	Atlantis II FZ	SW Indian	Johnson & Dick (1992)	71.06	22.72	5.51	0.71	0.00	100.00	Johnson & Dick (1992)
RC27-9:35-49	Atlantis II FZ	SW Indian	Johnson & Dick (1992)	75.96	19.53	4.05	0.45	0.00	99.99	Johnson & Dick (1992)
RC27-9:35-80	Atlantis II FZ	SW Indian	Johnson & Dick (1992)	74.52	20.28	5.01	0.19	0.00	100.00	Johnson & Dick (1992)
RC27-9:44-1	Atlantis II FZ	SW Indian	Johnson & Dick (1992)	73.56	21.33	4.64	0.47	0.00	100.00	Johnson & Dick (1992)

Supplementary Data Table 3-1, Part 1, Page 2

Sample Number	Location	Ridge Segment	Source Ref. (modes)	Modal Data						Source Ref. (Cpx TE)
				OL	OPX	CPX	SP	Plag	Sum	
RC27-9:46-1	Atlantis II FZ	SW Indian	Johnson & Dick (1992)	67.69	25.90	5.21	1.20	0.00	100.00	Johnson & Dick (1992)
RC27-9:46-2	Atlantis II FZ	SW Indian	Johnson & Dick (1992)	74.71	22.24	2.09	0.96	0.00	100.00	Johnson & Dick (1992)
RC27-9 35-80	**Atlantis II FZ**	**SW Indian**	**Johnson & Dick (1992)**	**74.52**	**20.28**	**5.01**	**0.19**	**0.00**	**100.00**	**Salters and Dick (2002)**
RC 27-9 25-138	**Atlantis II FZ**	**SW Indian**	**Johnson & Dick (1992)**	**71.08**	**18.26**	**9.50**	**1.13**	**0.04**	**100.01**	**Salters and Dick (2002)**
RC27-9 30-44	Atlantis II FZ	SW Indian	Johnson & Dick (1992)	65.03	24.51	9.51	0.95	0.00	100.00	Salters and Dick (2002)
RC27-9 34-62	Atlantis II FZ	SW Indian	Johnson & Dick (1992)	68.06	23.78	7.29	0.79	0.07	99.99	Salters and Dick (2002)
RC27-9 18-51	Atlantis II FZ	SW Indian	Johnson & Dick (1992)	75.09	19.50	2.36	0.82	2.23	100.00	Salters and Dick (2002)
RC27-9 6-3	**Atlantis II FZ**	**SW Indian**	**Johnson & Dick (1990)**	**67.10**	**25.60**	**6.62**	**0.64**	**0.00**	**99.96**	**Salters and Dick (2002)**
RC27-9 35-49	**Atlantis II FZ**	**SW Indian**	**Johnson & Dick (1992)**	**75.96**	**19.53**	**4.05**	**0.45**	**0.00**	**99.99**	**Salters and Dick (2002)**
RC27-9 6-8	**Atlantis II FZ**	**SW Indian**	**Johnson & Dick (1990)**	**66.60**	**25.80**	**6.61**	**0.80**	**0.00**	**99.81**	**Salters and Dick (2002)**
PS86-6-26	10-16 deg E	SW Indian	Dick (1984) & unpubl.	60.65	26.23	12.26	0.85	0.00	99.99	Salters and Dick (2002)
ANTP 134 HD3	Vema FZ	Central Indian	Dick (1984) & unpubl.	69.60	25.30	4.50	0.60	0.00	100.00	Hellebrand et al. (2002)
"	Vema FZ	Central Indian	Dick (1984) & unpubl.	69.60	25.30	4.50	0.60	0.00	100.00	Hellebrand et al. (2002)
ANTP 134 HD4	Vema FZ	Central Indian	Dick (1984) & unpubl.	78.80	16.20	4.20	0.60	0.00	99.80	Hellebrand et al. (2002)
"	Vema FZ	Central Indian	Dick (1984) & unpubl.	78.80	16.20	4.20	0.60	0.00	99.80	Hellebrand et al. (2002)
ANTP 134 HD7	Vema FZ	Central Indian	Dick (1984) & unpubl.	62.60	35.10	1.30	0.90	0.00	99.90	Hellebrand et al. (2002)
ANTP 134 HD8	Vema FZ	Central Indian	Dick (1984) & unpubl.	78.00	17.20	4.40	0.20	0.00	99.80	Hellebrand et al. (2002)
"	Vema FZ	Central Indian	Dick (1984) & unpubl.	78.00	17.20	4.40	0.20	0.00	99.80	Hellebrand et al. (2002)
CIRCE 93 HD2	CIR axis 12° S	Central Indian	Dick (1984) & unpubl.	90.4	9.3	0.2	0.04	0	99.94	Hellebrand et al. (2002)
"	CIR axis 12° S	Central Indian	Dick (1984) & unpubl.	90.4	9.3	0.2	0.04	0	99.94	Hellebrand et al. (2002)
RC27-9:46-1	Atlantis II FZ	SW Indian	Johnson & Dick (1992)	67.69	25.90	5.21	1.20	0.00	100.00	Johnson & Dick (1992)
RC27-9:46-2	Atlantis II FZ	SW Indian	Johnson & Dick (1992)	74.71	22.24	2.09	0.96	0.00	100.00	Johnson & Dick (1992)
RC27-9 35-80	**Atlantis II FZ**	**SW Indian**	**Johnson & Dick (1992)**	**74.52**	**20.28**	**5.01**	**0.19**	**0.00**	**100.00**	**Salters and Dick (2002)**
RC 27-9 25-138	**Atlantis II FZ**	**SW Indian**	**Johnson & Dick (1992)**	**71.08**	**18.26**	**9.50**	**1.13**	**0.04**	**100.01**	**Salters and Dick (2002)**
"	CIR axis 12° S	Central Indian	Dick (1984) & unpubl.	90.4	9.3	0.2	0.04	0	99.94	Hellebrand et al. (2002)
CIRCE 93 HD4	CIR axis 12° S	Central Indian	Dick (1984) & unpubl.	75.50	21.70	2.20	0.70	0.00	100.10	Hellebrand et al. (2002)
"	CIR axis 12° S	Central Indian	Dick (1984) & unpubl.	75.50	21.70	2.20	0.70	0.00	100.10	Hellebrand et al. (2002)
CIRCE 93 HD7	CIR axis 12° S	Central Indian	Dick (1984) & unpubl.	83.10	16.70	0.10	0.10	0.00	100.00	Hellebrand et al. (2002)
ANTP 126 HD2	Argo FZ	Central Indian	Dick (1984) & unpubl.	70.10	23.40	6.10	0.40	0.00	100.00	Hellebrand et al. (2002)
ANTP 126-HD5	Argo FZ	Central Indian	Dick (1984) & unpubl.	71.30	20.90	7.00	0.80	0.00	100.00	Hellebrand et al. (2002)
"	Argo FZ	Central Indian	Dick (1984) & unpubl.	71.30	20.90	7.00	0.80	0.00	100.00	Hellebrand et al. (2002)
ANTP 126 D5	Argo FZ	Central Indian	Dick (1984) & unpubl.	74.60	20.80	3.70	0.90	0.00	100.00	Hellebrand et al. (2002)
"	Argo FZ	Central Indian	Dick (1984) & unpubl.	74.60	20.80	3.70	0.90	0.00	100.00	Hellebrand et al. (2002)
ANTP 84 HD11	Marie Celeste FZ	Central Indian	Dick (1984) & unpubl.	76.70	19.50	3.70	0.10	0.00	100.00	Hellebrand et al. (2002)
ANTP 87 HD5	Marie Celeste FZ	Central Indian	Dick (1984) & unpubl.	80.80	17.90	1.00	0.30	0.00	100.00	Hellebrand et al. (2002)
ANTP 87 HD9	Marie Celeste FZ	Central Indian	Dick (1984) & unpubl.	82.70	17.10	0.04	0.14	0.00	99.98	Hellebrand et al. (2002)
ANTP 89 HD1	Marie Celeste FZ	Central Indian	Dick (1984) & unpubl.	71.30	27.80	0.40	0.40	0.00	99.90	Hellebrand et al. (2002)

Supplementary Data Table 3-1, Part 1, Page 3

Sample Number	Location	Ridge Segment	Source Ref. (modes)	Modal Data						Source Ref. (Cpx TE)
				OL	OPX	CPX	SP	Plag	Sum	
ANTP 89 HD2	Marie Celeste FZ	Central Indian	Dick (1984) & unpubl.	76.10	21.20	2.20	0.30	0.00	99.80	Hellebrand et al. (2002)
ANTP 89 HD5	Marie Celeste FZ	Central Indian	Dick (1984) & unpubl.	73.10	20.50	4.90	0.50	1.00	100.00	Hellebrand et al. (2002)
ANTP 89 HD8	Marie Celeste FZ	Central Indian	Dick (1984) & unpubl.	75.80	19.90	3.80	0.30	0.00	99.80	Hellebrand et al. (2002)
ANTP 89 HD15	Marie Celeste FZ	Central Indian	Dick (1984) & unpubl.	85.10	14.40	0.50	0.04	0.00	100.04	Hellebrand et al. (2002)
ANTP 89 HD17	Marie Celeste FZ	Central Indian	Dick (1984) & unpubl.	81.00	16.90	1.90	0.10	0.00	99.90	Hellebrand et al. (2002)
ME33/2-31GTV	Green Rock Hill	Central Indian	Hellebrand et al. (2002)	70.00	28.00	1.40	0.60	NA	100.00	Hellebrand et al. (2002)
SO92-60GTV	Green Rock Hill	Central Indian	Hellebrand et al. (2002)	74.00	22.80	2.60	0.60	NA	100.00	Hellebrand et al. (2002)
SO92-74GTV	Green Rock Hill	Central Indian	Hellebrand et al. (2002)	74.00	23.50	1.90	0.60	NA	100.00	Hellebrand et al. (2002)
G96-39/36	Romanche FZ	Mid-Atlantic	Tartorotti et al. (2002)	66.60	25.00	6.80	1.10	0.50	100.00	Tartorotti et al. (2002)
G96-39/36	Romanche FZ	Mid-Atlantic	Tartorotti et al. (2002)	66.60	25.00	6.80	1.10	0.50	100.00	Tartorotti et al. (2002)
895B 1R-1, 71-76	Site 895	East Pacific Rise	Dick and Natlland (1996)	87.70	11.30	0.31	0.62	0.12	100.05	Dick and Natlland (1996)
895C 1R-1, 28-32	Site 895	East Pacific Rise	Dick and Natlland (1996)	82.60	14.90	1.22	1.24	0.00	99.96	Dick and Natlland (1996)
895C 1R-1, 28-32	Site 895	East Pacific Rise	Dick and Natlland (1996)	82.60	14.90	1.22	1.24	0.00	99.96	Dick and Natlland (1996)
895C 3R-1, 35-39	Site 895	East Pacific Rise	Dick and Natlland (1996)	81.30	16.20	1.43	1.04	0.00	99.97	Dick and Natlland (1996)
895D 3R-1 116-120	Site 895	East Pacific Rise	Dick and Natlland (1996)	82.20	15.90	1.16	0.79	0.00	100.05	Dick and Natlland (1996)
895D 4R-3 97-101	Site 895	East Pacific Rise	Dick and Natlland (1996)	78.00	18.70	2.41	0.87	0.00	99.98	Dick and Natlland (1996)
895D 7R-2, 129-133	Site 895	East Pacific Rise	Dick and Natlland (1996)	82.20	15.60	1.71	0.48	0.00	99.99	Dick and Natlland (1996)

Supplementary Data Table 3-1, Part 2, Page 1

Sample Number	CPX Trace Element Content Concentration in ppm															
	cpx Sc	cpx V	cpx Cr	cpx La	cpx Ti	cpx Sr	cpx Zr	cpx Ce	cpx Nd	cpx Sm	cpx Eu	cpx Gd	cpx Dy	cpx Er	cpx Yb	cpx Y
Vulc5:41-13(5)	49.00	279.00	5637.00		2615.00	5.10	10.60	0.43	1.83	1.22	0.60		2.87	1.87	1.71	
Vulc5:41-15(8)	49.00	297.00	5925.00		2879.00	5.40	11.50	0.50	1.92	1.24	0.57		2.56	1.79	1.61	
Vulc5:41-30(3)	53.00	309.00	7530.00		1979.00	1.00	2.60	0.06	0.71	0.78	0.35		1.94	1.22	1.18	
Vulc5:41-33(6)	54.00	298.00	6759.00		1547.00	2.10	5.00	0.17	0.60	0.70	0.32		1.78	1.14	1.18	
Vulc5:41-45(7)	50.00	355.00	7928.00		1554.00	1.30	1.50	0.04	0.40	0.41	0.20		1.75	1.06	1.10	
Vulc5:34-56(3)	64.00	274.00	7579.00		796.00	0.60	0.60	0.01	0.08	0.15	0.08		0.87	0.49	0.32	
Vulc5:35-1(4)	70.00	300.00	7158.00		754.00	0.80	0.60	0.02	0.10	0.22	0.11		1.05	0.72	0.54	
Vulc5:35-19(2)	56.00	270.00	5876.00		1893.00	3.10	4.50	0.33	0.61	0.50	0.21		1.71	1.01	0.74	
Vulc5:35-22(4)	61.00	295.00	8150.00		886.00	1.80	0.30	0.01	0.04	0.12	0.07		0.82	0.64	0.57	
Vulc5:35-30(8)	54.00	321.00	8955.00		779.00	3.80	0.30	0.02	0.12	0.17	0.09		1.16	0.79	0.89	
Vulc5:37-3(2)	84.00	367.00	8275.00		1335.00	1.10	3.20	0.05	0.56	0.58	0.30		1.78	0.98	0.78	
AII107:40-6(5)	50.00	342.00	10227.00		244.00	1.20	0.10	0.01	0.02	0.05	0.02		0.55	0.46	0.57	
AII107:40-8(6)	70.00	285.00	6534.00		363.00	0.70	0.10	0.04	0.13	0.08	0.04		0.48	0.50	0.63	
AII107:40-11(9)	54.00	297.00	8392.00		443.00	0.50	0.10	0.01	0.02	0.05	0.03		0.70	0.57	0.70	
AII107:40-13(5)	53.00	291.00	8519.00		368.00	1.20	0.10	0.01	0.01	0.05	0.03		0.38	0.43	0.46	
AII107:40-27(5)	73.00	274.00	6518.00		326.00	0.80	0.20	0.02	0.04	0.07	0.03		0.52	0.52	0.53	
IO11/76:56-57(4)	73.00	301.00	6042.00		1608.00	0.60	2.20	0.02	0.48	0.60	0.27		1.79	1.01	1.10	
IO11/76:56-10(10)	44.00	278.00	6925.00		1320.00	0.60	1.40	0.02	0.47	0.48	0.30		2.12	1.57	1.57	
IO11/76:56-54(4)	57.00	276.00	7793.00		1606.00	1.40	2.80	0.06	0.60	0.63	0.34		2.17	1.58	1.49	
IO11/76:58-34(4)	52.00	278.00	6053.00		1113.00	20.20	1.10	1.55	0.60	0.34	0.18		1.46	1.01	0.69	
PS86:6-37(3)	52.00	293.00	6829.00		2674.00	5.40	11.00	0.87	2.16	1.37	0.56		2.65	1.70	1.67	
Prot5:15-90(8)	41.00	290.00	9462.00		1083.00	0.40	0.50	0.02	0.24	0.39	0.18		1.18	0.69	0.74	
Prot5:19-2(8)	78.00	258.00	7433.00		598.00	8.00	2.10	1.02	0.58	0.26	0.12		0.95	0.71	0.62	
Prot5:29-26(6)	74.00	276.00	7765.00		527.00	1.20	0.90	0.07	0.13	0.13	0.06		0.56	0.51	0.48	
Prot5:38-1(3)	62.00	282.00	7124.00		567.00	0.60	0.40	0.03	0.15	0.15	0.08		1.02	0.74	0.54	
RC27-9:6-3(7)	55.00	305.00	7051.00		1525.00	1.20	2.10	0.04	0.62	0.62	0.33		1.93	1.17	0.78	
RC27-9:6-8(8)	47.00	338.00	6959.00		1702.00	0.60	1.70	0.03	0.76	0.76	0.39		2.67	1.72	1.74	
RC27-9:25-142(6)	38.00	308.00	7334.00		1843.00	1.20	3.10	0.11	0.92	0.92	0.47		2.40	1.50	1.63	
RC27-9:18-23	56.00	326.50	5909.50		1875.50	1.01	2.50	0.06	0.75	0.80	0.39		2.22	1.33	1.39	
RC27-9:18-45	53.33	327.50	5617.50		1790.00	0.97	2.42	0.05	0.62	0.72	0.34		2.18	1.29	1.36	
RC27-9:25-138								0.12	0.98	0.88	0.40		2.17	1.29	1.35	
RC27-9:30-32			8673.33		1356.67	3.14	3.61	0.20	1.04	0.87	0.42		2.17	1.38	1.29	
RC27-9:30-40			7596.33		1747.00	1.29	3.06	0.10	0.97	0.90	0.43		2.62	1.70	1.59	
RC27-9:34-58			8690.00		537.00	0.44	0.20	0.02	0.04	0.13	0.06		0.86	0.61	0.64	
RC27-9:34-63			8771.50		687.00	0.60	0.37	0.01	0.07	0.15	0.08		1.05	0.67	0.72	
RC27-9:35-49			8608.50		598.25	0.59	0.23	0.02	0.07	0.13	0.08		0.99	0.66	0.75	
RC27-9:35-80			9007.67		571.67	0.77	0.16	0.01	0.05	0.11	0.07		0.93	0.64	0.66	
RC27-9:44-1			8811.00		929.00	2.89	0.42	0.03	0.17	0.31	0.16		1.58	0.93	0.96	
RC27-9:46-1			7605.33		1521.33	0.71	1.29	0.03	0.43	0.67	0.30		2.35	1.47	1.54	
RC27-9:46-2			8395.50		1135.00	0.53	1.08	0.03	0.37	0.50	0.24		1.87	1.16	1.15	

Supplementary Data Table 3-1, Part 2, Page 2

Sample Number	CPX Trace Element Content Concentration in ppm															
	cpx Sc	cpx V	cpx Cr	cpx La	cpx Ti	cpx Sr	cpx Zr	cpx Ce	cpx Nd	cpx Sm	cpx Eu	cpx Gd	cpx Dy	cpx Er	cpx Yb	cpx Y
RC27-9 35-80					**572.00**	**0.77**	**0.16**	**0.01**	**0.05**	**0.11**	**0.07**		**0.93**	**0.64**	**0.66**	
RC 27-9 25-138	**30.23**		**5507.37**		**2109.95**	**4.87**	**6.74**	**0.34**	**1.93**	**1.07**	**0.47**		**2.53**	**1.53**	**1.40**	
RC27-9 30-44	29.04		7499.34		518.02	0.65	0.37	0.00	0.07	0.13	0.07		0.92	0.72	0.68	
RC27-9 34-62	22.87		4792.70		1103.61	1.06	1.69	0.06	0.56	0.49	0.19		1.53	1.02	0.95	
RC27-9 18-51	21.01		6182.36		660.96	0.58	0.43	0.01	0.17	0.25	0.11		1.05	0.80	0.69	
RC27-9 6-3					**1535.00**	**1.19**	**2.32**	**0.04**	**0.47**	**0.57**	**0.33**		**1.64**	**1.23**	**1.18**	
RC27-9 35-49					**627.17**	**0.60**	**0.27**	**0.01**	**0.07**	**0.14**	**0.08**		**1.00**	**0.65**	**0.72**	
RC27-9 6-8					**1863.00**	**1.27**	**1.10**	**0.03**	**0.57**	**0.77**	**0.38**		**2.66**	**1.72**	**1.74**	
PS86-6-26			5801.6	0.007	1325.7	1.740	2.483	0.093	0.834	0.611	0.267		1.842	1.125	0.994	
ANTP 134 HD3				0.0014	790.00	0.63	0.62	0.014	0.240	0.340	0.140	0.660	1.220	0.840	0.860	6.200
"				0.0023	668.00	1.35	1.00	0.016	0.250	0.250	0.120		0.860	0.620	0.560	6.000
ANTP 134 HD4				0.0020	657.00	0.88	0.54	0.036	0.260	0.270	0.130	0.680	1.090	0.730	0.830	5.700
"					628.00	1.07	1.00	0.035	0.310	0.300	0.120		0.780	0.550	0.570	5.800
ANTP 134 HD7					858.00	1.30	1.60	0.025	0.280	0.250	0.120		0.850	0.590	0.560	6.500
ANTP 134 HD8				0.0018	601.00	0.65	0.47	0.024	0.190	0.190	0.080	0.650	0.930	0.540	0.580	4.700
"					641.00	0.98	1.20	0.033	0.290	0.260	0.140		0.870	0.560	0.620	6.100
CIRCE 93 HD2				0.0140	965	1.19	0.40	0.028	0.060	0.120	0.065	0.420	0.750	0.640	0.720	5.400
"					825	1.60	0.76		0.120	0.140	0.070		0.640	0.510	0.490	4.800
CIRCE 93 HD4				0.0030	551.00	0.44	0.19	0.013	0.110	0.110	0.050	0.370	0.890	0.630	0.740	5.000
"					451.00	1.18	0.53	0.016	0.130	0.140	0.060		0.850	0.600	0.580	5.100
CIRCE 93 HD7				0.0150	601.00	3.24	3.50	0.095	0.500	0.460	0.210	0.840	0.840	0.440	0.530	4.200
ANTP 126 HD2				0.0090	391.00	0.54	0.21	0.049	0.040	0.070	0.040	0.250	0.730	0.610	0.660	4.500
ANTP 126-HD5				0.0100	388.00	0.47	0.17	0.045	0.060	0.070	0.040	0.340	0.740	0.620	0.750	4.600
"								0.041	0.090	0.090	0.050		0.610	0.470	0.570	
ANTP 126 D5				0.0050	516.00	0.58	0.17	0.020	0.050	0.130	0.060	0.390	0.940	0.710	0.840	5.200
"								0.020	0.080	0.120	0.080		0.760	0.540	0.620	
ANTP 84 HD11					130.00	0.19	0.07	0.002	0.005	0.009	0.003	0.060	0.290	0.290	0.400	2.000
ANTP 87 HD5				0.0025	259.00	0.25	0.08	0.002		0.030	0.020	0.130	0.420	0.460	0.490	2.800
ANTP 87 HD9				0.0050	345.00	0.48	0.11	0.007	0.020	0.040	0.040	0.220	0.560	0.470	0.590	3.800
ANTP 89 HD1				0.0024	913.00	0.72	0.78	0.013	0.210	0.300	0.130	0.760	1.330	0.840	0.950	6.800
ANTP 89 HD2				0.0019	767.00	0.40	0.28	0.006	0.060	0.160	0.100	0.550	1.220	0.840	0.910	6.700
ANTP 89 HD5				0.0010	791.00	0.27	0.21	0.005	0.130	0.230	0.130	0.730	1.380	0.950	1.080	7.500
ANTP 89 HD8				0.0030	817.00	0.29	0.26	0.006	0.120	0.210	0.130	0.750	1.330	0.970	0.990	7.100
ANTP 89 HD15				0.0015	1419.00	0.63	0.95	0.008	0.170	0.210	0.130	0.710	1.260	0.930	0.920	7.200
ANTP 89 HD17				0.0140	575.00	0.33	0.13	0.013	0.012	0.060	0.040	0.240	0.640	0.570	0.720	4.200
ME33/2-31GTV				0.0020	523.00	0.39	0.16	0.004	0.040	0.060	0.030	0.230	0.610	0.430	0.580	3.400
SO92-60GTV				0.0050	500.00	0.42	0.13	0.017	0.030	0.090	0.040	0.270	0.600	0.430	0.580	3.500
SO92-74GTV				0.0013	460.00	0.29	0.12	0.003	0.020	0.040	0.020	0.180	0.390	0.330	0.330	3.200
G96-39/36	53.00	249.00	10400.00	0.01	353.00	0.24	0.41	0.05	0.14	0.11	0.06	0.32	1.03	1.02	1.00	8.30
G96-39/36	68.00	261.00	10210.00		445.00	0.44	0.80	0.07	0.22	0.19	0.07	0.47	1.37	1.28	1.07	10.80

Supplementary Data Table 3-1, Part 2, Page 3

Sample Number	CPX Trace Element Content Concentration in ppm															
	cpx Sc	cpx V	cpx Cr	cpx La	cpx Ti	cpx Sr	cpx Zr	cpx Ce	cpx Nd	cpx Sm	cpx Eu	cpx Gd	cpx Dy	cpx Er	cpx Yb	cpx Y
895B 1R-1, 71-76		215.00	6387.00		147.00	0.500	0.400	0.013	0.111	0.167	0.036		0.135	0.161	0.212	0.800
895C 1R-1, 28-32		194.00	7511.00		150.00	0.400	0.200	0.010	0.023	0.021	0.006		0.126	0.165	0.229	1.000
895C 1R-1, 28-32		227.00	7165.00		173.00	0.700	0.500	0.004	0.015	0.010	0.002		0.018	0.033	0.071	0.900
895C 3R-1, 35-39		201.00	6740.00		184.00	0.800	0.300	0.010	0.018	0.014	0.007		0.132	0.168	0.204	1.000
895D 3R-1 116-120		201.00	6535.00		156.00	0.600	0.400	0.002	0.016	0.033	0.007		0.117	0.163	0.218	0.900
895D 4R-3 97-101		202.00	7599.00		208.00	0.400	0.300	0.015	0.033	0.046	0.009		0.142	0.186	0.231	0.800
895D 7R-2, 129-133		219.00	7137.00		163.00	0.900	0.600	0.019	0.044	0.063	0.020		0.137	0.193	0.215	0.900

Supplementary Data Table 3-1, Part 3, Page 1

Sample Number	Calculated Whole Rock Trace Element Content Concentration in ppm											
	bulk rock Ti	bulk rock Sr	bulk rock Zr	bulk rock Ce	bulk rock Nd	bulk rock Sm	bulk rock Eu	bulk rock Gd	bulk rock Dy	bulk rock Er	bulk rock Yb	bulk rock Y
Vulc5:41-13(5)	333.80475	0.477810	1.889013	0.041236	0.180080	0.126382	0.064766	NaN	0.345861	0.266281	0.290742	NaN
Vulc5:41-15(8)	454.52213	0.676931	2.558331	0.064056	0.251890	0.170089	0.081226	NaN	0.401014	0.323966	0.333464	NaN
Vulc5:41-30(3)	193.39778	0.064311	0.454765	0.004055	0.050593	0.060998	0.029590	NaN	0.195579	0.156983	0.184595	NaN
Vulc5:41-33(6)	210.87544	0.218953	0.974458	0.018154	0.065806	0.080774	0.038518	NaN	0.238524	0.179634	0.217903	NaN
Vulc5:41-45(7)	190.63695	0.116698	0.277990	0.003698	0.038203	0.041610	0.021351	NaN	0.211703	0.154238	0.190196	NaN
Vulc5:34-56(3)	88.92315	0.047434	0.094848	0.000811	0.006681	0.013285	0.007417	NaN	0.091352	0.061979	0.049549	NaN
Vulc5:35-1(4)	72.72330	0.051398	0.089130	0.001331	0.006922	0.016433	0.008723	NaN	0.097137	0.083152	0.077864	NaN
Vulc5:35-19(2)	203.54483	NaN	0.762347	NaN	0.048688	0.042898	0.019115	NaN	0.180015	0.131182	0.116810	NaN
Vulc5:35-22(4)	60.64670	NaN	0.036028	NaN	0.001560	0.005336	0.003432	NaN	0.051074	0.054662	0.065567	NaN
Vulc5:35-30(8)	63.87800	NaN	0.041322	NaN	0.006320	0.009916	0.005683	NaN	0.089064	0.079375	0.115259	NaN
Vulc5:37-3(2)	79.98319	0.029496	0.306072	0.001423	0.017074	0.020325	0.011555	NaN	0.088741	0.068508	0.078051	NaN
AII107:40-6(5)	17.38195	NaN	0.011972	NaN	0.000860	0.002416	0.001054	NaN	0.036111	0.040605	0.067233	NaN
AII107:40-8(6)	24.56603	NaN	0.012012	NaN	0.005292	0.003706	0.002042	NaN	0.031006	0.044094	0.074267	NaN
AII107:40-11(9)	29.55918	NaN	0.010780	NaN	0.000735	0.002081	0.001363	NaN	0.040176	0.044713	0.075927	NaN
AII107:40-13(5)	21.50500	NaN	0.010929	NaN	0.000293	0.001741	0.001181	NaN	0.020011	0.032618	0.048700	NaN
AII107:40-27(5)	23.00745	NaN	0.022334	NaN	0.001630	0.003192	0.001483	NaN	0.031906	0.042827	0.059494	NaN
IO11/76:56-57(4)	136.21770	0.029390	0.340106	0.001039	0.026537	0.037048	0.018227	NaN	0.148235	0.110254	0.151336	NaN
IO11/76:56-10(10)	143.68200	0.045738	0.224013	0.001569	0.038108	0.041487	0.027278	NaN	0.220162	0.198368	0.242752	NaN
IO11/76:56-54(4)	193.18173	0.121979	0.507286	0.005385	0.055633	0.062116	0.035270	NaN	0.255496	0.224265	0.252542	NaN
IO11/76:58-34(4)	81.68029	NaN	0.159788	NaN	0.028696	0.018563	0.010921	NaN	0.111857	0.105044	0.091659	NaN
PS86:6-37(3)	378.88240	0.591089	2.234232	NaN	0.248582	0.165690	0.070616	NaN	0.371060	0.278872	0.318693	NaN
Prot5:15-90(8)	117.23475	0.030080	0.084838	0.001557	0.019408	0.033862	0.016566	NaN	0.125355	0.090230	0.117445	NaN
Prot5:19-2(8)	41.47878	NaN	0.281158	NaN	0.024671	0.012701	0.006526	NaN	0.065913	0.067646	0.077174	NaN
Prot5:29-26(6)	56.86989	NaN	0.169556	NaN	0.010921	0.011856	0.005871	NaN	0.064176	0.073039	0.081874	NaN
Prot5:38-1(3)	50.43465	0.034112	0.063142	0.001794	0.009480	0.010459	0.006044	NaN	0.092789	0.086936	0.078769	NaN
RC27-9:6-3(7)	157.09406	0.086446	0.365686	0.003003	0.048714	0.052837	0.030101	NaN	0.206209	0.156391	0.125961	NaN
RC27-9:6-8(8)	176.41230	0.043251	0.298787	0.002255	0.059791	0.064866	0.035641	NaN	0.285895	0.230472	0.281370	NaN
RC27-9:25-142(6)	238.16168	0.117452	0.698379	0.011207	0.097846	0.105252	0.057386	NaN	0.337447	0.257944	0.322856	NaN
RC27-9:18-23	205.39304	0.076585	0.401810	0.004864	0.060371	0.069088	0.035423	NaN	0.229707	0.167119	0.213806	NaN
RC27-9:18-45	108.48071	0.026237	0.273391	0.001499	0.019916	0.026962	0.014197	NaN	0.121835	0.102058	0.148670	NaN
RC27-9:25-138	NaN	NaN	NaN	0.012668	0.101734	0.095896	0.045467	NaN	0.273349	0.190775	0.236186	NaN
RC27-9:30-32	250.10150	0.504841	1.097559	0.033140	0.178155	0.157957	0.079335	NaN	0.459141	0.342989	0.350348	NaN
RC27-9:30-40	224.96774	0.126492	0.596380	0.010499	0.101109	0.099481	0.050138	NaN	0.341781	0.264367	0.290273	NaN
RC27-9:34-58	37.91421	0.017329	0.027618	0.000645	0.001975	0.006618	0.003745	NaN	0.063615	0.061655	0.082820	NaN
RC27-9:34-63	63.84291	0.035978	0.057649	0.000821	0.004608	0.010866	0.006497	NaN	0.097016	0.078776	0.105135	NaN
RC27-9:35-49	46.66126	0.026737	0.030126	0.000712	0.003563	0.007249	0.004594	NaN	0.073162	0.064547	0.094525	NaN
RC27-9:35-80	49.37056	NaN	0.023042	NaN	0.003047	0.007242	0.004712	NaN	0.078473	0.068860	0.090057	NaN
RC27-9:44-1	77.80027	NaN	0.059662	NaN	0.009395	0.019480	0.010867	NaN	0.129194	0.099020	0.129307	NaN
RC27-9:46-1	139.50056	0.041328	0.213146	0.001656	0.027880	0.047583	0.023285	NaN	0.219081	0.177224	0.228200	NaN
RC27-9:46-2	69.07184	0.013864	0.132466	0.000894	0.011642	0.018811	0.010172	NaN	0.108243	0.096041	0.129585	NaN

Supplementary Data Table 3-1, Part 3, Page 2

Sample Number	Calculated Whole Rock Trace Element Content Concentration in ppm											
	bulk rock Ti	bulk rock Sr	bulk rock Zr	bulk rock Ce	bulk rock Nd	bulk rock Sm	bulk rock Eu	bulk rock Gd	bulk rock Dy	bulk rock Er	bulk rock Yb	bulk rock Y
RC27-9 35-80	49.39935	NaN	0.023037	NaN	0.003047	0.007242	0.004712	NaN	0.078473	0.068860	0.090057	NaN
RC 27-9 25-138	280.07410	0.483614	1.237919	0.034323	0.201335	0.116933	0.053253	NaN	0.319749	0.226115	0.246283	NaN
RC27-9 30-44	68.50270	NaN	0.074477	NaN	0.008000	0.014191	0.008134	NaN	0.124150	0.115096	0.127148	NaN
RC27-9 34-62	121.73116	0.083303	0.298858	0.005141	0.046956	0.044630	0.018671	NaN	0.170892	0.139780	0.156208	NaN
RC27-9 18-51	41.07591	0.016437	0.049331	0.000301	0.005740	0.009570	0.004594	NaN	0.059938	0.064351	0.075293	NaN
RC27-9 6-3	158.66144	0.085964	0.404637	0.002996	0.037181	0.049032	0.030350	NaN	0.175126	0.165196	0.189989	NaN
RC27-9 35-49	48.91665	0.027076	0.035147	0.000704	0.003379	0.007527	0.004564	NaN	0.073531	0.063412	0.091149	NaN
RC27-9 6-8	193.28625	0.091674	0.193443	0.002057	0.044900	0.065512	0.035070	NaN	0.285448	0.231091	0.282083	NaN
PS86-6-26	209.94257	0.224078	0.576202	0.012326	0.112972	0.086754	0.039571	NaN	0.301579	0.213940	0.214725	NaN
ANTP 134 HD3	65.44163	0.032111	0.094844	0.000756	0.013785	0.021785	0.009802	0.049248	0.104509	0.094553	0.121370	0.827773
"	55.33545	0.068810	0.152974	0.000864	0.014359	0.016019	0.008402	NaN	0.073670	0.069789	0.079032	0.801071
ANTP 134 HD4	52.47788	0.040347	0.066668	0.001697	0.013025	0.014861	0.007671	0.042214	0.077545	0.067483	0.101165	0.658673
"	50.16150	0.049059	0.123459	0.001673	0.015530	0.016513	0.007081	NaN	0.055491	0.050843	0.069475	0.670229
ANTP 134 HD7	45.48473	0.027633	0.243477	0.000635	0.008436	0.009662	0.005607	NaN	0.056391	0.058782	0.071795	0.774008
ANTP 134 HD8	48.35045	0.031254	0.059301	0.001203	0.009987	0.010963	0.004951	0.042333	0.069205	0.052023	0.072930	0.560548
"	51.56845	0.047121	0.151406	0.001654	0.015243	0.015002	0.008664	NaN	0.064740	0.053950	0.077960	0.727520
CIRCE 93 HD2	38.15369	0.005052	0.024670	0.000150	0.000408	0.001268	0.000849	0.006294	0.017105	0.025849	0.051830	0.358780
"	32.61844	0.006792	0.046874	NaN	0.000817	0.001479	0.000914	NaN	0.014596	0.020598	0.035273	0.318915
CIRCE 93 HD4	33.65233	0.011938	0.022949	0.000386	0.003600	0.004262	0.002196	0.017730	0.051899	0.052460	0.083562	0.528592
"	27.54483	0.032017	0.064016	0.000476	0.004255	0.005424	0.002635	NaN	0.049566	0.049962	0.065495	0.539164
CIRCE 93 HD7	23.31880	0.016102	0.289229	0.000660	0.004669	0.006660	0.003901	0.018271	0.026202	0.023476	0.044677	0.326327
ANTP 126 HD2	38.14694	NaN	0.033987	NaN	0.002901	0.005514	0.003372	0.022144	0.072359	0.076053	0.100951	0.655516
ANTP 126-HD5	41.73910	NaN	0.028118	NaN	0.004820	0.006027	0.003643	0.032273	0.077590	0.079808	0.117619	0.689754
"	NaN	NaN	NaN	0.003175	0.007230	0.007749	0.004553	NaN	0.063959	0.060500	0.089391	NaN
ANTP 126 D5	39.29340	0.024315	0.022731	0.000888	0.002365	0.006904	0.003484	0.024149	0.067696	0.068310	0.105310	0.615510
"	NaN	NaN	NaN	0.000888	0.003784	0.006373	0.004646	NaN	0.054733	0.051954	0.077729	NaN
ANTP 84 HD11	9.54850	NaN	0.008795	NaN	0.000233	0.000470	0.000171	0.003634	0.020420	0.027224	0.049354	0.233081
ANTP 87 HD5	12.46761	0.003562	0.007673	0.000029	NaN	0.000728	0.000572	0.004157	0.017481	0.029623	0.046490	0.246829
ANTP 87 HD9	13.23075	0.002142	0.009177	0.000045	0.000179	0.000566	0.000733	0.004746	0.017417	0.025150	0.049806	0.295489
ANTP 89 HD1	38.95086	0.007600	0.093206	0.000180	0.003704	0.007449	0.004073	0.027643	0.064111	0.064795	0.101489	0.671045
ANTP 89 HD2	45.72279	0.010807	0.032785	0.000177	0.001949	0.006145	0.004347	0.026066	0.070364	0.069150	0.101955	0.702862
ANTP 89 HD5	68.00623	0.014540	0.029816	0.000281	0.007688	0.014917	0.009067	0.053685	0.115175	0.101880	0.146693	0.967107
ANTP 89 HD8	61.28521	0.012387	0.033482	0.000270	0.005743	0.011236	0.007576	0.046483	0.095605	0.092671	0.123606	0.837610
ANTP 89 HD15	60.25429	0.005313	0.075515	0.000081	0.002081	0.003558	0.002670	0.016563	0.040635	0.049247	0.077290	0.559808
ANTP 89 HD17	32.25031	NaN	0.013079	NaN	0.000329	0.001954	0.001468	0.009576	0.031536	0.040660	0.073180	0.399382
ME33/2-31GTV	27.71900	0.008035	0.020937	0.000096	0.001109	0.002096	0.001244	0.010707	0.035602	0.037538	0.067640	0.368867
SO92-60GTV	32.27500	NaN	0.016549	NaN	0.001118	0.003912	0.001955	0.014326	0.038200	0.038378	0.068827	0.389639
SO92-74GTV	26.59375	0.007120	0.014708	0.000082	0.000612	0.001478	0.000850	0.008427	0.022471	0.027626	0.037387	0.338638
G96-39/36	37.58568	0.017735	0.072515	NaN	0.011242	0.009549	0.005560	0.031106	0.111241	0.137029	0.161878	1.281852
G96-39/36	47.38138	NaN	NaN	NaN	NaN	NaN	NaN	0.045686	0.147962	0.171958	0.173209	1.667952

Supplementary Data Table 3-1, Part 3, Page 3

Sample Number	Calculated Whole Rock Trace Element Content Concentration in ppm											
	bulk rock Ti	bulk rock Sr	bulk rock Zr	bulk rock Ce	bulk rock Nd	bulk rock Sm	bulk rock Eu	bulk rock Gd	bulk rock Dy	bulk rock Er	bulk rock Yb	bulk rock Y
895B 1R-1, 71-76	6.25485	NaN	NaN	NaN	NaN	NaN	NaN	NaN	0.003564	0.007269	0.016187	0.056440
895C 1R-1, 28-32	8.01188	NaN	NaN	NaN	NaN	NaN	NaN	NaN	0.005033	0.010026	0.020876	0.084906
895C 1R-1, 28-32	9.24036	NaN	NaN	NaN	NaN	NaN	NaN	NaN	0.000719	0.002005	0.006473	0.076416
895C 3R-1, 35-39	10.07630	NaN	NaN	NaN	NaN	NaN	NaN	NaN	0.005766	0.010970	0.019496	0.089130
895D 3R-1 116-120	8.01060	NaN	NaN	NaN	NaN	NaN	NaN	NaN	0.004756	0.010129	0.020193	0.077586
895D 4R-3 97-101	13.23400	NaN	NaN	NaN	NaN	NaN	NaN	NaN	0.008033	0.014810	0.025271	0.082114
895D 7R-2, 129-133	9.05873	NaN	NaN	NaN	NaN	NaN	NaN	NaN	0.006265	0.012929	0.020940	0.081931

Supplementary Data Table 3-2. Mineral compositions in average DMM.

	Mineral Modes				
	ol	opx	cpx	sp	sum
	0.57	0.28	0.13	0.02	1
	Mineral Trace element compositions (ppm)				
	ol	opx	cpx	sp	sum [a]
Rb	-	0.005	0.371	-	0.050
Ba	-	0.062	4.197	-	0.563
Th	-	0.0001	0.061	-	0.008
U	-	0.0002	0.024	-	0.003
K	-	0.541	389.6	-	50.800
Nb	0.058	0.167	0.443	0.575	0.149
Ta	0.004	0.011	0.029	0.037	0.010
La	0.0002	0.026	1.414	0.016	0.192
Ce	0.0005	0.137	3.930	0.027	0.550
Pb	0.00002	0.005	0.129	0.001	0.018
Pr	0.0002	0.034	0.744	0.003	0.107
Nd	0.002	0.194	4.044	0.013	0.581
Sr	0.004	1.312	56.11	-	7.664
Zr	0.657	6.574	20.28	11.50	5.082
Hf	0.013	0.131	0.836	0.228	0.157
Sm	0.004	0.109	1.585	0.003	0.239
Eu	0.002	0.056	0.611	0.001	0.096
Ti	101.8	1018	2715	1018	716.3
Gd	0.007	0.239	2.209	0.004	0.358
Tb	0.003	0.051	0.415	0.001	0.070
Dy	0.026	0.396	2.916	0.010	0.505
Ho	0.010	0.096	0.633	0.003	0.115
Y	0.751	3.266	15.25	0.147	3.328
Er	0.036	0.363	1.735	0.012	0.348
Yb	0.086	0.376	1.615	0.017	0.365
Lu	0.016	0.065	0.235	0.003	0.058

Chapter 4:

Volatile and Trace Elements in Basaltic Glasses from Samoa: Implications for Water Distribution in the Mantle

Abstract

We report volatile (H_2O, CO_2, F, S, Cl) and trace element data for submarine alkalic basalt glasses from the three youngest Samoan volcanoes, Ta'u, Malumalu and Vailulu'u. Most samples are visibly sulfide saturated, so have likely lost some S during fractionation. Cl/K ratios (0.04 – 0.15) extend to higher values than pristine MORBs, but are suspected to be partly due to source differences since Cl/K roughly varies as a function of $^{87}Sr/^{86}Sr$. There are no resolvable differences in the relative enrichment of F among sources, and compatibility of F during mantle melting is established to be nearly identical to Nd. Shallow degassing has affected CO_2 in all samples, and H_2O only in the most shallowly erupted samples from Vailulu'u. Absolute water contents are high for Samoa (0.63 – 1.50 wt%), but relative enrichment of water compared to trace element enrichment is low. H_2O/Ce (58 – 157) and H_2O/La (120 – 350) correlate inversely with $^{87}Sr/^{86}Sr$ compositions (0.7045 – 0.7089). This leads us to believe that, because of very fast diffusion of hydrogen in olivine, recycled lithospheric material with high initial water content will lose water to the drier ambient mantle during storage within the inner Earth. The net result is the counter-intuitive appearance of greater dehydration with greater mantle enrichment.

1. Introduction

Volatile elements such as hydrogen, carbon, fluorine, sulfur and chlorine track not only the melt phase in magmatic systems, but also the gas and fluid phases. Because of their ability to decouple from lithophile elements, especially at or near the Earth's surface, these elements provide a possible fingerprint of processes that are not actively recorded by the standard suite of incompatible trace elements (e.g. Sr, Rb, U, Th, and the rare earth elements). They have been used extensively to study volatile-driven arc magmatism, but have not been as widely applied to ocean island volcanism. It is now well established that the distribution of water in the mantle (primarily in nominally anhydrous minerals) strongly determines the locations and extents of mantle melting (Asimow and Langmuir, 2003) along with mantle rheology (Hirth and Kohlstedt, 1996; 2003), so it is important to understand the abundance of water in all mantle materials.

Lavas from the Samoan islands and seamounts have unique geochemical characteristics compared to other ocean island basalts (OIBs) as well as mid-ocean ridge basalts (MORBs), including extreme $^{87}Sr/^{86}Sr$ (up to 0.7089), low $^{143}Nd/^{144}Nd$ (down to 0.5125), and highly trace element enriched lavas (Wright and White, 1986; Farley et al., 1992; Workman et al., 2004). These characteristics define the Enriched Mantle 2 reservoir (EM2; Zindler and Hart, 1986). EM2 has classically been interpreted as oceanic crust and terrigeneous sediment that had been recycled back to the mantle through subduction zones (e.g. Weaver, 1991). Upon closer inspection, the standard recycling model of ocean crust/sediment fails as an explanation for producing EM2, due to smooth trace element patterns, low $^{187}Os/^{188}Os$ ratios, incorrect Pb isotope compositions, and high $^{3}He/^{4}He$ ($>8R_A$) in Samoan lavas (Workman et al., 2004). Instead, the origin of EM2 has been modeled with the ancient formation of metasomatised oceanic lithosphere, followed by storage in the deep mantle and return to the surface in the Samoan plume. Although Samoa is strongly EM2 in character, other mantle reservoirs, such as HIMU (high $^{238}U/^{204}Pb$ mantle; Zindler and Hart, 1986) and PHEM (**P**rimitive **He**lium **M**antle; Farley et al., 1992), are thought to contribute to the Samoan lavas, and hence in one location there is extreme compositional heterogeneity.

Here we report a study of volatile element concentrations in Samoan lavas in order to assess their relative enrichment compared to other trace element and isotope signatures, and to use them as potential clues to the origin of compositional variations in the mantle. We

find that water enrichment (identified by H_2O/Ce and H_2O/La ratios) in EM2 lavas has an inverse relationship to lithophile element enrichment (e.g. high Rb/Sr and $^{87}Sr/^{86}Sr$ ratios). The model for the formation of EM2 (Workman et al., 2004) would not result in fractionation of water from the lithophile elements. However, the fast diffusion of water through mantle minerals (Mackwell and Kohlstedt, 1990) provides a very effective means of losing water from EM2 to a water-poor ambient mantle during the long-term (~2.5 Ga) storage of EM2 – to the point of there being very similar bulk water contents (<100 ppm) in EM2 and the Depleted MORB Mantle (DMM). This finding leads credence to the idea that enriched mantle plumes are indeed "hot-spots" (Morgan, 1971; Sleep, 1990; Campbell and Griffiths, 1990) and not "wet-spots" (Schilling, et al., 1980; Green and Falloon, 1998).

2. Background

2.1. Geological and Geochemical Setting

The Samoan islands and seamounts are centered on 14°S latitude, stretch from 169-177.5°W longitude (fig. 1), and rest on the outer rim of the geophysical "superplume" of the South Pacific (Su et al., 1994). Seismic tomography images from beneath Samoa show a slow velocity anomaly extending into the lowermost mantle (Montelli et al., 2003), supporting a deep origin for upwelling mantle material feeding the Samoa hotspot. The tectonic setting of Samoa is complicated by having the northern termination of the Tonga Trench only 100 km to the south of the island chain. Hart et al. (2004a) have given a synthesis of the regional tectonic history and how plume-trench interaction has influenced the distribution of Samoan volcanism, specifically the *en-echelon* topographic ridges seen in Figure 1. Hart et al. (2004a) also established, from K-Ar dating and isotope geochemistry of seamounts extending to the west of Savai'i, that the Samoan plume has been active for at least 25 million years, producing a 1700 km long volcanic chain.

The easternmost, leading-edge Samoan volcano is the seamount, Vailulu'u (fig. 1); it rises from a 5000 m deep seafloor to a summit depth of 590 m and rests 45 km east of its nearest neighbor, Ta'u Island (Hart et al., 2000). Vailulu'u has been shown to be both volcanically and hydrothermally very active (Hart et al., 2000; Hart et al., 2003; Staudigel et al., 2004; Konter et al., 2004). The power output from Vailulu'u's summit crater is estimated to be 610-760 MW, the equivalent of 20-100 Mid-Ocean Ridge black smokers;

Mn export is estimated at 240-300 kg/day, or the equivalent of about 10 black smokers (Staudigel et al., 2004; Hart et al., 2003). The presence of ^{3}He anomalies in the water column show that at least this volatile element is actively degassing from upwelling magmas beneath Vailulu'u (Staudigel et al., 2004). We suspect that the hydrothermal circulation of seawater and degassing of magmas observed at Vailulu'u is representative of all the Samoan volcanoes at this stage of growth.

One goal of this study is to understand volatile enrichments/depletions as a function of mantle source composition. Each of these Samoan volcanoes has a distinct and well-characterized geochemical signature, discussed in detail by Workman et al. (2004). In summary, Malumalu displays the most extreme EM2 signature yet documented from ocean island basalts, with $^{87}Sr/^{86}Sr$ up to 0.7089 and extreme trace element enrichment. Ta'u shows some of the least enriched lavas from Samoa, with Sr-Nd-Pb isotopic values that are close to the mantle component PHEM (**P**rimitive **He**lium **M**antle of Farley et al. [1992]; $^{87}Sr/^{86}Sr = 0.7045$); for Ta'u this corresponds to $^{3}He/^{4}He$ up to 18 R_A and a lesser degree of trace element enrichment. Vailulu'u lavas are of intermediate enrichment and are thought to contain a small component of HIMU mantle, giving Vailulu'u the highest $^{206}Pb/^{204}Pb$ (19.4) in Samoa.

2.2. Samples and Volcano ages

Glass samples from the three youngest Samoan volcanoes, Vailulu'u, Malumalu, and Ta'u, have been taken from glassy rims of pillow basalts dredged during the 1999 AVON2/3 cruise aboard the R/V Melville. In this paper, we report data on samples obtained from 11 dredges ranging from 780 to 4170 meters deep – 6 from Vailulu'u, 2 from Ta'u and 3 from Malumalu (see Table 1). All Ta'u and Malumalu dredges are from a similar depth of 2300 – 3600 meters, whereas the shallowest and deepest dredges are from Vailulu'u.

All samples have some vesicles, most with less than 10% by volume and none over about 30%, indicating that these samples have experienced volatile exsolution during eruption. All dredges except 72 (Vailulu'u) and 75 (Ta'u) have sulfides present in nearly every sample (see Table 1); these occur as 10-50 μm spheres and are visible under reflected light in the glass chips that were analyzed. Micro-phenocryts of olivine, spinel, and clinopyroxene are common within the glasses. In a few of the olivine phenocrysts, melt inclusions have been fortuitously exposed, so these were analyzed for their volatile contents

to compare with volatile abundances in the matrix glass, but they have not been properly studied for major elements and mineral-melt equilibration.

U-series data have been collected for samples from each Vailulu'u and Malumalu dredge (Sims and Hart, 2004), including the following samples studied here: 63-13, 70-01, 71-02, 71-09, 72-02, 73-01, 73-03, 73-12, 76-01, 78-01. All show $^{230}Th/^{238}U$ excesses and are interpreted to be less than 300 thousand years old. The $^{230}Th/^{238}U$ excesses shown from Malumalu are similar to those on Vailulu'u, suggesting that Malumalu is not significantly older than Vailulu'u. Two samples from Vailulu'u (63-13 and 70-09) show ^{210}Pb disequilibria are interpreted to be less than 100 years old (Hart et al., 2000).

The oldest K-Ar age from Tau Island is 0.3 Ma (McDougall, 1985). The youngest volcanic series on Tau (Faleasao) is probably younger than 37,000 years, based on ^{14}C ages of coral inclusions in these volcanics (Hart, unpublished). Additionally, there was an underwater eruption just west of Tau in 1866 (see description in Keating, 1992).

3. Analytical Techniques

Multiple glass chips from the quenched rims of dredged pillow basalts were hand-picked and mounted with epoxy for ion microprobe analyses. Volatile abundances (H_2O, CO_2, F, S and Cl) were determined by triplicate analyses on the Cameca IMS 6f ion microprobe at the Department of Terrestrial Magmatism with a 5-10 nA Cs^+ primary beam. See Hauri et al. (2002) for a full description of the mircobeam method. Trace elements were determined on the same area of glass using the same instrument, but with an O^- primary beam. Analytical uncertainties are ±10% for H_2O and ±5% for all other elements. All calibrations were made against mafic glass standards.

For Sr isotope analyses, glass chips were hand-picked and leached for 1 hour in 6N HCl. Sr was separated by a standard cation exchange procedure described in Taras and Hart (1987). Isotopic analyses were carried out on the NEPTUNE multi-collector ICP/MS at W.H.O.I.; $^{87}Sr/^{86}Sr$ values are corrected to 0.71024 for NBS 987 and carry a 2σ precision equal to ±25 ppm (Hart et al., 2004b).

4. Results

Volatile and other trace element concentrations for Samoan glasses are listed in Table 1. Major element abundances of the glasses were analyzed by electron microprobe at MIT and

have been previously published (Workman et al., 2004). Sr, Nd and Pb isotope measurements have been made on a few whole rock samples (for which we now report glass data) and are also published in Workman et al. (2004). New $^{87}Sr/^{86}Sr$ measurements on glass samples are reported in Table 1, and range from 0.70452 to 0.70841, within the previously established range for whole rock analyses of Samoan lavas (Workman et al., 2004). The $^{87}Sr/^{86}Sr$ compositions of glass and whole rock pairs for individual samples have been found to be within analytical error (Jackson et al., unpubl.), so using $^{87}Sr/^{86}Sr$ values from "mixed material" is inconsequential to our data analysis.

4.1. Trace elements and fractionation correction

All the glasses presented here are evolved beyond clinopyroxene saturation, as identified by: 1) low Mg#'s (molar percent of $Mg/[Mg+Fe^{+2}]$), ranging from 39 to 61; 2) positive correlations between Mg# and CaO; 3) presence of clinopyroxene phenocrysts in whole rock samples; and 4) liquid lines of descent predicted by the pMELTS model (see fig. 2). They are all alkali basalts, with SiO_2 from 45.5 to 48.9 wt% and total alkalis (K_2O+Na_2O) from 3.2 to 6.1 wt%. The glasses are generally further along on fractionation trends than their whole rocks (fig. 2) due to the exclusion of phenocrysts in the glasses. Mg#'s of aphyric whole rocks are equal to or slightly higher than their glasses, but some glasses come from picritic samples with Mg#'s up to 81-84.

Trace element patterns of the glasses closely parallel whole rock trace element patterns (from Workman et al., 2004) of each volcano. La/Sm and Sm/Yb for glass and whole rock pairs are usually within analytical error, showing that the fractionation of olivine and clinopyroxene has had little effect on incompatible element ratios. Hence, using the data in this way (as elemental ratios) would be the most reliable in assessing primary melt characteristics.

La/Sm values of the glasses range from 3.3 to 7.5 and correlate positively with $^{87}Sr/^{86}Sr$, a proxy for source enrichment (i.e. Ta'u has the lowest and Malumalu has the highest La/Sm; not shown). Sm/Yb, on the other hand, does not correlate with enrichment, and the three volcanoes overlap in values from 2.9 – 5.6. For comparison, N-MORB La/Sm and Sm/Yb ratios are each ~1.0 (Hofmann, 1988). The steepness of Samoan rare-earth element slopes is a strong indication of melting within the stability field of garnet lherzolite (Hauri et al., 1994; Salters et al., 2002), as to be expected with melting beneath an old tectonic plate where the bottom of the lithosphere (e.g. Li et al., 2004) is near the garnet to spinel transition (Kogiso et al., 1998; Robinson and Wood, 1998; Klemme and O'Neill, 2000).

In order to estimate the compositions of primitive Samoan magmas, we have corrected the raw glass data for crystal fractionation by using the pMELTS trends (Ghiorso et al., 2002) to calculate the remaining liquid mass as a function of Mg#. The degree of fractionation ranges from 17% to 66%, with the majority of lavas falling within the range of 30 – 46% fractionated. Figure 2 shows that Malumalu and Ta'u lavas lie along very similar fractionation lines. Vailulu'u lavas are on a separate trend at higher CaO, with shallow dredges (63, 68, 70 and 73) being more fractionated on average than deep dredges (70 and 71).

The same fractionation corrections have been applied to the volatile contents, assuming that crystal fractionation happened at vapor under-saturated conditions. Figure 3 shows the fractionation-corrected abundances of volatile elements and a select group of trace elements, listed in the order of increasing compatibility during mantle melting. Concentrations are normalized to primitive upper mantle (PUM); most values for PUM are taken from McDonough and Sun (1995) except for CO_2 and H_2O, which are calculated assuming that PUM has a CO_2/Nb ratio of 239 (Saal et al., 2002) and an H_2O/Ce ratio of 200 (the value for FOZO observed by Dixon et al., 2002). This plot allows for a brief overview of the relative enrichments of volatile elements compared to the trace elements, suspending (for the moment) any interpretation about loss of volatiles by degassing. For all volcanoes, the negative anomalies for CO_2, H_2O, and S indicate that these volatiles are less enriched in the lavas than lithophile elements of similar compatibility; the opposite is true for the positive anomaly at Cl for most of the Vailulu'u lavas. F is the only volatile element that is consistently "conformable" with the lithophile elements in all samples. In the following sections, we attempt to discern which of these signals are primary and how they can be used to understand the composition and evolution of the mantle.

4.2. Water and carbon dioxide in glasses

The Samoan lavas show a large range in raw H_2O (0.63 – 1.50 wt%) and CO_2 (6 – 233 ppm) contents (fig. 4a; Table 1). Such water contents are highly elevated over MORBs (fig. 4b), but are very similar to Hawaii's submarine lavas from Loihi Seamount (Dixon and Clague, 2001) and the North Arch lava field (Dixon et al., 1997), and to melt inclusion data from the Austral Islands (Lassiter et al., 2002). Water in OIB lavas is generally lower than in arc lavas (up to ~ 6 wt%) but in the same range as back-arc basin lavas (e.g. Newman et al., 2000, for the Marianas system).

The presence of vesicles (1-30 vol%; Table 1) in every sample indicates that these lavas were all vapor saturated during eruption onto the seafloor. Some vapor loss can be accounted for by correcting for vesicle gases (i.e. the manifestation of closed system degassing). As a test for the severity of water loss, vesicle abundances were determined in 3 of the most vesicle-rich samples, 73-01, 73-03, and 78-03, by point-counting standard-sized thin sections. By volume, these contain 31%, 20% and 24% vesicles, respectively. Adding equilibrium vapor compositions back into the glasses, following the procedure described in Dixon et al. (2002), results in increases in bulk water content on the order of 0.03 to 0.05 wt%; yet these samples still have the lowest water abundances. Because this level of correction is within error of the analyses, we chose not to make vesicle corrections for all samples in the Samoan suite. It is likely that the volume of vesicles present in the glasses at eruption does not represent the total amount of degassing experienced by these lavas; in other words, we think it is likely that these lavas have lost gas via open-system degassing with bubble loss, prior to their final eruption and emplacement on the seafloor.

H_2O-CO_2 solubility models (Stolper and Holloway, 1988; Dixon et al., 1995; Dixon, 1997) show that CO_2 is much more insoluble than H_2O in basaltic magmas. As a result, with Samoan water contents, vapor compositions during open-system degassing are almost entirely CO_2 until pressures drop below ~100 bars (ocean depth of 1000 meters) (Newman and Lowenstern, 2002). In Figure 4a, the arrow at the end of the degassing trend marks the sharp change from CO_2-dominated to H_2O-dominated vapor compositions; above this point, open-system degassing results in nearly negligible water loss.

In Figure 4c, calculated equilibrium saturation pressures (using the Dixon [1997] model for H_2O-CO_2 saturation in alkali basalts) are plotted with collection depth. Lavas that lie very close to the 1:1 line erupted close to their dredge depth. Lavas below the 1:1 line are interpreted to have erupted more shallowly and flowed down slope; lavas above the line experienced incomplete degassing (i.e. rapid quenching). Note that some scatter is because dredges are along flanks of the volcanoes and hence may traverse 100's of meter of depth contours (see fig.1); the quoted dredge depth is the average for each dredge and may not represent every sample accurately.

As indicated by carbon dioxide concentrations and pressures of equilibration, both the most and the least degassed samples are from Vailulu'u: the deep dredges (71 and 72 from 4200 m and 3800 m deep, respectively) show water contents up to 1.50 wt%, and the shallowest dredges (63, 68, 70, and 73 at or near 1000 m) have water contents down to 0.63 wt%. The low water in the shallow dredges is the result of degassing a water-rich vapor (fig.

4a). Ta'u and Malumalu lavas all have high enough pressures of equilibration (fig. 4c) to preclude loss of significant water by open system degassing.

In summary, degassing has affected CO_2 in all samples, and H_2O only in the most shallowly-erupted samples from Vailulu'u. Additional support for minimal water loss is that fact that the most melt inclusions have water contents that are identical (within error) to their host matrix glasses, but with equal or higher CO_2 (Tables 1 and 2; the one exception is a melt inclusion from sample 71-03, which has lower CO_2 and H_2O than its matrix glass). One melt inclusion from sample 72-12 shows the highest pressure of vapor saturation at 818 bars, indicating a minimum crystal fractionation depth of 1.6 km within the oceanic crust (3840 meters dredge depth plus 1600 meters igneous crust at a rock density of 2800 kg/m^3).

4.3. Water and carbon dioxide in primary magmas

After fractionation-correction (see section 4.1), we estimate primary magmas to have H_2O in the range of 0.4 – 1.1 wt%. Shallowly erupted Vailulu'u lavas are once again at the lower limit of this range, representing the greatest losses of water by both open- and closed-system degassing.

Original CO_2 concentrations in the primary magmas can be estimated using the observation that CO_2/Nb ratios are roughly constant in volatile under-saturated MORB melt inclusions from the Siquieros Transform (Saal et al., 2002) – it is still highly uncertain whether or not this ratio applies to OIBs. Using fractionation-corrected Nb concentrations and CO_2/Nb equal to 239 (Saal et al., 2002), 95% of the data suggest primary CO_2 contents in the narrow range of 0.8 to 1.2 wt%.

We have used the H_2O-CO_2 degassing program by Newman and Lowenstern (2002) to estimate the maximum water loss from deep, open-system degassing, and find that a primary magma with 47 wt% SiO_2 and initial volatile content of 1.2 wt% H_2O and 1.0 wt% CO_2 will still have 1.15 wt% H_2O after CO_2 has degassed to ~10 ppm. This difference is within the analytical error for water and evidence that the observed water contents for all lavas except those from the shallow Vailulu'u dredges (63, 68, 70 and 73) are robust estimates of original abundances of water.

At the pMELTS-modeled fractionation pressures of 3-4 kbar, the data indicate that CO_2 is the only strongly oversaturated volatile component, as it is very insoluble in basaltic magmas (Stolper and Holloway, 1988; Dixon et al., 1995; Dixon, 1997). Carbonitite

metasomatism has been documented in Samoan xenoliths (Hauri et al., 1993), and is further evidence for deep CO_2 degassing.

4.4. Fluorine

Raw F contents range from 800 to 1890 ppm and are well correlated with incompatible trace elements including P, Na, K and Ti (fig. 5; Table 1). Fractionation-corrected values for F are 480 to 880 ppm and closely overlap primitive Hawaiian melt inclusions that have 300 to 1000 ppm F (Hauri, 2002). These values are similar to other plume related lavas, but are significantly higher than in MORBs (e.g. Schilling et al., 1980; fig. 5).

There are no resolvable differences in the relative enrichment of F between the different volcanoes or the different dredges; instead there is a constant F/Nd ratio of 21.7±2.6 (2σ) across the whole sample suite, indicating F compatibility equal to that of Nd. Figure 5 shows that Samoa glasses, together with normal MORBs (PETBD database: http://beta.www.petdb.org/), very depleted MORBs (from the Siquieros Transform; Saal et al., 2002; Saal et al., unpubl.) and Primitive Upper Mantle (McDonough and Sun, 1995), all fall along a F/Nd line of 21. Siquieros samples alone (Saal et al., 2002) show a mean F/Nd of 19.4±2.6 (1σ), whereas all MORBs show F/Nd = 20.1±5.8 (1σ). Continental crust is also estimated to have a F/Nd ratio within this range (at 20.7; Wanke et al., 1984). To our knowledge, the only basalts that fall dramatically off this line are melt inclusions from the Austral Islands showing F/Nd ratios that are generally 60-70 (Lassiter et al., 2002). Elevated F may be a characteristic of the HIMU mantle end-member that is represented by lavas from the Austral island chain (Hauri and Hart, 1993). However, Vailulu'u glasses, which are thought to contain a small HIMU component (Workman et al., 2004), show no systematic elevation of F.

4.5. Sulfur

Sulfur in the Samoan glasses ranges from 781 – 2651 ppm, consistent with other oceanic basalts (Wallace and Carmichael, 1992). As discussed above, most glasses are saturated with a sulfide phase, so have likely lost some S by sulfide fractionation. Figure 6 shows the rough positive correlation between S/Dy and Mg# of the whole suite of Samoan glasses (note that S and Dy have been suggested to have similar compatibilities during mantle melting [Saal et al., 2002], so S/Dy should not change as a function of melting or olivine/clinopyroxene crystallization, but will decrease if sulfides are fractionated from a

melt). However, for a given Mg#, there is a very wide range of S/Dy, suggesting that fractionation of sulfides may not be the only factor in controlling relative S depletions.

At the FeO contents of Samoan glasses (10.5 – 14.2 wt%), S concentrations are higher than they are in sulfide-saturated MORBs, possibly because Samoan lavas have higher oxygen fugacities (see Dixon, 1997; Dixon and Clague, 2001). Sulfide saturation is a complicated function of fO_2, temperature, pressure and melt composition (e.g. Wallace and Carmichael, 1992), making further analysis of S beyond the scope of this paper.

4.6. Chorine

Raw Cl contents of the Samoan glasses fall within the range of 451-1815 ppm (Table 1); fractionation-corrected values are 269-1412 ppm, similar to other plume related magmas (e.g. Dixon and Clague, 2001; Simons et al., 2002), but much greater than estimated parental MORBs (<100; Michael and Cornell, 1998). Glasses from Vailulu'u and dredge 76 from Malumalu have the highest Cl, while Ta'u glasses fill the lower half of the whole range. Cl saturation in basaltic melts is greater than 2 wt% at these water contents (Webster et al., 1999), so we expect that there was no Cl degassing at any point in the evolution of the magmas. Curiously, of all the volatile and trace elements, Cl is best correlated with S across the whole Samoan suite (fig. 7). There is no reason to expect these two elements to have either similar compatibilities or similar behavior in magmatic systems.

Cl concentrations are roughly correlated with other incompatible elements for certain groups of dredges. Figure 8 shows one example of this with the relationship between Cl and K (the element most often used in assessing relative Cl enrichments; see below). The lowest Cl/K ratios (~0.04) are found primarily in glasses from Ta'u and Malumalu (dredge 78), and the highest ratios are from a collection of Vailulu'u dredges that define a Cl/K line of approximately 0.12. Two dredges, 73 and 76, fall "across-trend" in between these two groups of Cl/K. It is important to note that this layout is not unique to Cl and K concentration space, and instead looks very similar for Cl with almost all trace elements.

There is much precedent for interpreting high Cl concentrations in oceanic basalts as being the product of seawater assimilation (Michael and Cornell, 1998; Kent et al., 1999; Lassiter et al., 2002; Simons et al., 2002; Stroncik and Haase, 2004) due to very high concentrations of Cl in seawater and especially in brines (Kent et al., 1999). A study by Michael and Cornell (1998) found that Cl/K ratios in MORBs that are unaffected by seawater contamination range from 0.01 – 0.07, with depleted MORBs at the low end and enriched MORBs at the high end of this range. Samoan glasses overlap with the MORB

range and extend to higher Cl/K (up to 0.15; fig. 8). The question is: how much of this Samoan signal is primary and how much is caused by assimilation? We address this question in the paragraphs below.

By omitting samples that fall along brine assimilation trends, Stroncik and Haase (2004) recently found Cl/K ratios in OIBs to be a function of source signatures, as recognized by their correlation with Sr and Pb isotopic values. Enriched mantle (EM1 and EM2) lavas have low Cl/K ratios (down to 0.02) and HIMU lavas have Cl/K ratios up to 0.08 (Stroncik and Haase, 2004). Also, plume-influenced glasses from the Easter Seamount Chain, having Cl concentrations interpreted as primary based on good correlations between Cl and La, show Cl/K ratios from 0.05 up to 0.12 (Simons et al., 2002), similar to our Samoan glasses.

The relationship between Cl/K and $^{87}Sr/^{86}Sr$ for Samoa is displayed in Figure 8. The most extreme EM2 lavas (Malumalu, dredge 78) at high $^{87}Sr/^{86}Sr$ have some of the lowest Cl/K. With decreasing $^{87}Sr/^{86}Sr$, Cl/K ratios increase up to a maximum value of 0.15 in the Vailulu'u lavas (that have a small HIMU component; see background section above) and then drop to MORB-type values in Ta'u. This result is in general agreement with Stroncik and Haase (2004), despite our absolute Cl/K and $^{87}Sr/^{86}Sr$ ranging to significantly higher values.

The minimum Cl/K ratio from each volcano is ~0.04 and could be taken as the primary composition for all of Samoan magmas before Cl contamination. However, enumerated below are reasons to believe that the Cl signal in Samoa is largely primary, with scatter caused by minimal assimilation:

1. There are correlations between high Cl and other trace elements that are not enriched in brines (for example, Cl and Nb show a similar relationship as do Cl and K in fig. 7). A 15% brine derived from seawater contains about 10 wt% Cl (Kent et al., 1999), and it would take only 1% of this brine to elevate a magma's Cl content from 500 to 1500 ppm (almost the full range in Samoa). With the same amount of brine, there would be a negligible effect on most other trace elements (including K), yet we observe increased trace element concentrations with increased Cl. Also, Kent et al. (1999) claim that assimilated material is high in B as well as Cl, but B is not elevated in high Cl Samoan glasses; in fact the highest B concentrations occur is glasses from dredge 78, which have some of the lowest Cl and lowest Cl/K ratios.

2. Michael and Cornell (1998) clearly demonstrate that high levels of assimilation occur in lavas that are highly evolved. The opposite is observed for the Samoan glasses: the least evolved Vailulu'u samples (see fig. 2) show the highest Cl and Cl/K ratios (fig. 8).

3. The few melt inclusions we have analyzed (Table 2) have Cl contents usually within error of their host matrix glasses. However, this evidence alone may not prove the Cl is primary, since it is possible that Cl in the inclusions was assimilated at the depth of crystal fractionation.

4. There is a correlation between Cl/K and $^{87}Sr/^{86}Sr$ (fig. 8), which in general mimics the observation of Stroncik and Haase (2004) that EM sources and depleted mantle have low Cl/K while HIMU has higher Cl/K. However, Vailulu'u is in no way end-member HIMU, but instead is EM2 with a small component of HIMU.

5. Figure 7 indicates that high Cl magmas also have high S, and no known assimilant contains Cl and S in the required 1:1 ratio. Either high Cl is a primary feature of the lavas, or the correlation between Cl and S is coincidental.

A study on chlorine isotopes (e.g. Magenheim et al., 1995) might provide compelling evidence against an assimilation origin for the high Cl, and ultimately may be the only way to define the proportion of igneous- to seawater-derived Cl.

5. Source Variations In Water Enrichment

Since CO_2 is severely degassed, S is subject to sulfide fractionation, Cl is sensitive to seawater contamination, and F abundances do not vary relative to trace element abundances, we focus our attention here on the source variations of water.

During mantle melting, the compatibility of water is similar to Ce and La, as determined both observationally (e.g. Michael, 1995; Danyushevsky et al., 2000) and experimentally (Hauri et al., in revision). As such, ratios of H_2O/Ce and/or H_2O/La have been used as direct indicators of source compositions and the extent to which water is enriched or depleted. For example, low H_2O/Ce ratios in Loihi magmas (Dixon and Clague, 2001) and plume-influenced MORBs (Dixon et al., 2002) have been used to argue for the presence of recycled oceanic crust and sediment that had been efficiently dehydrated during subduction.

The relationship between H_2O/La and $^{87}Sr/^{86}Sr$ in Samoan basalts (fig. 9) extends the observation by Dixon et al. (2002) that enriched mantle sources have relative depletion of water (note that H_2O/La is used rather than H_2O/Ce since H_2O and La are most similar in compatibility during melting of garnet lherzolite [Hauri et al., in revision]). The Samoan glasses have a wide range in $^{87}Sr/^{86}Sr$ (0.7045 – 0.7089) that is inversely correlated with H_2O/La (ranging from 120 to 316). The highest H_2O/La ratios in Samoa overlap with the low H_2O/La end of the plume-influenced Discovery lavas from the S. Atlantic (Dixon et al.,

2002). Otherwise, all Samoa glasses have much lower H_2O/La ratios than do average MORBs or average Loihi lavas (Dixon and Clague, 2001; Dixon et al., 2002). Ultimately, it seems that the greater the "enrichment" of the mantle (in terms of heavy isotopes and trace elements), the greater the apparent dehydration.

We do not believe that this relationship is an artifact of secondary processes in Samoan glasses. There is no coincidental correlation between $^{87}Sr/^{86}Sr$ and dredge depth (i.e. possible degassing). In the above section on water and carbon dioxide, we have shown that degassing has not resulted in significant water loss for any of the samples plotted in Figure 9. As supporting evidence, water contents in melt inclusions are equal to or less than the water contents in the glasses at equal or higher CO_2 (Tables 1 and 2). The slightly higher water in some glasses may reflect a greater degree of fractionation of these melts – this is not confirmed since we lack major element compositions for the melt inclusions. For the sake of argument, if the water content in samples from dredge 78 was the same as the highest water in Samoa, then the H_2O/La ratio would be ~200 (instead of 120) – still well below values for MORB, Loihi and Discovery. Finally, if water has been assimilated from seawater or brine, then the H_2O/La ratios plotted in Figure 9 would be maximum values, and the signal we observe would be a dampened one; however, H_2O/La does not correlate with any potential "assimilation" proxies such as Cl/K.

6. Origin Of EM2's "Dehydration"

The origin of the EM2 mantle end-member is classically explained as the recycling of oceanic crust plus terrigeneous sediment through subduction zones (e.g. Weaver, 1991). However, our recent work on extreme EM2 lavas from Samoa (found at Malumalu, in particular) argues against simple mixing of a sedimentary component into depleted mantle based on trace element and isotopic trends in the Samoan lavas (see Workman et al. [2004] for detail). Instead, the origin of EM2 is explained as ancient (2.5 Ga), recycled, metasomatized lower oceanic lithosphere; a small degree, upper mantle melt (like those imagined to be formed at depth beneath mid-ocean ridges or island arcs) impregnated a depleted lithosphere, then the material was subducted and stored in the mantle (Workman et al., 2004). This is simply one scenario that works to explain the observations in Samoa that the EM2 source has a trace element pattern more reflective of upper mantle magmatic fractionation processes than sedimentary compositions, but does not completely rule out a

subduction-related origin for EM2 (in other words, we do not necessarily know *where* the metasomatism has taken place).

The above model for the *formation* of EM2 cannot account for the low H_2O/La ratios observed in the Samoan glasses since (non-arc) mantle melting cannot produce large fractionations of water from La owing to their similar compatibilities. In addition, since the model EM2 reservoir is created in the lower oceanic lithosphere, it will be isolated from the subduction zone dehydration processes affecting the crust/sediment package in the upper part of the subducted slab. However, the *aging* of EM2 *can* account for our observations. This is how: very fast diffusion of hydrogen in olivine (Mackwell and Kohlstedt, 1990) will cause recycled material with high initial water content to lose water to the drier ambient mantle during storage within the deep Earth.

Mackwell and Kohlstedt (1990) provide an Arrhenius equation for the temperature dependence of hydrogen diffusion in olivine; this leads to a diffusion coefficient of 8.9×10^{-9} m^2/s at 1500°C, for the fast [100] direction. Using a constant temperature of 1500°C, in 2.5 Ga (the estimated age of EM2), a 26 km thick slab can be fully equilibrated with the ambient mantle using the approximation that equilibrated distance, $x = \sqrt{(\text{diffusion coefficient} \times \text{time})}$. At an assumed upwelling rate of 1 cm/yr, water abundance can be fully equilibrated over 4 km with the surrounding mantle during convective transport through the upper mantle (660 km) alone. Since much of the mantle is at temperatures higher than 1500°C, these are conservative estimates; the effects of enhanced diffusion through grain boundaries will also serve to aid equilibration. It is unknown whether or not similar diffusion rates for hydrogen apply to other major mantle minerals. If helium can be used as an analogue for H, at 1500°C, He diffusion in clinopyroxene and garnet is equal or faster than that in olivine (Trull et al., 1991; Dunai and Roselieb, 1996). In contrast to water, most other elements will have much smaller equilibration distances; for example, rare-earth-element diffusion rates at the same temperature results in the full equilibration of less than 10 meters in 4 billion years (Hofmann and Hart, 1978; Van Orman et al., 2001). As a result, the enhanced solid-state mobility of hydrogen in the mantle can potentially shift the H_2O/La ratio in the absence of any melting or mantle-fluid interactions.

Figure 10 is a conceptual diagram for the diffusive equilibration of water during the recycling and storage of EM2. Workman et al. (2004) give an estimate for the trace element composition of EM2: La = 0.895, Ce = 1.923, and if H_2O/Ce was initially like the common mantle, FOZO (i.e. 200; Dixon et al., 2002), then the starting H_2O content of EM2 would be 385 ppm. The Depleted MORB Mantle (DMM) is estimated to contain 0.19 ppm La and

0.55 ppm Ce (Workman and Hart, 2005). At an H_2O/Ce ratio of 150 (Dixon et al., 2002), H_2O in DMM = 82.5 ppm, less than 25% that of EM2. Assuming all reservoirs here are peridotite lithologies, when "wet" EM2 is introduced to "dry" depleted mantle, water will diffuse out of EM2 and into the "infinite sink" of ambient depleted mantle until their water activites are equal (at DMM = 82.5 ppm). When EM2 equilibrates with the depleted mantle and the two components have the same water content, the resulting H_2O/Ce is 43 and H_2O/La is 92 in the EM2 component; these values are nearly identical to the values seen in the high $^{87}Sr/^{86}Sr$ glasses from Malumalu (see fig. 9 for H_2O/La). Less-enriched sources, lying initially between EM2 and DMM along a H_2O/La = 500 line, will lose water when recycled to the mantle until they reach the 82.5 ppm water line. Thus, in aged sources, H_2O/La increases as the degree of enrichment decreases. This analysis shows that the observed differences in H_2O/La ratios in these mantle sources are not the result of different water contents, but instead are due to differences in REE enrichment at similar water contents.

The above discussion is focused on *dehydration* of enriched reservoirs, but the same thinking will apply to *re-hydration* of dry mantle reservoirs. If subducted material becomes extensively dehydrated (e.g. as called upon by Dixon et al. [2002]), storage within the mantle will result in a *re-hydration* of the slab until the slab and mantle are in chemical equilibrium in terms of water content. This is a nearly unavoidable consequence of recycling, unless slab temperatures stay very cold (much less than 1500°C) or recycling times are very rapid (< 50 million years).

7. Discussion

Volatile and trace element abundances for nearly 100 submarine basaltic glasses from the three youngest Samoan volcanoes have been presented here. We have found that water abundance relative to trace element abundance correlates inversely with source enrichment. This leads us to believe that, because of very fast diffusion of hydrogen in olivine (Mackwell and Kohlstedt, 1990), recycled material with high initial water content will lose water to the drier ambient mantle during storage within the Earth. However, this is a somewhat incomplete picture since 1) the greatest budget of water in an upper mantle peridotite is not contained in olivine, but in clinopyroxene and orthopyroxene (Hirth and Kohlstedt, 1996; Hauri et al., in revision) and 2) other lithologies (especially pyroxenites,

with little olivine) may be present in the mantle as subducted oceanic crust (e.g. Hirschmann and Stolper, 1996).

The water content of EM2 is estimated to be close to that of the upper mantle (~100 ppm), and differences in the H_2O/La ratio of Samoan mantle components are due to local diffusive homogenization of their water contents during long-term storage in the mantle. Therefore, the differences in water concentrations between Samoan lavas and MORBs are more a difference in degree of melting than source composition. La, H_2O and Ce are enriched in Samoan lavas about 60-fold over their estimated EM2 source concentrations, requiring a degree of melting on the order of 1% (with $D_{Ce,\ water} = 0.01$ and aggregated fractional melting). This contrasts with an estimated degree of melting at 6-7% to generate MORB liquids from the upper mantle (Workman and Hart, 2005).

If the diffusion rates of hydrogen in other mantle minerals are similar to olivine, water may be one of the only elements whose abundance is nearly constant over great distances in the mantle, assuming similar source lithologies. This "diffusive dehydration" model has important implications for the interpretation of mantle H_2O/La and H_2O/Ce ratios. Whether or not subducted materials have higher or lower H_2O/La than the upper mantle, slabs and mantle wedge material stored in the deep Earth for significant periods of time will experience temperature-dependent diffusive mobility of hydrogen and will likely lose hydrogen to the ambient mantle.

The direction of diffusive hydrogen transport will depend not on the H_2O/La ratio but on the bulk H_2O contents of juxtaposed mantle sources. Indeed, subducted oceanic crust and sediment could enter the deep mantle with a low H_2O/La ratio but a bulk H_2O content that is still higher than the surrounding mantle, and thereby lose even more water via "diffusive dehydration". Alternatively, if dehydration and melting are extremely efficient in subduction zones, then recycled material may enter the deep mantle extremely dry, and become re-hydrated via diffusive exchange with the surrounding mantle. Either way, an evaluation of the absolute abundance of water in mantle sources requires more than simply knowing the ratio of H_2O to REE in derivative lavas. Robust estimates of lithophile element concentrations, from accurate inversion of complete major element, trace element and isotopic data, must be the starting point for investigating the variability of water in the mantle in any tectonic setting.

Acknowledgements

Many thanks go to Mark Kurz for allowing us to raid his collection of glasses he diligently collected during the 1999 cruise of the R/V Melville. During the preparation of this manuscript, discussions with Jackie Dixon, Nobu Shimizu, Alberto Saal, Glenn Gaetani and Jeff Standish were very helpful and much appreciated. DTM's hospitality during their 100th year anniversary made a two-week session of data collection an especially enjoyable experience.

References

Asimow, P. D. and C. H. Langmuir, The importance of water to oceanic mantle melting regimes, *Nature*, 421, 815-820, 2003.

Campbell, I.H. and R.W. Griffiths, Implications of mantle plume structure for the evolution of flood basalts, *Earth Planet. Sci. Lett.*, 99, 79-83, 1990.

Danyushevsky, L.V., S.M. Eggins, T.J. Faloon, and D.M. Christie, H_2O Abundance in Depleted to Moderately Enriched Mid-ocean Ridge Magmas; Part I: Incompatible Behaviour, Implications for Mantle Storage, and Origin of Regional Variations, *J. Petrology*, 41 (8), 1329-1364, 2000.

Dixon, J.E., Degassing of alkalic basalts, *Am. Minerologist*, 82, 368-378, 1997.

Dixon, J.E., E.M. Stolper, and J. Holloway, An Experimental Study of Water and Carbon Dioxide Solubilities in Mid-Ocean Ridge Basaltic Liquids. Part I: Calibration and Solubility models, *J. Petrology*, 36 (6), 1607-1631, 1995.

Dixon, J.E., D.A. Clague, P. Wallace, and R. Poreda, Volatiles in Alkalic Basalts from the North Arch Volcanic Field, Hawaii: Extensive Degassing of Deep Submarine-erupted Alkalic Series Lavas, *J. Petrology*, 38 (7), 911-939, 1997.

Dixon, J.E., and D.A. Clague, Volatiles in Basaltic Glasses from Loihi Seamount, Hawaii: Evidence for a relatively dry plume component, *J. Petrology*, 42 (3), 627-654, 2001.

Dixon, J.E., L. Leist, C. Langmuir, and J.-G. Schilling, Recycled dehydrated lithosphere observed in plume-influenced mid-ocean-ridge basalts, *Nature*, 420, 385-389, 2002.

Dunai, T.J. and K. Roselieb, Sorption and diffusion of helium in garnet: implications for volatile tracing and dating, *Earth Planet. Sci. Lett.*, 139, 411-421, 1996.

Farley, K. A., Natland, J.H., and Craig, H., Binary mixing of enriched and undegassed (primitive?) mantle components (He, Sr, Nd, Pb) in Samoan lavas, *Earth Planet. Sci. Lett.*, 111, 183-199, 1992.

Ghiorso, M. S., Hirschmann, M.M., Reiners, P.W., and Kress, V.C. III, The pMELTS: A revision of MELTS for improved calculation of phase relations and major element partitioning related to partial melting of the mantle to 3 GPa, *Geochemistry, Geophysics, Geosystems, 3*(5), 10.1029/2001GC000217, 2002.

Green, D.H. and T.J. Falloon, Pyrolite: A Ringwood concept and its current expression, in: The Earth's Mantle: Composition, Structure and Evolution, ed., I.N.S. Jackson, Cambridge University Press, Cambridge, 311-378, 1998.

Hart, S. R., Staudigel, H., Koppers, A.A.P., Blusztajn, J., Baker, E.T., Workman, R., Jackson, M., Hauri, E., Kurz, M., Sims, K., Fornari, D., Saal, A., and Lyons, S., Vailulu'u undersea volcano: The New Samoa, *Geochemistry, Geophysics, Geosystems, 1*, 2000GC000108, 2000.

Hart, S. R., H. Staudigel, R. Workman, A.A.P. Koppers, A.P. Girard, A fluorescein tracer release experiment in the hydrothermally active crater of Vailulu'u Volcano, Samoa, *J. Geophysical Research*, v. 108, n. B8, 2377, 2003.

Hart, S.R., M. Coetzee, R.K. Workman, J. Blusztajn, K.T.M. Johnson, J.M. Sinton, J.W. Hawkins, Genesis of the Western Samoa Seamount Province: Age, Geochemical Fingerprint and Tectonics, *Earth and Planet. Sci. Letters*, 227, 37-56, 2004a.

Hart, S. R., L. Ball and M. Jackson, Sr Isotopes by Laser Ablation PIMMS: Application to Cpx from Samoan Peridotite Xenoliths, WHOI Plasma Facility Open File Report 11, available at: http://www.whoi.edu/science/GG/people/shart/open_file.htm, 2004b.

Hauri, E. H., and Hart, S.R., Re-Os isotope systematics of HIMU and EMII oceanic island basalts from the south Pacific Ocean, *Earth Planet. Sci. Lett., 114*, 353-371, 1993.

Hauri, E. H., Shimizu, N., Dieu, J.J., and Hart, S.R, Evidence for hotspot-related carbonatite metasomatism in the oceanic upper mantle, *Nature,* 365, 221-227, 1993.

Hauri, E.H., T.P. Wagner, T.L. Grove, Experimental and natural partitioning of Th, U, Pb and other trace elements between garnet, clinopyroxene and basaltic melts, *Chemical Geology*, 117, 149-166, 1994.

Hauri, E.H., J. Wang, J.E. Dixon, P.L. King, C. Mandeville, and S. Newman, SIMS analysis of volatile in silicate glasses, 1: Calibration, matrix effect and comparisons with FTIR, *Chemical Geology*, 183, 99-114, 2002.

Hauri, E.H., SIMS analysis of volatile in silicate glasses, 2: isotopes and abundances in Hawaiian melt inclusions, *Chemical Geology*, 183, 115-141, 2002.

Hauri, E.H., G.A. Gaetani, and T.H. Green, Partitioning of water during melting of the upper sources of oceanic basalts, *Nature*, in revision, 2005.

Hirschmann, M.M. and E.M. Stolper, A possible role for garnet pyroxenite in the origin of the "garnet signature" in MORB, *Contrib. Mineral. Pet.*, 124 (2), 185-208, 1996.

Hirth, G. and D.L. Kohlstedt, Water in the oceanic upper mantle: implications for rheology, melt extraction, and the evolution of the lithosphere, *Earth and Planet. Sci. Lett.*, 144, 93-108, 1996.

Hirth, G. and D.L. Kohlstedt, Rheology of the Upper Mantle and the Mantle Wedge: A View from the Experimentalists, In: *Inside the Subduction Factory*, Ed. J. Eiler, AGU

Monograph 138, 2003.

Hofmann, A.W., Chemical differentiation of the Earth: the relationship between mantle, continental crust and oceanic crust, *Earth Planet. Sci. Lett.*, 90, 297-314, 1988.

Hofmann, A. and S. R. Hart, An assessment of local and regional isotopic equilibrium in the mantle, *Earth Planet. Sci. Lett.*, 38, 44-62, 1978.

Keating, B. H., The geology of the Samoan Islands. In: *Geology and offshore mineral resources of the Central Pacific basin*, eds. B. H. Keating and B. R. Bolton, Circum-pacific Council for Energy and Mineral Resources Earth Science Series, 14, 127-178, 1992.

Kent, A.J.R., M.C. Norman, I.D. Hutcheon, and E.M. Stolper, Assimilation of seawater-derived components in an oceanic volcano: evidence from matrix glasses and glass inclusions from Loihi seamount, Hawaii, *Chemical Geology*, 156, 299-319, 1999.

Klemme, S. and H. O'Neill, The near-solidus transition from garnet to spinel lherzolite, *Contrib. Min. Pet.*, 138, 237-248, 2000.

Kogiso, T., K. Hirose and E. Takahashi, Melting experiments on homogeneous mixtures of peridotite and basalt: application to the genesis of ocean island basalts, *Earth Planet. Sci. Lett.*, 162, 45-61, 1998.

Konter, J. G., H. Staudigel, S. R. Hart and P. M. Shearer, Seafloor seismic monitoring of an Active Submarine Volcano: Local Seismicity at Vailulu`u Seamount, Samoa, *Geochem., Geophys., Geosyst.*, 5, 2004GC000702, 2004.

Lassiter, J.C., E.H. Hauri, I.K. Nikogosian, and H.G. Barsczus, Chlorine-potassium variations in mlet inclusions from Raivavae and Rapa, Austral Islands: constraints on chlorine recycling in the mantle and evidence for brine-induced melting of oceanic crust, *Earth Planet. Sci. Lett.*, 202, 525-540, 2002.

Li, X., R. Kind, X. Yuan, I. Wolbern, and W. Hanka, Rejuvenation of the lithosphere by the Hawaiian plume, *Nature*, 427, 827-829, 2004.

Mackwell, S.J., and Kohlstedt, Diffusion of Hydrogen in Olivine: Implication for Water in the Mantle, *J. Geophys. Res.*, 95 (B4), 5079-5088, 1990.

Magenheim, A.J., A.J. Spivack, P.J. Michael and J.M. Gieskes, Chlorine stable isotope composition of the oceanic crust: Implication for Earth's distribution of chlorine, *Earth Planet. Sci. Lett.*, 131, 427-432, 1995.

McDonough, W. F. and S.-s. Sun, The composition of the Earth, *Chemical Geology*, 120, 223-253, 1995.

McDougall, I., Age and Evolution of the Volcanoes of Tutuila, American Samoa, *Pacific*

Science, 39, 311-320, 1985.

Michael, P., Regionally distinctive sources of depleted MORB: Evidence from trace elements and H_2O, *Earth Planet. Sci. Lett.,* 131, 301-320, 1995.

Michael, P. and W.C. Cornell, Influence of spreading rate and magma supply on crystallization and assimilation beneath mid-ocean ridges: Evidence from chlorine and major element chemistry of mid-ocean ridge basalts, *J. of Geophys. Res.*, 103 (B8), 18,325-18,356, 1998.

Montelli, R., G. Nolet, F.A. Dahlen, G. Masters, E.R. Engdahl, S-H. Hung, Finite-Frequency Tomography Reveals a Variety of Plumes in the Mantle, *Science*, 10.1126/science.1092485, 2003.

Morgan, W.J., Convection plumes in the lower mantle, *Nature*, 230, 42-43, 1971.

Newman, S., E. Stolper, and R. Stern, H_2O and CO_2 in magmas from the Mariana arc and back arc system, *Geochem., Geophys., Geosyst.*, 1, 10.1029/1999GC000027, 2000.

Newman, S. and J.B. Lowenstern, VolatileCalc: a silicate melt-H_2O-CO_2 solution model written in visual basic for excel, *Computers and Geosciences*, 28, 597-604, 2002.

Robinson, J.A.C. and B.J. Wood, The depth of the spinel to garnet transition at the peridotite solidus, *Earth Planet. Sci. Lett.,* 164, 277-284, 1998.

Saal., AE., E.H. Hauri, C.H. Langmuir, and M.R. Perif, Vapor undersaturation in primitive mid-ocean-ridge basalt and the volatile content of Earth's upper mantle, *Nature*, 419, 451-455, 2002.

Salters, V. J. M., Longhi, J.E., and Bizimis, M., Near mantle solidus trace element partitioning at pressures up to 3.4 GPa, *Geochem., Geophys., Geosyst., 3*(7), 10.1029/2001GC000148, 2002.

Schilling, J.-G., M.B. Bergeron, and M.B. Evans, Halogens in the mantle beneath the North Atlantic, *Philos. Trans. Royal Soc. London*, Ser. A 297, 147-178, 1980.

Simons, K., J. Dixon, J.-G. Schilling, R. Kingsley, and R. Poreda, Volatile in basaltic glasses from the Easter-Salas y Gomez Seamount Chain and Easter Microplate: Implications for geochemical recycling of volatile elements, *Geochem., Geophys., Geosyst.*, 3(7), 10.1029/2001GC000173, 2002.

Sims, K.W.W. and S.R. Hart, Th, Nd, Sr and Pb isotopes in Samoan lavas: Implications for mantle heterogeneity, *Eos. Trans. AGU*, 85(47), Fall Meeting Suppl., Abstract V53A-0608, 2004.

Sleep, N.H., Hotspots and mantle plumes: Some phenomenology, *J. Geophys, Res.*, 95, 6715-6736, 1990.

Staudigel, H., S.R. Hart, A.A.P. Koppers, C. Constable, R. Workman, M.D. Kurz, E.T. Baker, Hydrothermal Venting at Vailulu'u Seamount: The Smoking End of the Samoan Chain, *Geochem. Geophys. Geosyst.*, 5, Q02003, 10.1029/2003GC000626, 2004.

Stolper, E.M., and J.R. Holloway, Experimental determination of the solubility of carbon dioxide in molten basalt at low pressure, *Earth and Planet. Sci. Lett.*, 87, 397-408, 1988.

Stroncik, N.A. and K.M. Haase, Chlorine in oceanic intraplate basalts: Constraints on mantle sources and recycling processes, *Geology*, 32(11), 945-948, 2004.

Su, W., R.L. Woodward and A.M. Dziewonski, Degree 12 model of shear velocity heterogeneity in the mantle, *J. Geophys, Res.*, 99, 6945-6980, 1994.

Taras, B.D., and S.R. Hart, Geochemical evolution of the New England seamount chain: isotopic and trace-element constraints, *Chemical Geology*, 64, 35-54, 1987.

Trull, T.W., M.D. Kurz and W.J. Jenkins, diffusion of cosmogenic ^{3}He in olivine and quartz: implications for exposure age dating, *Earth Planet. Sci. Lett.,* 103, 241-256, 1991.

Van Orman J.A., T.L. Grove and N. Shimizu, Rare earth element diffusion in diopside: Influence of temperature, pressure and ionic radius, and an elastic model for diffusion in silicates, *Contrib. Min. and Pet.*, 141, 687-703, 2001.

Wallace, P., and I.S.E. Carmichael, Sulfur in basaltic magmas, *Geochim. et Cosmochim. Acta*, 56, 1863-1874, 1992.

Wänke, H., G. Dreibus, and E. Jagoutz, Mantle chemistry and accretion of the Earth, in *Archean Geochemistry*, eds. A. Kröner, G.N. Hanson, and A.M. Goodwin, Springer-Verlag, Berlin, pp. 1-24, 1984.

Webster, J.D., R.J. Kinzler, and E.A. Mathez, Chloride and water solubility in basalt and andesite melts and implications for magmatic degassing, *Geochim. et Cosmochim. Acta*, 63(5), 729-738, 1999.

Weaver, B. L., The origin of ocean island basalt end-member compositions: trace element and isotopic constraints, *Earth Planet. Sci. Lett., 104*, 381-397, 1991.

Workman, R.K., S.R. Hart, M. Jackson, M. Regelous, K. Farley, J. Blusztajn, M. Kurz, and H. Staudigel, Recycled Metasomatized Lithosphere as the Origin of the Enriched Mantle II (EM2) End-member: Evidence from the Samoan Volcanic Chain, *Geochem. Geophys. Geosyst.*, 5, Q04008, doi:10.1029/2003GC000623, 2004.

Workman, R.K. and S.R. Hart, Major and Trace Element Composition of the Depleted MORB Mantle (DMM), *Earth and Planet. Sci. Letters*, 231, 53-72, 2005.

Wright, E., and White, W.M., The origin of Samoa: new evidence from Sr, Nd, and Pb

isotopes, *Earth Planet. Sci. Lett., 81*, 151-162, 1986/87.

Zindler, A., and Hart, S.R., Chemical Geodynamics, *Annual Rev. Earth and Planet. Sci.*, 14, 493-571, 1986.

Figures

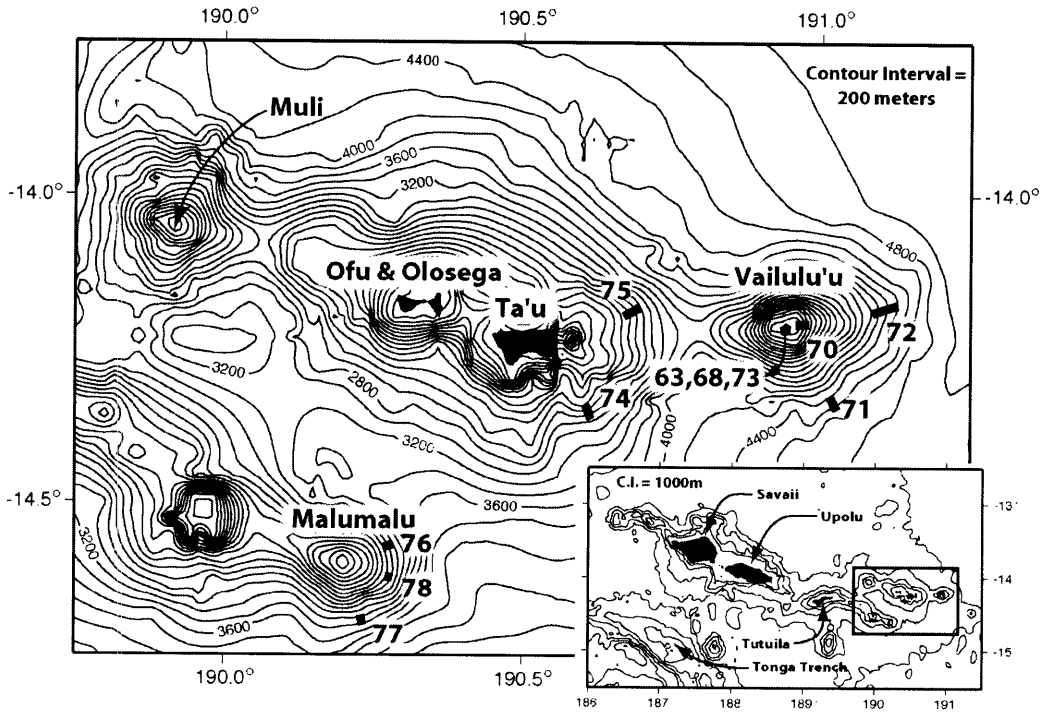

Figure 4-1. Location map for Samoan glasses. Thick lines with adjacent numbers mark individual dredges; note that some dredges traverse more contours than others. Depth contours are plotted using AVON 2/3 shipboard bathymetry data. Inset shows greater Samoan region, including the northernmost extent of the Tonga Trench.

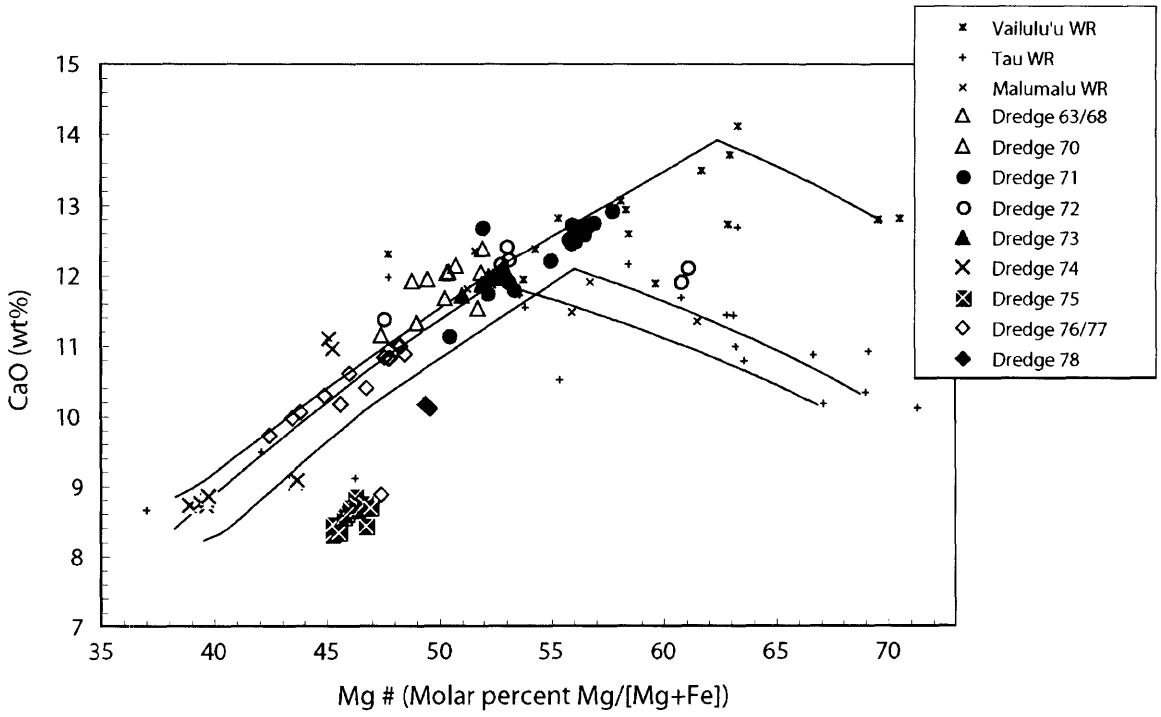

Figure 4-2. CaO plotted with Mg# for Samoan whole rocks (Workman et al., 2004) and glasses (this study). Crystal fractionation trends plotted here have been calculated using pMELTS predicted liquid lines of decent (Ghiorso et al., 2002), starting with some of the most primitive whole rock compositions. Best fits to the observed glass compositional trends are from pMELTS anhydrous runs at pressures of 3-4 kbar. Runs with 1wt% water are nearly identical to those plotted here, but with 1 kbar higher pressure.

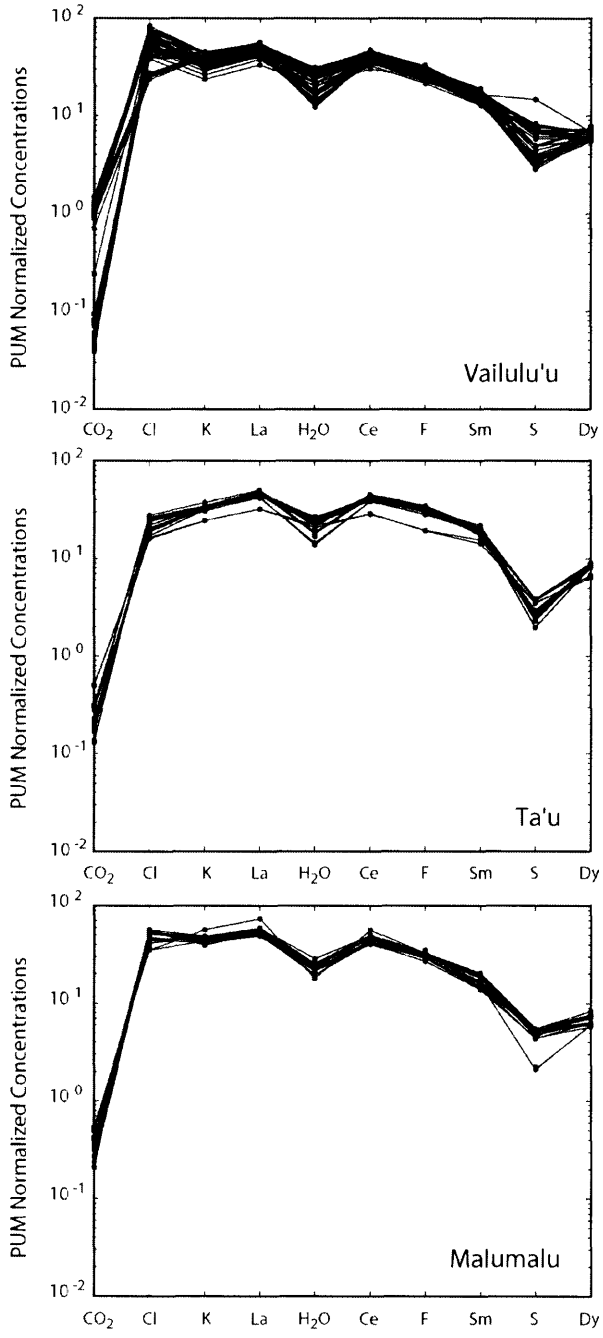

Figure 4-3. Fractionation-corrected trace and volatile element concentrations, listed in the order of increasing compatibility during mantle melting. Values are normalized to Primitive Upper Mantle (PUM) of McDonough and Sun (1995), except for water (at 335 ppm assuming $H_2O/Ce = 200$) and carbon dioxide (at 157 ppm assuming $CO_2/Nb = 239$ [Saal et al., 2002]).

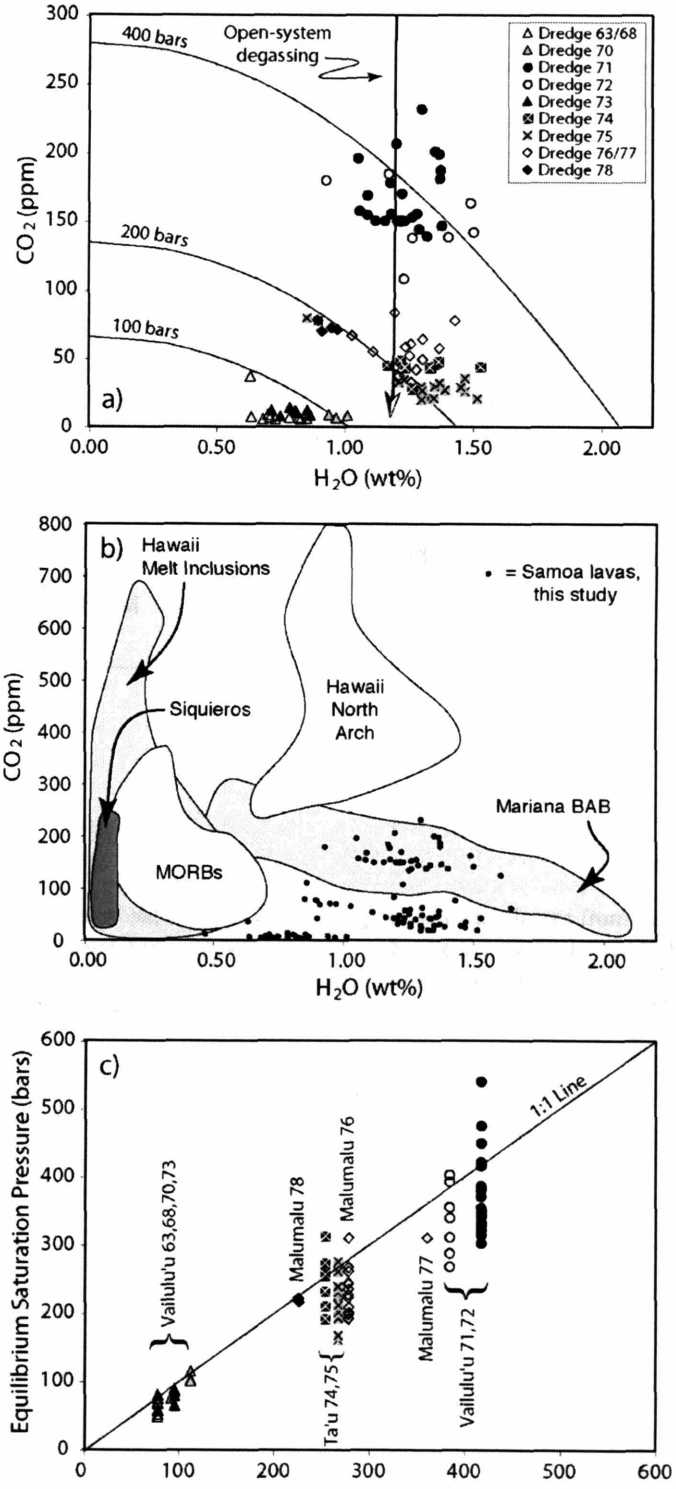

Figure 4-4. Panel a) shows water and carbon dioxide contents of Samoan glasses plotted with equilibrium vapor saturation curves and degassing trends of Dixon (1997); because open-system degassing trends are nearly vertical on this diagram, we expect that water loss has been negligible for all glasses except those at pressures less than 100 bars. Panel b) compares H_2O and CO_2 contents of Samoan glasses from this study to magmas in other settings. Panel c) plots average dredge depths for individual dredges with calculated saturation pressures (Dixon, 1997) for each sample; most lavas lie near the 1:1 line, so 1) are saturated with an H_2O-CO_2 vapor and 2) did not flow downhill from shallower extrusion depths. Each dredge traverses multiple depth contours (up to 800 meters; see fig. 1), so there is some ambiguity about the exact collection depth.

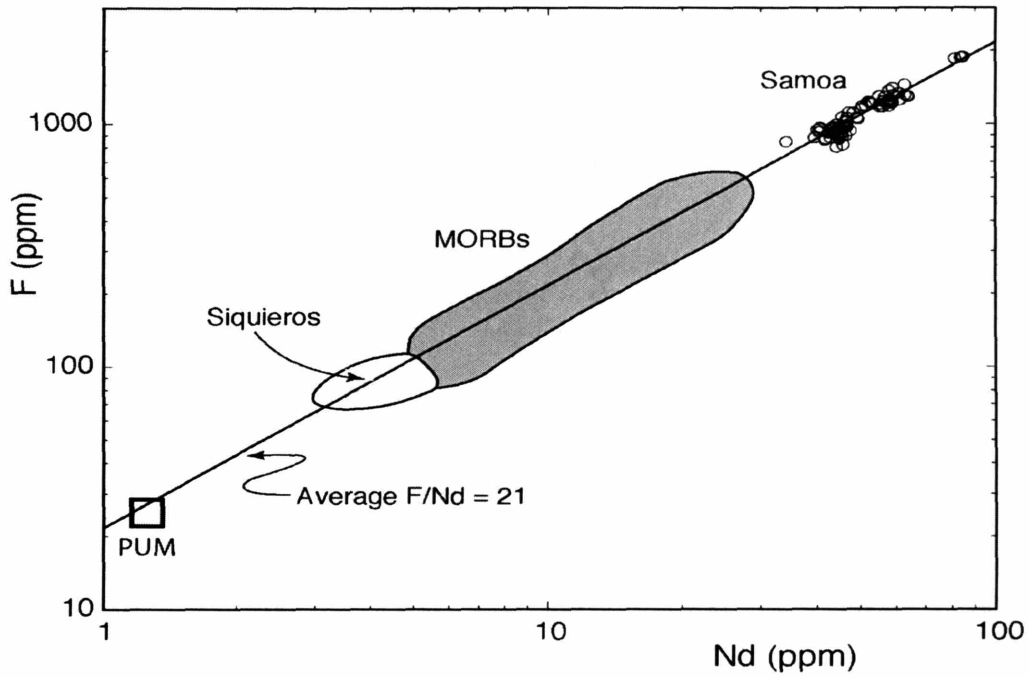

Figure 4-5. Plot of Nd and F concentrations in Samoan glasses from this study, normal MORBs (from the PETBD online database: http://beta.www.petdb.org/), very depleted MORBs (Saal et al., 2002; Saal et al., unpubl.) and Primitive Upper Mantle (McDonough and Sun, 1995). Collectively these oceanic lavas define a constant F/Nd ratio of 21, showing that F has a compatibility equal to Nd during upper mantle melting.

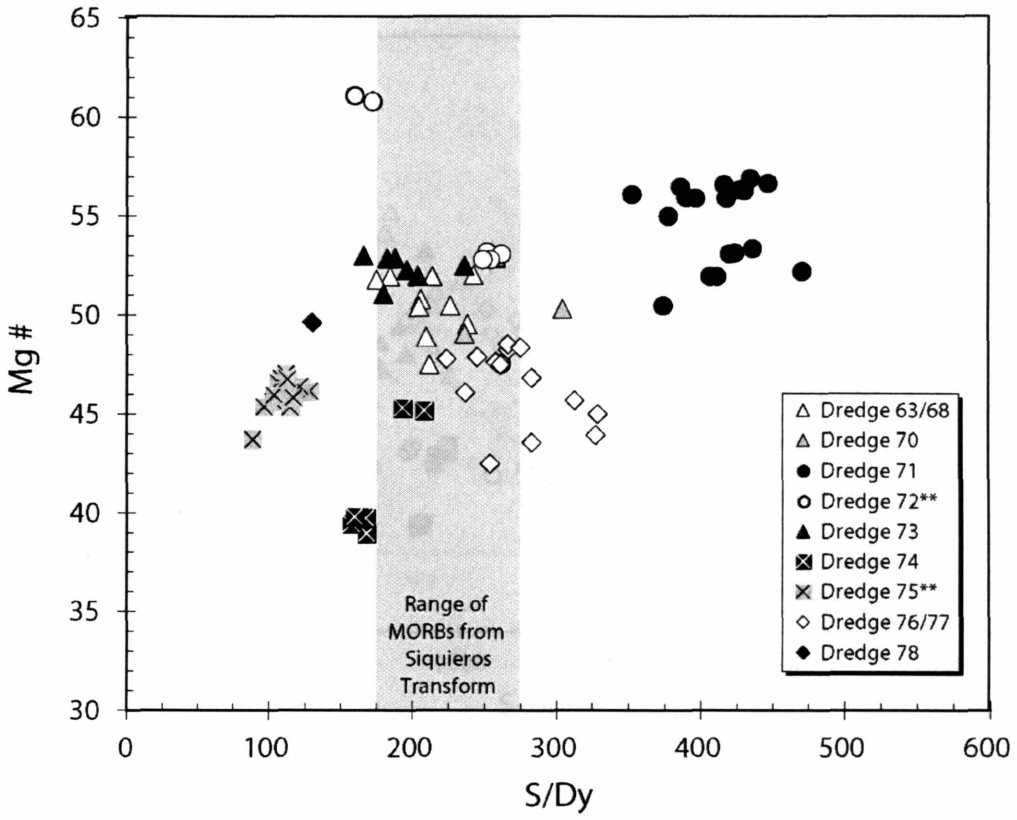

Figure 4-6. Plot of S/Dy with Mg# of the Samoan glasses. Mg# = molar percent Mg/(Mg+0.85Fe). S has been suggested to have similar compatibility to Dy, so S/Dy ratios of melts should be similar to that of their source as long there has been no sulfide fractionation or SO_2 degassing. Since sulfides were observed in all dredges except those marked with **, and there is a rough positive correlation between S/Dy (as well any S/REE ratio) and Mg#, we interpret these lavas to have lost some of their initial sulfur content by sulfide fractionation.

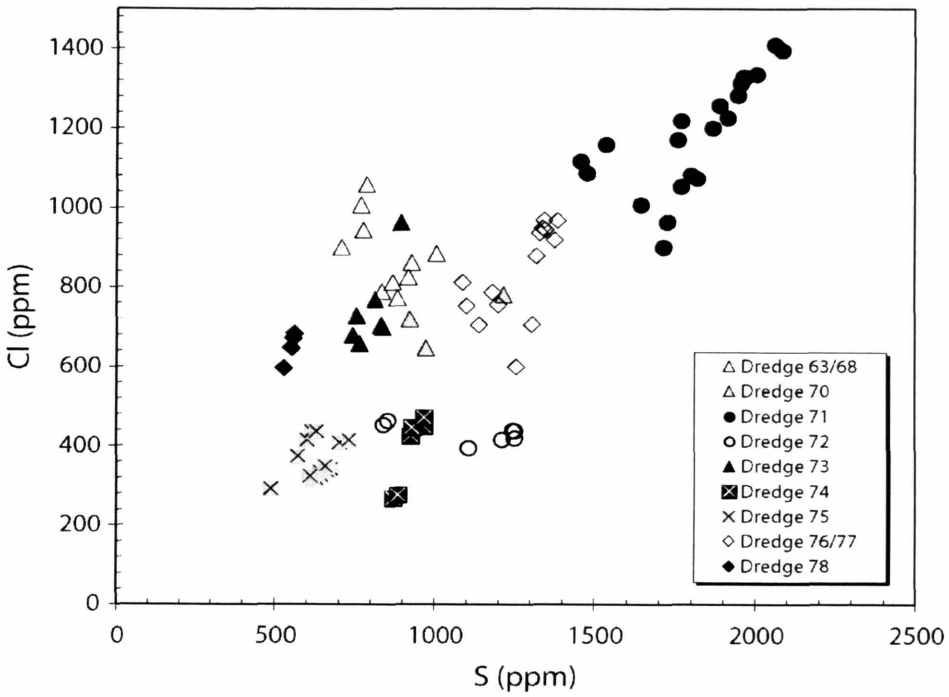

Figure 4-7. Fractionation-corrected S and Cl concentrations in Samoan basaltic glasses. Note from Figure 2 that the glasses with highest S and Cl are from the least evolved glasses of the Samoan suite. Although most glasses are saturated with sulfides, the correlation between Cl and S suggests that S loss by fractionation of a Fe-S liquid may be minimal.

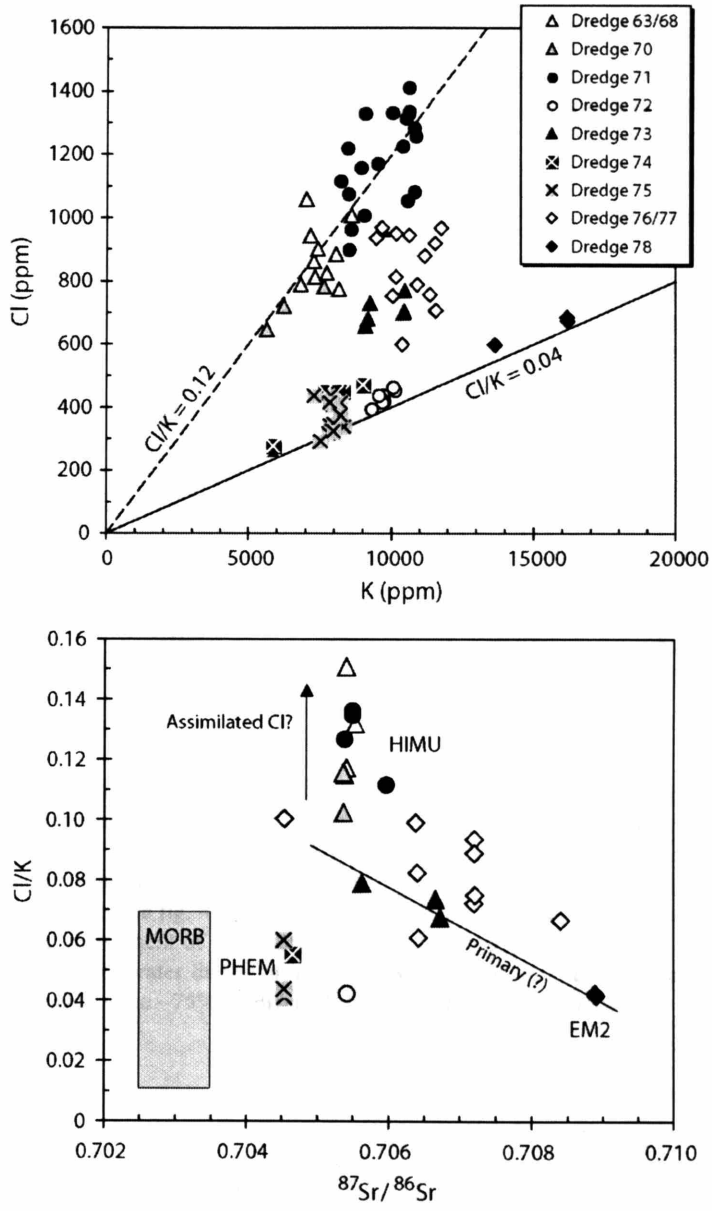

Figure 4-8. Two-panel diagram to show the systematics of Cl in Samoan glasses. Top panel shows fractionation-corrected concentrations of K and Cl; Vailulu'u lavas define a high Cl/K sub-suite, while Ta'u and dredge 78 from Malumalu define a low Cl/K array. The lower panel shows that Cl/K ratios vary with the $^{87}Sr/^{86}Sr$ source proxy.

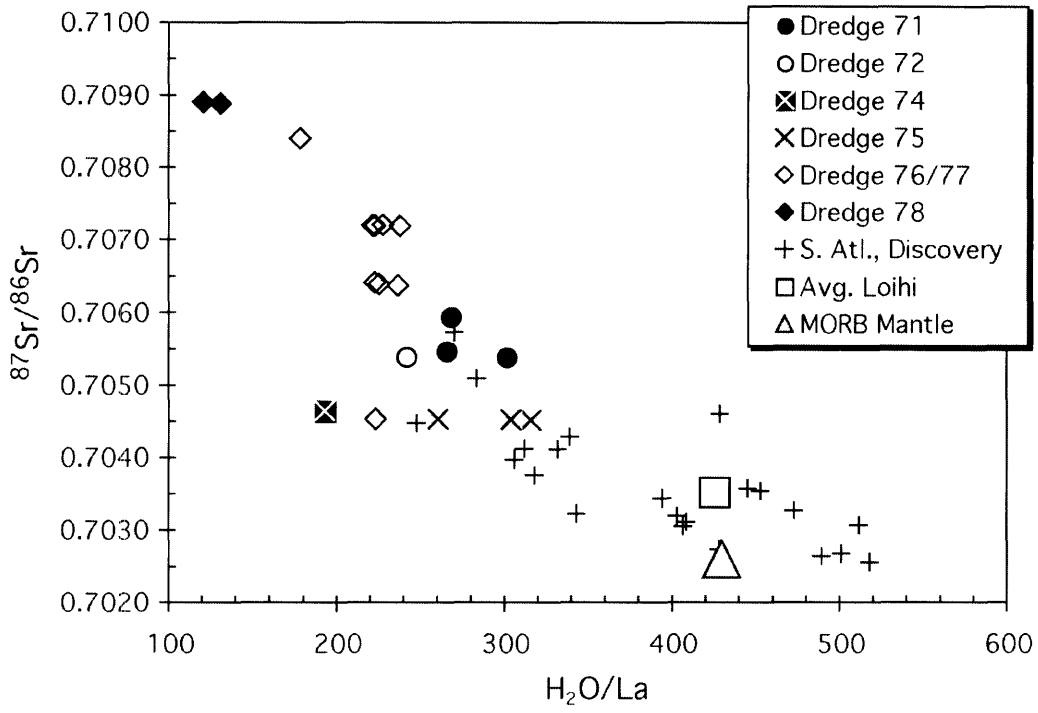

Figure 4-9. Plot of H_2O/La against $^{87}Sr/^{86}Sr$ in Samoan submarine glasses from this study along with plume-influenced glasses from the Discovery anomaly in the S. Atlantic (Dixon et al., 2002), average Loihi glasses (Dixon and Clague, 2001), and average normal MORB based on an H_2O/Ce ratio of 150 (Dixon et al., 2002). Note that the shallowly dredged, degassed Vailulu'u samples (from dredges 63, 68, 70 and 73) are not included on this plot (see fig. 4). The negative slope here indicates that increasingly enriched mantle has decreasing relative enrichment of water in its source. This water depletion in EM2 is interpreted to be the result of diffusive loss of water during storage of EM2 in a dry ambient mantle. The amount of water lost from EM2 is estimated to be ~75% its original (i.e. "pre-recycled") abundance.

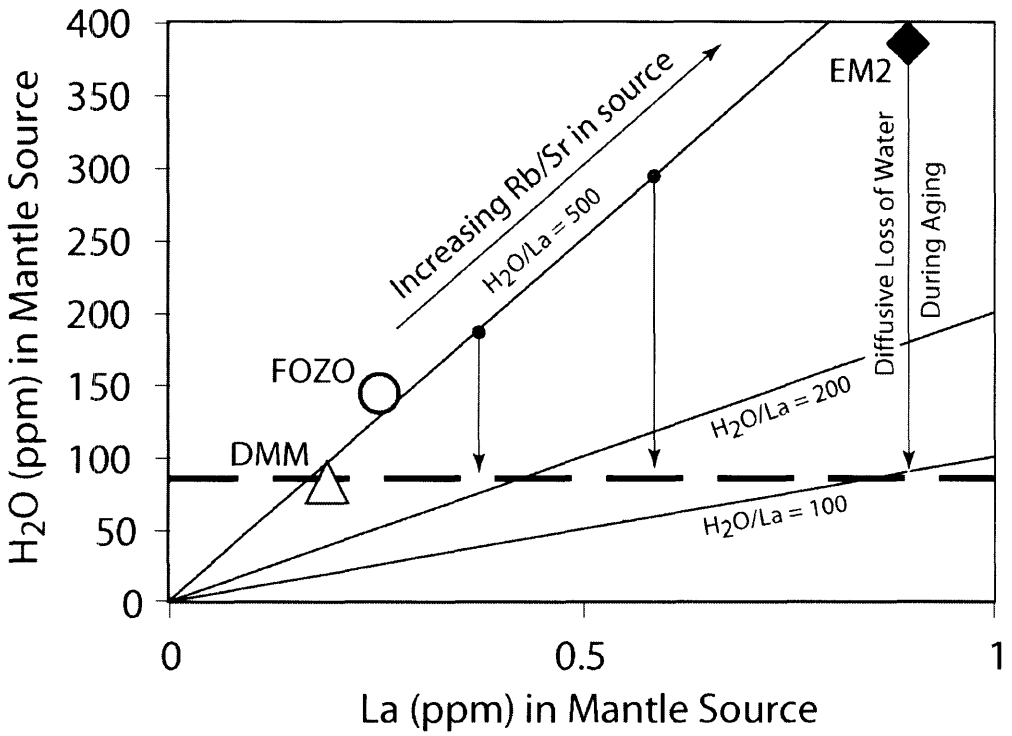

Figure 4-10. This plot is a conceptual diagram for the diffusive equilibration of water during the recycling and storage of EM2. At its formation, EM2 had "normal" enrichment of water, with H_2O/Ce of 200 and H_2O/La of 430 at 385 ppm H_2O. During storage of this material with high H_2O in an ambient mantle with lower H_2O, water is diffusively lost from EM2 – but La is not due to their contrasting rates of diffusion. When EM2 has equilibrated with the upper mantle (82.5 ppm, heavy dashed line), this otherwise enriched reservoir has an H_2O/La ratio of 92. Less enriched sources (that lay in-between EM2 and DMM), will likewise lose water while stored in a drier mantle, but, as a result of lower REE abundance, will equilibrate to higher H_2O/La. This leads to the negative relationship between H_2O/La and $^{87}Sr/^{86}Sr$ seen in Figure 9.

Tables

Table 4-1. Chemical data for Samoan Glasses, including Major Elements and Fractionation correction factors.

Sample	63-13	68-03	68-03 Rpt	68-34	68-35	68-36	68-37	68-38	68-43	68-44	70-01	70-02	70-09
Volcano	Vailulu'u	Vailulu'u	Vailulu'u	Vailulu'u	Vailulu'u	Vailulu'u	Vailulu'u	Vailulu'u	Vailulu'u	Vailulu'u	Vailulu'u	Vailulu'u	Vailulu'u
Sulfides [a]	y	y	y	y	y	n	y	y	n	y	y	n	y
Vesicles [b]	l	l	l	h	h	h	h	h	h	h	l	l	l
Volatile Content													
H_2O (wt%)	0.83	0.63	0.70	0.82	0.73	0.68	0.85	0.78	0.71	0.64	0.97	1.01	0.94
CO_2 (ppm)	6	37	9	7	6	6	7	7	7	8	7	9	9
F (ppm)	1113	929	924	909	896	884	936	876	915	889	843	935	855
S (ppm)	1318	1127	1153	1472	1353	1322	1469	1044	1410	1361	1387	1876	1484
Cl (ppm)	1603	1478	1553	1295	1278	1235	1364	1329	1267	1189	922	1207	1158
# Analyses	2	1	2	3	3	3	3	3	3	3	6	3	3
Equil. Press. (bars) [c]	77	69	69	77	60	53	82	71	59	49	104	116	102
Dredge Depth (bar) [d]	92	78	78	78	78	78	78	78	78	78	113	113	113
Major Elements (wt%)[g]													
Mg# [h]	47.4	51.9	51.9	52.0	48.8	50.8	49.5	51.8	50.4	50.4	52.8	50.3	49.0
Liquid mass [i]	58.9	68.2	68.2	68.3	61.8	65.8	63.2	67.8	65.1	65.0	70.1	64.8	62.2
Trace Elements (ppm)													
Li	8.6	5.9	7.0	5.8	6.0	5.8	6.4	6.0	6.0	5.8	7.0	5.6	6.2
B	3.9	2.7	3.6	2.9	3.0	2.8	3.3	2.9	3.0	2.7	3.7	2.9	3.1
P	2798	1729	2336	1911	1996	1943	2065	1813	1989	1843	2257	1908	2020
K	12153	12597	10298	11785	11034	11126	11509	10927	11877	12551	8030	11785	10023
Ti	20607	20450	19118	21234	21782	21547	20999	19980	21312	21782	17786	21156	20372
Rb	23	30	19	26	25	24	24	25	26	30	14	27	21
Sr	459	582	478	564	563	565	559	510	583	619	411	552	444
Y	30	29	26	29	30	29	29	28	29	31	25	30	30
Zr	283	271	253	270	283	278	271	266	280	285	225	272	265
Nb	58	56	50	53	54	54	54	54	55	57	39	56	51
Ba	280	304	243	288	278	278	282	255	295	315	171	280	232
La	47	43	39	41	42	42	41	41	42	44	31	43	39
Ce	100	94	87	91	94	94	90	91	93	97	72	94	87
Nd	47.2	43.8	40.5	43.5	44.5	45.6	42.9	42.8	44.6	46.5	34.1	44.1	41.7
Sm	9.1	8.5	8.5	9.0	9.6	8.6	8.7	8.2	8.8	9.1	7.4	8.1	8.3
Eu	2.8	3.1	2.4	3.0	3.0	3.0	3.1	2.9	2.9	3.3	2.1	2.9	2.7
Gd	7.0	8.8	6.5	8.1	8.3	8.4	8.0	8.1	8.4	9.3	6.1	8.3	7.4
Dy	6.2	6.1	5.4	6.1	6.4	6.4	6.2	6.0	6.2	6.6	5.4	6.2	6.3
Yb	2.5	2.6	2.0	2.4	2.5	2.5	2.1	2.7	2.5	2.5	1.7	2.7	2.6
Hf	6.9	5.9	6.1	6.0	6.5	6.5	6.1	6.2	6.1	6.2	4.9	5.8	6.2
Th	8.1	5.7	6.5	5.8	5.8	5.9	6.1	5.8	6.0	5.7	5.5	6.1	6.1
U	1.8	1.3	1.3	1.4	1.4	1.3	1.4	1.3	1.3	1.3	1.1	1.3	1.4
$^{87}Sr/^{86}Sr$ [e]	0.70552	0.705396	0.705396								0.705371	0.705359	0.705352

[a] Presence of sulfides in glass chips; y = observed, n = not observed.

[b] Vesicle abundance in glass chips; l = low (0-5 vol%), m = moderate (5-10 vol%), h = high (10-30 vol%).

[c] Equilibrium vapor saturation pressure calculated following Dixon (1997).

[d] Average dredge depth for each dredge; 10 meters = 1 bar.

[e] Sr Isotope analyses on whole rocks previously published by Workman et al. (2004) are in plain text, new analyses on glasses are in bold.

[f] Repeat analyses are from different glass chips of the same sample.

[g] Major Elements previously published in Workman et al. (2004).

[h] Mg# = Molar percent $Mg/(Mg+Fe^{2+})$. Fe^{2+} taken as 0.85 of total reported FeO.

[i] Liquid mass = percent of liquid mass remaining after fractionation of soilds from a Mg# 73 initial composition as predicted by pMELTS (Ghiorso et al., 2002). Multiply trace and volatile elements by this number/100 to get fractionation corrected compositions. Amount of solid fractionation = (100 - Liquid remaining).

Table 4-1, Page 2

Sample	71-02	71-03	71-04	71-05	71-06	71-06Rpt	71-09	71-10	71-10Rpt	71-11	71-13	71-13D	71-14
Volcano	Vailulu'u	Vailulu'u	Vailulu'u	Vailulu'u	Vailulu'u	Vailulu'u	Vailulu'u	Vailulu'u	Vailulu'u	Vailulu'u	Vailulu'u	Vailulu'u	Vailulu'u
Sulfides [a]	y	y	y	y	y	y	y	y	y	y	y	y	y
Vesicles [b]	l	l	l	l	l	l	l	l	l	l	l	l	l
Volatile Content													
H_2O (wt%)	1.18	1.22	1.09	1.06	1.28	1.37	1.18	1.26	1.37	1.23	1.12	1.37	1.22
CO_2 (ppm)	179	171	156	158	156	188	156	154	182	151	151	199	152
F (ppm)	903	980	937	865	972	1064	947	966	1026	915	878	967	949
S (ppm)	2337	2612	2474	2060	2574	2404	2508	2572	2508	2568	2441	2406	2537
Cl (ppm)	1490	1752	1651	1558	1718	1478	1656	1744	1610	1522	1366	1267	1708
# Analyses	3	3	3	2	3	4	3	3	4	3	3	3	3
Equil. Press. (bars) [c]		356	304	333	382	451	323	352	418	355	335	477	332
Dredge Depth (bar) [d]	417	417	417	417	417	417	417	417	417	417	417	417	417
Major Elements(wt%)[g]													
Mg# [h]		57.7	55.9	55.0	51.9	51.9	56.6	55.9	55.9	53.1	53.1	53.3	56.3
Liquid mass [I]		79.7	76.3	74.4	68.2	68.2	77.5	76.2	76.2	70.7	70.6	71.1	77.0
Trace Elements(ppm)													
Li	5.8	6.3	6.1	6.3	6.5	6.3	6.1	6.2	5.8	5.8	5.7	6.2	5.6
B	3.0	3.3	3.3	3.3	3.7	3.3	3.3	3.6	3.0	3.0	2.9	3.3	2.7
P	1560	1735	1733	1771	1883	1729	1733	1777	1750	1724	1741	1756	1641
K	13317	14206	11969	13900	13210	13884	13869	13593	11984	12137	11938	13609	12413
Ti	20215	21156	18727	21038	20685	20685	20764	20764	19353	19040	19118	20764	19510
Rb	32	36	29	33	30	34	34	33	29	28	28	32	30
Sr	567	607	544	597	568	588	591	585	545	543	545	586	566
Y	28	29	27	29	28	29	28	29	27	27	28	30	29
Zr	271	285	260	286	270	279	278	282	260	263	258	294	264
Nb	55	59	53	58	55	58	57	57	53	53	52	57	54
Ba	305	327	287	319	299	314	321	314	284	279	276	312	296
La	44	47	41	46	45	45	45	46	41	39	39	44	41
Ce	96	103	89	102	98	97	98	100	88	86	87	99	92
Nd	45.4	47.5	41.8	46.7	45.6	44.9	45.9	46.3	42.4	39.5	40.7	45.5	42.9
Sm	8.2	8.8	8.9	9.0	9.2	8.5	9.4	9.1	8.1	8.4	8.2	8.1	8.3
Eu	3.2	3.2	2.8	3.2	2.8	3.4	3.2	3.2	2.8	2.8	2.7	3.0	3.0
Gd	9.0	9.3	7.5	9.3	7.9	9.2	9.1	9.0	8.2	8.1	8.3	8.9	8.8
Dy	6.0	6.4	5.5	6.3	5.9	6.0	6.2	6.3	6.1	5.8	5.5	5.9	6.1
Yb	2.3	2.5	2.2	2.5	2.4	2.4	2.3	2.5	2.5	2.4	2.7	2.4	2.7
Hf	5.9	6.1	6.0	6.1	6.4	6.1	5.8	6.2	5.9	5.3	5.8	5.9	6.0
Th	5.8	6.4	5.5	6.2	6.8	5.9	6.0	6.5	5.3	5.0	5.4	5.9	5.5
U	1.4	1.4	1.3	1.4	1.5	1.4	1.4	1.4	1.2	1.2	1.2	1.3	1.3
$^{87}Sr/^{86}Sr$ [e]	0.705943								0.705394				

Table 4-1, Page 3

Sample	71-15	71-16	71-22	71-22Rpt	71-23	71-24	71-25	71-26	71-27	71-28	71-28Rpt	72-02	72-04
Volcano	Vailulu'u	Vailulu'u	Vailulu'u	Vailulu'u	Vailulu'u	Vailulu'u	Vailulu'u	Vailulu'u	Vailulu'u	Vailulu'u	Vailulu'u	Vailulu'u	Vailulu'u
Sulfides [a]	y	y	y	n	y	y	y	y	y	y	n	n	n
Vesicles [b]	l	l	l	l	l	l	l	l	l	l	l	m	l
Volatile Content													
H_2O (wt%)	1.38	1.32	1.09	1.30	1.22	1.29	1.15	1.20	1.05	1.20	1.35	1.23	1.26
CO_2 (ppm)	147	140	169	233	151	145	151	151	197	207	202	109	139
F (ppm)	918	944	957	1110	960	983	962	973	990	1056	1077	1188	1060
S (ppm)	2619	2569	2232	2261	2551	2651	2563	4834	2323	2304	2435	1870	1757
Cl (ppm)	1545	1775	1715	1670	1726	1818	1711	1754	1400	1377	1570	670	623
# Analyses	3	3	3	3	3	3	3	3	3	3	4	3	3
Equil. Press. (bars) [c]		373	388	542	330	344	316	331	346	386	423	270	313
Dredge Depth (bar) [d]	417	417	417	417	417	417	417	417	417	417	417	384	384
Major Elements(wt%)[g]													
Mg# [h]		52.2	50.5	50.5	56.3	56.7	56.9	55.8	56.5	56.1	56.1	47.5	53.1
Liquid mass [I]		68.8	65.2	65.2	77.1	77.7	78.2	76.0	77.3	76.6	76.6	59.1	70.6
Trace Elements(ppm)													
Li	5.6	5.8	6.0		7.4	6.3	6.2	6.5	6.3	6.2		7.1	6.2
B	2.7	3.0	3.4		4.0	3.5	3.4	3.6	3.2	3.3		4.0	3.4
P	1641	1781	1764		2229	1754	1779	1898	1780	1809		2105	1870
K	12413	12260	12567		11739	13624	13547	13149	13953	13747		15708	13716
Ti	19510	19353	19040		19824	20764	20764	20999	20842	20921		24760	23663
Rb	30	28	31		24	32	31	32	34	32		37	33
Sr	566	554	575		492	583	582	567	592	591		665	616
Y	29	28	27		26	29	29	28	29	29		34	33
Zr	264	261	270		258	284	280	280	278	280		321	302
Nb	54	54	55		54	56	58	57	57	57		67	59
Ba	296	287	298		259	313	311	310	321	316		361	322
La	41	40	41		42	46	45	45	46	46		51	47
Ce	92	88	90		90	97	97	98	100	101		112	103
Nd	42.9	40.1	40.5		43.2	45.5	43.3	43.5	46.4	46.8		51.4	49.2
Sm	8.3	7.7	8.5		8.9	8.8	7.6	8.8	9.2	9.3		10.9	10.2
Eu	3.0	2.9	3.0		2.6	2.9	3.2	2.9	3.0	3.1		3.7	3.3
Gd	8.8	8.4	8.5		6.8	8.6	8.5	8.2	8.8	8.8		10.3	9.7
Dy	6.1	5.5	6.0		6.0	5.9	5.9	6.2	6.0	6.5		7.2	7.0
Yb	2.7	2.4	2.4		2.0	2.5	2.7	2.3	2.4	2.4		2.9	2.7
Hf	6.0	5.6	6.0		6.3	6.1	6.2	6.2	6.2	6.2		7.1	6.9
Th	5.5	5.4	5.5		6.8	5.8	5.9	6.4	6.3	6.5		6.8	6.0
U	1.3	1.3	1.2		1.5	1.4	1.3	1.4	1.4	1.5		1.5	1.4
$^{87}Sr/^{86}Sr$ [e]			0.705473	0.705473								0.705395	

Table 4-1, Page 4

Sample	72-07	72-10	72-12	72-12Rpt	72-13	73-01	73-03	73-04	73-07	73-12	73-13	73-15	74-01
Volcano	Vailulu'u	Vailulu'u	Vailulu'u	Vailulu'u	Vailulu'u	Vailulu'u	Vailulu'u	Vailulu'u	Vailulu'u	Vailulu'u	Vailulu'u	Vailulu'u	Ta'u
Sulfides [a]	n	n	n	n	n	n	y	y	n	n	y	n	-
Vesicles [b]	l	l	l	l	l	31%	20%	h	h	h	l	h	l
Volatile Content													
H_2O (wt%)	1.49	0.93	1.40	1.50	1.17	0.75	0.71	0.87	0.78	0.81	0.85	0.81	1.26
CO_2 (ppm)	164	181	139	143	185	8	13	9	15	12	13	11	28
F (ppm)	1148	867	1050	1109	921	989	998	1022	955	982	969	932	801
S (ppm)	1771	1010	1728	1784	1041	1209	1138	1227	1055	1162	1091	1293	984
Cl (ppm)	598	547	596	628	567	1022	1098	1025	965	1097	940	1390	651
# Analyses	3	3	2	5	3	3	3	3	3	3	2	3	3
Equil. Press. (bars) [c]	405	289	357	394	341	66	66	87	80	80	90	80	
Dredge Depth (bar) [d]	384	384	384	384	384	96	96	96	96	96	96	96	254
Major Elements(wt%)[g]													
Mg# [h]	53.0	61.1	52.8	52.8	60.8	52.3	51.0	52.0	53.0	52.9	52.8	52.5	
Liquid mass [l]	70.5	83.0	69.9	69.9	82.0	68.9	66.4	68.3	70.4	70.1	70.0	69.3	
Trace Elements(ppm)													
Li	6.4	6.2	6.3	6.2	5.9	5.5	6.2	5.5	5.7	5.6	5.7	5.8	
B	3.5	3.5	3.6	3.9	3.4	4.0	3.0	4.0	2.7	4.0	2.8	4.5	
P	1885	1816	1853	1802	1831	1763	1886	1773	1764	1813	1746	1986	
K	13793	12168	13808	13639	12245	15156	13930	15264	13026	14911	12965	13961	
Ti	23741	19824	23585	23428	20215	19432	20529	19432	19902	19589	19745	19275	
Rb	33	31	32	32	30	37	32	37	32	35	31	30	
Sr	620	559	612	599	570	585	566	589	570	587	567	543	
Y	33	29	33	32	30	29	29	29	29	29	28	27	
Zr	300	280	300	297	291	287	281	287	275	283	269	280	
Nb	60	55	59	58	56	58	58	58	55	58	55	58	
Ba	324	294	321	314	297	388	325	392	306	379	308	354	
La	47	43	46	45	44	52	45	52	44	52	42	51	
Ce	104	93	101	99	97	109	97	109	96	109	93	105	
Nd	50.3	44.9	49.5	48.4	45.4	46.6	44.2	46.5	42.9	45.5	43.6	44.1	
Sm	9.3	8.6	9.4	10.7	9.5	8.4	8.8	9.0	8.8	8.8	8.4	8.0	
Eu	3.4	3.1	3.3	3.4	3.0	3.1	3.3	3.1	3.1	3.1	3.2	2.9	
Gd	9.9	8.7	9.7	9.6	9.3	8.9	8.8	8.5	8.1	8.8	8.5	7.3	
Dy	6.8	6.4	6.8	7.2	6.1	6.2	6.3	6.0	6.4	6.2	6.0	5.5	
Yb	2.9	2.4	3.1	2.7	2.5	2.4	2.6	2.5	2.6	2.5	2.5	2.4	
Hf	6.9	5.9	6.6	6.4	6.2	6.3	6.2	6.1	5.8	6.3	5.9	6.0	
Th	5.8	5.7	5.9	5.9	6.0	7.3	6.3	7.5	6.1	7.8	5.9	8.3	
U	1.4	1.3	1.4	1.2	1.3	1.5	1.4	1.5	1.3	1.3	1.3	1.5	
$^{87}Sr/^{86}Sr$ [e]						0.70672	0.705616			0.706653			0.704686

Table 4-1, Page 5

Sample	74-02	74-03	74-05	74-10	74-11	74-12	74-13	74-14	75-01	75-02	75-03	75-04	75-05
Volcano	Ta'u	Ta'u	Ta'u	Ta'u	Ta'u	Ta'u	Ta'u	Ta'u	Ta'u	Ta'u	Ta'u	Ta'u	Ta'u
Sulfides [a]	n	n	n	n	n	n	y	y	n	n	n	n	n
Vesicles [b]	l	l	l	l	l	l	l	l	m	m	m	m	m
Volatile Content													
H_2O (wt%)	1.36	1.16	1.34	1.37	1.22	1.24	1.33	1.53	1.33	1.52	1.35	1.30	1.39
CO_2 (ppm)	46	45	44	48	49	44	44	44	21	21	21	20	27
F (ppm)	1872	802	1871	1866	1856	818	1854	1887	1339	1371	1235	1338	1262
S (ppm)	2107	1462	2092	2044	2017	1498	2022	2098	998	1034	1132	999	1189
Cl (ppm)	982	451	975	990	928	469	971	1023	689	734	657	692	674
# Analyses	4	3	3	3	3	3	3	3	3	3	3	3	3
Equil. Press. (bars) [c]	263	193	256	275	233	212	258	314	214	271	220	205	240
Dredge Depth (bar) [d]	254	254	254	254	254	254	254	254	268	268	268	268	268
Major Elements(wt%)[g]													
Mg# [h]	38.9	45.3	39.8	39.4	39.7	45.1	39.7	39.8	45.6	45.3	46.3	46.8	46.1
Liquid mass [i]	44.1	59.5	46.1	45.2	45.9	59.2	46.0	46.1	60.3	59.6	62.1	63.2	61.6
Trace Elements(ppm)													
Li	10.2	6.0	10.3	10.3		5.9	10.2	10.2	8.4	9.0	8.0	8.8	7.8
B	6.4	3.4	6.5	6.6		3.4	6.6	6.8	5.1	5.8	4.8	5.5	4.7
P	4327	2003	4351	4364		1965	4313	4341	3330	3865	3077	3757	3031
K	18191	9854	17961	17900		9900	16720	19509	13655	12229	12766	12475	12720
Ti	24211	37767	23741	23741		37532	23271	23898	24368	23428	26797	23976	27189
Rb	38	21	38	39		23	36	40	28	24	27	24	27
Sr	664	599	664	671		616	650	679	730	670	735	685	734
Y	58	35	59	60		35	57	59	45	43	43	45	44
Zr	587	314	594	604		308	557	585	445	431	429	442	427
Nb	86	49	86	88		48	86	88	65	61	61	63	62
Ba	373	209	370	383		213	366	388	287	262	275	271	270
La	69	35	69	71		35	67	71	50	48	47	50	47
Ce	161	81	162	166		80	158	165	116	112	109	117	109
Nd	84.3	44.3	84.1	84.5		45.8	81.3	84.9	61.0	58.0	58.4	60.7	58.0
Sm	17.3	9.7	17.6	17.8		10.6	17.1	18.0	12.7	11.7	12.2	13.3	12.5
Eu	5.6	3.3	5.7	5.8		3.2	5.6	5.7	4.5	4.0	4.2	4.2	4.4
Gd	17.4	9.7	17.5	18.3		10.0	17.1	18.1	13.2	11.5	12.9	11.5	12.8
Dy	12.5	7.6	12.7	13.0		7.2	12.1	13.1	9.7	9.0	9.3	9.2	9.3
Yb	5.1	3.0	4.9	5.1		2.9	5.1	5.5	3.7	3.5	3.7	3.7	3.7
Hf	12.7	6.9	12.4	12.8		6.9	12.6	13.4	9.4	9.7	9.2	9.8	9.3
Th	8.2	4.2	8.2	7.9		4.0	8.2	8.7	5.7	6.5	5.2	6.7	5.4
U	2.1	0.9	2.1	2.2		1.0	2.2	2.2	1.5	1.6	1.3	1.5	1.4
$^{87}Sr/^{86}Sr$ [e]				**0.704645**						**0.704521**			

Table 4-1, Page 6

Sample	75-07	75-08	75-10	75-11	75-12	75-13	75-14	75-15	75-16	75-17	75-18	76-01	76-02
Volcano	Ta'u	Ta'u	Ta'u	Ta'u	Ta'u	Ta'u	Ta'u	Ta'u	Ta'u	Ta'u	Ta'u	Malumalu	Malumalu
Sulfides [a]	n	n	n	n	n	n	n	n	n	n	n	y	y
Vesicles [b]	m	m	m	m	m	m	m	m	m	m	m	l	l
Volatile Content													
H_2O (wt%)	1.21	1.30	1.23	1.35	1.47	0.85	1.37	1.47	1.45	0.90	1.30	1.37	1.30
CO_2 (ppm)	33	30	35	30	26	80	32	36	29	78	27	58	64
F (ppm)	1291	1240	1234	1245	1448	1299	1216	1311	1219	1294	1175	1222	1220
S (ppm)	1086	1027	1039	1040	960	908	1024	1084	1004	904	969	1923	1991
Cl (ppm)	551	534	526	531	629	536	519	574	520	541	514	1283	1361
# Analyses	3	3	3	3	3	3	3	3	3	3	3	3	3
Equil. Press. (bars) [c]	193	216	202	231	263	162	240	276	262	168	213	268	262
Dredge Depth (bar) [d]	268	268	268	268	268	268	268	268	268	268	268	279	279
Major Elements(wt%)[g]													
Mg# [h]	46.3	46.5	46.3	47.0	45.3	43.7	46.0	45.8	45.9	43.6	46.7	46.0	43.5
Liquid mass [i]	62.1	62.6	62.0	63.7	59.6	54.2	61.4	60.8	61.1	54.1	63.0	61.4	55.3
Trace Elements(ppm)													
Li	7.7	7.7	7.8	7.9	8.3	8.6	7.9	8.0	7.6	8.6	7.8	9.2	10.7
B	4.9	4.7	4.7	4.8	4.9	5.4	4.8	5.2	4.8	5.6	4.8	4.3	4.6
P	3012	3039	3037	3017	3307	3234	3027	3165	3009	3302	3009	2377	2046
K	12613	12700	12775	13107	13762	13805	12977	13103	12773	13935	12648	17745	18166
Ti	26879	27134	27455	27338	24666	31122	27424	25222	27040	31020	26915	26750	24204
Rb	28	28	28	29	30	30	28	28	29	30	28	43	42
Sr	737	751	745	740	751	666	739	749	755	650	747	734	658
Y	43	44	44	44	46	49	44	44	44	49	43	36	33
Zr	416	424	427	428	458	471	431	428	427	471	421	371	321
Nb	60	61	61	62	65	67	61	63	61	66	61	70	74
Ba	269	272	275	278	297	287	274	282	275	286	270	403	402
La	46	47	47	48	52	51	47	48	47	50	47	58	57
Ce	106	111	110	111	120	119	110	113	110	119	108	125	122
Nd	56.8	58.5	58.6	58.9	62.7	63.6	58.8	59.2	57.7	64.2	55.5	57.3	52.8
Sm	12.1	12.2	12.4	14.0	13.8	14.7	12.4	12.8	12.7	14.3	11.6	12.2	10.2
Eu	4.1	4.3	4.3	4.3	4.5	4.9	4.4	4.2	4.2	4.3	4.2	4.2	3.7
Gd	12.4	13.2	12.9	13.1	13.5	13.9	13.3	13.1	13.1	13.8	13.1	11.8	10.6
Dy	8.9	9.6	9.3	9.3	9.9	10.2	9.1	9.3	9.7	10.1	8.6	8.1	7.0
Yb	3.6	3.7	3.8	3.8	4.1	4.3	4.0	3.7	3.7	4.2	3.8	2.8	2.8
Hf	9.0	9.1	9.0	9.1	9.5	9.9	8.9	9.3	8.8	10.1	8.6	8.0	6.8
Th	5.1	5.3	5.2	5.2	5.6	5.5	5.3	5.4	5.2	5.8	5.0	7.1	7.4
U	1.3	1.3	1.4	1.3	1.5	1.5	1.3	1.4	1.4	1.5	1.3	1.6	1.6
$^{87}Sr/^{86}Sr$ [e]			0.704533					**0.704527**				0.707192	**0.707202**

Table 4-1, Page 7

Sample	76-03	76-04	76-05	76-06	76-07	76-08	76-10	76-11
Volcano	Malumalu	Malumalu	Malumalu	Malumalu	Malumalu	Malumalu	Malumalu	Malumalu
Sulfides [a]	y	y	y	y	y	n	y	y
Vesicles [b]	l	l	l	l	l	l	l	l
Volatile Content								
H_2O (wt%)	1.25	1.11	1.20	1.03	1.30	1.21	1.26	1.24
CO_2 (ppm)	52	55	84	67	50	37	33	59
F (ppm)	1180	1237	1182	1236	1300	1236	1409	1228
S (ppm)	1735	2023	1936	1894	2391	1992	2065	2277
Cl (ppm)	1074	1348	925	1195	1725	1403	1541	1615
# Analyses	3	3	3	3	3	3	3	3
Equil. Press. (bars) [c]	228	192	311	194	244	199	209	236
Dredge Depth (bar) [d]	279	279	279	279	279	279	279	279
Major Elements(wt%)[g]								
Mg# [h]	47.7	47.6	47.4	46.8	43.9	48.2	42.5	44.9
Liquid mass [I]	65.5	65.1	64.8	63.2	56.1	66.7	52.7	58.7
Trace Elements(ppm)								
Li	8.9	9.0	8.6	12.8	10.6	10.9	9.9	9.9
B	4.4	4.5	3.9	6.0	4.6	5.3	5.0	4.6
P	2369	2499	2059	2605	2214	3200	2730	1982
K	17639	17133	16015	17961	17195	14176	19264	17287
Ti	26758	26484	25308	23820	24055	24682	25857	23976
Rb	44	41	37	41	39	28	46	42
Sr	728	709	641	608	633	594	783	670
Y	35	35	34	30	33	33	35	33
Zr	365	368	301	310	321	333	380	319
Nb	69	70	66	65	72	62	78	71
Ba	402	390	354	386	390	320	439	394
La	56	57	51	58	58	51	61	56
Ce	123	123	112	119	122	116	131	120
Nd	57.9	57.6	50.6	52.2	55.2	56.2	59.0	52.5
Sm	11.2	11.7	10.5	10.5	10.8	12.0	11.5	9.9
Eu	4.1	3.9	3.7	3.1	3.4	3.1	4.4	3.9
Gd	11.2	11.1	10.0	8.5	10.2	8.5	11.7	10.8
Dy	7.8	7.8	7.4	6.7	7.3	7.5	8.1	6.9
Yb	2.7	2.8	2.7	2.1	2.5	2.2	3.1	3.0
Hf	8.5	8.1	6.7	7.7	7.2	7.6	8.0	6.9
Th	7.0	7.6	6.8	10.3	8.7	8.3	8.0	7.6
U	1.6	1.7	1.5	1.9	1.7	1.9	1.8	1.7
$^{87}Sr/^{86}Sr$ [e]	**0.706413**			**0.708405**	**0.704530**	0.706374		**0.707196**

Table 4-1, Page 8

Sample	76-12	76-13	76-14	77-06	78-01	78-02	78-03	78-10
Volcano	Malumalu	Malumalu	Malumalu	Malumalu	Malumalu	Malumalu	Malumalu	Malumalu
Sulfides [a]	y	y	y	y	-	y	-	y
Vesicles [b]	l	l	l	h	h	h	24%	h
Volatile Content								
H_2O (wt%)	1.20	1.28	1.26	1.43	0.91	0.95	0.97	0.89
CO_2 (ppm)	44	42	61	78	70	73	72	78
F (ppm)	1245	1221	1211	1173	1254	1226	1310	1206
S (ppm)	2089	2053	2225	1947	831	821	838	781
Cl (ppm)	1396	1436	1562	1055	1004	968	1021	886
# Analyses	3	3	3	3	3	3	3	3
Equil. Press. (bars) [c]	202	224	245	311		218		223
Dredge Depth (bar) [d]	279	279	279	361	226	226	226	226
Major Elements(wt%)[g]								
Mg# [h]	47.8	48.5	45.6	48.3		49.4		49.6
Liquid mass [i]	65.8	67.3	60.4	66.9		67.0		67.4
Trace Elements(ppm)								
Li	8.9	8.7	10.1	10.3	11.5		12.1	13.5
B	4.5	4.4	4.5	5.3	6.2		6.3	7.8
P	2434	2409	1976	2390	2078		2114	2685
K	17532	17440	17578	17287	24137		24106	20214
Ti	26640	26484	23898	25230	21234		20921	19824
Rb	42	42	43	41	61		60	46
Sr	723	720	650	644	723		704	620
Y	36	36	32	33	33		32	30
Zr	370	372	318	343	384		371	358
Nb	71	70	71	71	78		77	72
Ba	397	398	392	380	481		477	405
La	57	57	56	57	76		74	71
Ce	124	125	119	124	155		151	140
Nd	58.1	59.0	53.3	56.1	61.4		63.0	55.5
Sm	11.9	12.4	10.6	11.3	10.7		10.8	9.5
Eu	4.2	3.9	3.5	3.3	3.9		3.9	3.0
Gd	11.5	11.8	10.8	9.8	11.5		10.9	8.7
Dy	8.5	7.7	7.1	7.1	7.1		7.2	6.0
Yb	2.7	2.9	2.6	2.8	2.7		2.6	2.2
Hf	8.0	7.7	6.6	8.0	8.1		8.1	7.9
Th	7.4	7.2	7.8	8.4	11.6		11.1	12.6
U	1.7	1.7	1.6	1.7	2.2		2.3	2.3
$^{87}Sr/^{86}Sr$ [e]		0.706395	**0.707198**		0.708901		0.708886	

Table 4-2. Volatile Composition of Olivine-Hosted Melt Inclusions

	68-34 mi	71-03mi	71-03mi	71-06 mi	72-12 mi	72-12 mi
H_2O (wt%)	0.88	1.22	0.67	1.21	1.48	1.32
CO_2 (ppm)	35	164	53	453	509	515
F (ppm)	935	860	879	874	1107	1022
S (ppm)	2028	2265	1979	2242	2348	2220
Cl (ppm)	1296	1598	1256	719	541	517

	76-07 mi	76-08 mi	76-10 mi	76-13 mi	76-14 mi	77-06 mi
H_2O (wt%)	1.10	1.14	0.93	1.12	1.08	1.35
CO_2 (ppm)	95	37	26	388	57	161
F (ppm)	1129	1233	1182	1150	1170	1239
S (ppm)	2195	2019	1661	2121	2033	1952
Cl (ppm)	1403	1411	1279	1295	1470	1051

Chapter 5:

Assessment of recycled, slab-derived material in enriched lavas from Samoa: evidence from oxygen isotopes

Abstract

Oxygen isotope compositions of olivine phenocrysts from Samoan lavas, ranging from $\delta^{18}O$ of 5.1-5.6‰, reconfirm that lavas from Enriched Mantle 2 (EM2) plumes display higher primary $\delta^{18}O$ values than any other mid-ocean ridge or hotspot setting. We find that $\delta^{18}O$ correlates well with $^{87}Sr/^{86}Sr$, $^{208}Pb/^{204}Pb$ and incompatible element ratios such as La/Sm. There is no correlation between $\delta^{18}O$ and Mg#'s of whole-rocks or olivines, so we interpret the $\delta^{18}O$ values to represent primary melt compositions. Clinopyroxene phenocrysts were also analyzed from a few samples and show a similar range in $\delta^{18}O$ as the olivines; unlike a typical equilibrium fractionation of ~0.4‰ for $\delta^{18}O_{Cpx} - \delta^{18}O_{Ol}$, most clinopyroxenes are lower in $\delta^{18}O$ than their coexisting olivines. We test two models for the origin of EM2's enrichment in ^{18}O, incompatible trace elements and Sr-Nd-Pb radiogenic isotopes; both are based almost entirely on comparisons of trace element patterns between a calculated source for the most EM2-rich lavas and our two model outputs. The first model is inspired by the classic interpretation that EM2 represents mantle that has been enriched by recycled marine sediments. The second model is one in which a subduction-zone-delineated mantle wedge is metasomatized by a melt from oceanic crust that has been subducted to eclogite facies pressure-temperature conditions. Each model has significant discrepancies with trace element patterns observed for Samoa, but the metasomatic model overall shows a better fit.

1. Introduction

Oxygen isotopes have become a commonly used proxy for the identification of ancient, recycled crustal components in arcs and mantle plumes and/or as a means to identify recent crustal contamination of mantle-derived igneous rocks (Eiler, 2001). The use of oxygen isotopes as a crustal tracer is made possible by the fact that only materials at or near the Earth's surface show great variability in $\delta^{18}O$ as a result of low temperature equilibrium fractionation effects. However, $\delta^{18}O$ variations in mantle-derived lavas and their phenocrysts are often small and care must be taken not to interpret secondary processes as mantle source signals.

The range in $\delta^{18}O$ of olivines from MORBs and upper mantle peridotites is small ($5.1 \pm 0.2‰$; Mattey, 1994; Chazot et al., 1997; Eiler et al., 1997; Eiler, 2001) and overlaps with values obtained from lunar rocks (Clayton et al., 1971; Clayton et al., 1972, Wiechert et al., 2000). Deviations from these 'primary' mantle values have been found in ocean island basalts (OIBs) and attributed to the addition of sediment/upper-crustal material (in the case of high $\delta^{18}O$) or lower oceanic crust (in the case of low $\delta^{18}O$), either as a present-day assimilant or as a component in the mantle plume (see the review by Eiler, 2001). Most detailed studies of $\delta^{18}O$ compositions in OIBs have focused on locations where $\delta^{18}O$ is either very similar to MORB (Pitcairn, Hawaii) or is lower than MORB (Hawaii, Iceland, Canaries) (Eiler, 2001). Here we expand on the observation by Eiler et al. (1997) that the EM2 mantle component (Enriched Mantle 2), found most extremely in the Samoan hotspot track and more weakly in the Society Islands, is the only one to consistently show $\delta^{18}O$ values that are elevated over MORBs. The Samoan islands and seamounts are now very well characterized in terms of major and trace elements, water content and Sr-Nd-Pb-Hf-Os-He isotopic composition, so there is abundant context in which to put the new oxygen isotope data that is presented in this paper.

Eiler et al. (1997) interpreted the high $\delta^{18}O$ in Samoa as the occurrence of recycled marine sediment in the Samoan plume. Such an explanation for the origin of enrichment in EM2 followed previous suggestions for EM2's origin, but was subsequently refuted by Workman et al. (2004) based on a large suite of trace element and isotopic data. Instead, Workman et al. (2004) called upon metasomatism of the lithospheric mantle (by an upper mantle melt) to explain the formation of EM2; however, their model cannot directly account for elevated $\delta^{18}O$ compositions.

Here we present new $\delta^{18}O$ analyses of olivine and clinopyroxene phenocrysts from Samoan lavas and test two models for the generation of EM2. The first is the standard sediment-recycling model. The second expands upon the metasomatic model of Workman et al. (2004) by identifying a *location* for the metasomatism (the mantle wedge), and more accurately defining what the metasomatising agent *is* (an eclogite melt). Each model shows some major misfits to characteristics of end-member Samoan lavas, although the metasomatic model requires less 'special pleading'.

2. Samples and Methods

The samples analyzed in this study have already been well characterized in terms of major and trace element abundances and isotopic (Sr-Nd-Pb-He-Os) compositions (Workman et al., 2004). Samples selected here are a subset of a much larger collection discussed by Workman et al. (2004) and are used as the result of their containing olivine phenocrysts plentiful enough for separation. Samples with names beginning with a letter (T, U or S) are subaerial samples from the Samoan Islands, and those beginning with numbers are dredged from Vailulu'u and Malumalu Seamounts as well as submarine portions of Ta'u Island.

Whole rock samples were crushed and sieved to obtain a 300-660 μm size fraction. The sieved fraction was then rinsed in acetone and deionized water. Olivine and clinopyroxene phenocrysts were hand-picked under binocular microscope either dry or from a water bath. The only mineral grains picked for $\delta^{18}O$ analyses were those with the fewest visible melt inclusions, mineral inclusions or surface discolorations.

Oxygen isotope compositions ($\delta^{18}O = 1000*(^{18}O/^{16}O_{sample}/^{18}O/^{16}O_{SMOW}) - 1$), where SMOW = standard mean ocean water at an $^{18}O/^{16}O$ ratio of 0.0020052) were determined by laser fluorination (LF) at the Caltech laboratory based on methods described by Valley et al. (1995) and Eiler et al. (2000a). Over 3 days of LF analyses, 16 runs of the GMT-2 garnet show a 1σ reproducibility of 0.07‰ about a mean of 5.83‰ – within error of the accepted, long-term average of 5.80‰ (see Valley, 1995; Eiler et al., 2000a).

Sample runs contain 1-2 mg of multiple mineral grains, and each sample is ideally run in triplicate, although some samples presented here only have 1 or 2 analyses. During LF analyses, some (not all) sample runs showed a high value of the contaminant mass 47 (i.e. ~100 times normal). This unknown contaminant was also enriched in mass 48, resulting in highly elevated $\delta^{18}O$ values (generally 10-20‰, but up to 37‰) that were all discarded.

This was a problem that was never encountered on a standard run. Consequently, sample splits were heat-treated at 1000° C for 1 and 10 minutes in air, thereby greatly improving the frequency of good runs. Although the heat treatment causes visible oxidation of olivine grains, there is no systematic difference in $\delta^{18}O$ between sample splits that were and were not pre-treated; in other words, heat-treated sample splits are both higher and lower than, but within 2σ error of, their non-treated splits with successful LF runs (see Table 1).

The range in $\delta^{18}O$ shown by replicate analyses of olivine from a given sample is slightly greater than the quoted reproducibility of the standard. For example, samples 71-2 (n=4) and 78-3 (n=3) both show variations on the order of 0.2‰. Although this is only barely beyond the limit of 2σ reproducibility of the standard, it may be suggestive of minor sample heterogeneity, as shown strongly in a SIMS study of single olivine phenocrysts from Iceland (Gurenko and Chaussidon, 2000) as well as multiple olivine analyses from a single lava flow (also from Iceland; Eiler et al., 2000b).

3. Results

Olivine phenocrysts from 20 Samoan shield lavas have $\delta^{18}O$ compositions of 5.11-5.55‰ (Table 1). The lower end of the Samoan range overlaps with olivines in MORBs and upper mantle peridotites (5.1 ± 0.2‰) that are either measured directly (Mattey, 1994; Eiler et al., 1997) or inferred from melt compositions (Eiler et al., 2000c). No lavas from any other mantle components, including another enriched mantle, EM1 (found at Pitcairn Island; Eiler et al., 1995), have $\delta^{18}O$ extending to such high values (see Eiler et al., 1997; Eiler, 2001); exceptions are from lavas that have undergone extensive crystal fractionation (e.g. Muehlenbachs and Byerly, 1982; Geist et al., 1998; Harris et al., 2000) or recent assimilation of altered crustal components (Garcia et al., 1998).

Clinopyroxene (cpx) phenocrysts have been analyzed for $\delta^{18}O$ from 5 samples and show a nearly equivalent range in $\delta^{18}O$ (4.97-5.53‰) as the olivines. Figure 1 shows that for individual samples, the $\delta^{18}O$ compositions of cpx's are similar to or lower than their coexisting olivines. This feature is directly opposite of measured and theoretical equilibrium $\delta^{18}O$ partitioning between cpx and olivine, in which cpx is generally 0.4‰ higher than olivine (Chiba et al., 1989; Mattey et al., 1994; Chazot et al., 1997; Macpherson et al., 1998; Harris et al., 2000). From this perspective, if we only had cpx data, the $\delta^{18}O$ values found in Samoa would not be an ^{18}O-enriched anomaly in the global database of oceanic basalts, as the implied $\delta^{18}O$ of equilibrium melts would be fully below the upper limit of MORB melts

(basaltic melts are assumed to be 0.5‰ heavier than olivines and hence 0.1‰ heavier than cpx; Anderson et al., 1971; Kyser et al., 1981; Eiler, 2001). Although precise knowledge of equilibrium $\delta^{18}O$ fractionations as a function of mineral and melt major element compositions, temperature and volatile content are lacking, it is possible that olivine and cpx are seemingly out of equilibrium because they record $\delta^{18}O$ at different stages in the evolution of the melts. Because olivine is the first mineral to become saturated in Samoan magmas (along with spinel), we henceforth use olivine as a proxy for $\delta^{18}O$ compositions of primary liquids.

Increasing $\delta^{18}O$ values of olivine strongly correlate with increasing incompatible element ratios and heavy isotope compositions (figs. 2-4). Figure 2 shows the relationship between $\delta^{18}O$ and La/Sm, but there are similarly good correlations with other element ratios such as K/Na, K/Ti and Rb/Sr, suggesting that high $\delta^{18}O$ derives from sources that are enriched in the highly incompatible elements. The highest $\delta^{18}O$ occurs in Malumalu lavas (samples 78-1 and 78-3), which also have the highest La/Sm (6.4), $^{208}Pb/^{204}Pb$ (39.86) and $^{87}Sr/^{86}Sr$ (0.7089). These Malumalu lavas define the most extreme EM2 basalts in the current global database and therefore equilibrium olivine from end-member EM2 is established to have $\delta^{18}O$ equal to 5.5‰. Sources with the lowest $^{87}Sr/^{86}Sr$, marked primarily by lavas from Ta'u and Upolu, are almost entirely separate from Malumalu by having lower oxygen and Sr isotopic compositions along with lower La/Sm (figs. 2-4). Vailulu'u olivines show the greatest range in $\delta^{18}O$ of any volcano (~0.4‰), but all other source proxies are nearly identical for the 6 Vailulu'u samples. On the other hand, Malumalu shows the greatest range in $^{87}Sr/^{86}Sr$ (0.7067-0.7089) of these volcanoes, but has $\delta^{18}O$ values that vary by only 0.22‰ (fig. 4).

The differences in source characteristics between eastern and western Samoa are highlighted in Figure 3. Western Samoan, comprised of the islands Savai'i and Upolu, overlaps the eastern shield lavas in $\delta^{18}O$ but is distinctly lower in $^{208}Pb/^{204}Pb$. Workman et al. (2004) claim that, of all the Samoan volcanoes, Savai'i and Upolu have the least abundant EM2 component and instead are strongly influenced by depleted mantle (for Upolu) and another, yet unidentified, source with low $^{206}Pb/^{204}Pb$ and $^{208}Pb/^{204}Pb$ but high $^{207}Pb/^{204}Pb$ (for Savai'i). The one Savaiian sample presented here is from the oldest volcanic series exposed on the island and yields a $\delta^{18}O$ composition (5.38‰) that is mid-range of the whole Samoan suite. Olivine in two young, post-erosional lavas from Savai'i, analyzed by Eiler et al. (1996), have $\delta^{18}O$ values (5.48‰ and 5.67‰) extending higher than the end-member EM2 value (5.5‰), but it is unclear if this represents a source signal or is a product

of shallow assimilation of older, altered Savaiian shield. Since all lavas from Savai'i have similar Sr-Nd-Pb isotopic signatures (Workman et al., 2004), we suggest that the lower $\delta^{18}O$ value for Savai'i is primary and the elevated $\delta^{18}O$ in post-erosional samples is from secondary processes. No further attempt is made to explain the characteristics of post-erosional lavas, as the primary focus of this work is to determine the origin of high $\delta^{18}O$ in the EM2 mantle component.

4. Process Control

The inference of small variations of $\delta^{18}O$ in mantle sources based on small variations of $\delta^{18}O$ in mantle-derived lavas must be validated with an assessment of melt generation and fractionation processes. Eiler (2001) shows that joint olivine and plagioclase fractionation, as appropriate for MORBs, results in a nearly negligible net change of $\delta^{18}O$ (<0.1‰, over a large range of MgO) since light olivine is 'buffered' by heavy plagioclase. However, the Samoan lavas from this study have liquid lines of descent that are saturated with olivine ± clinopyroxene (Workman et al., 2004), minerals that are both lighter than equilibrium melts (see discussion above). A simple calculation, assuming an olivine-melt $\delta^{18}O$ fractionation of 0.5‰, indicates that 40% olivine fractionation (an upper limit for magmas presented here) will increase a melt's $\delta^{18}O$ composition by 0.2‰. Greater increases in a melt's $\delta^{18}O$ can only occur if minerals with greater mineral-melt $\delta^{18}O$ differences are fractionated. Spinel and chromite are two such minerals (Eiler, 2001) that are present in Samoan lavas, but at a possible fractionated mass of ~2% and mineral-melt $\delta^{18}O$ fractionation of 2‰, melt $\delta^{18}O$ will increase by less than 0.1‰. Fractionation of titanomagnetite has been shown to cause increases in $\delta^{18}O$ of silicic Galapagos lavas (Muehlenbachs and Byerly, 1982), but there is no evidence this phase has played a role in Samoan fractionation trends.

An assessment of crystal fractionation effects on melt $\delta^{18}O$ values would benefit from more detailed modeling of an AFC-type process (Assimilation-Fractional-Crystallization; DePaolo, 1981) suggested to occur in some OIB lavas. However, an AFC process to create high $\delta^{18}O$ may be more important in the formation of EM2 mantle than in the present-day generation of Samoan melts; there is no reason to think that EM2 hotspot chains are unique in the way they generate or process melts, and no other OIB's show elevated $\delta^{18}O$ values.

Olivines with higher $\delta^{18}O$ tend to come from whole rocks with lower SiO_2 and CaO than do the lower $\delta^{18}O$ olivines (fig. 5). This negative correlation is slightly deceptive because picritic samples (with low SiO_2 and CaO) are generally from Vailulu'u and

Malumalu (with high $\delta^{18}O$). This observed relationship is not the result of crystal fractionation or accumulation since $\delta^{18}O$ does not correlate with Mg#'s (molar fraction of $Mg/[Mg+Fe^{2+}]$) of whole rocks or of olivines (Jackson et al., unpubl.). Whole rock samples with the lowest Mg#'s are from Upolu, and are the only obvious candidates for showing possible effects of olivine fractionation on $\delta^{18}O$, as other lavas have Mg#'s too high to have fractionated enough olivine to significantly change a melt's $\delta^{18}O$. It is, of course, possible that a melt has experienced crystal fractionation and then accumulated 'foreign' olivine.

The above factors may play in role in causing scatter in plots such as those in Figures 2 through 4, but do not negate the fact that $\delta^{18}O$ values are enriched in olivines from EM2 end-member lavas. Fractionations of $\delta^{18}O$ upon the *generation* of melt from a peridotite lithology will likewise not lead to the observed variation in Samoa's $\delta^{18}O$ values; Eiler (2001) shows that, in theory, the $\delta^{18}O$ composition of a melt is a function of Na_2O content, but the Samoan lavas are within a relatively narrow range of Na_2O (~1-3 wt%) where there is very little leverage on $\delta^{18}O$ (0.1‰). Also, there is no correlation between $\delta^{18}O$ and Na_2O, even if lavas are fractionation-corrected to Mg# 73 by incremental addition or subtraction of equilibrium olivine.

5. Source Control

The correlations of $\delta^{18}O$ (olivine) with trace element and Sr-Pb isotopic enrichment in whole rocks (figs. 2-4) robustly indicate that ^{18}O-enrichment exists in the EM2 source. Eiler et al. (1997) made the same observation with analyses from Savai'i (the post-erosional samples discussed above) and the Society Islands, another EM2 hotspot chain (although not as extreme in EM2 as Samoan lavas). Their interpretation was that EM2 represents a mixture of depleted mantle and 2-6% marine sediment having $\delta^{18}O$ = 15‰ and $^{87}Sr/^{86}Sr$ = 0.710. They also suggest that extensive metasomatism could potentially elevate a source's $\delta^{18}O$, as evidenced by high $\delta^{18}O$ found in olivines (5.3-5.5‰) and pyroxenes (5.7-5.8‰) from metasomatised Savaiian xenoliths. In an earlier study, Hauri et al. (1993) showed that cpx separates from these xenoliths have $^{87}Sr/^{86}Sr$ up to 0.7128, higher than any values seen in the Samoan lavas; however, the genetic relationship of the xenoliths to the lavas is unclear since Pb isotopic compositions of cpx in the xenoliths do not lay on an extension of trends formed by the lavas (see Workman et al., 2004).

With new light from data presented here and in Workman et al. (2004), it has become clear that the composition of end-member EM2 lavas is much lower in $\delta^{18}O$ and higher in $^{87}Sr/^{86}Sr$ than reported by Eiler et al. (1997). To model the new $\delta^{18}O$ – $^{87}Sr/^{86}Sr$ trend, sediment having $\delta^{18}O$ of 15-25‰ must have $^{87}Sr/^{86}Sr$ of 0.720 to 0.732 if mixing with primitive mantle and a more narrow range of 0.715 to 0.720 if mixing with depleted mantle; the mass of sediment added would be 2-4%, with less sediment needed as the $\delta^{18}O$ of the sediment increases (see fig. 4). Although the data is roughly fit in these two dimensions, a sediment origin for EM2 is not guaranteed by this calculation alone – there are many more parameters to be checked in order to assess the plausibility of this scenario. Accordingly, in the section below (5.1), we compare a sediment plus mantle mixture to the whole trace element pattern of end-member Samoan lavas.

Marine sediments are not the only material characterized by heavy oxygen. Altered upper oceanic crust (AOC) has been found to have δ18O values up to ~15-20‰ (Staudigel et al., 1981, Staudigel et al., 1995; Alt, 2003). When AOC is subducted at convergent margins, elements that are enriched in the ocean crust by low temperature alteration on the seafloor (Rb, Ba, U, K, Pb; Hart and Staudigel , 1989; Staudigel et al., 1996; Bach et al., 2003; Kelley et al., 2003) are also lost from the crust by dehydration and metamorphism, as seen in compositions of eclogites, the high temperature/pressure assemblage of oceanic crust (e.g. Becker et al., 2000). On the contrary, there is evidence from metabasalts and eclogites (Matthews et al., 1984; Neal et al., 1990; Nadeau et al., 1993; Putlitz et al., 2000) that deeply subducted materials do not lose the high δ18O compositions they acquired from seafloor alteration. Although bulk addition of subducted AOC (i.e. eclogite) would never result in enrichments of the highly-incompatible and light-rare-earth elements, it is possible that a melt derived from such material could have the required trace element enrichments as well as high δ18O. Below we test a second model for the generation of EM2: metasomatism of the mantle wedge by an eclogite melt derived from a subducting slab. This model expands on the one put forth by Workman et al. (2004) by providing a location (the mantle wedge) and an agent (an eclogite melt) for their proposed mantle metasomatism; however, it is very different in the regard that this is potentially a much more complicated process, involving a greater variety of minerals as well as a greater numbers of 'steps' in the processing of materials.

There are a couple of fairly convincing arguments against a fluid being the enriching component in EM2 mantle: 1) Samoan lavas have slight negative anomalies in the fluid-mobile elements – for example, even though the absolute abundances of U and K are high,

U/Nb and K/La (ratios of 'neighboring' elements in the order of compatibility) are less than in the primitive mantle; and 2) end-member Malumalu lavas have low relative Cl enrichment (see Chapter 4), whereas fluids in subduction zone systems are documented to have high Cl abundances (Kent et al, 2002; Scambelluri et al., 2004).

In summary, the following constraints for EM2, based on isotope and trace elements, must be satisfied in any plausible model for its origin: 1) high time-integrated Rb/Sr and Nd/Sm; 2) elevated δ18O; 3) lack of significant anomalies across the high-field-strength elements; 4) slight depletions in the fluid-mobile elements.

5.1. Test for a sediment source of enrichment

Present-day assimilation of local marine sediments with high $\delta^{18}O$ cannot explain the origin of the Samoan lavas because Pb isotopic compositions of the sediments are too low in $^{206}Pb/^{204}Pb$ and $^{208}Pb/^{204}Pb$ to be the enriched component of the end-member Malumalu lavas (see Plank and Langmuir, 1998; Workman et al., 2004). Therefore, we must approach the problem as one of recycling ancient marine sediments back to the mantle at convergent margins, as melting and dehydration processes in the subduction zone have the potential to alter trace element compositions, hence parent/daughter ratios and, consequently over time, radiogenic isotopic compositions. However, difficulties in this problem arise since we have collectively little knowledge about past sediment compositions (that are, in part, a function of the redox state of the oceans), melting and dehydration processes in the subduction zone, and partitioning of trace elements between sediment/fluid and sediment/melt. There is some experimental evidence to suggest that subducted sediments will still look basically like unsubducted sediments (in term of the general sense of anomalies in their trace element patterns), even after dehydration and partial melting, due to sediment/fluid and sediment/melt partition coefficients being close to 1 and often higher (Johnson and Plank, 1999); this does not mean that trace element ratios will not change, but rather that generally enriched or depleted elements will stay generally enriched or depleted, respectively.

There is seemingly no foolproof way of 'selecting' a marine sediment composition to test as an enriching component in EM2, given the many unknowns listed above. Trace elements in sediments that are not thought to fractionate from each other during subduction zone alteration (i.e. Th/La; Plank, 2005) have the potential to fractionate during small-degree mantle melting to make the Samoan lavas. On the other hand, elements that may have similar compatibilities during mantle melting (i.e. Th/U, Ba/Th, K/U, Ce/Pb, Sr/Nd) are likely to

fractionate from each other during dehydration of sediments in subduction zones because of slightly differing fluid mobilities (Johnson and Plank, 1999).

We have chosen to use La/Th and Nb/Th ratios in order to identify a 'test' sediment because these elements are thought to be immobile in sediment-derived fluids and therefore their ratios will not be fractionated by dehydration processes (Johnson and Plank, 1999; Plank, 2005). These ratios show a good correlation with each other for the Samoan lavas (fig. 6) and decent correlations with $^{87}Sr/^{86}Sr$ compositions, so must be largely reflective of source variations. We also use Ba/Th as another 'filter' for choosing a sediment; Ba is more fluid-mobile than the other elements used (Johnson and Plank, 1999), but the enormous range of Ba/Th in marine sediments (Plank and Langmuir, 1998) compensates for this possible fractionation in the subduction zone. Using compositions of individual marine sediments from the GLOSS study by Plank and Langmuir (1998), we have found 7 sediments (most of clay-dominated lithology) that lay on an extension of the Samoan trace element trends in La/Th-Nb/Th-Ba/Th space (fig. 6). The average of these 7 selected sediments is reported in Table 2. These 7 out of the 43 sediment compositions reported by Plank and Langmuir (1998) are most distinct from GLOSS by having negative Ba and Sr anomalies.

Figure 7 shows a comparison between trace element patterns of a calculated Malumalu (i.e. EM2) source with mixtures of the selected sediment and depleted or primitive mantle. See Table 2 for details of calculating the Malumalu source composition. Each mixture contains 2% by mass of the sediment and will satisfy the observed $\delta^{18}O$ of Malumalu if the sediment has a $\delta^{18}O$ composition of 25‰. To the right of La, the Malumalu source falls between the two sediment-mantle mixtures, except for Pb. To the left of La, the Malumalu source falls below either mixture, except for Nb and Ta, which fall above. Sediment melting is thought to be common beneath arc volcanoes (Elliot et al., 1997; Hoogewerff et al., 1997; Plank and Langmuir, 1998; Johnson and Plank, 1999) and, if it occurred before mixing with the mantle, could potentially account for the excess abundance of Rb, Ba, Th, U and K, but will not be able to explain the low Nb and Ta (Johnson and Plank, 1999), unless a minor phase such as rutile (with high Nb and Ta compatibility; e.g. Rudnick et al., 2000) is present in the sediment during melting. Because of experimental challenges (e.g. Johnson and Plank, 1999), there is very little accurate information about Pb mobility during dehydration and melting. The great enrichment of Pb in the continental crust (42 ppm and 84 times the abundance in primitive upper mantle; Rudnick and Fountain, 1995) must be due to greatly enhanced mobility of Pb at some stage in its generation – whatever that process is could be

the same to mobilize Pb from sediments and decrease the high positive anomaly in the sediment-mantle mixtures of Figure 7.

In summary, if sediment recycling to the mantle is the reason for trace element and hence isotopic enrichment in EM2, very specific changes must be made to the sediment before it is mixed and stored with the mantle. While these changes appear unlikely at present, future advancements in the understanding of subduction zone processes may either rule-out or rule-in a 'sediment scenario'.

5.2. Test for an eclogite melt source of enrichment

The trace element composition of eclogite, to be used in the calculation discussed below, is based on eclogite samples with MORB protoliths reported by Becker et al. (2000), and is listed in Table 2. As mentioned above, the addition of bulk eclogite to either primitive or depleted mantle will not result in the required LILE and LREE enrichment in the EM2 reservoir, since these elements are not preferentially enriched over MREE or HREE in eclogites (fig. 8). Even 2 to 3 billion years ago, oceanic crust was most likely not preferentially enriched in these elements, as there is evidence that a depleted upper mantle already existed at that time (Machado et al., 1986; Bowring and Housh, 1995; Vervoort et al., 1996).

Here we test a model in which the mantle wedge (the mantle in-between a subducted slab and the volcanic arc) is metasomatized by a melt from subducted oceanic crust. Recent thermal models for the mantle wedge and subducted slab (van Keken et al., 2002; Kelemen et al., 2003a) suggest that temperatures at the slab-wedge interface may exceed the water-saturated solidus of basaltic compositions beneath the volcanic front, and certainly will at more deeply subducted locations. Melting experiments on garnet pyroxenite show a very narrow temperature range between the solidus and liquidus (Kogiso et al., 2003), meaning melt productivity (as a function of temperature; dF/dT), will be much greater than in peridotite melting.

The upper panel in Figure 8 shows the trace element pattern of our 'test' eclogite. A 30% melt of this eclogite (using partition coefficients in Table 2) is mixed with 1) primitive mantle and 2) depleted mantle. Adding 5% of the melt to each melt-mantle mixture results in trace element patterns that show a fairly decent match to our calculated Malumalu source, especially given the potential errors in the chosen compositions and partition coefficients; to match the $\delta^{18}O$ of Malumalu, the eclogite melt must have a $\delta^{18}O$ composition of 15‰. The two mixtures bound the Malumalu source for most elements, with the only major misfit

being at U. Since U is a fluid-mobile element, it is possible that eclogites subducted to greater depths will lose additional U by further dehydration reactions.

This scenario has promise in explaining the origin of enrichment in EM2. The caveat if this: the eclogite melt produced from the slab must not be extracted from the mantle wedge, but instead get 'stuck' in it. This may be possible if the melting takes place at subducted depths greater than occur beneath the volcanic arc and the enriched wedge is effectively 'swept away' into greater depths of the mantle.

6. Discussion

Each proposed option for elevated $\delta^{18}O$ in enriched mantle lavas from Samoa requires some form of 'special pleading'. No single scenario can successfully explain the complete array of observation in the lavas, although many fewer discrepancies exist with the model involving metasomatism of the mantle wedge by eclogite melts. Likewise, no single scenario can be confidently ruled out as a possibility due to our limited knowledge base about ancient and present-day subduction zone processing of slabs, as well as compositions of ancient sediments and altered oceanic crust.

If ancient metasomatism by an eclogite melt is a plausible origin for the trace element enrichment in EM2, the reality must be a mixture of sediment and eclogite melts as the enriching component, since the solidus temperatures for these two materials can be very similar (Nichols et al., 1994; Johnson and Plank, 1999; Poli and Schmidt, 2000). This is nearly unavoidable, given the close proximity of sediment overlaying the igneous crust, and the observation that metabasalts and metapelites are often severely intermingled (for example, see Hansteen and Troll, 2003). The exchange of 1% eclogite melt for 0.5% bulk sediment slightly improves the fit of Rb and the Pr-Nd-Sr sedment of the trace element pattern, but makes the negative anomaly in Pb turn positive.

It is possible that some of the second-order variations in the trace element pattern for the Samoan lavas are due to recent alterations to the EM2 source beneath Samoa. For example, recent carbonatite metasomatism has been documented in xenoliths from Savai'i (Hauri et al., 1993). If such a metasomatising material was extracted from the EM2 (Malumalu) source before Malumalu lavas were generated, then the trace element patterns of Malumalu lavas falsely represent their ancient composition. We will need to take great care in understanding the sequence of events in the history of a given source and its derivative melts from the time of their formation until the day of our sampling.

Acknowledgements

We thank Erik Hauri for inspiring us to think of the mantle wedge as a possible place to generate EM2. We would also like to acknowledge Nami Kitchen for her talent and time spent with the LF analyses presented here. Nobu Shimizu has been a wonderful sounding board and resource for this work.

References

Alt, J.C., Stable isotope composition of upper oceanic crust formed at a fast spreading ridge, ODP Site 801, *Geochem. Geophys. Geosyst.*, 4 (5), doi:10.1029/ 2002GC000400, 2003.

Anderson, A.T., R.N. Clayton and T.K. Mayeda, Oxygen isotope thermometry of mafic igneous rocks, *J. Geology*, 79, 714-729, 1971.

Bach, W., B. Peucker-Ehrenbrink, S.R. Hart and J.S. Blusztajn, Geochemistry of hydrothermally altered oceanic crust: DSDP/ODP Hole 504B – Implications for seawater-crust exchange budgets and Sr- and Pb-isotopic evolution of the mantle, *Geochem. Geophys. Geosyst.*, 4 (3), doi:10.1029/2002GC000419, 2003.

Becker, H., K.P. Jochum and R.W. Carlson, Trace element fractionation during dehydration of eclogites from high-pressure terranes and the implications for element fluxes in subduction zones, *Chemical Geology*, 163, 65-99, 2000.

Bowring, S.A. and T. Housh, The Earth's Early Evolution, Science, 269, 1535-1540, 1995.

Chazot, G., D. Lowry, M. Menzies and D. Mattey, Oxygen isotopic composition of hydrous and anhydrous peridotites, *Geochimica et Cosmochimica Acta,* 61, 161-169, 1997.

Chiba, H., T. Chacko, R.N. Clayton and J.R. Goldsmith, Oxygen isotope fractionations involving diopside, forsterite, magnetite and calcite; application to geothermometry, *Geochimica et Cosmochimica Acta,* 53, 2985-2995, 1989.

Clayton, R.N., N. Onuma and T.K Mayeda, Oxygen isotope fractionation in Apollo 12 rocks and soils, *Proc. 2nd Lunar Sci. Conf.*, 1417-1420, 1971.

Clayton, R.N., J.M. Hurd and T.K. Mayeda, Oxygen isotope abundances in Apollo 14 and 15 rocks and minerals, *Lunar Sci. Inst. Contrib.*, 88, 141-143, 1972.

DePaolo, D.J., Trace element and isotopic effects of combined wallrock assimilation and fractional crystallization. *Earth Planet. Sci. Lett.*, 53, 189–202, 1981.

Eiler, J.M., K.A. Farley, J.W. Valley, E.M. Stolper, E.H. Hauri and H. Craig, Oxygen isotope evidence against bulk recycled sediment in the mantle sources of Pitcairn island lavas, *Nature,* 377, 138-141, 1995.

Eiler, John M., K.A. Farley, J.W. Valley, E.H. Hauri, H. Craig, S.R. Hart and E.M. Stolper, Oxygen isotope variations in ocean island basalt phenocrysts, *Geochimica et Cosmochimica Acta,* 61, 2281-229, 1997.

Eiler, J.M., A.J. Crawford, T.R. Elliott, K.A. Farley, J.W. Valley, and E.M. Stolper, Oxygen isotope geochemistry of oceanic-arc lavas, *Journal of Petrology,* 41, 229-256, 2000a.

Eiler, J.M., K. Gronvold, and N. Kitchen, Oxygen isotope evidence for the origin of chemical variations in lavas from theistareykir volcano in iceland's northern volcanic zone, *Earth and Planetary Science Letters,* 184, 269-286, 2000b.

Eiler, John M., P. Schiano, N. Kitchen and E. M. Stolper, Oxygen-isotope evidence for recycled crust in the sources of mid-ocean-ridge basalts, *Nature,* 403, 530-534, 2000c.

Eiler, J.M., Oxygen isotope variations of basaltic lavas and upper mantle rocks, in: *Stable Isotope Geochemistry*, Reviews in Mineralogy and Geochemistry, 43, eds. J.W. Valley and D.R. Cole, 319-364, 2001.

Elliot, T., T. Plank, A. Zindler, W. White and B. Bourdon, Element transport from slab to volcanic front at the Mariana Arc, *J. Geophys. Res.*, 102, 14,991-15,019, 1997.

Garcia, M.O., E. Ito, J.M. Eiler and A.J. Pietruszka, Crustal comtamination of Kilauea Volcano magmas revealed by oxygen isotope analyses of glass and olivine from Puu Oo eruption lavas, *J. Petrology*, 39, 803-817, 1998.

Geist, D., T. Naumann and P. Larson, Evolution of the Galapagos Magmas: Mantle and crustal fractionation without assimilation, *J. Petrology*, 39, 953-971, 1998.

Gurenko, A.A. and M. Chaussidon, Oxygen isotope variations in primitive tholeiites of iceland; evidence from a SIMS study of glass inclusions, olivine phenocrysts and pillow rim glasses, *Earth and Planetary Science Letters,* 205, 63-79, 2002.

Hansteen, T.H. and V.R. Troll, Oxygen isotope composition of xenoliths from the oceanic crust and volcanic edifice beneath Gran Canaria (Canary Islands); consequences for crustal contamination of ascending magmas, *Chemical Geology,* 193, 181-193, 2003.

Harris, C., H.S. Smith and A.P. le Roux, Oxygen isotope composition of phenocrysts from Tristan da Cunha and Gough Island lavas: variation with fractional crystallization and evidence for assimilation, *Contrib. Mineral, Petrol.*, 138, 164-175, 2000.

Hart, S. R., and H. Staudigel, Isotopic characterization and identification of recycled components, 15-28. In: *Crust/Mantle Recycling at Convergence Zones*, eds. S. R. Hart and L. Gulen, NATO ASI Series, Vol. 258, Series C, Kluwer Academic Publishers, Dordrecht, The Netherlands, 1989.

Hauri, E. H., N. Shimizu, J.J. Dieu, and S.R. Hart, Evidence for hotspot-related carbonatite metasomatism in the oceanic upper mantle, *Nature,* 365, 221-227, 1993.

Hofmann, A.W., Chemical differentiation of the Earth: the relationship between mantle, continental crust, and oceanic crust, *Earth and Planet. Sci. Letters*, 90, 297-314, 1988.

Hoogewerff, J.A., M.J. van-Bergen, P.Z. Vroon, J. Hertogen, R. Wordel,, A. Sneyers, A. Nasution, J.C. Varekamp, H.L.E. Moens and D. Mouchel, U-series, Sr-Nd-Pbisotope and trace element systematics across an active island arc-continent collision zone: Implications for element transfer at the slab-wedge interface, *Geochimica et Cosmochimica Acta,* 61, 1057-1072, 1997.

Johnson, M.C., and T. Plank, Dehydration and Melting Experiments Constrain the Fate of Subducted Sediments, *Geochemistry, Geophysics, Geosystems,* 1, 1999GC000014, 1999.

Kelemen, P.B., J. Rilling, E.M. Parmentier, L. Mehl and B.R. Hacker, Thermal structure due to solid-state flow in the mantle wedge beneath arcs, in: *Inside the Subduction Factory*, ed. J. Eiler, AGU Monogr. 138, 293-311, 2003a.

Kelemen, P.B., G.M. Yogodzinski and D.W. Scholl, Along-strike variation in lavas of the Aleutian island arc: Implications for the genesis of high Mg# andesite and the continental crust, In: *Inside the Subduction Factory*, Ed. J. Eiler, AGU Monograph 138, 2003b.

Kelley, K.A., T. Plank, J. Ludden and H. Staudigel, Composition of altered oceanic crust at ODP Sites 801 and 1149, *Geochem. Geophys. Geosyst.*, 4 (6), doi:10.1029/2002GC000435, 2003.

Kent, A.J.R., D.W. Peate, S. Newman, E.M. Stolper and J.A. Pearce, Chlorine in submarine glasses from the Lau Basin: seawater contamination and constraints on the composition of slab-derived fluids, *Earth and Planet. Sci. Letters*, 202, 361-377, 2002.

Kogiso, T., M.M. Hirschmann and D.J. Frost, High-pressure partial melting of garnet pyroxenite: possible mafic lithologies in the sources of ocean island basalts, *Earth and Planet. Sci. Letters*, 216, 603-617, 2003.

Kyser, T.K., J.R. O'Neil and I.S.E. Carmichael, Oxygen isotope thermometry of basic lavas and mantle nodules, *Contrib. Mineral, Petrol.*, 77, 11-23, 1981.

Machado, N., C. Brooks and S. R. Hart, Determination of initial $^{87}Sr/^{86}Sr$ and $^{143}Nd/^{144}Nd$ in primary minerals from mafic and ultramafic rocks: Experimental procedure and implications for the isotopic characteristics of the Archaean mantle under the Abitibi greenstone belt (Canada). *Geochim. Cosmochim. Acta*, 50, 2335-2348, 1986.

Mattey, D., D. Lowry and C. Macpherson, Oxygen isotope composition of mantle peridotite, *Earth and Planet. Sci. Letters*, 128, 231-241, 1994.

Matthews, A. and M. Schliestedt, Evolution of the blueschist and greenschist facies rock of Sifnos, Cyclades Greece: a stable isotope study of subduction-related metamorphism,

Contrib. Min. Petrol., 88, 150-163, 1984.

Macpherson, C.G., J.A. Gamble and D. Mattey, Oxygen isotope geochemistry of lavas from an oceanic to continental arc transition, Kermadec-Hikurangi margin, SW Pacific, *Earth and Planet. Sci. Letters*, 160, 609-621, 1998.

McDonough, W.F., and S.-s. Sun, The composition of the Earth, *Chemical Geology*, 120, 223-253, 1995.

Muehlenbachs, K. and G. Byerly, ^{18}O-enrichment of silicic magmas caused by crystal fractionation at the Galapagos Spreading Center, *Contrib. Mineral, Petrol.*, 79, 76-79, 1982.

Nadeau, S., P. Philppot and F. Pineau, Fluid inclusion and mineral isotopic compositions (H-C-O) in eclogitic rocks as tracers of local fluid migration during high-pressure metamorphism, *Earth and Planet. Sci. Letters*, 114, 431-448, 1993.

Neal, C.R., L.A. Taylor, J.P. Davidson, P. Holden, A.N. Halliday, P.H. Nixon, J.B. Paces, R.N. Clayton and T.K. Mayeda, Eclogites with oceanic crustal and mantle signature from the Bellsbank kimberlite, South Africa, part 2: Sr, Nd, and O isotope geochemistry, *Earth and Planet. Sci. Letters*, 99, 362-379, 1990.

Nichols, G.T., P.J. Wyllie and C.R. Stern, Subduction zone melting of pelagic sediments constrained by melting experiments, *Nature*, 371, 785-788, 1994.

Plank, T., Constraints from Thorium/Lanthanum on sediment recycling at sunduction zones and the evolution of the continents, *J. Petrology*, in press, 2005.

Plank, T. and C.H. Langmuir, The chemical compositions of subducting sediments and its consequences for the crust and mantle, *Chem. Geol., 145*, 325-394, 1998.

Poli, S. and M.W. Schmidt, Petrology of subducted slabs, *Annu. Rev. Earth and Planet. Sci.*, 30, 207-235, 2002.

Putlitz, B., A. Matthews and J.W. Valley, Oxygen and hydrogen isotope study of high-pressure metagabbros and metabasalts (Cyclades, Greece): implications for the subduction of oceanic crust, *Contrib. Mineral, Petrol.*, 138, 114-126, 2000.

Rudnick, R.L., M. Barth, I. Horn, W.F. McDonough, Rutile-bearing Refractory Eclogites: Missing Link Between Continents and Depleted Mantle, *Science*, 287, 278-281, 2000.

Rudnick, R.L. and D.M. Fountain, Nature and composition of the continental crust: a lower crustal perspective, *Rev. Geophysics* 33, 267-309, 1995.

Scambelluri, M., J. Fiebig, N. Malaspina, O. Müntener and T. Pettke, Serpentinite Subduction: Implications for fluid processes and trace-element recycling, *International Geology Rev.*, 46, 595-613, 2004.

Staudigel, H., Davies, G., Hart, S. R., Marchant, K. M. and Smith, B. M., Large Scale Isotopic Sr, Nd and O isotopic anatomy of altered oceanic crust at DSDP/ODP Sites 417/418, *Earth Planetary Science Letters*, 130, 169-185, 1995.

Staudigel, H., K. Muehlenbachs, S. H. Richardson and S. R. Hart, Agents of low temperature ocean crust alteration, *Contrib. Mineral Petrol.*, 77, 150-157, 1981.

Staudigel, H., T. Plank, B. White and H.-U. Schminke, Geochemical fluxes during seafloor alteration of the basaltic upper oceanic crust: DSDP Sites 417 and 418, in: *Subduction: Top to Bottom*, Geophys. Monogr. Ser., 96, ed. G.E. Bebout, pp. 19-38, 1996.

Valley, J.W, N. Kitchen, M.J. Kohn, C.R. Niendorf and M.J. Spicuzza, UWG-2, a garnet standard for oxygen isotope ratios: Strategies for high precision and accuracy with laser heating, *Geochim. et Cosmochim. Acta*, 59, 5223-5231, 1995.

van Keken, P.F., B. Kiefer and S.M. Peacock, High-resolution models of subduction zones: Implications for mineral dehydration reactions and the transport of water into the deep mantle, *Geochem. Geophys. Geosyst.*, 3, doi:10.1029/2001GC000256, 2002.

Vervoort, J.D., P.J. Patchett, G.E. Gehrels, A.P. Nutman, Constraints on early Earth differentiation from hafnium and neodymium isotopes, *Nature*, 379, 624-627, 1996.

Wiechert, U.H., A.N. Halliday, D.C. Lee, G.A. Snyder, L.A. Taylor and D. Rumble, Oxygen- and tungsten-isotopic constraints on the early development of the moon, *Meteoritics Planetary Sci.*, 35, A169, 2000.

Workman, R.K., S.R. Hart, M. Jackson, M. Regelous, K. Farley, J. Blusztajn, M. Kurz, and H. Staudigel, Recycled Metasomatized Lithosphere as the Origin of the Enriched Mantle II (EM2) End-member: Evidence from the Samoan Volcanic Chain, *Geochem. Geophys. Geosyst.*, 5, Q04008, doi:10.1029/2003GC000623, 2004.

Workman, R.K. and S.R. Hart, Major and Trace Element Composition of the Depleted MORB Mantle (DMM), *Earth and Planet. Sci. Letters*, 231, 53-72, 2005.

Figures

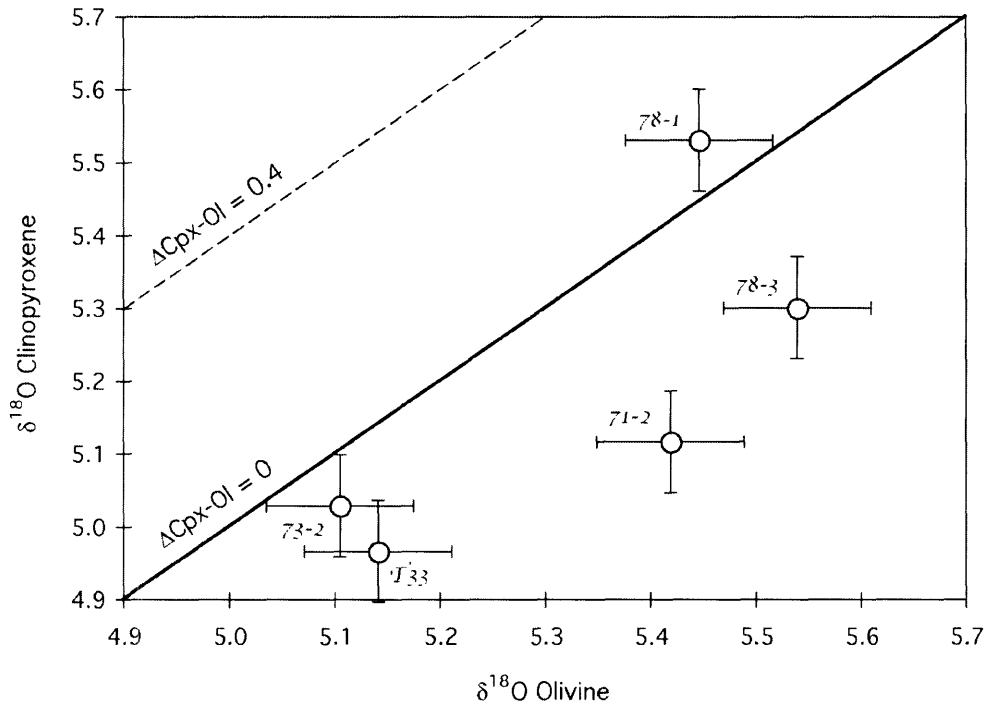

Figure 5-1. Oxygen isotope compositions of coexisting olivine and clinopyroxene from 5 Samoan lavas. ΔCpx-Ol = $\delta^{18}O_{Cpx}$ - $\delta^{18}O_{Olivine}$. Equilibrium ΔCpx-Ol fractionation is typically reported to be 0.4‰ (Chiba et al., 1989; Chazot et al., 1997; Macpherson et al., 1998; Harris et al., 2000), but the Samoan samples show near zero or negative values. The disequilibrium may be due to olivine and cpx recording magmatic $\delta^{18}O$ compositions at different stages in the magmas' evolution. Since olivine is the first phase on the liquidus of Samoan melts, we interpret olivine to be the more reliable recorder of primary magmas. Error bars are plotted as 1σ analytical error (0.07‰).

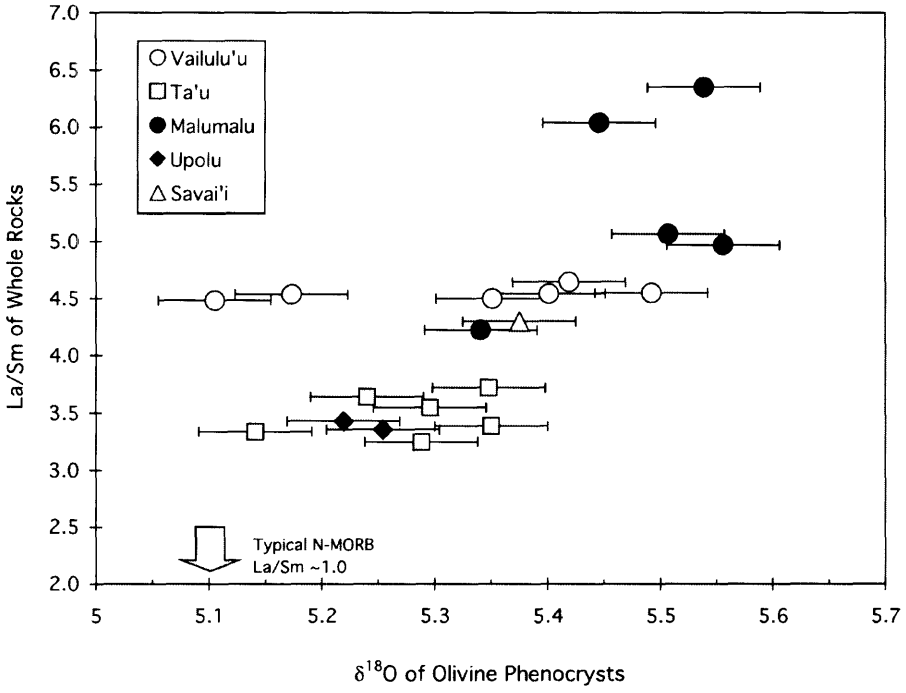

Figure 5-2. Correlation between La/Sm (ppm/ppm) and $\delta^{18}O$ in Samoan lavas. La/Sm ratios can vary as a function of degree of melting, but this is not suspected to control the correlation seen here since La/Sm also correlates well with $^{87}Sr/^{86}Sr$. There are similarly good correlations between $\delta^{18}O$ and other element ratios such as K/Na, K/Ti and Rb/Sr, indicating general enrichment of incompatible elements in sources with elevated $\delta^{18}O$. Error bars are plotted as 1σ standard error (0.05‰) for a sample run in duplicate.

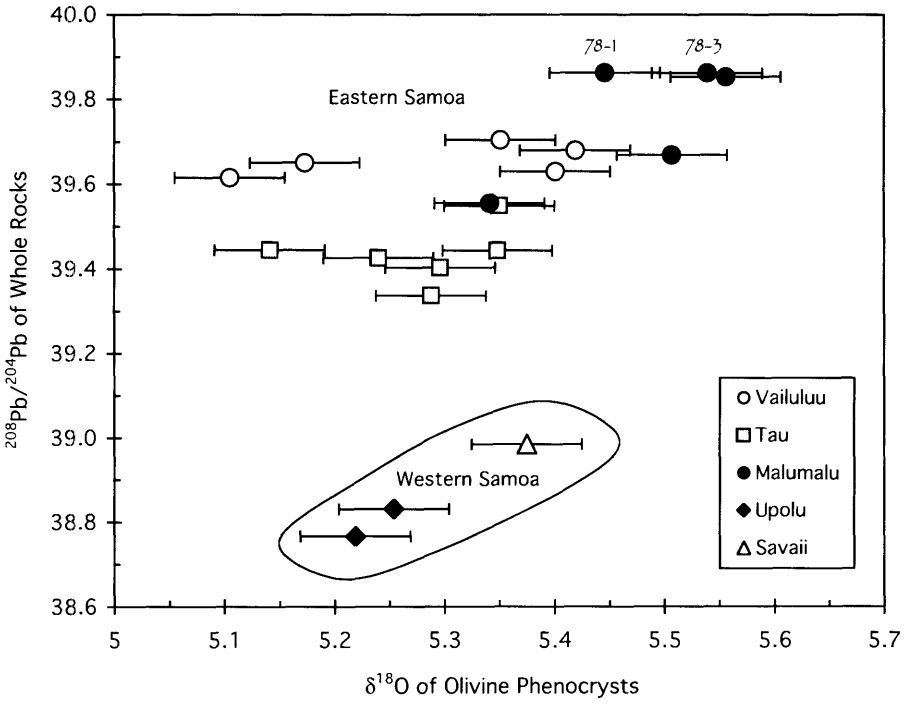

Figure 5-3. Relationship between oxygen and lead isotopes in Samoan lavas. Although the fields for Western Samoa (Savai'i and Upolu) and Eastern Samoa (Vailulu'u, Ta'u and Malumalu) overlap in $\delta^{18}O$ values, they are distinct and entirely separate in $^{208}Pb/^{204}Pb$. The source characteristics for Western Samoa lavas are discussed elsewhere (Workman et al., 2004), and the main topic of discussion in this paper is the origin for the extreme mantle enrichment displayed by Malumalu lavas (the two samples with the highest $^{87}Sr/^{86}Sr$ in Samoa, 78-1 and 78-3, are identified for reference). Note that there is no Pb isotopic data for the highest $\delta^{18}O$ sample from Vailulu'u. Error bars are plotted as 1σ standard error (0.05‰) for a sample run in duplicate.

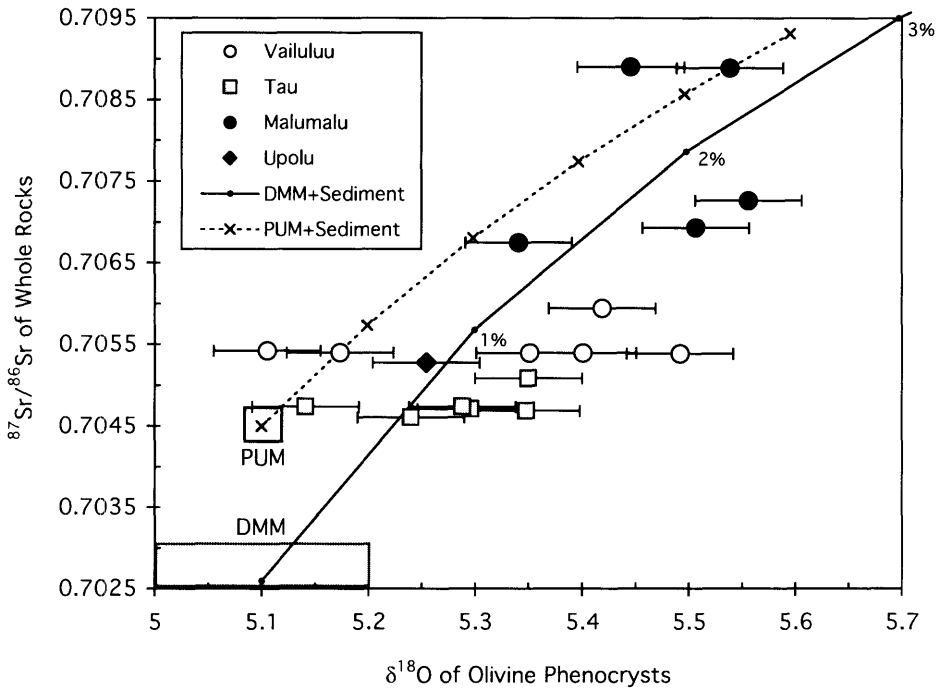

Figure 5-4. Relationship between oxygen and strontium isotopes for Samoan lavas. This positive correlation for enriched mantle lavas has previously been interpreted to represent recycling of sediments from subduction zones back to the mantle (Eiler et al., 1997). Two mixing calculations are shown for reference: Primitive Upper Mantle (PUM) contains 19.9 ppm Sr (McDonough and Sun, 1995), and is mixed with a hypothetical sediment having 170 ppm Sr, $^{87}Sr/^{86}Sr$ of 0.720 and $\delta^{18}O$ of 15‰; Depleted MORB Mantle (DMM) contains 8 ppm Sr (Workman and Hart, 2005) and is mixed with the same sediment except with heavier $\delta^{18}O$ (25‰). Tick marks are in increments of 1% sediment addition. Error bars are plotted as 1σ standard error (0.05‰) for a sample run in duplicate.

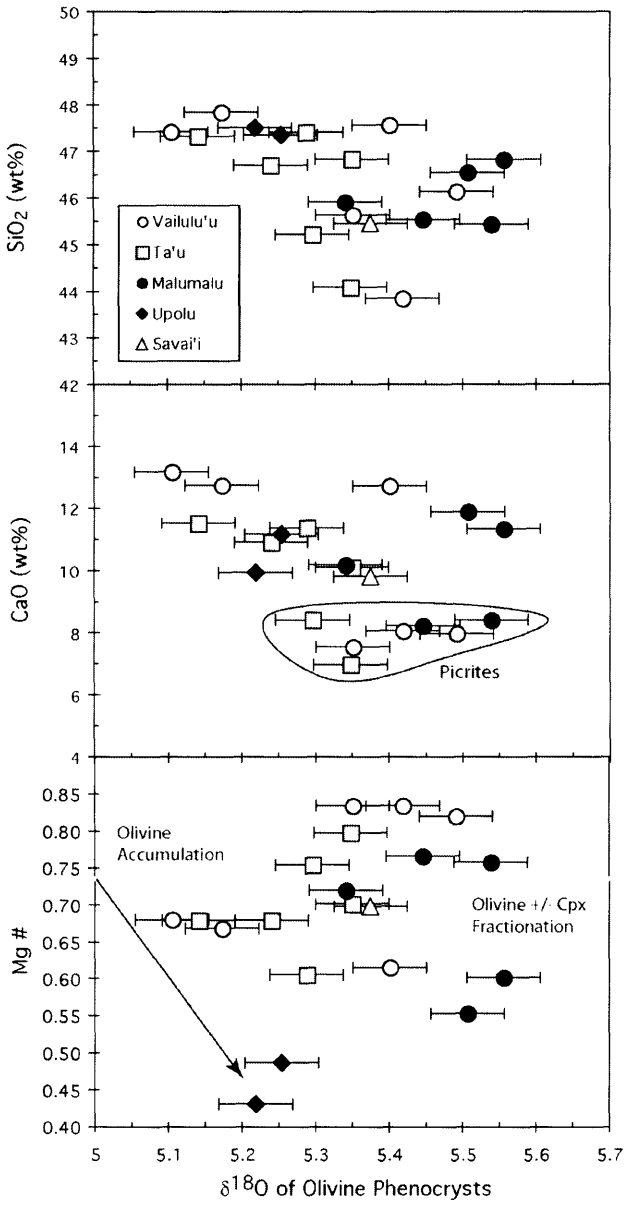

Figure 5-5. Relationships between $\delta^{18}O$ compositions of olivine and whole-rock major element compositions of their host lavas. The line, drawn across the bottom plot at Mg# 73, marks the position of a melt in equilibrium with Fo_{90} mantle olivine. Lavas above this line are picrites that have accumulated olivine and below this line have fractionated olivine ± clinopyroxene. The arrow shows the effect on $\delta^{18}O$ from fractional crystallization of 40% olivine. Because there is no correlation between $\delta^{18}O$ and Mg#, $\delta^{18}O$ values are not the result of crystal fractionation.

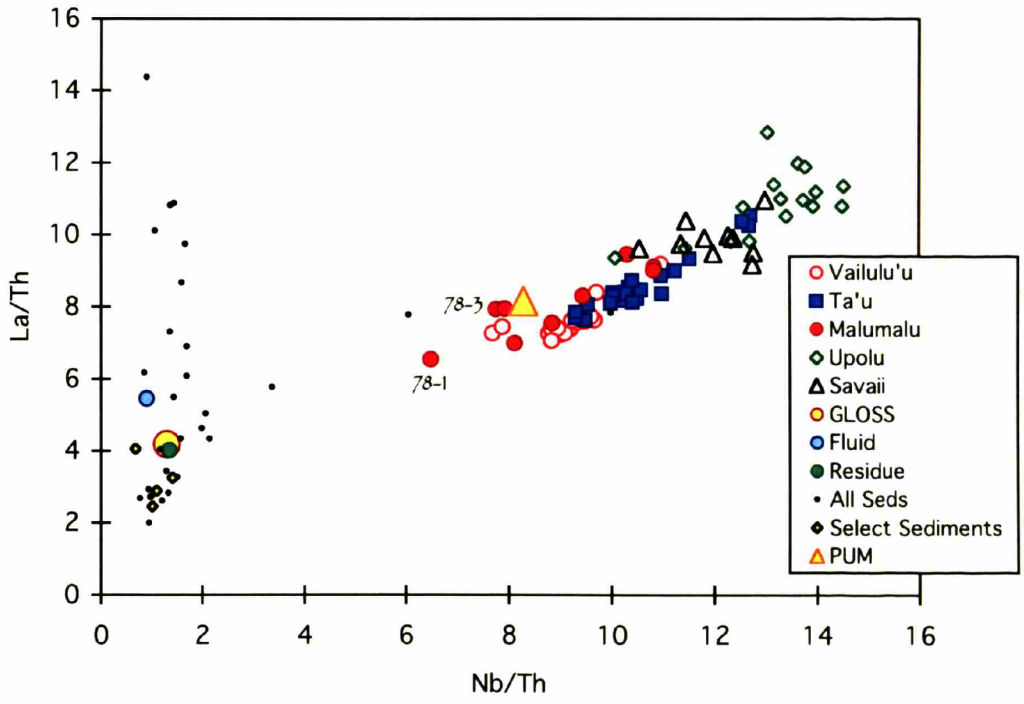

Figure 5-6. Plot of Nb/Th with La/Th ratios of whole rock Samoan basalts (Workman et al., 2004) compared to marine sediments from Plank and Langmuir (1998) used to identify sediment that would be a plausible component of EM2. These ratios were selected because they involve fluid-immobile elements (see Johnson and Plank, 1999; Plank, 2005), so will not be greatly altered by subduction-zone dehydration processes. Since Th is the denominator of each ratio, mixing lines will be linear on this diagram. For reference, DMM has Nb/Th = 18.8 and La/Th = 24.3 (Workman and Hart, 2005). PUM is Primitive Upper Mantle from McDonough and Sun (1995). GLOSS is an average of modern sediments being subducted in trenches today (Plank and Langmuir, 1998). 'All Seds' are individual sediments used to construct GLOSS. 'Select Sediments' are sediments chosen by us to be a plausible mixing component in EM2 based on their position on this plot as well as on a plot of La/Th-Ba/Th. 'Fluid' is a model for slab fluid from Eiler et al. (2000a), and 'Residue' is the residual composition after 7% of the 'Fluid' is removed from GLOSS, indicating insignificant compositional changes to sediment by dehydration (at least for the elements here).

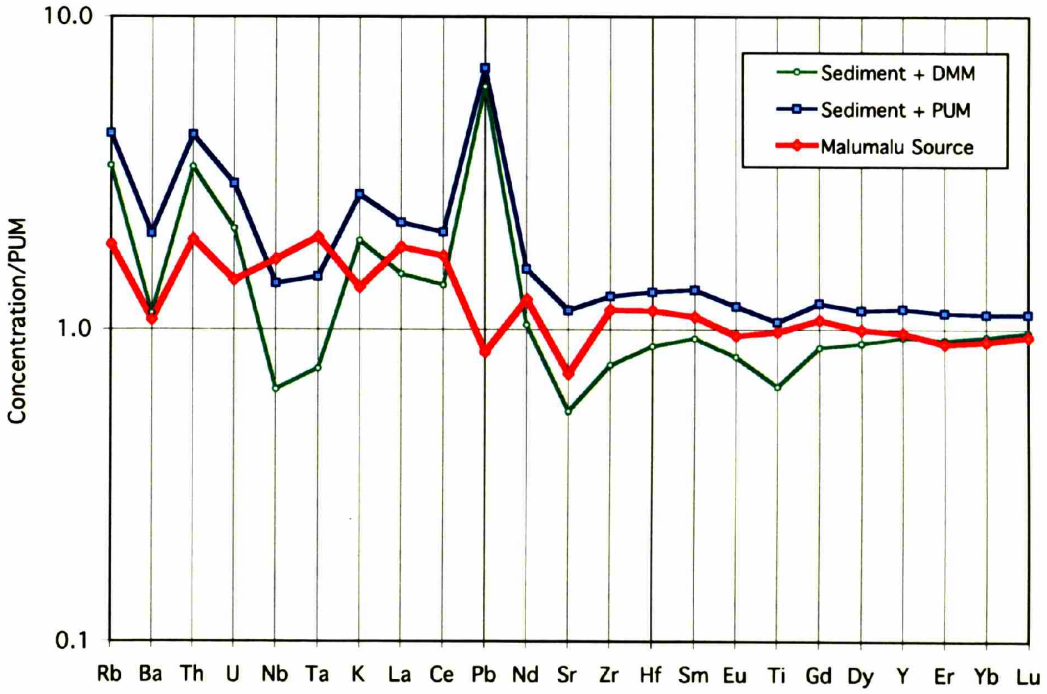

Figure 5-7. Test for mantle enrichment by marine sediments as the origin for EM2. Trace element concentrations are normalized to Primitive Upper Mantle (PUM; McDonough and Sun, 1995). Depleted MORB Mantle is from Workman and Hart (2005). See Figure 6 and Table 2 for sediment selection and derivation of Malumalu source. The Malumalu source is compared with mixtures of sediment with 1) PUM and 2) DMM. The mass fraction of sediment in each mixture is 2%, requiring the sediment to have $\delta^{18}O$ = 25‰ to match the $\delta^{18}O$ composition of EM2.

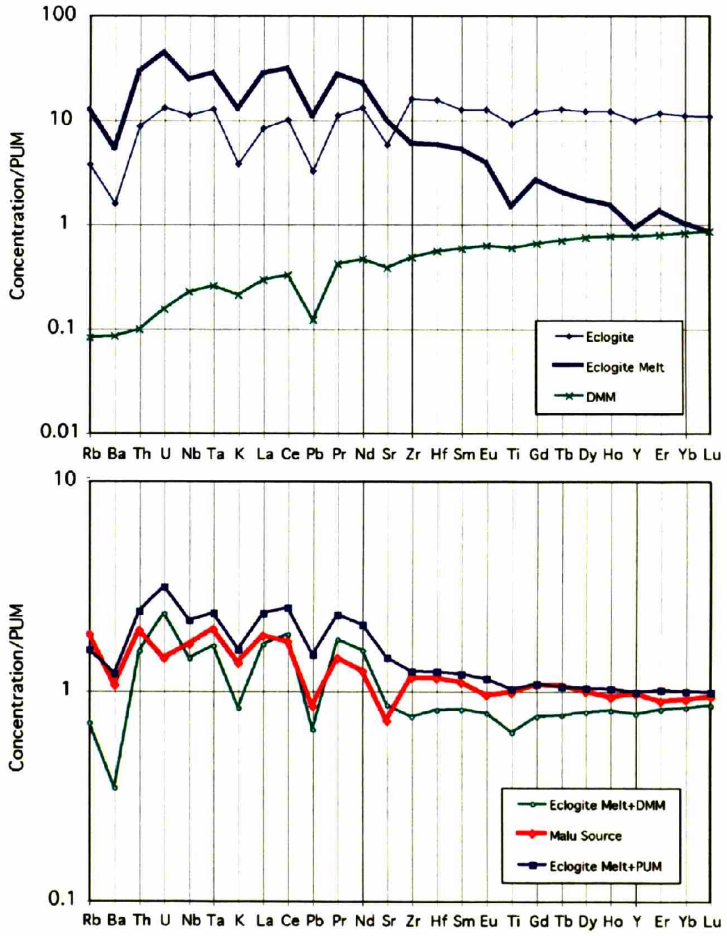

Figure 5-8. Test for metasomatism of depleted/primitive mantle by eclogitic melt as the origin for EM2. Trace element concentrations are normalized to Primitive Upper Mantle (PUM; McDonough and Sun, 1995). Top panel shows 1) the Depleted MORB Mantle (DMM; Workman and Hart, 2005); 2) an average of eclogites with MORB protoliths (Becker et al., 2000; weighted heavily to their sample W1); and 3) a 30% modal, aggregated fractional melt of the eclogite. Bottom panel shows 1) the source for Malumalu lavas assuming that the lavas represent 2.5% aggregated fractional melting; and 2) mixtures of DMM and PUM each with 5% of the eclogitic melt shown in the top panel. The eclogite melt is required to have $\delta^{18}O$ of 15‰ to match the $\delta^{18}O$ composition of EM2. Trace element compositions, partition coefficients and additional details can be found in Table 2. Because the mantle-melt mixtures show the same general pattern as the calculated Malumalu source (with the only exception being U), and the Malumalu source generally falls in-between the two mantle-melt mixtures (except for the Pr-Nd-Sr segment), we conclude that this scenario is a viable one for the formation of EM2.

Tables

Table 5-1. Oxygen isotope compositions of phenocrysts from Samoan lavas

		$\delta^{18}O$ of Individual Analyses									Cpx Phenocrysts
Sample	Volcano									Average	$\delta^{18}O$
63-2	Vailulu'u	0 min.*	5.492							5.49	
68-3	Vailulu'u	0 min.	5.173							5.17	
63-11	Vailulu'u	0 min.	5.389	0 min.	5.316	1 min.	5.348			5.35	
71-11	Vailulu'u	0 min.	5.381	0 min.	5.587	1 min.	5.569			5.40	
71-2	Vailulu'u	0 min.	5.291	0 min.	5.5	1 min.	5.352	10 min	5.531	5.42	5.03
73-2	Vailulu'u	0 min.	5.139	0 min.	5.07					5.10	5.03
74-1	Ta'u	0 min.	5.348							5.35	
T16	Ta'u	0 min.	5.243	1 min.	5.236					5.24	
T25	Ta'u	0 min.	5.22	0 min.	5.332	1 min.	5.336			5.30	
T33	Ta'u	0 min.	5.115	0 min.	5.166					5.14	4.97
T44	Ta'u	1 min.	5.35							5.35	
T54	Ta'u	0 min.	5.319	0 min.	5.326	1 min.	5.219			5.29	
76-9	Malumalu	0 min.	5.341							5.34	
77-1	Malumalu	0 min.	5.422	0 min.	5.583	1 min.	5.515			5.51	
77-9	Malumalu	0 min.	5.488	1 min.	5.641	10 min	5.54			5.56	
78-1	Malumalu	0 min.	5.529	0 min.	5.363					5.45	5.53
78-3	Malumalu	0 min.	5.443	0 min.	5.621	1 min.	5.552			5.54	5.30
U14	Upolu	0 min.	5.219							5.22	
U16	Upolu										5.42
U19	Upolu	0 min.	5.254							5.25	
S23	Savaii	0 min.	5.373	0 min.	5.376					5.37	

* *0 min., 1 min.* or *10 min.* indicate the number of minutes of heat-treatment before analysis of each sample split.

Table 5-2. Compositions and mineral/melt partition coefficients (D's) used in the calculations illustrated by Figures 7 and 8

(ppm)	Malumalu Lava	Lherzolite D's	Malumalu Source	Selected Sediment	Eclogite	Eclogite D's	30% Melt of Eclogite
Rb	44.7	0.00002	1.118	97.8	2.27	0.02	7.57
Ba	282.0	0.00012	7.05	344.0	10.54	0.015	35.15
Th	6.17	0.00087	0.154	12.8	0.699	0.015	2.330
U	1.164	0.00101	0.0291	1.978	0.269	0.022	0.895
Nb	44.0	0.0035	1.100	13.88	7.39	0.335	16.14
Ta	2.92	0.0035	0.0730	0.916	0.477	0.335	1.041
K2O (wt%)	1.574	0.0012	0.0393	2.48	0.110	0.02	0.368
La	44.3	0.009	1.186	39.4	5.44	0.059	18.08
Ce	82.2	0.020	2.875	89.3	16.96	0.139	52.2
Pb	4.35	0.013	0.127	44.1	0.488	0.052	1.62
Pr	9.16	0.026	0.364	-	2.84	0.267	6.97
Nd	34.9	0.031	1.558	36.22	16.48	0.495	28.21
Sr	379.1	0.023	14.32	167.8	115.4	0.5	196.1
Zr	205.4	0.046	12.11	154.8	168.3	3.02	62.4
Hf	5.20	0.050	0.325	4.82	4.40	3.02	1.630
Sm	7.15	0.049	0.446	7.25	5.10	2.67	2.122
Eu	1.991	0.061	0.147	1.581	1.938	3.69	0.596
TiO2 (wt%)	2.196	0.078	0.197	0.738	1.844	7.24	0.296
Gd	6.28	0.081	0.582	6.23	6.59	5.25	1.443
Tb	0.870	0.109	0.105	-	1.256	7.25	0.201
Dy	4.59	0.135	0.670	5.68	8.22	8.27	1.157
Ho	0.804	0.162	0.139	-	1.812	9.26	0.228
Y	21.89	0.180	4.166	38.46	42.85	12.8	3.93
Er	1.908	0.195	0.392	3.15	5.15	10.2	0.587
Yb	1.399	0.278	0.401	2.94	4.88	12.7	0.450
Lu	0.208	0.297	0.0635	0.449	0.736	15.2	0.057

Table 5-2. The Malumalu lava is the average trace element content of samples 78-1 and 78-3, both corrected to Mg# 73 by olivine subtraction. Partition coefficients (D's) are adapted from Kelemen et al. (2003b) for garnet lherzolite and eclogite lithologies, except the heaviest REE are smoothed in garnet lherzolite and D_{Sr} in eclogite melting is set to 0.5. Spinel lherzolite D's are taken from Workman and Hart (2005). The 'Lherzolite D's' represent a mixture of 15% garnet lherzolite and 85% spinel lherzolite D's. The Malumalu Source is calculated assuming the lava represents a 2.5% aggregated fractional melt; the inverted source has approximately the correct Rb/Sr, Sm/Nd and Lu/Hf to have developed its observed isotopic composition in 2.5 Ga of aging from PUM (see Workman et al., 2004). The 'Selected Sediment' is the average of 7 sediments from Plank and Langmuir (1998) chosen for their La/Th, Ba/Th and Nb/Th compositions (see fig. 6), and used to test a sediment source of enrichment for EM2. Note that 3 of the 7 sediments do not have Nb analyses, so are not plotted in Figure 6. The eclogite composition is based on eclogites with MORB protoliths reported by Becker et al. (2000); the REE elements not analyzed by Becker at al. (2000) have been filled-in here by assuming that the REE's will have a slope similar to N-MORB (Hoffman, 1988), and Ta has been calculated assuming Nb/Ta = 15.5. The 30% ecolgite melt assumes aggregated fractional melting of this eclogite.

Chapter 6:

Gravity-based calculation of crustal flux from the Samoan hotspot and its correlation with Pb-isotopes: a brief overview

Abstract

A Mantle Bouguer Anomaly (MBA) map has been calculated for Samoa from free air gravity and shipboard bathymetry, and then interpreted solely in terms of crustal thickness variations. We find that the western Samoan volcanoes have the greatest amount of excess igneous crust, and that integrated crustal flux decreases nearly monotonically approaching to Vailulu'u Seamount, the easternmost and youngest volcano. This trend shows excellent correspondence to increasing $^{206}Pb/^{204}Pb$ compositions of the lavas with decreasing age along the hotspot track. We speculate this correlation could be due to either a lithosphere thickening toward the east or decreasing potential temperature of the mantle plume.

1. Introduction

This chapter has been inspired by an age-old question about lavas that are sampled from ocean islands and mid-ocean ridges: are their compositions a product of their source, or a product of the way they are sampled and processed from a multi-component mantle? In other words, is there true spatial heterogeneity in the mantle or are the compositions of surface samples a function of how they are sampled from a 'homogeneously heterogeneous' mantle? The likely story is that both play an important role in magma compositions, but it is unclear how significant each factor could be. The issue of 'source vs. process' is difficult to address with geochemistry alone, as many of the needed physical constraints, such as lithospheric thickness, magma flux, thermal anomalies, and deep mantle structure are largely provided by geophysical observations.

With an extensive geochemical investigation of the Samoan Islands and Seamounts, we have documented systematic changes in lava composition with distance along the hotspot track; this is shown most strongly in the monotonically increasing $^{206}Pb/^{204}Pb$ compositions with distance from Savai'i toward Vailulu'u Seamount, the present-day hotspot center (see Chapter 2). The goal of this study is to determine whether or not geophysical parameters, specifically crustal flux, will also vary systematically along the volcanic chain.

Using a protocol similar to that of Van Ark and Lin (2004), we have calculated a mantle bouger anomaly map for the Samoan region and interpreted it as variations in total crustal thickness. Integrating excess crustal thickness (total crust minus 6 km of background ocean crust) in cross-sections along the Samoan lineament, we show that crustal flux is systematically decreasing with approach to Vailulu'u. Therefore, increasing $^{206}Pb/^{204}Pb$ compositions occur as crustal flux wanes. We have not yet developed a detailed model to explain how the geochemical and geophysical properties are linked, but speculate that it may be due to decreasing potential temperature of the Samoan mantle plume or increasing lithospheric thickness over the last 5 million years.

2. Calculations

The calculations described below have been applied to a map region from 168°E to 195°E and 4°S to 16°S within the southern Pacific Ocean (Figure 1). Although we only interpret the results from a small sub-area of this large region, it is as easy to calculate a

large region as it is a small region and we envision the regional scale maps to be used more fully in the future. For example, Hart et al. (2004) have shown that seamounts with a Samoan signature extend back as far as ~175°E, making the oldest known Samoan volcanism ~23 million years old. It would be interesting to compare excess crust and geochemistry in this older section of the Samoan, as we do here for the youngest expression of the Samoan plume.

We employ two kinds of data for this study: free air gravity (FAA) and measured bathymetry. The free air gravity map of Sandwell and Smith (1997) is publicly available at http://topex.ucsd.edu/WWW_html/mar_grav.html and was obtained from satellite altimetry measurements taken during the Geosat and ERS1 missions. It has 1-minute by 1-minute resolution and determines the maximum resolution of our calculations since some of the bathymetry data is of higher resolution. The FAA map of our study region is shown in Figure 2. Bathymetry data is taken from two sources: 1) real bathymetry points from the Smith and Sandwell (1997) predicted bathymetry map (also available publicly at: http://topex.ucsd.edu/WWW_html/mar_topo.html) and 2) SeaBeam bathymetry in the region of the Samoan Islands and Seamounts obtained during the 1999 AVON 2 and 3 cruises of the R/V Melville (Hart et al., 2000). The coverage of real bathymetry is shown in Figure 3, with masking of grid nodes that have no data within a 1-minute radius. We have not considered the effect of sediment coverage in our calculations because sediment thicknesses are less than 1000 meters for the entire study region and less than 200 meters for the sub-region involved in our interpretations (fig. 4) (Divins, 2001).

The mantle Bouguer anomaly (MBA) map shown in Figure 5 is calculated, using the Parker (1972) algorithm, by subtracting the attraction of seafloor topography (fig. 3) and a reference model of 6 km thick ocean crust from the free air anomaly (fig. 2). We assume density values of 1.03, 2.7 and 3.3 g/cm^3 for seawater, the oceanic crust and the upper mantle, respectively (e.g., Kuo and Forsyth, 1988; Lin et al., 1990). The MBA map and all others to follow have been trimmed by 0.5° on each side in order to edit out the 'edge-effect' of our calculations. Negative values on the MBA map represent regions of excess low-density material (i.e., oceanic crust greater than 6 km); the opposite is true for positive anomalies.

A map of depth to the Moho (base of the oceanic crust), shown in Figure 6, is calculated through a downward continuation of the MBA anomalies to a depth of 11 km (estimated combined depth of 5 km ocean depth plus 6 km reference oceanic crust thickness), as described in greater detail by Van Ark and Lin (2004). This assumes that the entire MBA

signal is due to excesses or deficits in crustal thickness; if there are any mantle thermal effects contributing to the MBA signal, we will have over-estimated depth to the Moho at those locations. The Moho is offset by a constant +3 km in order to force the 'background' Moho depth to be near 11 km, which is the depth of the Moho if the oceanic crust is 6 km thick at locations away from islands or seamounts – for example at 190°E and 12.5°S. Total crustal thickness, shown in Figure 7, is calculated by subtracting the seafloor topography from the calculated Moho depth. Excess crustal thickness is the remaining crust after removing a 6 km thick layer we assume to be 'original' oceanic crust produced at a spreading ridge (fig. 8).

3. Results

Figure 9 show a close-up of excess crustal thickness for the part of the Samoan volcanic chain that is the subject of Chapters 2, 4 and 5; the boundaries of this map are defined by the red box in Figure 1, and coordinates are expressed in kilometers. Although the islands are not plotted here (so as not to obscure the thickness variations), the outlines of islands are clear from the contours of excess crustal thickness (i.e., compare to Figure 1). The calculated maximum excess crust for this area is ~25 km; it occurs beneath Savai'i and is displayed in the cross-section of Savai'i in Figure 9. Moving southeast from Savaii, it is clear from Figure 9 alone that crustal thicknesses are waning. The last volcano of the Samoan chain, Vailulu'u, is shown in cross-section in Figure 9 and has a mixiumum crustal thickness of ~7 km.

To estimate the crustal flux (i.e., erupted volume flux) from the Samoan plume through time, we have integrated excess crustal thicknesses for 200 km-long cross-sections at every 1 km along the Samoan lineament. Crustal flux along the chain is shown in Figure 10 and is reported as km^3 of crust for a 200 km by 1 km map area. Using a Pacific plate speed of 7 cm/yr (Sella et al., 2002), the unit of crustal flux reported in Figure 10 translates to the number of km^3 of crust erupted from the Samoan plume in a period of 14,300 years. From Savai'i to Vailulu'u, the calculated crustal flux decreases (almost monotonically except for over the Tutuila-Malumalu ridge) by ~75%. The bottom panel of Figure 10 shows the strong inverse correlation of $^{206}Pb/^{204}Pb$ to crustal flux. Low $^{206}Pb/^{204}Pb$ indicates a contribution from trace-element-depleted mantle components to the lavas (i.e., FOZO and DMM) and high $^{206}Pb/^{204}Pb$ indicates a contribution of trace-element-enriched mantle components to the lavas (i.e., EM2 and HIMU) (see Chapter 2, Figure 16 for correlations

between trace element enrichment and Pb isotopes). Hence, periods of high crustal flux are accompanied by sampling of more depleted mantle components and periods of low crustal flux are accompanied by samples of more enriched mantle components. However, it may be slightly misleading to interpret the crustal thickness variations as if they directly represent temporal changes in magma production from the Samoan plume since recent eruptions have been documented for both Savaii and Vailulu'u (see Chapter 2). Not all the crustal volume from Savaii was produced 5 million years ago (its apparent age from plate motion), but it is unclear what proportion of the crust represents shield versus rejuvenated volcanism.

4. Discussion

The strong relationship between the geochemistry of Samoan lavas and our gravity-based estimate of crustal flux along the chain suggests there is a process-oriented mechanism for producing variations in lava compositions, meaning that lava compositions are a function of what materials are sampled from a multi-component mantle. Below we address two parameters that, if varied systematically, could potentially result in a systematic change in the composition of melts produced from the upwelling plume: lithospheric thickness and potential temperature of the plume.

A very interesting model for melting of a heterogeneous mantle has recently been developed by Ito and Mahoney (2005). They show that the same mantle (composed of multiple components) can produce magmas of varying composition (in trace elements and heavy isotopes) depending on lithospheric thickness at the location of magma genesis. This is due to fundamental differences in the solidus temperatures of the different components and the depth at which melting is 'shut-off' by the lithospheric cap. They assume that, at a given pressure, depleted mantle will melt at a higher temperature than enriched mantle, so melting that is terminated deeply will result in magmas with strong enriched mantle signatures; on the other hand, if the melting column extends to more shallow depths, the enriched melt will be diluted by depleted mantle melts.

Applying this concept to Samoa would suggest that the lithosphere beneath western Samoa is thinner than beneath eastern Samoa, resulting in the production of more melt from the depleted mantle component and, in summation, a greater total melt volume. We will need to explore the implication that western Samoan lavas reflect a greater degree of melting than eastern Samoa lavas; at the present state of investigation, it is not clear if this is the case (as a

side-note, water concentrations in western Samoan lavas may be the key to this question, but such data has not yet been collected).

Changes in the potential temperature of the plume may also explain our observations by controlling the length of the melting column from the bottom instead of the top. At a constant lithospheric thickness, a cooling mantle plume will not be able to produce as much melt from its depleted mantle components, resulting in the geochemical and geophysical evolution from Savai'i to Vailulu'u. However, because of small melt productivity during deep melting (e.g., Asimow et al., 2004), it is possible this scenario will not be able to account for the large differences in crustal volume between western and eastern Samoa.

A changing composition of the Samoan plume (i.e., proportion of depleted to enriched material) would not easily account for coupled variation of calculated igneous flux and $^{206}Pb/^{204}Pb$. If the plume changes composition as it upwells beneath the Pacific Plate, but potential temperature and lithospheric thickness remain constant, we would expect the depleted material to produce less total melt volume because of a higher solidus temperature than the enriched material. Our observation is the opposite of this: depleted signatures occur with the greatest crustal volumes.

The last option is the one of coincidence. Consider that the average crustal volume (~1200 km^3; Figure 10) over Upolu and Tutuila is the 'constant' crustal volume of a full-grown Samoan shield volcano. Volcanoes to the east have not yet been fully developed, whereas Savai'i has entered a stage of extensive, post-shield, rejuvenated volcanism (as historically documented). From this perspective, geochemical variations would be independent of the igneous flux, unless the average Pb isotopic composition of a volcano changes with growth.

References

Asimow, P.D., J.E. Dixon and C.H. Langmuir, A hydrous melting and fractionation model for mid-ocean ridge basalts: Application to the Mid-Atlantic Ridge near the Azores, *Geochemistry, Geophysics, Geosystems,* 5(1), 2003GC000568, 2004.

Divins, D., Total sediment thickness of the world's oceans and marginal seas, World Data Center Mar. Geol. And Geophys., Boulder, CO, 2001. Available publicly at: http://www.ngdc.noaa.gov/mgg/sedthick/sedthick.html

Hart, S. R., Staudigel, H., Koppers, A.A.P., Blusztajn, J., Baker, E.T., Workman, R., Jackson, M., Hauri, E., Kurz, M., Sims, K., Fornari, D., Saal, A., and Lyons, S., Vailulu'u undersea volcano: The New Samoa, *Geochemistry, Geophysics, Geosystems,* 1, 2000GC000108, 2000.

Hart, S.R., M. Coetzee, R.K. Workman, J. Blusztajn, K.T.M. Johnson, J.M. Sinton, J.W. Hawkins, Genesis of the Western Samoa Seamount Province: Age, Geochemical Fingerprint and Tectonics, *Earth and Planet. Sci. Letters*, 227, 37-56, 2004a.

Ito, G. and J.J. Mahoney, Flow and melting of a heterogeneous mantle: 1. Method and importance to the geochemistry of ocean island and mid-ocean ridge basalts, *Earth Planet. Sci. Letters,* 230, 29-46, 2005.

Kuo, B.Y. and D.W. Forsyth, Gravity anomalies of the ridge-transform system in the South Atlantic between 31 and 34.5°S: Upwelling centers and variations in crustal thickness, *Mar. Geophys. Res.,* 10, 205-232, 1988.

Lin, J., G.M. Purdy, H. Schouten, J.-C. Sempere and C. Zervas, Evidence from gravity data for focused magmatic accretion along the Mid-Atlantic Ridge, *Nature*, 344, 627-632, 1990.

Parker, R.L., The rapid calculation of potential anomalies, *Geophys. J. Roy. Astro. Soc.*, 31, 447-455, 1972.

Sandwell, D.T. and W.H.F. Smith, Marine gravity anomaly from Geosat and ERS1 satellite altimetry, *J. Geophysical Research*, 102 (B5), 10039-10054, 1997.

Sella, G. F., Dixon, T.H., and Mao, A., REVEL: A model for recent plate velocities from space geodesy, *J. Geophys. Res., 107*, EGT 11-1 to 11-32, 2002.

Smith, W.H.F. and D.T. Sandwell, Global seafloor topography from satellite altimetry and ship depth soundings, *Science*, 277, 1957-1962, 1997.

Van Ark, E. and J. Lin, Time variation in igneous volume flux of the Hawaii-Emperor hot spot seamount chain, *J. Geophys. Res.*, 109 (B11), doi:10.1029/2003JB002949, 2004.

Figures

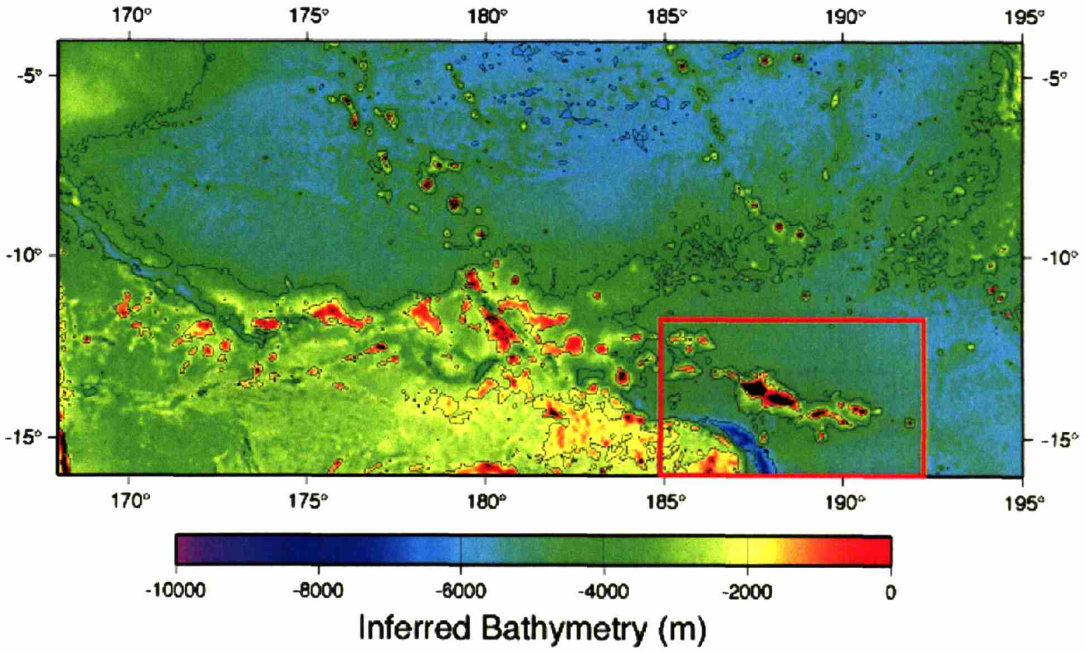

Figure 6-1. Smith and Sandwell (1997) predicted bathymetry for the study region based on a combination of shipboard bathymetric measurements and bathymetry calculated from free air gravity measured by satellite altimetry. The Samoan Islands are shown in black in the southeastern corner of the map. The red box around them marks the boundaries of the map shown in Figure 9.

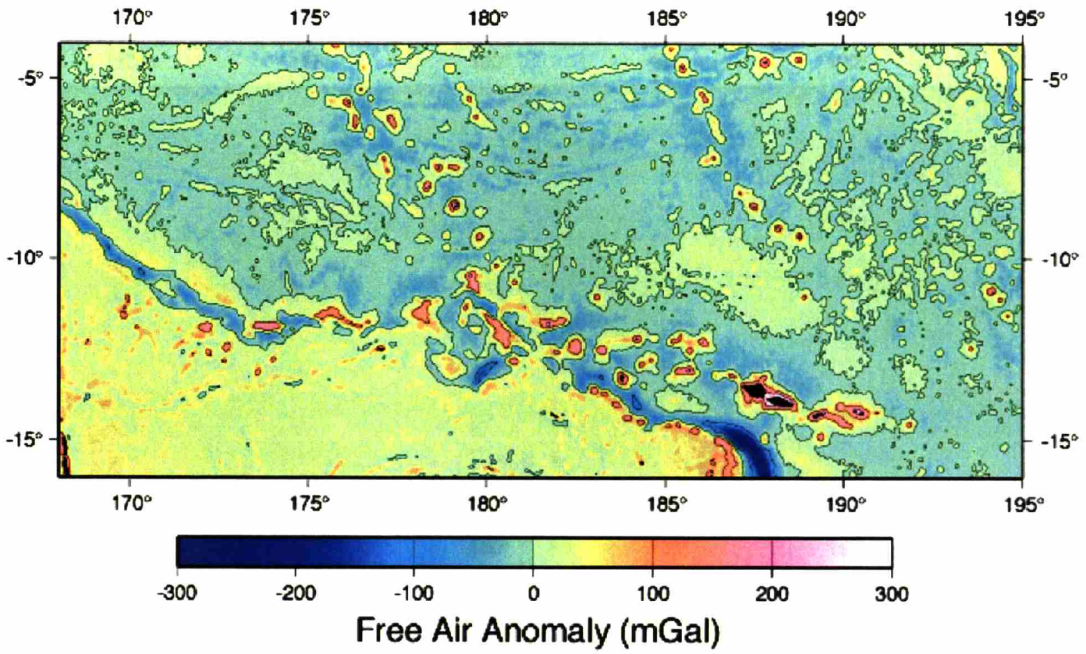

Figure 6-2. Free air anomaly map for the study region from Sandwell and Smith (1997).

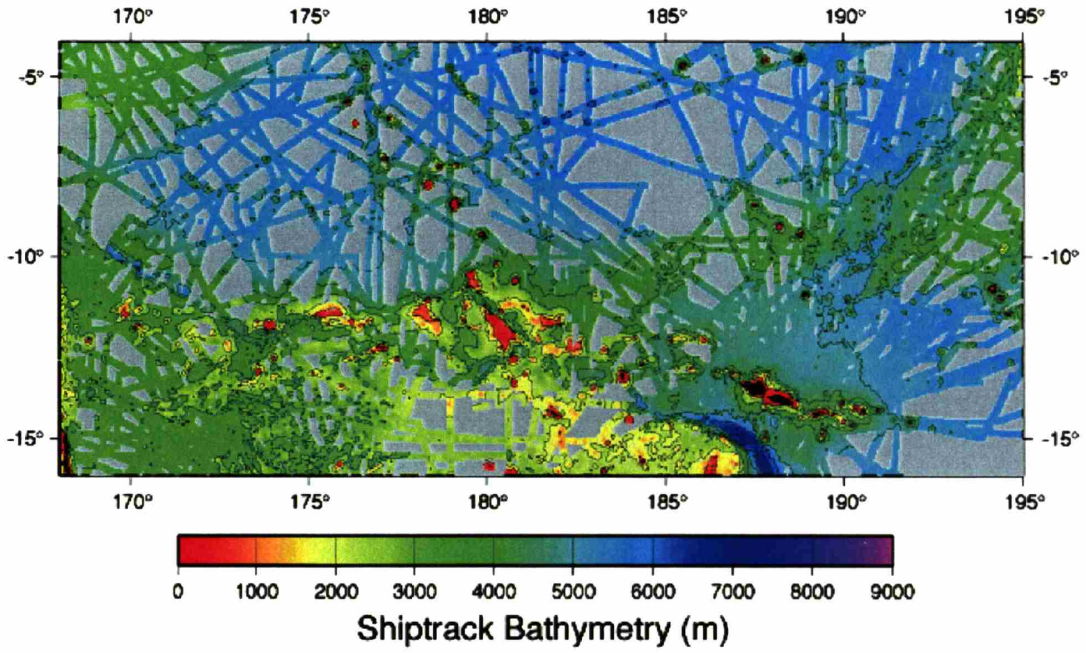

Figure 6-3. Real bathymetry measured by shiptrack. Data sources are Smith and Sandwell (1997) and SeaBeam data from the 1999 AVON 2 and 3 cruises of the R/V/ Melville.

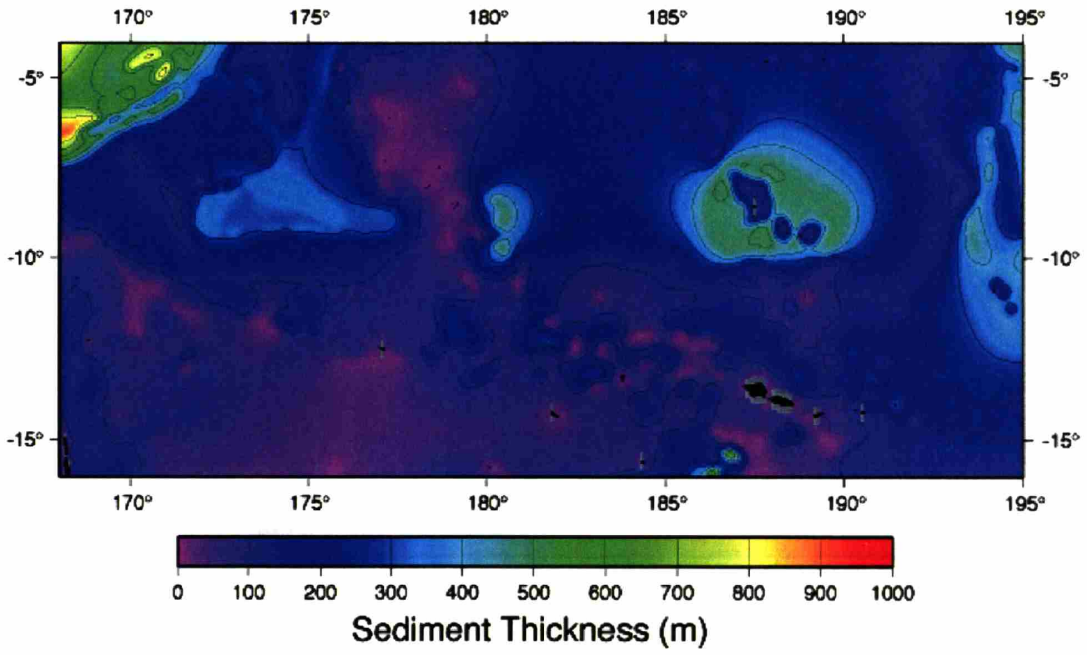

Figure 6-4. Regional sediment thickness map from Divins (2001). Since the sediment cover is generally very thin, we have not considered it in the calculation of MBA.

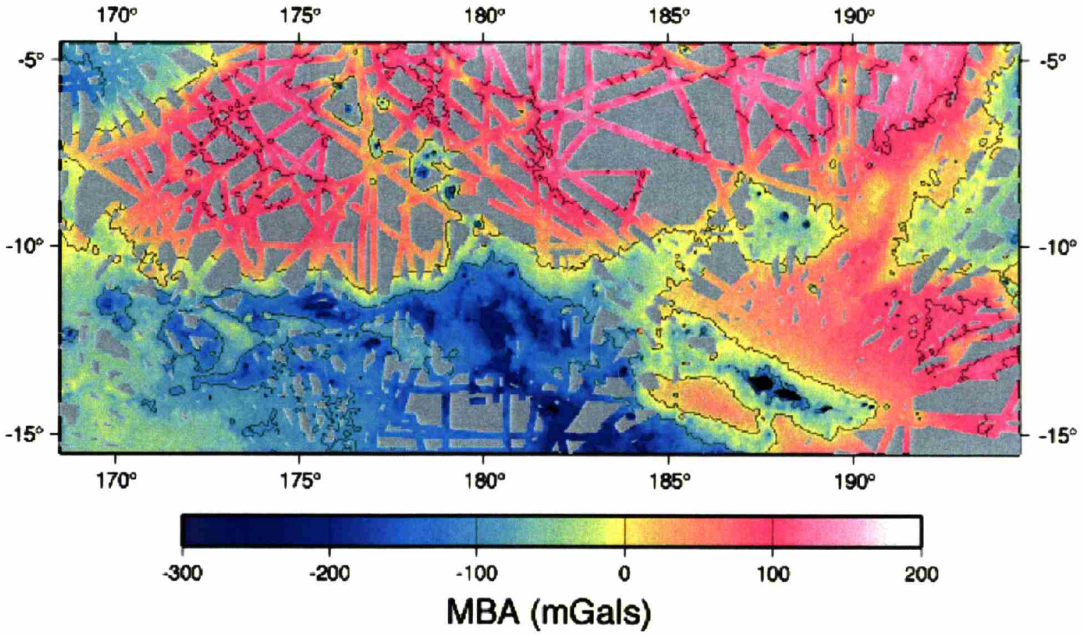

Figure 6-5. Mantle Bouguer anomaly map of the study region calculated according to the Parker (1972) algorithm as implemented by Kuo and Forsyth (1988) and Lin et al. (1990). Negative anomalies indicate excess low-density material, such as over the Samoan Islands and a large portion of the southwest quadrant of the map (some of which may be related to the Samoan plume).

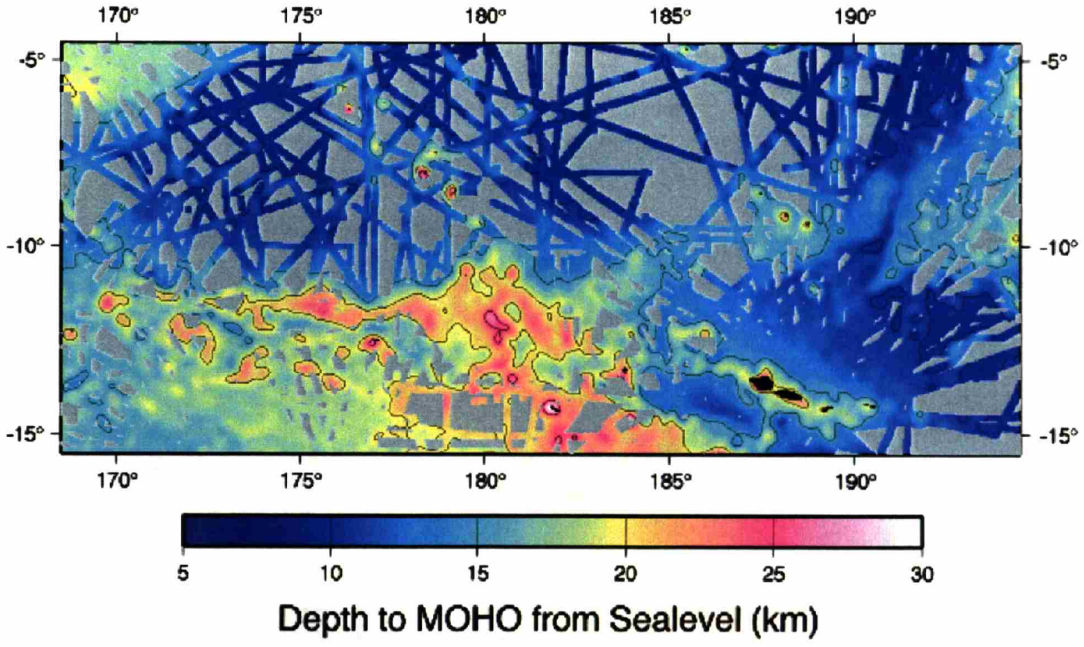

Figure 6-6. Depth to the Moho from sealevel calculated with a downward continuation of the MBA signal, assuming that all the MBA anomaly is due to crustal thickness variations.

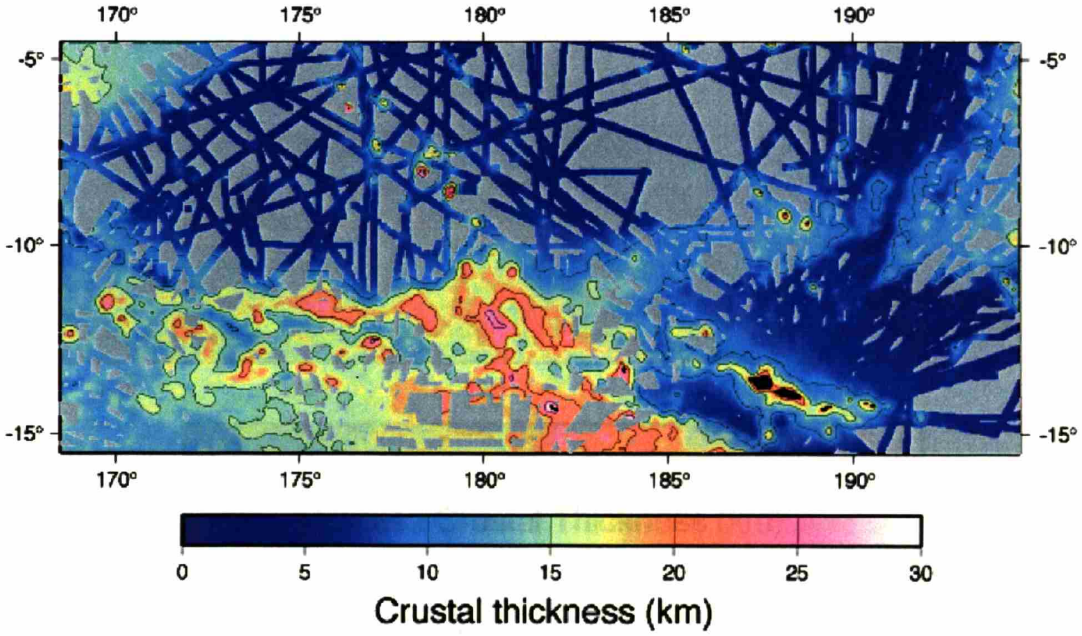

Figure 6-7. Crustal thickness map calculated by subtracting seafloor topography (fig. 3) from the Moho depth (fig. 6).

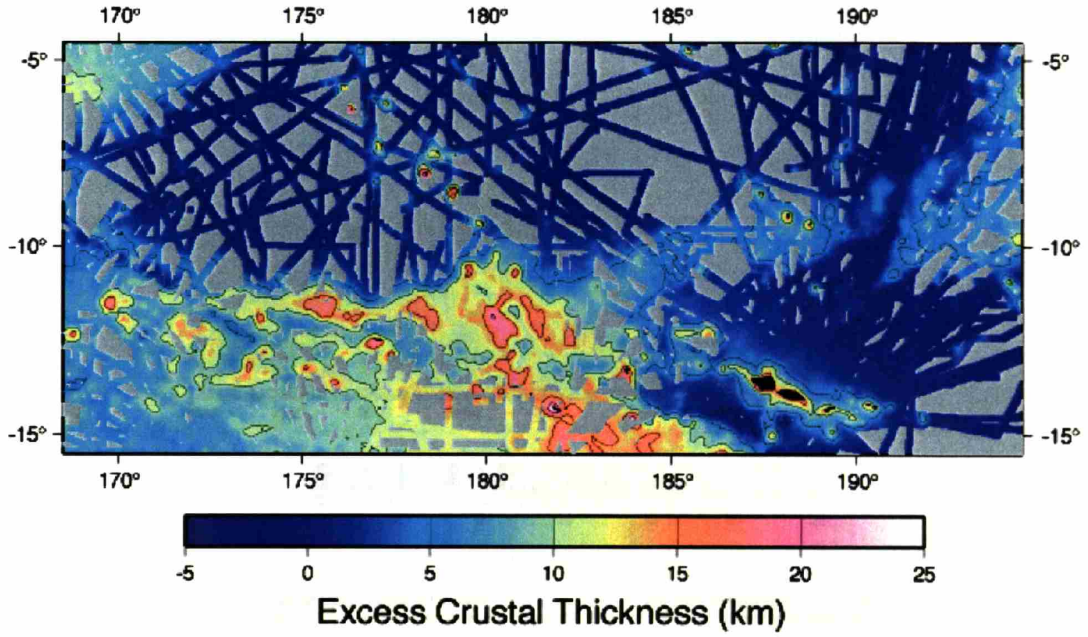

Figure 6-8. Excess crustal thickness calculated by subtracting 6 kilometers from the crustal thickness map in Figure 7. This provides an estimate of crustal flux associated with volcanism after formation of the plate at the East Pacific Rise.

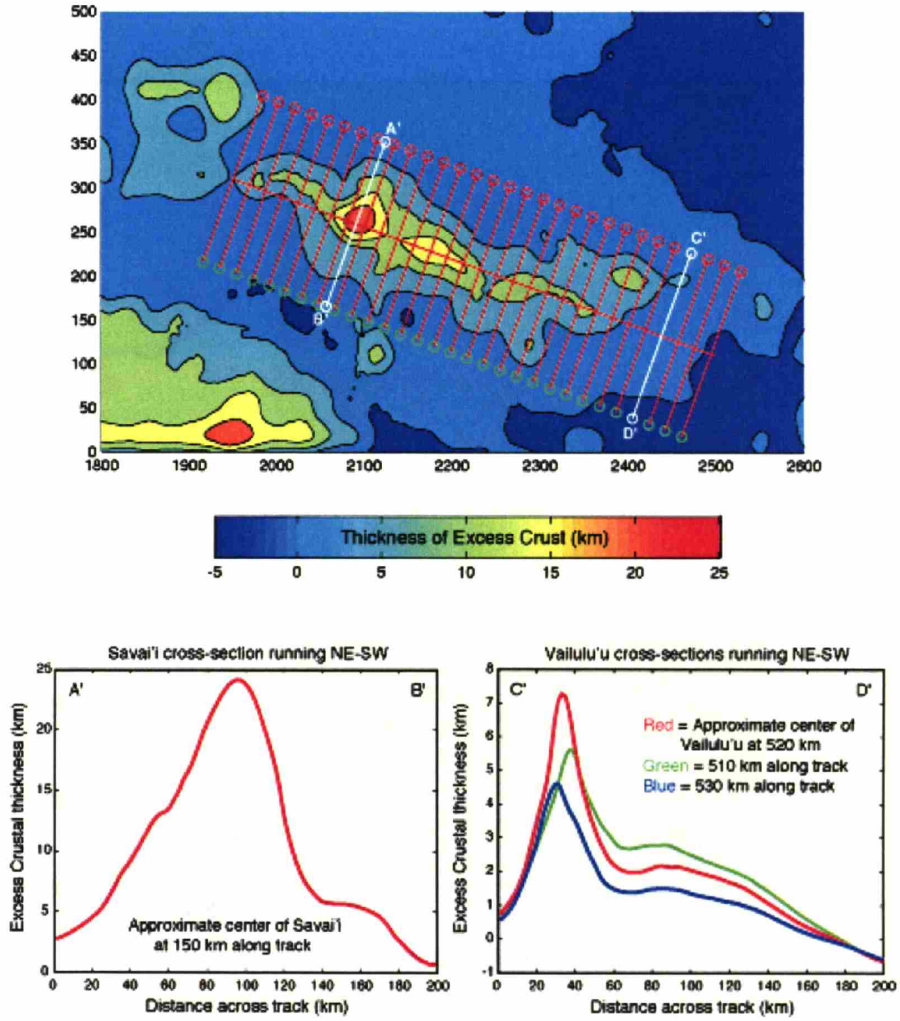

Figure 6-9. Top panel shows excess crustal thickness for the region around Samoa. The boundaries of this map are defined by the red box in Figure 1, but the coordinates here are expressed as kilometers, with the origin being the southwest corner of Figure 1. The 'along-axis' line runs from Savaii at its northwest end to Vailulu'u Seamount at its southeast end. The total distance of the along-axis line is 585 km. 'Across-axis' lines are perpendicular to the along-axis line and are 200 km wide. Plotted here are examples of across-axis lines every 20 km along-axis. Also plotted are two white cross axis lines that mark locations of the cross sections shown in the bottom two panels. Bottom left panel is a cross section of crustal thickness across the middle of Savaii, with a maximum of almost 25 km of crust. At the opposite end is Vailulu'u, shown in the bottom right panel. Maximum excess crustal thickness here is only ~7 km; the two additional cross-sections of Vailulu'u are shown for a semi-3D perspective. For reference, the large mass of excess crust shown at the coordinate (1950, 20) is related to the Tonga Arc, but is not a completely reliable estimate of crustal thickness due to 'edge effects' at this map boundary.

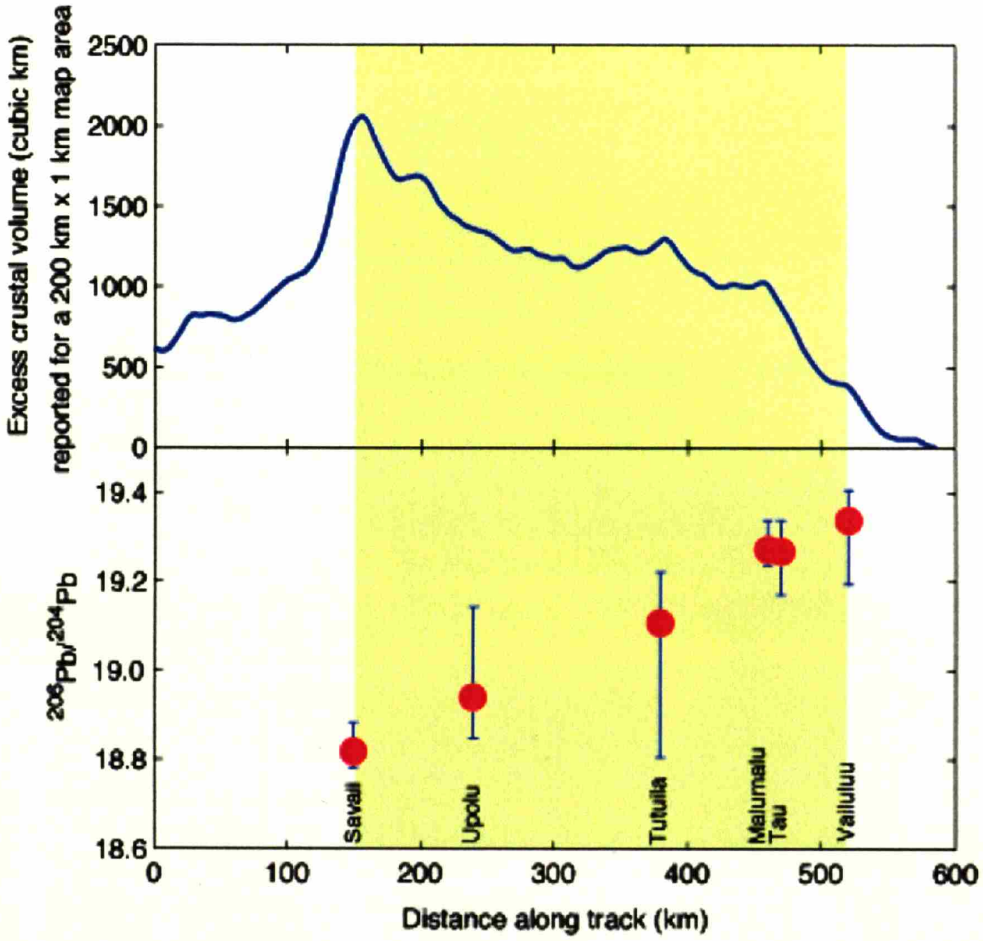

Figure 6-10. A two-panel plot illustrating crustal flux along the Samoan volcanic chain and its surprisingly good inverse correlation with $^{206}Pb/^{204}Pb$. Crustal flux is reported as the volume of crust in a 200 km by 1 km area (map view) along the axis shown in Figure 9; i.e., each point is an integration of a cross-section such as those shown in the bottom two panels of Figure 9. Mean $^{206}Pb/^{204}Pb$ values for each island or seamount are plotted in red, with upper and lower bars indicating the full ranges (data is from Chapter 2). As crustal flux is monotonically decreasing from west to east, mean $^{206}Pb/^{204}Pb$ is monotonically increasing. We speculate this relationship is due to increasing lithospheric thickness or waning potential temperatures of the Samoan plume over time.